PHYSICO-CHEMICAL STUDIES ON MICROEMULSIONS WITH SPECIAL EMPHASIS TO IONIC LIQUID

Thesis submitted to the University of North Bengal

For the Award of

Doctor of Philosophy in Chemistry

BY

SUJOY PAUL

GUIDE

DR. AMIYA KUMAR PANDA

Department of Chemistry

University of North Bengal

Darjeeling 734013

West Bengal

INDIA

2014

DECLARATION

I declare that the thesis entitled "PHYSICO-CHEMICAL STUDIES ON MICROEMULSIONS WITH SPECIAL EMPHASIS TO IONIC LIQUID" has been prepared by me under the guidance of Dr. Amiya Kumar Panda, Associate Professor, Department of Chemistry, University of North Bengal.

No part of this thesis has formed the basis for the award of any other degree or fellowship previously.

SUJOY PAUL

Department of Chemistry
University of North Bengal
Darjeeling 734013
West Bengal
INDIA

CERTIFICATE FROM THE GUIDE

I certify that Mr. Sujoy Paul has prepared the thesis entitled "PHYSICO-CHEMICAL STUDIES ON MICROEMULSIONS WITH SPECIAL EMPHASIS TO IONIC LIQUID", for the award of PhD degree of the University of North Bengal, under my guidance. He has carried out the work at the Department of Chemistry, University of North Bengal.

Amiya Kumar Panda

Date:

Dedicated to my family...

ACKNOWLEDGEMENT

The research work, as presented in the dissertation entitled "PHYSICO-CHEMICAL STUDIES ON MICROEMULSIONS WITH SPECIAL EMPHASIS TO IONIC LIQUID", has been carried out under the supervision of Dr. Amiya Kumar Panda, Department of Chemistry, University of North Bengal. I am immensely grateful to him for his constant inspiration and guidance during the tenure of my PhD work.

I bid my gratitude to the authority of University of North Bengal for providing the facilities and accessibilities related to the research work.

Financial supports from the Department of Science and Technology (DST), Govt. of India, are gratefully acknowledged.

I convey my sincere appreciation to all the faculty and staff members of the Department of Chemistry, University of North Bengal. I would like to specially acknowledge Prof. S. K. Saha, Prof. B. Basu, Prof. M. N. Roy, Dr. A. Mishra, Dr. P. Ghosh, Dr. S. Das, Dr. B. Sinha, Dr. P. Bandopadhyay, Prof. P. S. Roy and Dr. A. Majumder, Department of Chemistry, University of North Bengal for their valued guidance, advice and suggestions.

I also acknowledge them who have directly and indirectly given me the inspirations to make this work happen in a stipulated time.

My heartiest thanks go to my fellow colleagues Kausik Manna, Moumita Chakraborty, Sudarshana Majumdar, Pritam Guha, Biplab Roy, Prasant Nahak and Gourav Karmakar and my friends Soumik Bardhan, Sumanta Gupta, Suranjan Shil, Jayanta Das, Amitava Mandal and Tamal Goswami for their cooperation and constant support. I really enjoyed their criticisms, suggestions and encouragements which, I am sure, going to miss.

The work would not have materialized unless I am blessed with the patience, support and wishes from my parents and family members.

Last but not the least the constant inspiration and support from my wife Barnali and my little daughter Swarnabrita have made possible my dreams to reality.

ABSTRACT

Microemulsions are thermodynamically stable, macroscopically homogeneous but microscopically heterogeneous, mixtures of water and oil stabilized by surfactant monolayer. They have unique properties like ultralow interfacial tension, large interfacial area and the ability to solubilize otherwise immiscible liquids. In spite of several studies on microemulsions, knowledge on this domain of research are still fragmentary in research. Recently ionic liquids have been found to be good substituent as the polar component. Such a combined potential of ionic liquid and microemulsion have instigated to undertake different physicochemical studies on ionic liquid microemulsion. Sometimes ionic liquids as single polar components suffer from some limitations which may be overcome through the usage of ionic liquid in combination with another polar solvent, e.g., water. With this purview, it was thought to be worthy to carry out the works as outlined below:

Detailed studies on the pseudo-ternary water-in-oil microemulsion system, comprising water/(Tween-20+n-alkanol)/n-heptane, have been carried out by way of phase manifestation, method of dilution, viscosity and dynamic light scattering techniques. Such an initiative was made as point of reference so that the data set could be compared with the similar systems comprising ionic liquid in lieu of water. Tween-20, in combination with cosurfactants (of varying chain length, from n-butanol to n-octanol) were used in studying such systems in the temperature range 303 – 323 K. A clear dependence of the different phases on cosurfactant chain length was noted. By employing the method of dilution, associated thermodynamic parameters for the formation of water-in-oil microemulsion droplets were derived. Different associated structural parameters were derived through further computation of the data derived from the method of dilution. Unusual behavior of Tween 20, compared to the conventional ionic surfactants, was noted. Viscosity measurements, as carried out at different composition and temperature, revealed the temperature and water pool size dependency of the microemulsion systems. Viscosity data did not follow the same

trend during heating and the cooling process, due to condensation effect. This phenomenon was further confirmed by dynamic light scattering studies.

Although several studies on imidazolium based ionic liquid-in-oil microemulsion are available in the literature, however, studies on pyridinum bases ionic liquid microemulsion are not so common. Pyridinium based ionic liquids have superior yet unexplored properties when considered in the polar domain of microemulsion. 1-butyl-4-methyl pyridinium tetrafluoroborate ([b4mpy][BF_4]) / (Tween 20 + n-pentanol) / n-heptane microemulsion system has been studied by combined phase behavior, dynamic light scattering, viscosity and spectroscopic probing techniques. With the increasing amount of Tween 20/n-pentanol (S/CS) ratio, turbidity increased, although it was not possible to achieve a stable microemulsion without the cosurfactant. Dynamic light scattering and viscosity study revealed that the size of the μE droplets increased with increasing volume fraction (φ_d) of ionic liquid. Both the size and viscosity increased with φ_d. With the increasing amount of n-pentanol, the variation became less sensitive due to the better stabilizing effect induced by the alkanol. Increase in size of the microemulsion droplets was overshadowed by the increase in the fluidity of the medium, for which viscosity decreased with increasing temperature, as common for Newtonian fluids. State of the ionic liquid in the microemulsion was monitored by absorption and fluorescence spectroscopy with and without curcumin as the molecular probe. While a continuous increase in polarity of the IL domain occurred with increasing amount of IL, the fluorescence anisotropy results revealed that the rigidity of the domain passed through maxima for all S/CS ratio.

Physicochemical properties of an ionic liquid (IL) 1-butyl-3-methylimidazolium methanesulfonate, ([bmim][MS]), in combination with water, were evaluated through the density, viscosity, surface tension, conductance, cyclic voltammetry, absorption and emission spectroscopic measurements. Binary mixtures were studied both in the water rich and [bmim][MS] rich regions (0.01 mM to 4.96 M). The static and dynamic properties of the binary combinations were evaluated through density and viscosity measurements. [bmim][MS] decreased the surface tension of water wherefrom the surface excess and area per

molecule of the ionic liquid were determined at the air-liquid surface. Equivalent conductance of [bmim][MS] at infinite dilution was determined from the conductance data as the system obeyed Debye-Hückel-Onsager formalism. Cyclic voltammetry measurements revealed the formation of some metastable organized structures at specific compositions. Absorption and emission spectral behavior of the anionic dye eosin Y was found to be dependent on the concentration of [bmim][MS] in the water rich region. A significant change in steady state anisotropy and excited state life time of the fluorophore occurred above 1.0 M [bmim][MS] in water, which was correlated with the viscosity of the medium. It was concluded that aggregation of [bmim][MS] into micelle like aggregates above the specific concentration occurred, which significantly altered the different physiochemical parameters of [bmim][MS] binary mixture.

Combined phase behavior, method of dilution, viscosity, dynamic light scattering, electrical conductance and spectroscopic probing techniques were employed in understanding the physicochemical properties of pseudo ternary microemulsion system 1-butyl-3-methyl imidazolium methanesulfonate ([bmim][MS]±water) / (Tween-20+n-pentanol) / n-heptane. Phase manifestation revealed that the area under the clear region depended on ionic liquid (IL) / water mole ratio. Thermodynamic and structural parameters for the formation of (IL+water)-in-oil μE system were evaluated employing the method of dilution at different [polar domain]/[Tween-20] mole ratio and temperature; the parameters depended on the composition of the polar domain. IL+water comprising μE behaved differently, compared to the conventional water-in-oil μE system, especially at higher mole fraction of IL. Both the size and viscosity increased with the increasing volume fraction of the dispersed phase (IL+water), while they decreased with increasing temperature. Although having IL, the μEs were less conducting due to the strong interaction between the IL cation and the oxyethylene groups of the surfactants. Formation of micelle like aggregates within the polar domain further suppressed the conductivity. Combined studies on the absorption and emission spectra of eosinY, along with the excited state lifetime and anisotropy measurements, revealed the existence of different states of IL+water in the polar domain.

PREFACE

The present dissertation deals with the physicochemical studies on different types of microemulsions with a special prominence with ionic liquids. To begin with, introduction and corresponding literature studies have been presented; the reported information of understanding microemulsions and binary mixtures of ionic liquid and water in a general way has been reviewed followed by a description of the scope and perspective.

The present study comprises four different aspects:

1. A relatively simpler system comprising water/(Tween-20+n-alkanol)/n-heptane w/o μE was studied. During this study, effect on the variation of cosurfactant chain length, [water] / [surfactant] mole ratio (ω), (indicative of the water pool size), and temperature were investigated in detail.

2. The system comprising 1-butyl-4-methylpyridinium tetrafluoroborate [b4mpy][BF_4]+water/(Tween-20+n-pentanol)/n-heptane system was studied by combined phase behavior, viscosity, conductance and DLS approach in the oil rich microemulsion region and also spectral behavior on curcumin of the above said system would be studied.

3. After the investigation of the above μE, different physico-chemical studies such as density, viscosity, surface tension, conductance, cyclic voltammetry and spectral behavior of eosin Y in the binary mixture of the ionic liquid 1-butyl-3-methyl imidazolium methan sulfonate [bmim][MS] and water was investigated with an intention to study the μE whereby the water pool will be replaced by ionic liquid.

4. Then [bmim][MS]+water/(Tween-20+n-pentanol)/n-heptane μE system was studied by combined phase behavior, dilution, viscosity and DLS approach in the oil rich microemulsion region and also spectral behavior on eosin Y of the above said system were studied.

Finally attempts have been made to summarize and conclude based on the different experimental observations.

The study then follows the basic data and off-prints of the published papers.

CONTENT

LIST OF TABLES

Table 4.5. **145**

Scaling law parameters for volume (IL+water) induced percolation of ([bmim][MS]±water) / (Tween-20+n-pentanol) / n-heptane polar domain-in-oil microemulsion system at different temperatures.

LIST OF FIGURES & SCHEMES

CHAPTER 2

INTRODUCTION

INTRODUCTION

1. Amphiphiles and surfactants

The word "amphiphile" was coined by Paul Winsor more than fifty years ago. It comes from two Greek roots. The prefix 'amphi' means double and the word 'philos' expresses friendship or affinity, as in. An amphiphilic substance exhibits a double affinity, which can be defined from the physico-chemical point of view as a polar-apolar duality. A typical amphiphilic molecule consists of two parts: on the one hand a polar group which contains hetero atoms such as oxygen, sulphur or nitrogen included in functional groups such as alcohol, thiol, ether, ester, acid, sulfate, sulfonate, phosphate, amine, amide, etc. On the other hand the apolar group is in general comprised of hydrocarbon chain/s of the alkyl or alkylbenzene type; sometimes halogen atoms and even a few nonionizable oxygen atoms. The polar portion is often called 'hydrophilic part' or 'hydrophile' as it exhibits strong affinity to polar solvents, particularly water. The apolar part is called 'hydrophobe'or'lipophile'[1].

Some of the amphiphiles can undergo self-organization in solution through the formation of "association colloids" or "micelles."[2,3]. Micelles, formed by amphiphiles, can have several potential applications. Such amphiphiles are also termed as SURFACTANT. In English the term surfactant (acronym for surface-active-agent) designates a substance which exhibits some superficial or interfacial activities. It is worth remarking that all amhiphiles do not display such activity; in effect, only the amphiphiles with more or less equilibrated hydrophilic and lipophilic tendencies are likely to migrate to the surface or interface. It does not happen if the amphiphilic molecule is too hydrophilic or too hydrophobic, in which case it stays in one of the phases. Surfactants, through the process of interfacial adsorption, could substantially reduce the surface free energy (Gibbs adsorption)[4,5]. A schematic diagram of a typical surfactant molecule can be described as follows:

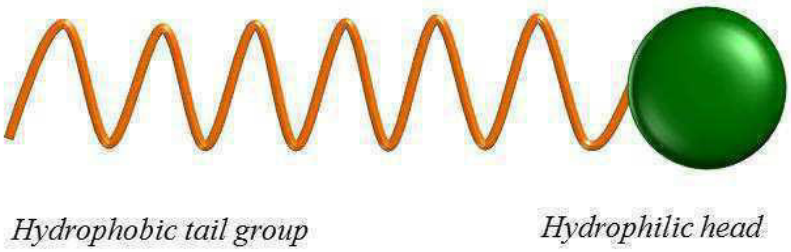

Figure 1. General structure of a surfactant molecule.

1.2. Classification of surfactants

1.2.1. Classification based on origin:

Based on the origin, surfactants are classified as soaps and detergents.

Soaps: Strictly speaking the term soap refers to the sodium or potassium salt of fatty acids. By extension the acid may be any carboxylic acid, and the alkaline metal ion may be replaced by any metallic or organic cation. Soaps are made from fats and oils, or their fatty acids, by treating them chemically with a strong alkali[6-8]. Examples include sodium palmitate, sodium oleate, sodium cholate, etc.

Detergents: In the late 1940 and early 1950 synthetic detergents displaced soaps in domestic washing particularly in washing machine use, because they displayed several advantages, such as better tolerance to hard water, better detergency, and cheaper price. Detergents refer to the synthetically prepared surfactants. Alkylbenzenesulfonates, a family of compounds that are similar to soap but are more soluble in hard water, because the polar sulfonate (of detergents) is less likely than the polar carboxylate (of soap) to bind to calcium and other ions found in hard water. Examples of detergents include sodium dodecyl benzene sulphonate (SDBS), sodium dodecyl sulfate (SDS), hexadecyltrimethylammonium (cetyltrimethylammonium) bromide (C_{16}TABr), cetylpyridinium chloride (CPC), polyoxyethylene sorbitan monolaurate (Tween 20 or Polysorbate 20), etc.

1.2.2. Classification based on the charge on the polar head groups:

Based on the charge carried by the hydrophilic head groups surfactants can be classified into non-ionic, ionic (cationic and anionic) and zwitterionic.

Nonionic Surfactants: These surfactants, because of their non-dissociable hydrophilic groups, they do not ionize in aqueous solution. A large portion of these nonionic surfactants are made hydrophilic by the presence of a

polyethylene glycol chain, obtained by the polycondensation of ethylene oxide. They are called polyethoxylated nonionics. Examples include polyoxyethylene sorbitanmonolaurate (Tween 20), t-octylphenoxypolyethoxyethanol (Triton X100), polyethylene glycol lauryl ether (Brij35), sorbitanmonolaurate (Span 20), etc.

Cationic Surfactant: Cationic surfactants are dissociated in water into amphiphilic cation and counter anion, most often of the halogen type. Long chain alktyltrimethylammonium bromide (CnTABr, n=10 – 18), cetylpyridinium chloride, benzylhexadecyltrimethylammonium chloride, etc., are some of the examples of cationic surfactants.

Anionic Surfactant: These are dissociated in water as an amphiphilic anion, and a cation, which is in general an alkaline metal (Na^+, K^+) or a quaternary ammonium. They include alkylbenzene sulfonates (detergents), (fatty acid) soaps, lauryl sulfate (foaming agent), di-alkyl sulfosuccinate (wetting agent), lignosulfonates (dispersants) etc. comes under this category.

Table 1: Classification of surfactants on the basis of charge on the polar head groups.

Type	Structure
Nonionic	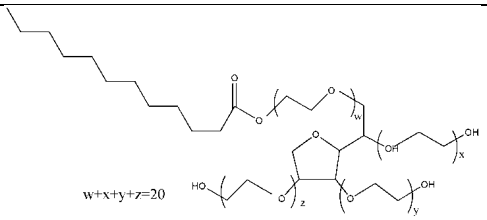 Polyoxyethylene sorbitan monolaurate (Tween 20)
Cationic	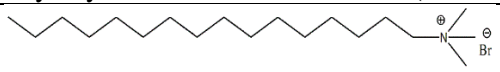 Cetyltrimethylammonm bromide (C_{16}TAB)
Anionic	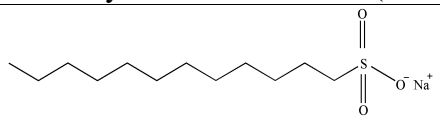 Sodium Dodecylsulfate (SDS)
Zwitterio-nic	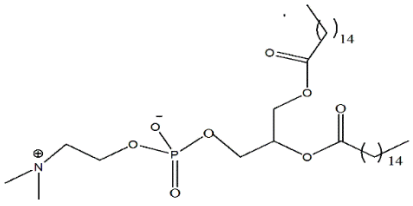 Dipalmitoylphosphatidylcholine

Zwitterionic Surfactants: When a single surfactant molecule exhibit both anionic and cationic dissociations it is called **amphoteric** or **zwitterionic**. 1,2-diacyl-sn-glycero-3-phosphatidylcholine (lecithin), 3-(ethyldimethylammonio) propane-1-sulfonate (NDSB-195) are some of the examples of this type of surfactant.

1.2.3. Other Classification: The other classes of surfactants which were developed with the advancement of surface chemistry are gemini surfactant, bolaamphiphile and catanionic surfactant.

Gemini Surfactants: These are surfactants which have special molecular structure where two amphiphilic moieties are linked through "spacer"[9-11]. The two terminal hydrocarbon tails can be short or long; the two polar head groups can be cationic, anionic or nonionic; the spacer can be short or long, flexible or rigid. The spacer can be attached directly to the identical ionic groups (Figure 2), each of which is in turn bonded to an identical hydrocarbon tail. Alternately, the two identical amphiphiles are joined midway[12-14].

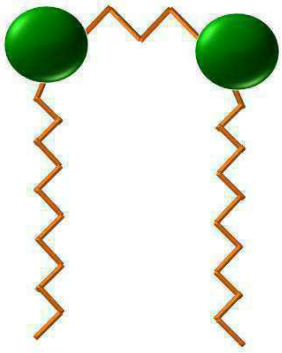

Figure 2. General structure of gemini surfactants.

Bolaamphiphile: Bolaamphiphiles (also known as bolaform surfactants, bolaphiles, or alpha-omega-type surfactants) are amphiphilic molecules that have hydrophilic groups at both ends of a sufficiently long hydrophobic hydrocarbon chain[15,16].

Figure 3. General Structure of bolaamphiphiles.

Catanionic Surfactant: In this class of surfactants, the heads of two oppositely charged surfactants (cationic and anionic) are linked with ionic bond[17-20 21-23].

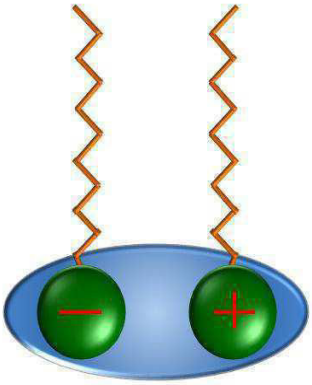

Figure 4. General Structure of catanionic surfactant.

2. Hydrophilic-Lipophilic Balance

The hydrophile-lipophile-balance (HLB) System simplifies the choice of surfactants to meet emulsion formulation requirements. It is based on the balance between the hydrophilic and the lipophilic proportions that give each surfactant its functionality. The most hydrophilic surfactants usually have the highest HLB values and vice versa[24-26].

HLB enables one to measure the emulsifying potential of a surfactant in terms of emulsion quality and stability. HLB value of a surfactant could be computed from its chemical structure and could be matched with the corresponding HLB of the oil phase to be dispersed. There are different empirical formulae to calculate the HLB value. The HLB values lie within a range of 0 - 20 on some arbitrary scale. Surfactants having highest HLB are usually highly soluble in water, could form stable o/w microemulsion. On the other hand, surfactants lying on the low end of the HLB scale are good for w/o microemulsion (μE) formulation[24-26].

The effectiveness of a given surfactant in stabilizing a particular emulsion system could be controlled by the balance between the HLBs of the surfactant and oil phase. HLB value for the nonionic surfactants possessing polyoxyethylene sorbitan group could be expressed as [26]:

$$HLB = \frac{\textbf{mole\% of the hydrophilic group}}{5} \quad \textbf{(1)}$$

Surfactants based on polyhydric alcohol-fatty acid esters such as glycerol monostearate can be handled by the following relationship: [26]

$$HLB = 20\left(1 - \frac{S}{A}\right) \quad \textbf{(2)}$$

Where, S is the saponification number of the ester and A is the acid number of the acid.

There are several other methods available in determining the HLB values of different surfactants. However, herein only the relevant equations have been presented. Tween 20 has an S value of 45.5 while it's A value is 276. Therefore it's HLB value is found to be 16.7. HLB values of the used surfactants are listed in Table 2.

Table 2. HLB values of some surfactants

Surfactant	Commercial Name	HLB value
POE(20) sorbitan monolaurate	Tween 20	16.7
POE(20) sorbitan monopalmitate	Tween 40	15.6
POE(20) sorbitan monostearate	Tween 60	14.9
POE(20) sorbitan monooleate	Tween 80	15.0
Hexadecyltrimethylammonium bromide	C_{16}TAB	21.4
Sodium dodecyl sulphate	SDS	40.0

3. Packing Parameter:

Israelachvili[27] suggested a parameter, called the packing parameter P, which gives a kind of measuring scale to recommend the shape of the amphiphilic aggregates. According to him, the nature of amphiphile-packing in micelles and their structural geometry can be predicted using a packing parameter (P) defined by the relation,

$$P = {}^{v}/_{Al_c} \quad \textbf{(3)}$$

$$R^M = {}^{3v}/_{A} \quad \textbf{(4)}$$

Where, P is the packing parameter, v is the volume of hydrophobic chain (nm^3) (considered as incompressible fluid), l_c is the maximum effective length of the hydrophobic chain of surfactant monomer (nm), R^M is the radius of the micelle (nm) and the surface area of the head group ($nm^2 molecule^{-1}$) at the micellar interface is denoted by A.

For the pure surfactants, the effective length for a saturated hydrocarbon chain (l_c) with n numbers of carbon atoms and their corresponding volumes (v) can be calculated using Tanford's formula [28]. Thus,

$$l_c \leq l_{max} \approx (0.154+0.1265n) \quad \textbf{(5)}$$

and

$$v = (0.0274+0.0269n) \quad \textbf{(6)}$$

where, l_{max} is the maximum length of the hydrophobic chain.

From the magnitude of packing parameter, the shapes of the aggregates formed can be predicted. For spherical micelle, $P < 0.333$; for non-spherical aggregates, $0.333 < P < 0.50$; for vesicles and bilayers, $0.50 < P < 1$ and for inverted structures, $P > 1$. For spherical micelles, the radius (R^M) should not exceed the critical chain length of the monomer[29].

4. Interfacial and Bulk Properties of surfactant solution:

Due to their amphiphilic nature, surfactants can lower the surface tension at the air-liquid interface and oil-water interface[30]. By virtue of this property they can assist solubilization, cleaning, emulsification and dispersion, etc. Under specific conditions (temperature, pressure, solvent nature, etc.) in solution the surfactant molecules, at a threshold or critical concentration, can undergo self-aggregation or self-organization, termed as critical micelle concentration, CMC.[1,31-35] The main driving force, also the causative factor of surfactant aggregation, is dependent on the contact area between the alkyl chain and water of a dissolved surfactant. The retarding factor for surfactant aggregation is the repulsive force between surfactant head-groups, especially in case of ionic surfactants. Usually micelles are of two types, viz., (i) normal micelles (formed in aqueous or polar solvents) and (ii) reverse micelles (in non-polar medium the formation topology is reversed and aggregates formed

therein). Both the types of micelles are guided by the equilibrium thermodynamic principle.[2,36,37]

In case of ionic surfactants, the high charge density around the micellar surface is counter balanced partially through the process of counter-ion binding. However, as nonionic surfactants do not have such counter ions in stabilizing their micellar aggregates, usually nonionic surfactants have lower CMC values in water than the corresponding ionic surfactants.[38]

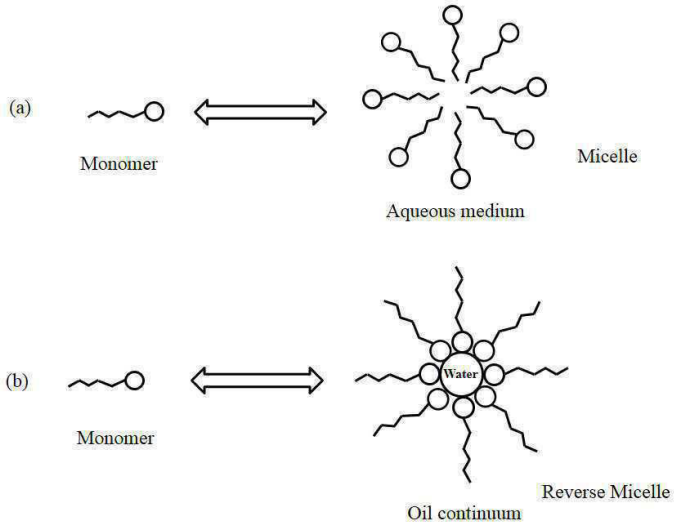

Figure 5. Schematic representation of (a) normal micelle and (b) reverse micelle.

Surfactants can get dissolved into water like common water soluble solutes. After the completion of surface adsorption, surfactants are compelled to congregate to form micelle. When some water-insoluble oil is used as solvent, reverse micelles are formed. The core of micelle is oil like which would accommodate additional oil molecules through the formation of swollen micelles. Further addition of oil results in the formation of oil-in-water emulsion.[28,30,39-55] The core of a reverse micelle on the other hand, is more hydrophilic. Thus it can solubilize some water molecules through forming swollen reverse micelle and subsequently water-in-oil emulsion.

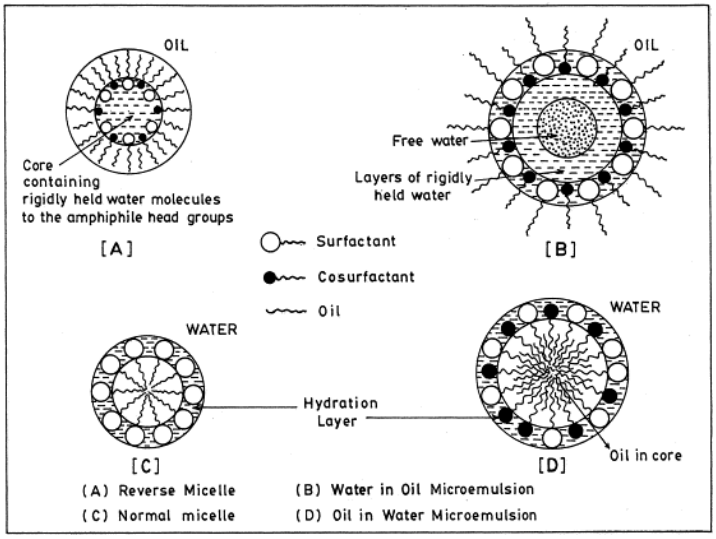

Figure 6. Pictorial representations of reverse micelles and microemulsions (adapted from ref. [39] [28]).

5. *Definition of Microemulsion (μE)*:

In 1943, the transparent dispersion of water-in-oil was termed as "oleopathichydromicelle" by Schulman and Hoar[28,56,57]. Later on Schulman, Stockenium and Prince coined the term "microemulsion"(μE).[58,59]. One of the best definitions of microemulsion is from Danielsson and Lindman [60] "a microemulsion is a system of water, oil and an amphiphile which is a single optically isotropic and thermodynamically stable liquid solution". Now-a-days, all the transparent combinations of oil, water and amphiphilic compounds forming thermodynamically stable, microheterogeneous and optically isotropic solutions, are defined as μEs as distinct from kinetically stable emulsion (macroemulsion)[37] [61] [28] [62]. In some respects, microemulsions can be considered as small-scale versions of emulsions, i.e., droplet type dispersions either of oil-in-water (o/w) or of water-in-oil (w/o), with a size range in the order of 1−100 nm in drop radius. Such a description, however, lacks precision since there are significant differences between microemulsion and ordinary emulsion (or macroemulsion). In emulsions, the average droplet size grows continuously with time so that phase separation ultimately occurs under gravitational force, i.e., they are thermodynamically unstable and their formation requires input of work. The drops of the dispersed phase are generally large (> 0.1 μm) so that they often take on a milky, rather than a translucent appearance. For microemulsions, once the conditions are right,

spontaneous formation occurs. As for simple aqueous systems, microemulsion formation is dependent on surfactant type and structure.

Though μEs usually comprise both the surfactant and co-surfactant (e.g., short chain alcohols, amines, alkyl amines and alkyl halides, etc.), in some cases (e.g., sodium dioctyl sulphosuccinate, AOT), μE can be formed without any co-surfactant [63,64]. Besides, the surfactant less μE (e.g., water, 2-propanol and toluene or hexane) can also be formed [65 66].

Actual structure of μE is still controversial. For emulsion (size 100-2000 nm) interfacial tension ($\gamma_{w/o}$) values is typically in the range of 0.1 – 1mJm^{-2}. For a μE, this value is as low as 0.001 mJ m^{-2}, i.e., it is 1000 fold lower. Surfactant molecules provide a protecting monomolecular film at the oil-water interface [59 67]. μEs, therefore, could be defined as thermodynamically stable, clear, isotropic dispersion of oil-in-water or vice versa, stabilized by monomolecular surfactant film [30 61 28 62]. The type of surfactants used determines the type of an emulsion (oil-in-water, O/W or water-in-oil, W/O). Nature of surfactant could also be categorized on the basis of their hydrophobicity or hydrophilicity. This is also alternately termed as hydrophilic-lipophilic balance (HLB). Judicial choice of surfactants, according to their HLB values, could help in the formulation of proper and desired μE.

5.1. Reason behind stability of microemulsions:

Microemulsion formation and stability can be explained on the basis of a simplified thermodynamic rationalization. The free energy of microemulsion formation can be considered to depend on the extent to which surfactant lowers the oil/water interfacial surface tension and the change in entropy of the system such that,

$$\Delta G = \Delta H - T\Delta S + \gamma\Delta A \qquad \textbf{(7)}$$

where, ΔG, ΔH and ΔS is the change in free energy, enthalpy and entropy (dispersion) associated with the microemulsification, γ is the surface tension of the oil/water interface, ΔA is the change in interfacial area and T is the temperature. When a microemulsion is formed, there is a large change in interfacial area (ΔA) due to the formation of large number of very small droplets. Though γ is positive at all times, on the onset of microemulsion

formation it is very small (γ <0.02mN/m). The dominant favourable entropic contribution is arising from the mixing of one phase into the other (in the form of large numbers of small droplets) and from other dynamic processes such as surfactant diffusion in the interfacial layer, monomer-micelle surfactant exchange etc. The first term (ΔH, a very small positive quantity) and the third term of equation (7) are offset by the entropic component. Thus, a negative free energy of formation is achieved when large reductions in surface tension are accompanied by significant favorable entropic change.

5.2. Water-in-oil (w/o) microemulsion:

The w/o microemulsion is topologically similar to the reverse micelles where the polar head groups of surfactants are oriented inwards and the hydrocarbon tails remain solubilized in the bulk oil phase [31]. In case of swollen reverse micelle the water molecules do not have the freedom to behave like bulk water. However, in case of w/o microemulsion the topology is little bit different. The very first layer of water remains immobilized as they are used up in hydrating the surfactant head groups and the counter ions (if present). After satisfying the hydration of the surfactant head group, the excess water would behave as bulk water.[34]

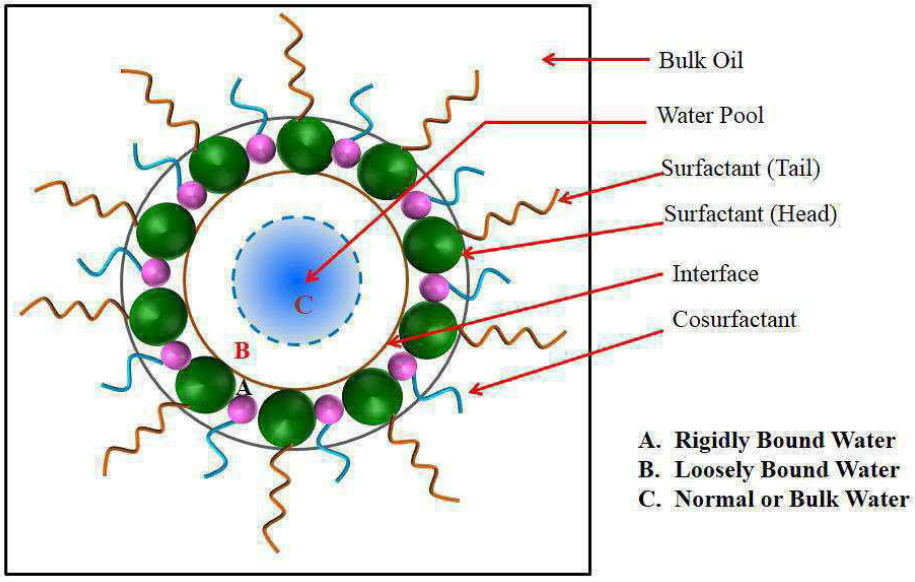

Figure 7. Schematic representation of W/O microemulsion.

6. Phase behavior of mixed water-oil-amphiphile (surfactant + cosurfactant) systems:

Winsor[68] described elaborately the different characteristics of phase manifestation of the ternary mixtures of water-surfactant-oil or the quaternary mixtures of water-surfactant-cosurfactant-oil. The concerned mixed systems fall into four catagories:

Winsor I: The surfactant is preferentially soluble in water and oil-in-water (o/w) microemulsions form. The surfactant-rich water phase coexists with the oil phase where surfactant is only present as monomers at small concentration.

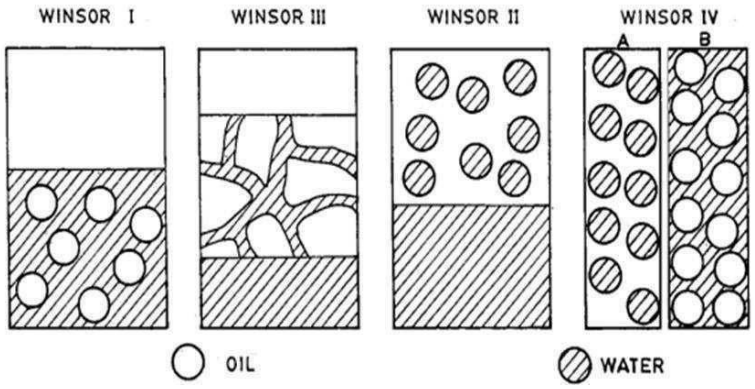

Figure 8. Different phase-forming situations for water-amphiphile-oil mixtures (adapted from ref. [30]).

Winsor II: The surfactant is mainly in the oil phase and water-in-oil (w/o) microemulsions form. The surfactant-rich oil phase coexists with the surfactant-poor aqueous phase.

Winsor III: A microemulsion phase which is in equilibrium with an excess oil phase and an excess water phase. Here both o/w and w/o dispersions are simultaneously present in the same domain in mixed state in separate contacts with both oil and water.

Winsor IV: A single-phase of dispersion either o/w or w/o not in contact with any other phase.

In spite of the above mentioned four categories there are also some reports [69-71]of simultaneous presence of two microemulsion phases in contact

with each other and one in separate contact with water and the other with oil. This may be considered as fifth category of Winsor's classification.

Size of w/o microemulsion could be controlled by varying the amount of water in it. The molar ratio, [water]/[surfactant] (ω) gives one a rough idea about the dimension of the water pool. [72] [28] [62] [30]

7. Role of cosurfactant in microemulsions:

The nature of the surfactant and the cosurfactant influence the phase diagram. In all four types of microemulsions, the interface is stabilized by an appropriate combination of surfactants or surfactant-cosurfactant combinations. The distribution of the cosurfactant between the oil and the interface imparts stability to the dispersion. Alcohols with short alkyl chain length are commonly added as 'cosurfactants', have the effect of further reducing the interfacial tension, while increasing the fluidity of the interface thereby increasing the entropy of the system. It also increases the mobility of the hydrocarbon tail and also allow greater penetration of the oil into this region. The alkyl chain length of cosurfactant have significant on the formation and physico-chemical properties of microemulsion. [73] [74]. The electrical conductance, dielectric constant, interfacial polarization are greatly influences by the chain length of alkanols[74]. Also the phase behavior and microstructure of a microemulsion is reported to be affected by the chain length of the cosurfactant [75]; [76]. The effect of alkyl chain length of oil on microemulsion formation is also studied by different research groups [77] [78]. The solubilization capacity of w/o microemulsion was interrupted by the partitioning of alcohol between oil, water and the interface depending on the chain length of oil and alcohol [78]. The shorter the carbon chain length of the oil and longer the carbon chain length of the alcohols, the higher is the solubilization capacity of the microemulsion.

8. Role of additives in microemulsions:

The microstructural state of a microemulsion may be affected by the presence of additives. Additives especially salts can significantly change the structural properties and hence the phase behavior of microemulsions. [79] [80] [81,82]. The droplet size of a microemulsion varies with increasing salinity and smaller droplets are formed for w/o microemulsion systems whereas it

increases in case of o/w microemulsion system [83]. Amaral et.al. investigated the structural effect of urea in water-AOT-n-hexane reverse micelles and found that the attractive intermicellar interaction increases as the urea concentration increases [84].The study of Kahlweit et al. [79]revealed that the influence of both lyotropic (decreases aqueous solubility of surfactants, e.g., NaCl) and hydrotropic salts (increases aqueous solubility of surfactants, e.g., $NaClO_4$) on the physico-chemical behavior of non-ionic microemulsion system is more or less similar. Dynamic light scattering studies of a polymer-reverse micelle indicated that the spherical droplet structure is preserved in presence of the polymer [85].Garcia-Rio et. al. [86] studied the effect of various alkyl amines on the percolation phenomenon of water/AOT/isooctane microemulsion and suggested the association of amine with AOT as the reason for the percolation. Eicke et.al. have investigated water-AOT-isooctane microemulsion system in presence of gelatin and block copolymers and found the formation of soft condensed microemulsion mediated polymer networks that can evident fluidity displaying viscous flow [87].

9. R- ratio

The R-ratio was first proposed by Winsor [68] to account for the influence of amphiphiles and solvents on interfacial curvature. The primary concept is to relate the energies of interaction between the amphiphile layer and the oil and water regions. Therefore, R-ratio is defined in terms of the cohesive interaction energy between those molecules residing within the surfactant layer. He also proposed that the cohesive energies act on amphiphilic compound positioned at the interfacial region and the cohesive energy ratio (CER), 'R' would explain the type of microemulsion formed. It is defined as:

$$R = \frac{C_{LO}}{C_{HW}} \qquad \textbf{(8)}$$

where, C_{LO} and C_{HW} are the interaction parameters between the lipophilic group and oil, and the hydrophilic group and water, respectively.

When R > 1, a w/o microemulsion is formed and for an o/w microemulsion R is less than 1. The cohesive energy ratio concept has been

used in the formulation of polymerization microemulsion [88]. When R= 1, the mutual solubility of amphiphile, oil and water is maximum and there is no tendency for the amphihile layer to be preferentially convex towards either oil or water, its optimum form will be planer (optical systems) where the micellar phase contains equal volumes of oil and water [89 90].

Taking in account of all the interaction terms (cohesive energies between oil molecules (C_{OO}), between lipophile molecules (C_{LL}), between water molecules (C_{WW}), between hydrophile molecules (C_{HH}), an extended definition of R is proposed by Bourrel et al. [91]

$$R = \frac{C_{LO} - C_{OO} - C_{LL}}{C_{HW} - C_{WW} - C_{HH}} \quad \textbf{(9)}$$

All the cohesive energy terms are found to be dependent on the chemical nature of the components of the microemulsion, their relative concentrations and the temperature.

10. Characterization of microemulsion:

10.2. Physico-chemical studies on microemulsion through phase manifestation:

Microemulsions comprising water, oil and surfactant-cosurfactant can exhibit ranges of phases, viz., viscous solution, lamellar liquid crystals, thin or thick gels, single phase (clear and transparent mixtures), two phase (turbidity appears followed by a phase separation) and three phase regions etc. depending upon the composition and nature of the ingredients, environmental condition (temperature, presence of additives)[28,92]. The knowledge on the areas of the formed phases is a useful characteristic of a multicomponent microemulsion forming system. The amount of surfactant and cosurfactant to be added and the percent of oil phase that can be incorporated shall be determined with the help of pseudo-ternary phase diagram. Usually, pseudo-ternary phase diagrams comprising of oil, water, and surfactant-cosurfactant (amphiphiles) are constructed at definite cosurfactant/surfactant weight ratios considering the mixture as a single component. Formation of monophasic/biphasic system is confirmed by visual inspection. The area covered by the monophasic points is considered as the

microemulsion region of existence. Experimentally, the weight percent compositions at the end points of all the above mentioned titrations (which are either appearance or disappearance of turbidity) are then plotted on a triangular coordinate to create a pseudo-ternary phase diagram, which illustrates different regions in it e.g. microemulsions and other types of entities as shown in Figure 9.

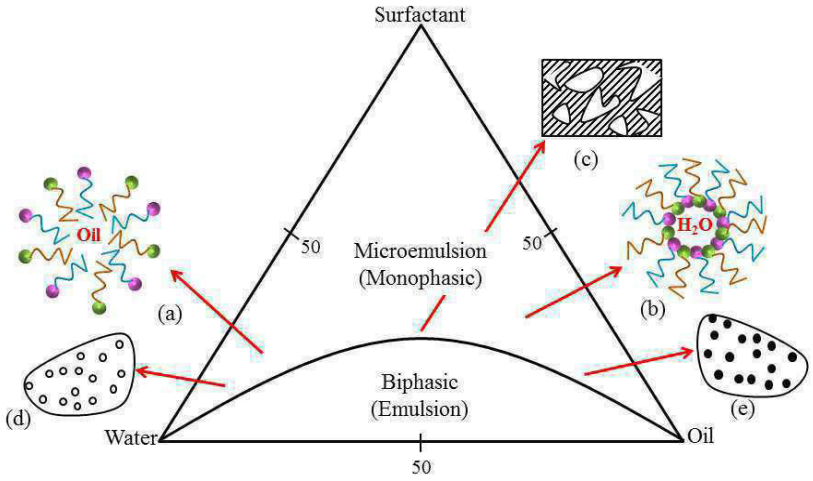

Figure 9. A comprehensive ternary phase diagram showing probable internal structures: (a), o/w microemulsion; (b), w/o microemulsion; (c), bicontinuous dispersion; (d), isolated and aggregated o/w dispersion; and (e), isolated and aggregated w/o dispersion.

10.3. Thermodynamics of w/o microemulsion formation by the method of dilution:

The energetics of formation of microemulsion systems can be obtained from a simple but a potential method, named dilution technique [93 94 28 95 74 96 97,98 99]. The w/o microemulsion consisted of dispersion of water droplets in oil continuum wherein the whole surfactant molecules were considered to populate the oil/water interface in partial association with the cosurfactant which remained distributed between the interface and the bulk oil besides its scanty residence in the water pool due to low solubility. The distribution constants at different temperatures lead to the evaluation of energetics of the process, and additionally the droplet density, size, interfacial population of surfactant and cosurfactant, etc. Such vital information on the dispersed w/o microemulsion system from the model experiments on dilution is a remarkable physico-chemical data generating procedure. In the dilution experiment, the stability of the aforesaid distribution was disturbed by the addition of oil and

was regained by subsequent addition of cosurfactant in the system. It was considered that the following relation holds by mass balance, [97,99 97].

$$n_a^t = n_a^w + n_a^i + n_a^o \quad \textbf{(10)}$$

where, n_a^t, n_a^w, n_a^i and n_a^o are total number of moles of cosurfactant present , moles of cosurfactant in water, its number at the interface and that in oil, respectively. At a constant temperature and ω, the n_a^o and n_o (number of moles of oil in the system) bear a constant ratio. Consequently, the mole fraction ratio of alkanol at the interface (X_a^i) and in oil (X_a^o) should also be constant. Thus,

$$n_a^o/n_o = k \quad \textbf{(11)}$$

and, $$k_d = \frac{X_a^i}{X_a^o} \quad \textbf{(12)}$$

where, k and k_d are constant and the distribution constant respectively. By replacing equation (12) in equation (11) one sets the following relation:

$$\frac{n_a^t}{n_s} = \frac{n_a^w + n_a^i}{n_s} + k\frac{n_o}{n_s} \quad \textbf{(13)}$$

n_s represents the number of moles of surfactant. The distribution constant k_d is related to the slope and intercept of equation (13) as:

$$k_d = \frac{X_a^i}{X_a^o} = \frac{n_a^i/(n_a^i+n_s)}{n_a^o/(n_a^o+n_o)} = \frac{n_a^i\left(1+\frac{n_a^o}{n_o}\right)}{n_a^o\left(1+\frac{n_a^i}{n_s}\right)} = \frac{\alpha(1+S)}{S(1+\alpha)} \quad \textbf{(14)}$$

where, $$\alpha = \left(I - \frac{n_a^w}{n_s}\right) = \frac{n_a^i}{n_s} \quad \textbf{(15)}$$

and S=K, I and S are the intercept and slope of equation (13). The number of moles of cosurfactant in water (n_a^w) was obtained from its solubility in water (for long chain alkanols, $n_a^w \approx 0$ because of their negligible solubility to make α = I).

The energetic parameters for the transfer of cosurfactant from oil to interface can then follow from the following relations,

$$\Delta G_t^0 = -RTlnk_d \quad \textbf{(16)}$$

$$\Delta H_t^0 = \left[\frac{\partial(\Delta G_t^0/T)}{\partial(1/T)}\right]_p \quad \textbf{(17)}$$

and, $$\Delta S_t^0 = \frac{\Delta H_t^0 - \Delta G_t^0}{T} \quad \textbf{(18)}$$

where, ΔG_t^0 and ΔH_t^0 represent standard Gibbs free energy, enthalpy and entropy of transfer respectively.

The results derived from the dilution experiments were used to evaluate structural parameters of the dispersed water droplets in microemulsion. The microemulsion droplets are approximated to have spherical shape in general, mono dispersed with a surface mono layer comprising surfactant and cosurfactant to be present at the interface. The total volume of the dispersed droplets (V_d) per unit volume (here in mL) can be expressed as follows:

$$V_d = \frac{4}{3}\pi {R_e}^3 N_d \quad \textbf{(19)}$$

R_e and N_d represents the effective diameter and total number of the droplets respectively. The droplet surface area (A_d) of droplets per unit volume is therefore:

$$A_d = 4\pi {R_e}^2 N_d = \left(n_S A_S + n_a^i A_a\right) N_A \quad \textbf{(20)}$$

where, A_S and A_a are the cross sectional area of the surfactant and cosurfactant molecules respectively, N_A Avogadro's constant.

The equation for R_e from equation (19) and (20) can be written as:

$$R_e = {3V_d}/{A_d} \quad \textbf{(21)}$$

Total volume of the dispersed phase, herein the water droplet embedded by the surfactant and n-alkanols at the oil-water interface, is the sum of the volume contribution of water (V_{H_2O}), surfactant (V_S) and the interfacial n-alkanol molecules (V_a^i) at the interface respectively. Thus one could write:

$$V_d = V_{H_2O} + V_S + V_a^i \quad \textbf{(22)}$$

One can determine the respective volumes using the values of number of moles (n_a^i), molar mass (M_a) and density of the components (ρ_a) according to the relation:

$$V_a^i = {n_a^i M_a}/{\rho_a} \quad \textbf{(23)}$$

The total droplet surface area (A_d) can be obtained from the equation:

$$A_d = \left(n_s A_s + n_a^i A_a\right) N_A \quad \textbf{(24)}$$

where, A_S and A_a are the polar head group area of surfactant and alkanol, respectively, and N_A is the Avogadro constant.

Putting the value of R_e in equation (19) we get the values of N_d

$$N_d = {3V_d}/{4\pi {R_e}^3} \quad \textbf{(25)}$$

The average aggregation number of surfactant (N_S) and cosurfactant (N_a) in a microemulsion droplet can be expressed as:

$$N_s = \frac{n_s N_A}{N_d} \quad \textbf{(26)}$$

$$N_a = \frac{n_a^i N_A}{N_d} \quad \textbf{(27)}$$

Volume of a microemulsion droplet is contributed by dispersed water, surfactant and cosurfactant molecules. Thus the radius of water pool in a

microemulsion droplet is related to the effective radius (i.e., the sum of pool radius and surfactant tail) according to the relation:

$$R_W = \left(\frac{V_{H_2O}+V_s^h+V_a^h}{V_d}\right)^{1/3} R_e \qquad \textbf{(28)}$$

where, V_{H_2O} , V_s^h and V_a^h are volume of water droplet, surfactant head group, and alkanol head group, respectively. Volume contribution due to surfactant head group and cosurfactant head group could be evaluated from the following two equations:

$$V_s^h = \frac{4}{3\pi^{1/2}} A_s{}^{3/2} N_s \qquad \textbf{(29)}$$

$$V_a^h = \frac{4}{3\pi^{1/2}} A_a{}^{3/2} N_a \qquad \textbf{(30)}$$

Various structural parameters, as described in the earlier section can be computed by employing the dilution data into the aforementioned equations.

10.4. Transport properties of microemulsion (Percolation of electrical conductance):

Microemulsions are good physical examples for dynamic percolation studies. They are thermally stable mixtures that respond reversibly to changes in relevant physical parameters. It can show striking conductance behavior. Normally, o/w systems with ionic amphiphiles have conductance levels comparable to electrolyte solutions: whereas w/o systems show poor conductance at low water content and at lower temperatures. The water droplets in a w/o microemulsion are in constant motion in the oil continuum. The droplets collide, fuse and subsequently break apart and during the process, exchange of mass between two fusing droplets may take place[34,100,101]. Although the continuous oil medium in w/o microemulsion is an insulator, w/o microemulsion (containing charged species in the water pool) are capable of electrical conduction. Depending upon this phenomenon the ion conduction of o/w, w/o and bicontinuous microemulsions are drastically different from one another. A water continuous o/w microemulsion behaves almost like normal aqueous medium and thus is good conducting, whereas oil continuous w/o

microemulsion is resistant to ion migration making it low conducting. Conductivity of a bicontinuous microemulsion is, however, significantly higher than w/o microemulsion, although not as high as o/w microemulsion[102]. The transfer of ions from one droplet to another progressing in certain direction under an applied electric field by way of fusion and fission can register increase in conductance which at a particular water content (ω) or temperature may show drastic change (normally increase). This phenomenon is called percolation and the threshold temperature or the threshold water concentration associated with the process are called percolation threshold [48 103 52,55,100,104-107].

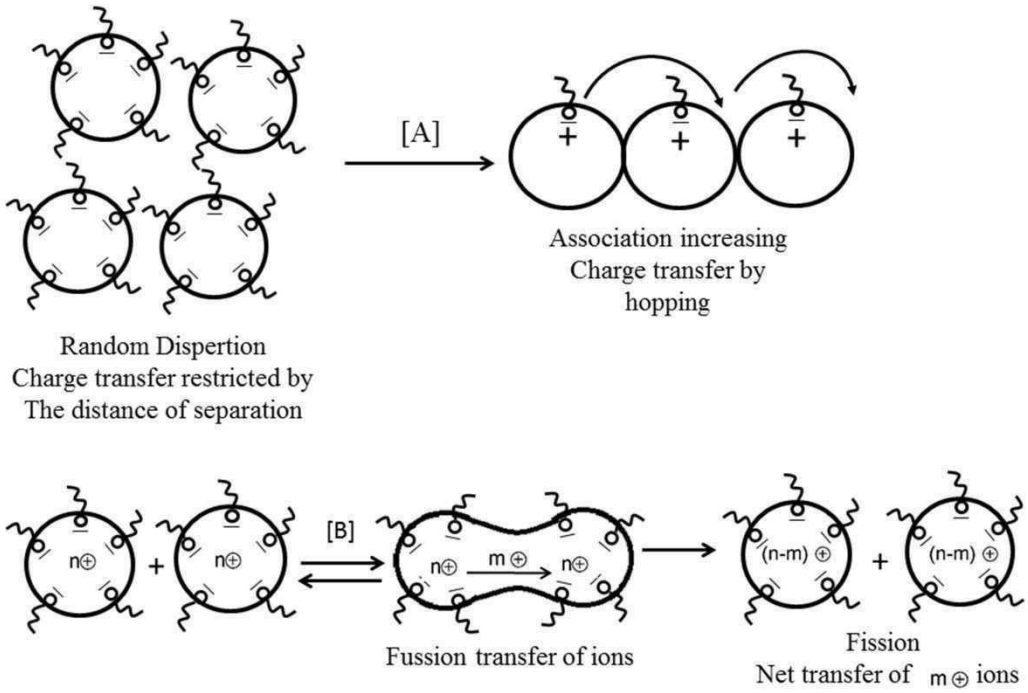

Figure 10. A Hopping mechanism. Ions hop in the direction indicated by the curl heads; B. Ion transport by fusion and fission. n ⊕ cations in the droplets. m⊕ cations are involved in the transfer process.

For microemulsion system, two types of percolation can arise (i) volume percolation [108 109 110 111,112 113 114] and (ii) temperature percolation[113 114 115 97 116 54]. In the first, at a fixed amount of amphiphile (surfactant + cosurfactant), increase in water content increases droplet size for their easier merging thus to provide increased mass transfer and conductance i.e. favoring percolation. At a constant ω, increased temperature may increase droplet collision, i.e., fusion among the microdroplets leading to infinite cluster formation; thus, easier transfer of mass or increased conductance increasing temperature percolation. In these situations, the systems change from

insulators to conductors. The droplets having surfactant ions on the surface and counter ions in the interior core come closer and the increased conductance has been considered to be due to (i) the hopping of the surfactant ions from one to another droplet[54 117] and (ii) the transfer of counter ions from one to another through water channels [118] formed by the clustering effect of the droplets; a channel opens during their 'sticky collusion' which result exchange of materials among the droplets[119]. The ion transfer in this process (fusion followed by fission) leads to increase in conductance. The difference between the percolation of a 'conductor-nonconductor' composite system and 'droplet-fusion-fission' associated microemulsion system is that the former produce 'static percolation' whereas the other results 'dynamic percolation'. The presence of additives can have striking effect on percolation, and various different additives including polymers have demonstrated different characteristics [116 85].

In w/o microemulsion, the droplets containing surfactant ions come to a threshold distance where transfer of charge between them occurs efficiently; they are physico-chemically dynamic and by diffusion they approach their neighbors to transfer charge [120]. This is how 'dynamic percolation' occurs after a threshold volume fraction (φ_t) at a constant temperature.

10.4.1. Mathematical rationale of percolation:

The phenomenon of percolation is guided by scaling law[94,115,121,122]. At a constant temperature and in the percolation range, the conductance of water droplets dispersed in oil in w/o microemulsions follows the relation,

$$\sigma = k(\varphi - \varphi_t)^m \quad \textbf{(31)}$$

or, $$ln\,\sigma = \ln k + m \ln(\varphi - \varphi_t) \quad \textbf{(32)}$$

where, σ is the specific conductance of the microemulsion system, k and m are constants and φ is the volume fraction of water, φ_t is the threshold value. Theoretically, the exponent 'm' should be 1.9 for both static and dynamic percolation [123].

At a fixed ω, the scaling law for the temperature percolation [124] [125] [126] in w/o microemulsion is,

$$\sigma = P(\theta - \theta_t)^n \quad \textbf{(33)}$$

or, $$ln\,\sigma = \ln P + n\ln(\theta - \theta_t) \quad \textbf{(34)}$$

where, θ is the temperature corresponding to the specific conductance σ, θ_t is the threshold temperature for transition and n is an exponent. Both φ_t and θ_t in equation (18) and (20), obtained from the plots between σ and φ, and σ and θ respectively, as showed in Figure 11.

Like m, the expected value of n is also 1.9[123,124]. In most of the cases the values of m and n found from experiments are at odds with the expected value of 1.9.

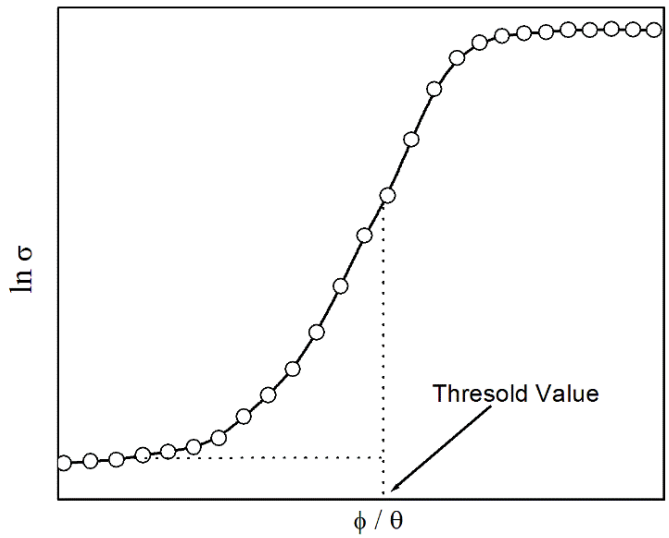

Figure 11. Schematic representation of volume and temperature percolation diagram of a w/o microemulsion system

11. Viscosity of microemulsions:

Viscosity measurement of microemulsion provides firsthand information on both the internal consistency of the colloidal dispersions and knowledge on the overall geometry of the particles of the dispersed phase. microemulsion systems have varied Newtonian and non-Newtonian flow behaviors. Newtonian flow behavior can be seen from low viscous

microemulsions. Non-Newtonian flow behavior is present in the bicontinuous type (Winsor III) of microemulsions and they can show plasticity. The viscosity data obtained for a microemulsion can be further computed to get the knowledge about the activation enthalpy (ΔH^*), which is equivalent to the activation energy, free energy (ΔG^*), entropy change (ΔS^*) and the change in specific heat capacity (ΔC_p) [38,114,127,128]. The activation enthalpy for the viscous flow and the associated entropy change can be expressed by the following equation,

$$\eta = \left(\frac{hN}{V}\right) e^{\Delta H^*/RT} e^{-\Delta S^*/RT} \quad \textbf{(35)}$$

Where, ΔS^*, h, N, and V are the activation entropy, Planck's constant, Avogadro number, and molar volume, respectively. The terms R and T have their usual significance. The logarithmic form of equation (21) gives:

$$\ln \eta = \left\{ ln\left(\frac{hN}{V}\right) - \frac{\Delta S^*}{R} \right\} + \frac{\Delta H^*}{RT} \quad \textbf{(36)}$$

The first term on the right hand side of Eq. (36) was considered to be constant so that a plot between $ln\ \eta$ and T^{-1} should have yielded ΔH^* from the slope. $ln\ \eta$ was found to vary with T^{-1} in a binomial way; hence one can derive ΔH^* from its differential with respect to temperature in the following way;

$$\ln \eta = a + bT + cT^2 \quad \textbf{(37)}$$

Thus, $$\frac{dln\eta}{dT} = -\frac{\Delta H^*}{RT^2} = b + 2cT \quad \textbf{(38)}$$

The fitting parameters a, b, and c have been found by computation, and the ΔH^* are then calculated at different temperatures using equation (38). $ln\ \eta$ has a nonlinear dependence on T^{-1}. Therefore, ΔH^* is not independent of temperature.

The change in heat capacity, ΔC_p, then follows from the relation,

$$\Delta C_p = \frac{d\Delta H^*}{dT} = -2RT(b + 3cT) \quad \textbf{(39)}$$

The ΔG^* values are obtained from the relation,

$$\Delta G^* = RTln\frac{\eta V}{hN} \quad \textbf{(40)}$$

and ΔS^* values are calculated using the Gibbs-Helmholtz equation,

$$\Delta S^* = \frac{\Delta H^* - \Delta G^*}{T} \quad \textbf{(41)}$$

12. Techniques for determination of microemulsion structure:

The characteristics of microemulsions have been established by different physical methods. Knowledge of the various methods available to thoroughly characterize a microemulsion system is essential. Both traditional methods (dilution method, conductance, viscosity, etc.) and emerging techniques such as dynamic light scattering (DLS), small angle X-ray scattering (SAXS), small angle neutron scattering (SANS), scanning electron microscopy (SEM), transmission electron microscopy (TEM), time resolved fluorescence quenching (TRFQ), NMR etc. are required for their characterization and property illumination. Among them DLS, SEM, TEM, cyclic voltammetry are most frequently used for the determination of internal structure of a microemulsion system.

12.2. Size of µE droplet as studied by dynamic light scattering technique:

DLS (also known as photon correlation spectroscopy or quasi-elastic light scattering) has gained potential importance in analyzing particle size and related physical characteristics of microemulsions [129 130 131]. When a coherent beam of light (as in lasers) interacts with colloidal particles in motion, the intensity correlation function provides information on the translational diffusion coefficient of the scattering particles and hence the hydrodynamic radious according to Stokes-Einstein equation.

$$D = \frac{kT}{3\pi\eta d} \quad \textbf{(42)}$$

where, k, T and η indicate the Boltzmann constant, temperature and viscosity respectively [132-134 135 136,137].

Dynamic light scattering provides insight into the dynamic properties of microemulsion by measuring single scattering events, meaning that each detected photon has been scattered by the sample exactly once. Usually, the measurements are taken at 90° in a dynamic light scattering spectrophotometer which uses a neon laser beam. The data processing is done in the built-in

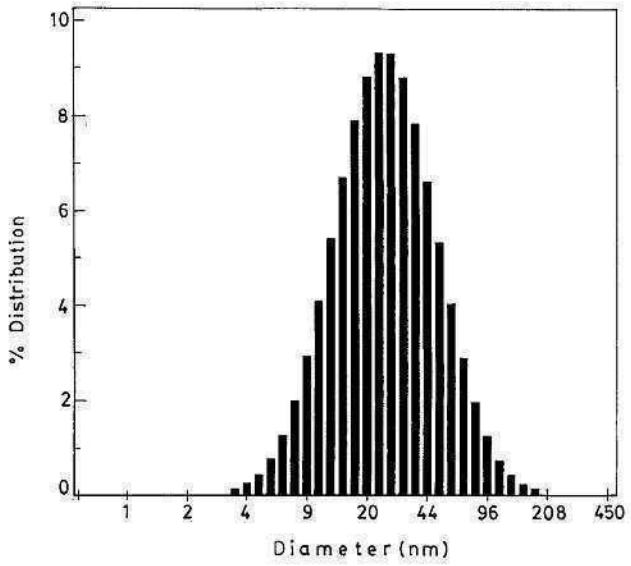

Figure 12. Droplet size distribution of H_2O/AOT/n-heptane system studied by dynamic light scattering technique (adapted from Ref. [101])

computer with the instrument. Acharya et. al. [38] have determined the diffusion coefficients and the polydispersity thorough DLS measurement of eucalyptol / polyoxyethylene(4)lauryl ether (Brij-30) / ethanol / water microemulsion system. Majhi et.al. [138] determined the particle size of the microwater droplets of microemulsion systems comprising AOT, water and different oils like heptane, octane, isooctane, decane, and eucalyptol. The structural study of water / sodium bis(2-ethylhexyl) phosphate / benzene microemulsion system by Feng et.al. [139] by DLS technique has revealed that at $\omega < 3$ rod shaped aggregates are formed whereas in water content dipolar crystallites dissolve successively and at $\omega > 3$, nonpolar reverse micelle overcome.

12.3. Spectroscopic investigation on microemulsion:

The local environment within a microemulsion droplet can be characterized with UV-Vis solvatochromic probes. As is well known, solubilization of a solute and chemical reactivity are dependent on the micro polarity of dispersed droplets in reverse microemulsions[140]. The

solvatochromic probes selected should be anchored to the polar core of the aggregates, to satisfy the procedural requirement of being soluble in the local environment media. Furthermore, this probe must be sensitive to the polarity of its environment and reflect the polarity through a shift of absorption maximum. Han and co-workers employed UV-Vis spectroscopy to monitor the extraction of trypsin solubilized in AOT/decane/water reverse micelles into compressed CO_2[141].Clarke et. al. investigated the the formation of water in supercritical carbon dioxide microemulsions stabilized by an ammonium carboxylate perfluoro polyether (PFPE) surfactant and found that the aqueous acidified $K_2Cr_2O_7$ is completely soluble in water-in-CO_2 microemulsion by UV-Vis spectroscopy[142].

The method of fluorimetry is based on the fluorescence spectra of a dye which varies substantially with its environment. The state of water in the waterpool of the w/o microemulsion has been elaborately investigated by a fluorescence probe technique by Hasegawa et.al. [143] for water/AOT/n-alkanes (C_6-C_{12}), using a viscosity sensitive fluorescence probe, auramine O and a xanthene dye. They found that upto ω 10, the microviscosity of the AOT anionic heads falls gradually till the upper limit of water tolerance. Sarkar et.al.[144] investigated the interaction of ionic liquid with water in 1-butyl-3-methylimidazolium hexafluorophosphate ([bmim][PF_6])/Triton X-100 (TX-100)/H_2Oternary microemulsions by the dynamics of solvent and rotational relaxation of coumarin 153 and coumarin 151 and found that for coumarin 153, the probe is located at the interfacial region of the microemulsions. Whereas, for, with an increase in the [bmim][PF_6] content the number of coumarin 151 molecules in the core of the microemulsions gradually increases.

12.4. Other Techniques:

12.4.1. Scanning electron microscope (SEM):

A scanning electron microscope (SEM) is a type of electron microscope that images a sample by scanning it with a high-energy beam of electrons (from 0.5 keV to 40 keV) in a raster scan pattern. The electrons interact with the atoms that make up the sample producing signals which contain information about the sample's surface topography, composition, and

other properties. In SEM, direct images of the microstructures of a microemulsion under varied conditions of dispersant composition and concentration can be taken. Due to the very narrow electron beam, SEM micrographs have a large depth of field yielding a characteristic three-dimensional appearance and very useful for understanding the surface structure of a sample. In modern instruments, the image (magnified by 10 to 500,000 times) is digitally captured and displayed on a computer monitor.

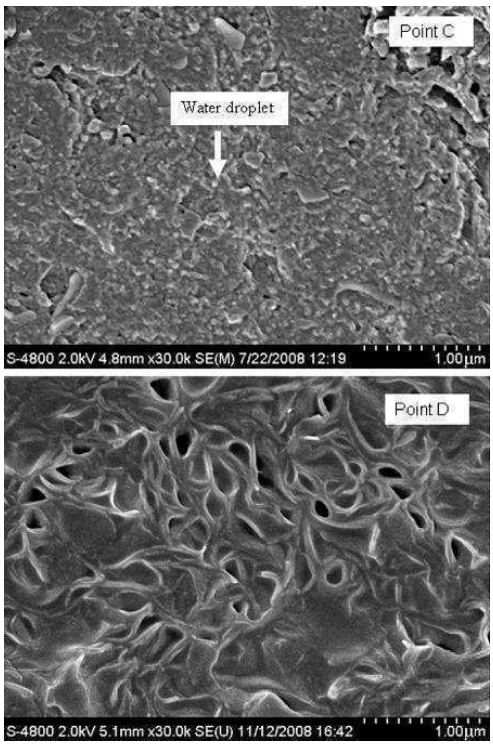

Figure 13. Cryo-SEM micrographs of microemulsion system CTAB/toluene–pentanol (1:1)/IL–water(1:1), two different points (C and D)[213]

12.4.2. Transmission electron microscopy(TEM):

Transmission electron microscopy (TEM) is a major analysis technique in both physical and biological sciences whereby a beam of electrons is transmitted through an ultrathin specimen, interacting with the specimen as it passes through it and the image formed by the interaction of the transmitted electrons of the specimen is magnified and detected by a sensor such as a CCD camera. TEMs are capable of imaging at a significantly higher resolution than light microscopes owing to the small de Broglie wavelength of electrons. TEM technique has been limitedly but potentially used in the understanding of the microstructure under varied conditions of dispersant composition and concentration [41 145-148].

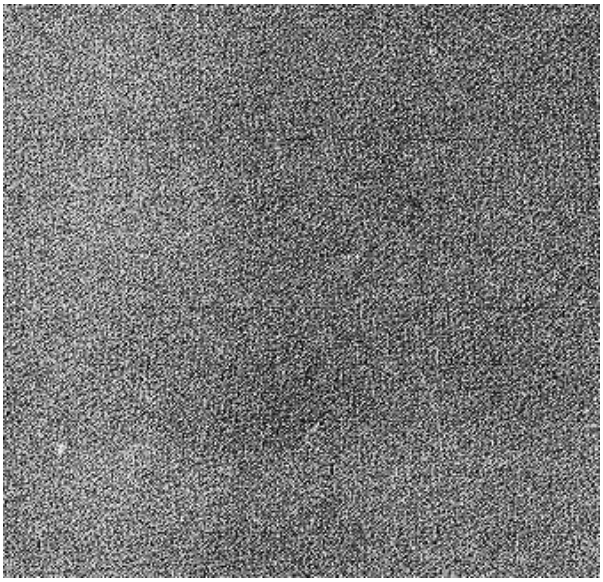

Figure 14. TEM of vitreous 20:1 diluted microemulsion on Triton-treated (at 139000X) grid showing higher droplet density and ordered structure[149].

12.4.3. NMR method:

The reverse micelles and microemulsions can be understood by the possibilities of determination of the self-diffusion coefficients of the constituting species; water, oil and amphiphile. The advantage of NMR method is that two- or three-phase characteristics can be monitored with single-phase domains on the micrometer scale. It also helps in finding out the degree of anisotropy and the presence of long-range discontinuities or continuities. Using high resolution ^{1}H, ^{2}H and ^{13}C NMR techniques, intermolecular interaction and structural rearrangement of non-ionic and anionic amphiphile-aided microemulsions have been investigated [150,151 ,152]. The technique can directly reveal the nature of mono- and polydispersity, as well as particle anisotropy [153]. According to Das et al. [154,155]NMR probing revealed glycerol-SDS-hexanol system to be structureless. A number of other NMR probed microemulsion structure elucidation have been carried out by other research groups [156-163].

12.4.4. Cyclic Voltammetry:

Mackay and co-workers have been first to suggest that electrochemical methods can be used to obtain information about the microstructure of microemulsions[164]. Electrochemical cyclic voltammetry has been successfully used to obtain information about the microstructure of micelles or

microemulsions [165-174].Changes in the microstructure were identified by using electrochemical probes such as ferrocene or its derivatives, ferricyanide, or methyl viologen. This detection was actually accomplished by determining diffusion coefficients of the probes which made it possible to investigate different microenvironments, in that the electrochemical reversibility of the probes was affected by the structure of the microemulsions and appeared to reflect the ease of mobility across interphases [166].Chokshi et. al.[175] and Shah et. al. [174] showed that the diffusion coefficients probed by electrochemical probes and cyclic voltammetric measurements could also be considered self-diffusion coefficients in microemulsion systems. Gao et.al. [176] investigated microemulsions consisting of the IL, 1-butyl-3-methylimidazolium hexafluorophosphate ([bmim][PF_6]), Tween 20 and water at various scan rates in order to verify the diffusion-controlled nature of the process.

13. Ionic liquid:

"The Structure and Properties of Ionic Melts" was the title of a Faraday Society Discussion held in Liverpool in 1961; it dispensed solely with molten inorganic salts [177]. An IL is a liquid that contains essentially only ions. Today, however, the term "ionic liquid" is commonly used for salts whose melting point is relatively low (below 100^0C). in particular, the salts that are liquid at room temperature are called room temperature ILs, or RTILs. There also exist mixtures of substances which have low melting points, called deep eutectic solvent, or DES, that have many similarities with ILs.

The earliest discovery of an IL can be dated to the middle of the nineteenth century, When some "red oil" was observed in a Friedel-Crafts reaction[178 179]. Ethanolammonium nitrate (m.p. 52–55 °C) was reported in 1888 by Gabriel and Weiner[180]. However one of the earlier known truly room temperature ILs was ethylammonium nitrate $[EtNH_3]^+$ $[NO_3]^-$ (m.p. 12 °C), synthesized in 1914 by Paul Walden. In the 1970s and 1980s ILs based on alkyl-substituted imidazolium and pyridinium cations, with halide or trihalogenoaluminate anions, were initially developed for use as electrolytes in battery applications. An important property of the imidazolium halogenoaluminate salts is that their physical properties such as viscosity,

melting point, and acidity could be adjusted by changing the alkyl substituents and the imidazolium/pyridinium and halide/halogenoaluminate ratios.

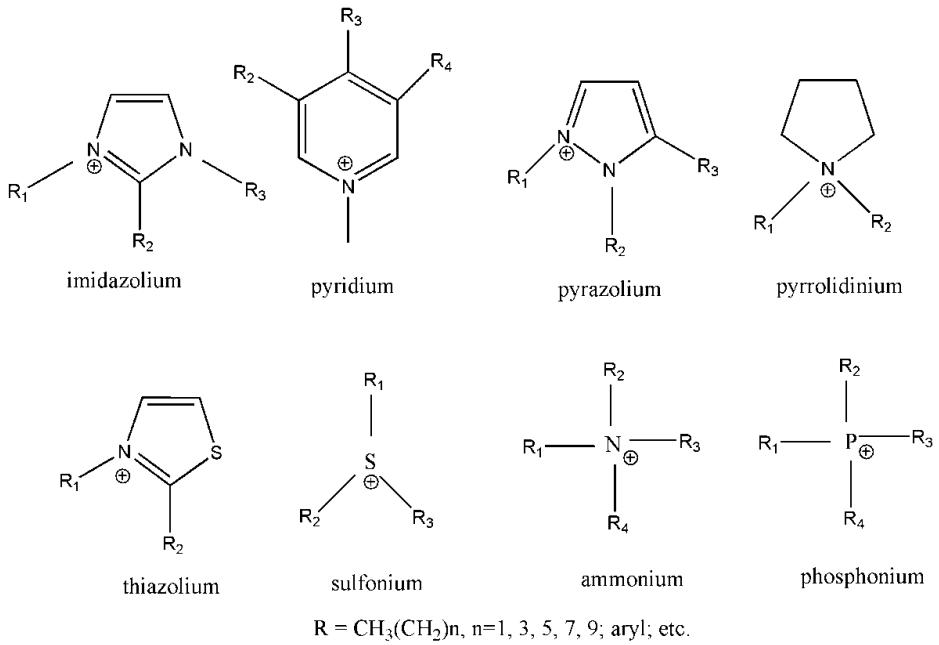

Figure 15A. Structures of some common types of ILs cations.

ILs are one of the most promising classes of new materials investigated in the last decade. They do not easily fit the conventional description of molecular fluids therefore promoting a necessary exploration of their physical properties at a microscopic level. Their negligible vapor pressure, high thermal stability, and properties tunability upon slight changes in the chemical architecture (including polarity, hydrophobicity, density, solvating activity etc.) have made these materials tailored for a constantly increasing range of applications[181-183]. Among these applications we find: catalysis[184,185], synthesis[186], pharmaceutics[187,188], electrochemistry[189,190] and green chemistry[191] in general.

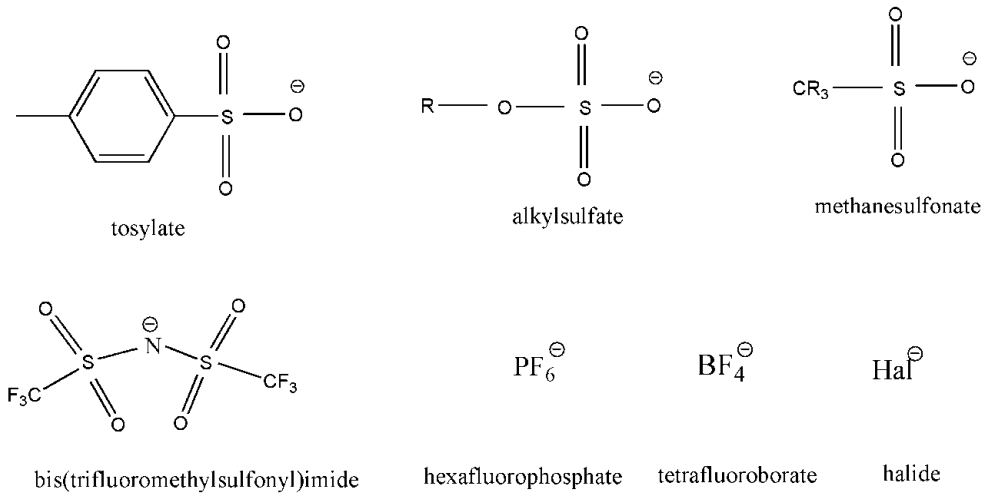

Figure 12B. Structures of some common types of ILs anions.

Two major drawbacks for some applications of ILs were moisture sensitivity and acidity / basicity. In 1992, Wilkes and Zawarotko [192] reported the preparation of ILs with alternative 'neutral', weakly coordinating anions such as hexafluorophosphate $[PF_6]$- and tetrafluoroborate $[BF_4]$-, allowing a much wider range of applications for ILs.

Most recently, people have been moving away from $[PF_6]^-$ and $[BF_4]^-$ since they are highly toxic [193], and towards new anions such as bistriflimide $[(CF_3SO_2)_2N]^-$ or even away from halogenated compounds completely like methanesulfonate $[MS]^-$. Moving towards less toxic cations have also been growing, with compounds like ammonium salts (such as choline) showing to be as flexible a support as imidazole.

14. Advantages of binary mixture comprising ionic liquid (ionic liquid + water):

The study of thermo physical properties is important in order to obtain sufficient information to predict properties and characteristics of ILs. The lack of physical property data and fundamental understanding of ILs prevent their further application to industry [194]. Water is the most abundant fluid on earth and is important in many biological and chemical systems. Water has unique physico-chemical properties based on strong hydrogen bonding [195]. Therefore, needless to mention that detailed investigation on IL-water binary mixtures have importance in terms of application and fundamental understanding. The presence of water may have a dramatic effect on properties of IL. Knowledge

of the physico-chemical and thermodynamic properties of binary mixtures formed by one or two components associated through hydrogen bonds is important and can give some information of the structural and energetic consequences of the interactions between ILs and water [196]. Even a small amount of water can dramatically influence the liquid properties of ILs without any reaction taking place. For example, the diffusion coefficient[197], viscosity,[198] polarity[199] and surface tension [200] of ILs varied considerably upon adding water. To facilitate the use of ILs in industrial processes, it is essential to assemble a frame of knowledge about these changes taking place in the physico-chemical properties of IL/water mixtures.

15. Ionic liquid microemulsion:

It is needless to mention that μE comprising ILs in the polar domain can have some unknown but some novel properties owing to the unique and combined features of the ILs and μEs. Research works involving IL microemulsion are ever increasing[202,210,214-216,348,356]. Different review works on IL μEs are available in the literature[191,213,347,349,357,358]. Ionic liquid microemulsions find application in various fields, viz., preparation and characterization of polymeric nanoparticles[236], synthesis of inorganic nanoparticles[237], renewable lubricants[238], and catalysis[239], etc. Han and co-workers[203] first reported the formation of μE comprising IL. Very recently Sarkar and co-workers [212] have reported a new strategy to prepare IL-in-oil μEs. IL based μEs in drug formulation has been explored by the research group of Moniruzzaman et al.[187] and Althanyan et al.[359] Estoe et al.[348], for the first time, have reported the characterization of IL μE using small angle neutron scattering (SANS) technique. Koetz and co-workers [213] have studied the structure of IL modified μE. Gao et al.[176,204,205] undertaken extensive works on μEs comprising of [bmim][PF_6] and water by different techniques. While Friberg et al.[349] have reported about the works on [bmim][BF_4] based μE, the structural studies of [bmim][BF_4]-in-oil μE have been reported by Gao et al.[176]. IL-in-oil μEs have also been extensively studied by Zheng and co-workers [360] using Triton X-100 and Tween 20. In the work of Gao et al.[91] comparative studies between the properties of microemulsions comprising TX-100 and Tween 20 have been reported. In another work of Zheng et al.[361]

extensive investigation were carried out on IL μE comprising Tween 80 as surfactant.

16. Microemulsion comprising IL+water:

A major drawback to use ILs is their inability to dissolve a number of chemicals including some hydrophilic substances, although the properties of ILs can be tuned [199,201]. To overcome this problem, the use of surfactants to create microemulsions containing water is an alternative method, as it is obvious that hydrophilic substances can be solubilized in the dispersed water phase. Furthermore, the microemulsion may possess some unexpected advantages in applications due to unique properties of ILs. Microemulsions with (IL+water) as polar cores or the microemulsions with nano-sized (IL+water) droplets dispersed in oil continuous phase by suitable surfactants may have some unknown properties and find various potential applications due to the unique features of ILs and microemulsions. Even so, these IL microemulsions have not been intensively investigated so far, especially their potential applications have rarely been reported. Cheng et.al.[202]demonstrated that 1-butyl-3-methylimidazolium tetrafluoroborate ([bmim][BF_4]) could form polar nanosized droplets dispersed in oil continuous phase. Gao et.al. [203] have prepared and characterized [bmim][BF_4]/TX-100/cyclohexane microemulsion with the ionic liquid as the polar core. Microemulsions consisting of water and a hydrophobic ionic liquid, 1-butyl-3-methylimidazolium hexafluorophosphate [bmim][PF_6], stabilized using Triton X-100 and Tween 20 have also been reported [204,205]. Atkin et. al. [206] studied the microstructure of the microemulsion comprising nonionic alkyl oligoethyleneoxide surfactants, alkanes, and a IL ethylammonium nitrate (EAN) through phase behavior and small angle X-ray scattering (SAXS). Gracia-Rio et.al.[207] investigated the IL based microemulsions of [bmim][BF_4]/Triton X-100/cyclohexane by absorption solvatochromic shifts, ^{1}H NMR in order to investigate the properties of the IL within the restricted geometry provided by microemulsions and the interactions of the ionic liquid with the interface. Zech et.al. [208] characterized high thermal stability of the microemulsions composed of 1-hexadecyl-3-methyl imidazolium chloride ([C_{16}mim][Cl]), an IL that exhibits surfactant properties, decanol as cosurfactant, dodecane as continuous

phase and the RTIL ethylammonium nitrate (EAN) as polar phase at ambient temperature. Very recently Klee et.al. [209] prepared magnetic microemulsion by the aid of a magnetic RTIL, [bmim][$FeCl_4$]. Such a magnetic microemulsion is a novel type of self-assembled system which due to its magnetic properties may open interesting paths for formulating functional and responsive systems. The increasing number of publications reflects the still growing interest in microemulsions containing room-temperature ILs [113,133-135,144,193,203,210-216].

AIMS AND SCOPES OF THE PRESENT STUDY

AIMS AND SCOPES OF THE PRESENT STUDY

Microemulsions are thermodynamically stable, macroscopically homogeneous but microscopically heterogeneous, mixtures of water and oil stabilized by surfactant monolayer. In spite of large number of studies, comprehensive knowledge on microemulsion are still considered to be fragmentary in nature. Ionic liquids are considered to have potentials as a substituent of the conventional polar component in μE. A combined individual potentials of ionic liquid and microemulsion have motivated to undertake different physico-chemical studies on ionic liquid microemulsion. Sometimes ionic liquids as single polar components suffer from some limitations which may be overcome through the usage of ionic liquid in combination with another polar solvent, e.g., water. With this purview, it was thought to be worthy to carry out the works as outlined below:

1. Formation, phase behaviour and physicochemistry of system comprising water/(Tween-20+n-alkanol)/n-heptane w/o μE were studied. The effect on the variation of cosurfactant chain length, [water] / [surfactant] mole ratio (ω), (indicative of the water pool size), and temperature were investigated in detail. Energetic and structural parameters were evaluated. The aim was to understand the effect of n-alkanol chain length on the formation stability and respective property of the derived w/o μE systems. Except a few cases studies on microemulsion using a series of n-alkanol are not available in the literature. Such an initiative was made as point of reference so that the data set could be compared with the similar systems comprising ionic liquid in lieu of water.

2. Although most of the studies on ILs are associated with the imidazolium ion, however, there has been a current trend to search for alternate, easily available but low cost ILs other than the imidazolium ion. Pyridinium based ILs have specific properties, viz., broad liquidous temperature range, inertness to air, moisture and superior solubilization capacity. In spite of high possible potentials, there have been a little research on 1-butyl-4-methylpyridinium tetrafluoroborate ($[b_4mpy][BF_4]$) comprising μE although it is one of the most reported pyridinium based IL. Another advantage of using this IL is that the system itself can be investigated without

any molecular probe (because of the presence of the pyridinium ring) in the UV-visible region.

Curcumin is a natural polyphenolic compound isolated from the rhizome of turmeric (Curcuma longa). Researches over the last few decades have shown that curcumin possesses a great variety of beneficial biological and pharmacological activities. Despite its highly promising features as a health-promoting agent, poor aqueous solubility in neutral aqueous medium of curcumin one of the major draw backs in its bioavailability, clinical efficiency and metabolism. A number of attempts have been made to increase the solubility in polar medium and hence the bioavailability of curcumin through encapsulation in different organized assemblies. Once used in the IL-in-oil microemulsion, curcumin may have a possibility to reside in the inner polar core of the μE because curcumin is not soluble in n-heptane. Thus the spectroscopic investigation involving curcumin in the microemulsion will be able to probe the microenvironment of the polar domain

3. Usually IL-in-oil μEs are more rigid and less temperature sensitive; such limitations can be overcome provided the pure IL is replaced with a binary mixture of IL and water. The aim of this study was to replace the water pool with ionic liquid of the aforementioned μE. However use of pure ionic liquid as polar domain in IL/O μE may have limitations such as rigidity, viscosity, salvation, etc. To overcome these problems, it is thought to be worthy to use a binary mixture of ionic liquid and water in place of pure ionic liquid. The investigation aims to derive the density, excess molar density and viscosity in understanding the synergistic and antagonistic behavior of all the combinations. Surface tension studies on aqueous solution of [bmim][MS] in the water rich region could evaluate the surface activity, surface excess and molecular area of the IL. Conductance measurements for all the combinations and cyclic voltammetry measurements in the IL rich region helped in understanding the states of aggregates in solution. Absorption and emission spectroscopic studies of an anionic xanthene dye eosin Y have been performed in the water rich region. Fluorescence lifetime and anisotropy measurements could shed light on the viscosity of the media. Efforts have also been made to correlate the life time and fluorescence anisotropy with the experimentally determined viscosity. Also we intended to correlate the data of the binary

mixture in the water rich region with the aggregation behavior of IL as there are several reports with conclude that [bmim] based ionic liquids can form micelle like aggregates in water after attainment of certain concentration. The choice of this anion is intentional as the anion is an alkyl group containing simple inorganic ion. Our main aim is to use the binary mixture of [bmim][MS] and water in microemulsion of oil continuum. However due to relatively higher melting point, this ionic liquid, in its pure form, was thought to be not useful for practical purpose. Moreover, imidazolium based ionic liquid containing [MS] anion would be less toxic compared to the fluorine based ILs. It is reported there that this particular ionic liquid could deactivate water above a certain concentration even if water is present in high amount (upto50 mole%). We also intended to check the validity of the generalization which subsequently have motivated us to undertake the physicochemical investigations on the binary mixture of [bmim][MS] and water. Such study is believed to help in understanding the interaction between [bmim][MS] and water at the molecular level as well as the orientation of the IL at the air solution interface which, in turn, will put new physical insight into the area of IL comprising binary mixtures.

4. Water is the "greenest" among all solvents. In our previous report, we showed that [bmim][MS] in combination with water exhibited some unusual behavior. The binary mixtures were studied using a number of techniques in the bulk condition. Different properties of the binary mixture could be tuned/altered by judicious mixing of the components. Previously, we have carried out systematic physicochemical investigations on water / (Tween 20 + n-pentanol) / n-heptane water-in-oil μE. It is, therefore, important to undertake the challenge in investigating the polar domain in oil microemulsion comprising the binary mixture of ionic liquid, [bmim][MS], in combination with water. Such studies are important in terms of their application as well as fundamental understanding point of view. However to the best our knowledge, no systematic studies have yet been carried out using a binary mixture of IL and water, which would be the novelty of the present work.

CHAPTER 1

CHAPTER 1

Physico-Chemical Studies on Microemulsion: Effect of Cosurfactant Chain Length on the Phase Behavior, Formation Dynamics, Structural Parameters and Viscosity of Water/(Tween 20+n-Alkanol)/n-Heptane Water-in-Oil Microemulsion

Abstract

The pseudo-ternary water-in-oil microemulsion system, comprising of water/(polyoxyethylene sorbitan monolaurate [Tween 20]+n-alkanol)/n-heptane, have been studied by phase manifestation, method of dilution, viscosity and dynamic light scattering measurements. Tween 20, in combination with equal mass of cosurfactants (of varying chain length, from n-butanol to n-octanol) were used in studying the systems in the temperature range 303 – 323 K. Appearance of turbidity was noted visually, which indicated the attainment of immiscibility or phase separation; a clear dependency of the different phases on cosurfactant chain length was noted. By employing the method of dilution, associated thermodynamic parameters for the formation of water-in-oil microemulsion droplets were derived. Different associated structural parameters were derived through further computation of the data derived from the method of dilution. Unusual behavior of Tween 20, compared to the conventional ionic surfactants, was noted. Viscosity measurements, as carried out at different composition and temperature, revealed the temperature and water pool size dependency of the microemulsion systems. Viscosity data did not follow the same trend during heating and the cooling process, due to condensation effect. This phenomenon was further confirmed by dynamic light scattering measurements.

J. Surfact. Deterg. **2011,** 14, 473-486

1. Introduction

Microemulsions (μEs) are thermodynamically stable isotropic dispersions of water-in-oil (w/o) or vice versa (o/w), stabilized by a surfactant monolayer[34,217]. The surfactant monolayer not only prohibits the direct contact between water and oil, but also reduces the interfacial tension between the two immiscible liquids. Beside water-in-oil or oil-in-water microemulsion, another type, like bi-continuous one is also possible. Type of microemulsion basically depends on the relative abundance of the two immiscible liquids[218]. Further details on the type and structure of microemulsion could be found in literature[30,219] and review[34]. Judicious mixing water, amphiphile and oil could spontaneously form a stable microemulsion. Thermodynamic stability, solubilizing capacity, optical transparency and isotropicity, etc., are some specific properties for which microemulsions find manifold applications in separation technology, food processing, cosmetics, drug encapsulations and nanoparticle synthesis, etc.[218] Besides, such compartmentalized entities could mimic biological systems too. Such applications of microemulsions have encouraged researchers around the globe in investigating different types of microemulsions. As there is no end in good science, research outcome in the field of microemulsions are considered to be fragmentary in nature.

A water-in-oil microemulsion is topologically similar to a reverse micelle[220]. When small amount of water is added to surfactant solution in oil, droplets of water get delineated from the non-polar phase. The delineation becomes possible due to the formation of a well-defined boundary by surfactant monolayer [221]. In most of the cases when single tailed surfactants are used as emulsifying agent, a fourth component becomes essential to maintain the curvature of the microemulsion droplets. Although small chain alkyl halides and amines could be used as the fourth component (known as cosurfactant) the most widely used cosurfactants are short chain n-alkanols[34]. Extensive research works have been done extensive works in studying the effect of n-alkanols as an additional stabilizer; still variations in different physico-chemical parameter such as the role of cosurfactant chain length are not so common in literature. Most commonly used cosurfactants include n-butanol, n-pentenol and n-hexanol for their better stabilizing efficiency in

microemulsion formation. However the exact reason on the better efficacy of these alkanols over the higher analogues are still not exactly known. Except a few cases studies on microemulsion using a series of n-alkanol are not available in the literature to the best of our knowledge[97,108,222-224]. This has motivated us in endeavoring the investigation on the water-in-oil microemulsion comprising of water/(Tween 20+n-alkanol)/n-heptane where the cosurfactant (n-alkanol) chain lengths were varied from n-butanol to n-octanol.

In this paper we have explored the effect of cosurfactant chain length on different physico-chemical parameters of w/o microemulsion as mentioned above. Cosurfactant chain length was varied from n-butanol to n-octanol. Also investigation on the physico-chemical properties of microemulsions have been carried out at different temperatures and different [water] / [Tween 20] mole ratio, ω. Above mentioned systems have been investigated by way of phase manifestation, method of dilution, viscosity and dynamic light scattering measurement. Such studies are believed to provide information on microemulsion in form of their formulation, energetics, and structural parameters.

2. Experimental

2.1. Materials

The non-ionic surfactant Tween 20 was purchased from Fluka, Switzerland. The cosurfactants n-butanol, n-pentanol, n-hexanol, n-heptanol and n-octanol were products from Lancster, England. All the materials were stated to be more than 99.5% pure and were used as received. HPLC grade n-heptane was obtained from E. Merck, Germany. Double distilled water was used throughout the experiment.

2.2. Methods

2.2.1. Construction of the phase diagram.

The pseudo ternary phase diagram comprising of water/(Tween 20+n-alkanol)/n-heptane was constructed by the method of titration and through visual inspection [211]. To investigate different regions (mainly two phase turbid,

2Φ and homogeneous single phase, 1Φ), known amount of Tween 20, mixed with n-alkanol in 1:1 ratio (w/w) were taken in different stoppered test tubes. Varying amount of oil (or water) was then added. Water (or oil) was progressively added by using Hamilton (USA) microsyringe under constant stirring condition where the temperature was controlled using a cryogenic circulatory water bath (of precession ±0.1K) at 303K. Appearance of the state of turbidity was noted visually, which indicated the onset of phase separation or immiscibility. The solutions were allowed to attain equilibrium for 30 minutes (we found that equilibrium was attained within thistime period in most of the systems).The process was followed for all the cosurfactants (n-butanol to n-octanol) [225].

2.2.2. Method of dilution

Thermodynamics of formation of water-in-oil (w/o) microemulsion (μE) comprising water/(Tween 20+n-alkanol)/n-heptane were evaluated by the method of dilution. In this method, besides using a series of alkanols, experiments were carried out at different [water] / [Tween 20] mole ratio, ω (5, 10, 15 and 20) and at five different temperatures (303, 308, 313, 318 and 323K). Temperature was controlled by a cryogenic circulatory water bath with an accuracy of ±0.1K. The method of dilution also helped in evaluating different structural parameters of the microemulsion under various conditions. Briefly, in the method of dilution, a fixed amount of water, surfactant and oil were taken in a stoppered test tube. The turbid solution was then titrated with cosurfactant under constant stirring unless a clear solution appeared. Sufficient time was allowed in attaining the equilibrium. At this point of clarity, composition of the mixture was then noted. A known quantity of n-heptane was then further added whereby the microemulsion got destabilized[12]. Clarity of the microemulsion was regained by further addition of n-alkanol under constant stirring; the amount of cosurfactant required was again noted. This method of destabilization and re-stabilization was repeated to obtain several points. Experiments were then done under different conditions, viz., [water]/[Tween 20] mole ratio, ω, temperature and cosurfactant chain length in order to evaluate thermodynamic and structural parameters. Each set of

experiment was carried out at least four times and the average of the values were used in obtaining the final result [226].

2.2.3. Viscosity measurements

Viscosity measurements were performed on monophasic microemulsions of known composition where 0.2 moldm^{-3} Tween 20 in n-heptane, mixed with 1:1 (w/w) alkanols were used. Choice of such composition was intended for comparative studies. Solutions of different ω were then used for viscosity measurements using a LVDV-II+PCP cone and plate type roto viscometer (Brookfield Eng. Lab, USA). A CPE-42 type spindle made by Brookfield Eng. Lab, USA was used. Viscosity of microemulsion at different temperature was measured where the temperature was controlled by circulatory water bath (±0.1K). Microemulsion comprising n-octanol as cosurfactant, at ω=20 could not be studied at 0.2 moldm^{-3} Tween 20 as the solution appeared turbid. During the measurement shear rates (D) were varied within the range 20 – 60 S^{-1} and corresponding shear stress (τ) were recorded. Finally viscosity of a solution was obtained using the zero shear rates according to the relation $\eta = \tau / D$ [114,127,128].

2.2.4. Dynamic light scattering (DLS) studies

Solutions, as prepared in the viscosity measurements, were used in measuring the dimension of the microemulsion droplets by dynamic light scattering method under different set of conditions (viz., cosurfactant chain length, ω and temperature). Diameter of the microemulsion droplets were determined using a Zetasizer Nano ZS90 (ZEN3690, Malvern Instruments Ltd, U.K.). A He-Ne laser of 632.8 nm wavelength was used and the measurements were made at a scattering angle of 90^0. Temperature was controlled by inbuilt Peltier heating-cooling device (±0.05K). Refractive index of each solution was recorded with an ABBE type refractometer, as it was required as an input in determining the size of the μE droplet by DLS technique. Viscosity data, as obtained from viscosity measurements, were also used in processing DLS data. Samples were filtered thrice using Milipore™ hydrophobic membrane filter of 0.25μ pore size. In actual DLS measurements,

the diffusion coefficient (D) of a solution is measured which is related to the diameter of a droplet (d) according to Stokes–Einstein equation [133-137]:

$$D = \frac{kT}{3\pi\eta d} \qquad \textbf{(1.1)}$$

where k, T and η indicate the Boltzman constant, temperature and viscosity respectively.

3. Results and discussion

3.1. Phase manifestation

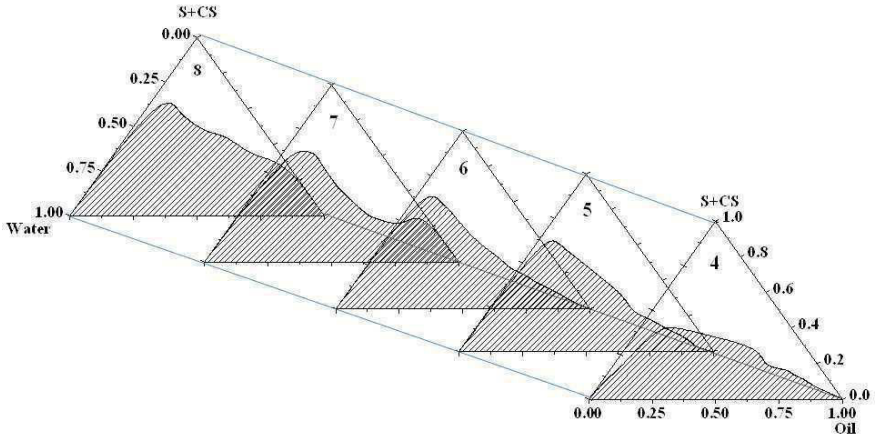

Figure 1.1. Pseudo-ternary phase diagram of water/(Tween 20 +n-alkanol)/n-heptane system at 303K. Tween 20 and n-alkanol were taken in 1:1 w/w ratio. n-alkanol chain lengths are mentioned inside each plot. Scale magnitudes were reduced by 1/100 in the plot.

Figure 1.1 describes the pseudo ternary phase diagram of water/(Tween 20+n-alkanol)/n-heptane systems. Solid line indicates the boundary region between the clear, single phase (1Φ) microemulsion region (un-shaded portions in the Figure) and two phase (2Φ) turbid region (shaded portions). From the Figure 1.1 it is also noticeable that the area under the clear region was dependent on the cosurfactant chain length. Results have further been clarified through Figure 1.2. With the increase in cosurfactant chain length, area under the monophasic region decreased with a small halt at n-hexanol. Area under the monophasic region was ~55 % (n-butanol) which decreased progressively upto ~25 % in case of n-octanol. n-pentanol and n-hexanol tendered more or less similar effects. It could be concluded, therefore, that increase in cosurfactant chain length (decrease in polarity) makes the

homogeneous system unstable, i.e., clear microemulsion formation becomes less favorable with the increasing cosurfactant (n-alkanol) chain length. Although different regions (viz., gel, viscous and clear fluid) were recorded in the monophasic region, for a simple and better understanding on the effect of n-alkanol chain length results have been described in terms of only two phases (1Φ and 2Φ).

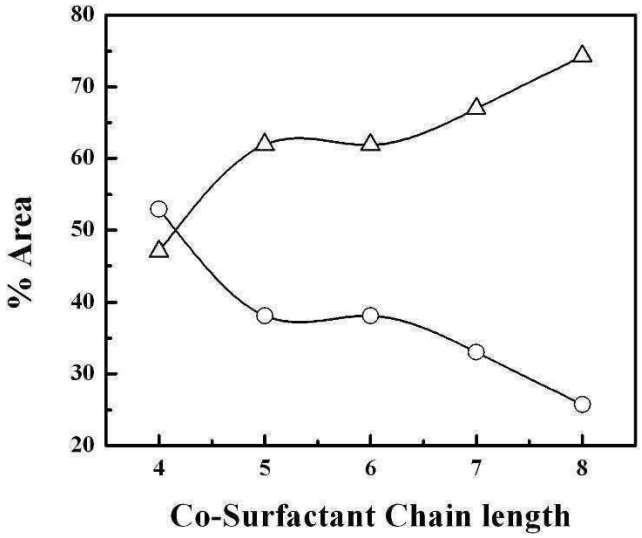

Figure 1.2. *Interdependence of the % area under clear (O) and turbid (Δ) region* with the cosurfactant chain length for water/(Tween 20 +n-alkanol)/n-heptane pseudo-ternary system at 303 K.

Construction of the phase diagram is the first and foremost job to be executed by a researcher, although the process is tedious in nature [34]. It is known that the phase behavior of pseudo-ternary system depends on various factors, viz., nature of the polar medium (herein water), surfactant and cosurfactant used, presence of additive, nature of the nonpolar medium (oil, herein n-heptane) and temperature, pressure, etc. [34,92] According to Ninham et al. the compactness/ease of microemulsion formation depends on the packing symmetry between the surfactant chain length and the combined chain length of oil and used cosurfactant [227]. Tween 20 has a hydrocarbon tail comprising of 12 carbon atoms. It is, therefore, not unexpected that n-pentanol and n-hexanol would have a matching symmetry when combined with n-heptane. Appearance of larger monophasic region in case of n-butanol could be explained by its higher miscibility with water[223]. Higher n-alkanols ($>C_6$) behaved more like oil than cosurfactant.

3.2. Dilution method

3.2.1. Evaluation of thermodynamic parameters

For a stable μE, the alkanol is distributed in water, interface and oil; the surfactant essentially remains at the interface. The total number of moles of n-alkanol (n_a^i) would thus follow the relation:

$$n_a^t = n_a^w + n_a^i + n_a^o \quad \textbf{(1.2)}$$

where the superscripts w, i and o stand for water, interface and oil respectively.

At a constant temperature and fixed ω, the ratio of number of moles of alkanol to the number of moles of alkanol in oil (n_a^o) will be constant (with respect to the total number of it in the oil, n_o). Consequently, the mole fraction ratio of alkanol at the interface (X_a^i) and in oil (X_a^o) should also be constant. Thus,

$$n_a^o/n_o = k \quad \textbf{(1.3)}$$

and $$\frac{X_a^i}{X_a^o} = k_d \quad \textbf{(1.4)}$$

where, k and k_d are constant and the distribution constant respectively.

By replacing equation (1.3) in equation (1.2) one sets the following relation:

$$\frac{n_a^t}{n_s} = \frac{n_a^w + n_a^i}{n_s} + k\frac{n_o}{n_s} \quad \textbf{(1.5)}$$

n_s represents the number of moles of surfactant.

In the dilution experiment, at a fixed n_s, n_a^t and n_o are varied to have a series of $\frac{n_a^t}{n_s}$ and $\frac{n_o}{n_s}$ which according to equation (1.5) can give $\frac{n_a^w + n_a^i}{n_s}$ and k

from the linear plot between $\frac{n_a^t}{n_s}$ and $\frac{n_o}{n_s}$ as intercept (I) and slope (S) respectively. For n-butanol, which is a lower alkanol, n_a^w can be obtained from its water solubility, and by this value $\frac{n_a^i}{n_s}$ can be evaluated. Higher n-alkanols are practically insoluble in water; thus $\frac{n_a^i}{n_s}$ could directly be obtained from the intercept. The plot of $\frac{n_a^t}{n_s}$ vs $\frac{n_o}{n_s}$ for n-hexanol at ω=10 have been presented in Figure 1.3. The distribution constant k_d is related to the slope and intercept of equation (1.5) as:

$$k_d = \frac{X_a^i}{X_a^o} = \frac{n_a^i/(n_a^i + n_s)}{n_a^o/(n_a^o + n_o)} = \frac{n_a^i(1+\frac{n_a^o}{n_o})}{n_a^o(n_a^i + n_s)} \qquad \textbf{(1.6)}$$

Alternately,

$$k_d = \frac{\alpha(1+S)}{S[1+(I-\frac{n_a^w}{n_s})]} = \frac{\alpha(1+S)}{S(1+\alpha)} \qquad \textbf{(1.7)}$$

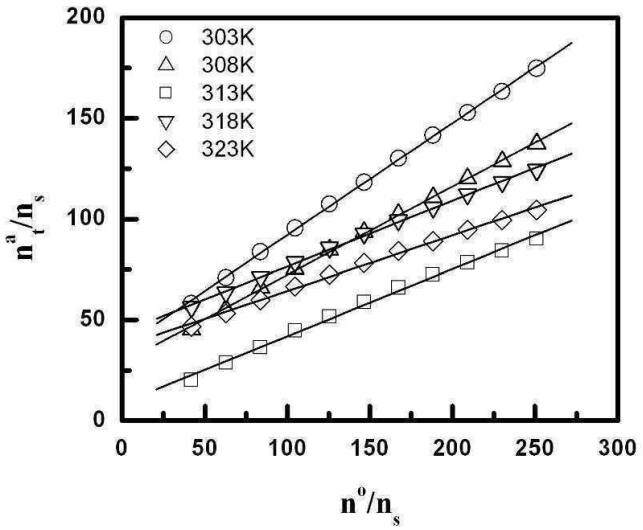

Figure 1.3. Plot of n_a^t/n_s vs n_o/n_s for water/(Tween 20 +n-hexanol)/heptane water-in-oil microemulsion system. A 1:1 (w/w) mixture of Tween 20 and n-hexanol was used at [water]/[Tween 20] mole ratio, ω=10. Temperatures are mentioned inside the Figure.

where, $$\alpha = (I - \frac{n_a^{\,w}}{n_s}) = \frac{n_a^{\,i}}{n_s} \qquad (1.8)$$

Therefore, by knowing I, S and α, one can obtain the value of k_d. For alkanols larger than n-butanol α =I, and equation (1.7) could be approximated as;

$$k_d = \frac{I(1+S)}{S(1+I)} \qquad (1.9)$$

Thus by using equations 1.5, 1.7 and 1.9 one can evaluate the values of $n_a^{\,i}$, $n_a^{\,o}$ and k_d which are useful information for the formation of w/o microemulsion. Evaluation of k_d value is required in obtaining the information on the thermodynamics of the involved process.

Changes in the standard Gibbs free energy of transfer (ΔG_t^o) of alkanol from oil to the interface could be expressed as:

$$\Delta G_t^o = - RT \ln k_d \qquad (1.10)$$

Changes in the standard enthalpy of transfer ΔH_t^o was evaluated by the van't Hoff equation:

$$[\frac{\partial(\Delta G_t^{\,o})}{\partial(1/T)}]_p = \Delta H_t^{\,o} \qquad (1.11)$$

In the present study, ΔG_t^o vs. T profile was found to follow a 2^0 polynomial equation as:

$$\Delta G_t^o = a + bT + cT^2 \qquad (1.12)$$

where a, b and c are the polynomial coefficients.

The polynomial coefficients thus helped in determining the ΔH_t^o values described in the following expression:

$$[\frac{d(\Delta G_t^{\,o}/T)}{d(1/T)}]_p = a - cT^2 = \Delta H_t^{\,o} \qquad (1.13)$$

The standard entropy of transfer (ΔS_t^o) of the associated process was then evaluated according to the following expression:

$$\Delta S_t^o = (\Delta H_t^o - \Delta G_t^o)/ T \qquad (1.14)$$

Figure 4 describes the variation of ΔG_t^o with [water]/[Tween 20] mole ratio (ω) at different temperature for water/(Tween 20+n-hexanol)/n-heptane as representative.

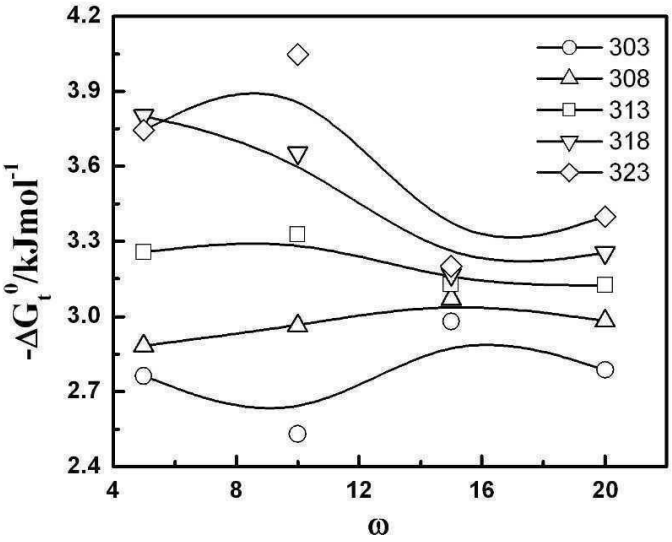

Figure 1.4. *ΔG_t^0 vs. ω plot* for water/(Tween 20 +n-hexanol, 1:1,w/w)/n-heptane water-in-*oil microemulsion at ω=10. Temperatures (in K) are mentioned inside the* Figure.

Results are also summarized in Tables 1.1 to 1.5.

Table 1.1. Thermodynamic parameters for the transfer of n-hexanol from oil to oil-water interface in the formation of water/(Tween 20+n-hexanol)/n-heptane water-in-oil microemulsion at different temperature and [water]/[Tween 20*] mole ratio, ω.*

Parameter		Temp. / K				
	ω	303	308	313	318	323
k_d	5	2.99	3.08	3.40	4.21	4.03
	10	2.73	3.18	3.59	3.98	4.51
	15	3.26	2.97	3.32	3.13	3.29
	20	3.09	2.82	2.47	2.65	3.54
$(-)\Delta G^0_t$/kJmol^{-1}	5	2.76	2.88	3.25	3.80	3.74
	10	2.53	2.96	3.32	3.65	4.04
	15	2.98	3.07	3.13	3.16	3.20
	20	2.80	2.98	3.12	3.25	3.39
ΔH^0_t /kJmol^{-1}	5	17.99	16.40	14.71	13.03	11.32
	10	22.00	21.00	19.98	18.94	17.90
	15	2.48	1.36	0.23	-0.92	-2.09
	20	8.15	7.20	6.23	5.24	4.25
ΔS^0_t/JK^{-1}mol^{-1}	5	68.51	62.51	57.41	52.93	46.64
	10	81.00	77.81	74.50	71.10	67.94
	15	18.04	14.40	10.73	7.06	3.42
	20	36.12	33.07	29.90	26.73	23.67

Table 1.2. Thermodynamic parameters for the transfer of n-alkanol from oil to oil-water interface in the formation of water/(Tween 20+n-alkanol)/n-heptane water-in-oil microemulsion at 313K and at different and [water]/[Tween 20] *mole ratio, ω.*

n-alkanol	Parameter				
	ω	k_d	$(-)\Delta G^0_t$ /kJmol^{-1}	ΔH^0_t /kJmol^{-1}	ΔS^0_t/JK^{-1}mol^{-1}
BuOH	5	3.01	2.86	27.42	96.75
	10	2.84	2.71	12.26	47.87
	15	2.38	2.08	11.56	0.043
	20	1.94	1.72	11.34	41.76
PentOH	5	3.41	3.19	13.41	53.05
	10	2.94	2.81	8.83	37.22
	15	2.60	2.50	-0.86	5.18
	20	2.47	2.35	4.30	21.29
HexOH	5	3.49	3.25	14.71	57.41
	10	3.59	3.32	19.99	74.50
	15	3.32	3.13	0.23	10.73
	20	2.47	3.12	6.23	29.90
HeptOH	5	3.52	3.43	7.67	35.47
	10	3.57	3.31	12.10	49.24
	15	3.30	3.39	6.18	30.59
	20	3.00	3.11	4.50	24.24
OctOH	5	4.34	3.82	11.76	49.78
	10	4.09	3.62	8.64	39.21
	15	3.48	3.24	2.27	17.62
	20	2.69	3.05	15.04	57.82

Table: 1.3. Free energy change ($-\Delta G^0_t$) for the transfer of n-alkanol from oil to oil-water interface in the formation of water/(Tween 20+n-alkanol)/n-heptane water-in-oil microemulsion at different temperatures and [water]/[Tween 20*] mole ratio, ω.*

System	$-\Delta G^0_t$ values at different temperatures					
	ω	**303**	**308**	**313**	**318**	**323**
BuOH	5	1.21	2.30	2.86	3.00	3.09
	10	2.23	2.31	2.71	2.84	3.16
	15	1.55	1.62	2.25	2.17	2.35
	20	1.49	1.65	1.72	2.30	2.22
PentOH	5	2.65	2.83	3.19	3.41	3.69
	10	2.54	2.79	2.81	3.17	3.29
	15	2.86	3.10	2.48	3.08	2.99
	20	2.16	2.25	2.35	2.50	2.56
HexOH	5	2.76	2.88	3.25	3.80	3.74
	10	2.53	2.96	3.32	3.65	4.04
	15	2.98	3.07	3.13	3.16	3.20
	20	2.78	2.98	3.12	3.25	3.39
HeptOH	5	3.09	3.26	3.43	3.60	3.80
	10	2.67	2.94	3.31	3.42	3.63
	15	3.01	3.21	3.39	3.53	3.61
	20	2.79	2.96	3.11	3.21	3.28
OctOH	5	3.04	3.68	3.82	3.75	4.28
	10	2.74	3.20	3.62	3.81	3.44
	15	2.89	3.11	3.24	3.27	3.29
	20	2.08	2.73	3.05	3.21	3.28

Table: 1.4. Enthalpy change ($-\Delta H^0_t$) for the transfer of n-alkanol from oil to oil-water interface in the formation of water/(Tween 20+n-alkanol)/n-heptane water-in-oil microemulsion at different temperatures and [water]/[Tween 20*] mole ratio, ω.*

System	ΔH^0_t values at different temperatures				
	ω	**303**	**308**	**313**	**318**	**323**
BuOH	5	67.48	46.36	24.91	3.11	-19.03
	10	8.85	10.56	12.30	14.06	15.85
	15	20.53	16.07	11.53	6.93	2.25
	20	11.23	11.29	11.34	11.40	11.45
PentOH	5	12.60	13.00	13.41	13.82	14.25
	10	7.40	8.12	8.83	9.56	10.30
	15	-10.28	-5.61	-0.86	3.96	8.86
	20	4.57	4.44	4.30	4.16	4.02
HexOH	5	17.99	16.36	14.71	13.03	11.32
	10	22.01	21.00	19.99	18.94	17.90
	15	2.48	1.37	0.23	-0.92	-2.09
	20	8.15	7.20	6.23	5.24	4.24
HeptOH	5	6.61	7.13	7.67	8.20	8.75
	10	18.99	15.58	12.10	8.56	4.98
	15	10.95	8.60	6.18	3.74	1.25
	20	8.79	6.65	4.48	2.26	0.02
OctOH	5	19.45	15.64	11.76	7.81	3.81
	10	42.03	25.48	8.64	-8.45	-25.82
	15	11.26	6.80	2.27	-2.33	-7.01
	20	38.50	26.86	15.04	3.01	-9.20

Table: 1.5. Entropy change ($-\Delta S^0_t$) for the transfer of n-alkanol from oil to oil-water interface in the formation of water/(Tween 20+n-alkanol)/n-heptane water-in-oil microemulsion at different temperatures and [Water]/[Tween 20*] mole ratio, ω.*

System	ΔS^0_t values at different temperatures					
	ω	**303**	**308**	**313**	**318**	**323**
BuOH	5	226.72	158.02	88.75	19.22	-49.33
	10	36.59	41.80	47.96	53.2	58.87
	15	72.90	57.40	44.06	28.64	14.24
	20	42.00	42.02	41.76	43.09	42.34
PentOH	5	50.33	51.41	53.05	54.22	55.54
	10	32.85	35.42	37.22	40.06	42.11
	15	-24.52	-8.14	5.18	22.15	36.71
	20	22.24	21.73	21.29	20.98	20.40
HexOH	5	68.51	62.51	57.41	52.93	46.64
	10	81.00	77.81	74.50	71.10	67.94
	15	18.04	14.40	10.73	7.06	3.42
	20	36.12	33.07	29.90	26.73	23.67
HeptOH	5	32.04	33.76	35.47	37.13	38.88
	10	71.49	60.15	49.24	37.70	26.67
	15	46.10	38.31	30.59	22.9	15.08
	20	38.25	31.23	24.24	17.24	10.23
OctOH	5	74.27	62.74	49.78	36.4	25.04
	10	147.8	93.13	39.21	-14.58	-69.29

System	ΔS^0_t values at different temperatures				
	ω	**303**	**308**	**313**	**318**	**323**
	15	46.72	32.20	17.62	2.96	-11.52
	20	133.95	96.12	57.82	19.59	-18.31

ΔG_t^o values were found to be negative in all the cases, which indicate the spontaneity of microemulsion formation. Tween 20, along with n-alkanol, can tune the curvature of the water droplets, delineated from the contact of oil. It is clear from the results that with the rise in temperature for a particular alkanol, the negative value of ΔG_t^o increased. Higher negativity of ΔG_t^o represents enhanced spontaneity of the microemulsion formation process. Increase in temperature would lead to the overall increase in the kinetic energy of the system, which subsequently eases the easier formation of droplet. Increase in temperature might lead to the opening up of the coiled surfactant head group, for which better efficacy of the system could have been achieved by Tween 20 at higher temperature [226].

A decrease in the negative value of ΔG_t^o with increasing [water]/[Tween 20] mole ratio ω was observed in general. Increase in the volume of the water droplet with increasing ω value requires larger coverage or delineation of water from the hydrophobic environment. At a fixed surfactant/cosurfactant composition, thus spontaneity of the microemulsion formation would be limited with the progressive increase in ω values.

While considering the effect of cosurfactant chain length, the spontaneity of the process is increased with the increase in cosurfactant chain length. However, no significant difference was noticed between n-heptanol and n-octanol. Increase in cosurfactant chain length leads to better accommodation of n-alkanol at the oil-water interface. However, the alkanols larger than n-heptanol behaved more like oil than cosurfactant. Overall values of ΔG_t^o were found to be within the range of -1 to -5 $kJ\,mol^{-1}$. The lower ΔG_t^o are indicative of weak interactions between the alkanol and Tween 20 at the interface [223].

While considering the ΔH_t^o value under various conditions (as described in Tables 1.1-1.2 and Table 4) it was found that, except a few case, the ΔH_t^o values were positive. Positive ΔH_t^o values indicate endothermicity involved in the microemulsion formation process. This was as expected; while water droplets getting dispersed into the oil continuum, due to area enhancement, there would be absorption of heat (energy). In general ΔH_t^o values decreased with the rise in ω value. It also decreased with the increase in temperature. With the rise in temperature overall structuredness of the system decreases, thus energy change associated with the process gets decreased. However, ΔH_t^o values were found to decrease with the increasing n-alkanol chain length. With the increase in n-alkanol chain length, partitioning of the cosurfactant at the oil-water interface becomes easier. Entropy values were found to be positive in most of the cases. Variation in the ΔS_t^o value was not so significant compared the associated enthalpy changes. ΔS_t^o values decreased with the rise in ω values; however, ΔS_t^o values increased linearly with the rise in cosurfactant chain length.

Investigation on the enthalpy entropy compensation could justify the similarities in the structuredness of a reverse micelle and water-in-oil microemulsion system. Normally the compensation effect is stated to be valid for surfactant aggregates [101]. Plot of ΔH_t^o vs ΔS_t^o have been shown in Figure 1.5. In this plot all the compositions/conditions were taken into account except n-butanol. Microemulsion system comprising n-butanol behaved differently for its significant solubility in water compared to its higher homologs 140. Nice correlation was observed for all sets of values (different n-alkanols, ω values and temperature). Compensation temperature, as obtained from the slope, was found to be 314K which was in good agreement with the average all the experimental temperature range (average temperature: 313K; experimental temperature range: 303, 308, 313, 318 and 323K). Although the energetic parameters have been indirectly computed, however they could also be experimentally evaluated by calorimetric measurements. Such studies could be considered as one of the future perspective.

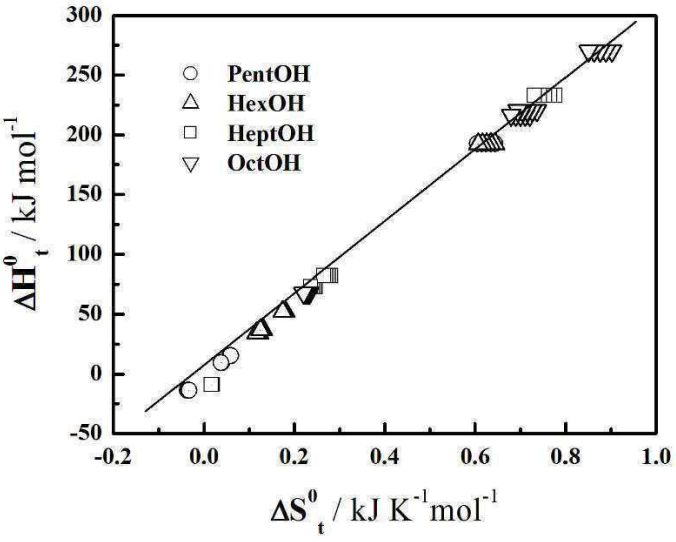

Figure 1.5. Enthalpy-entropy compensation for the formation of water/(Tween 20 + n-alkanol)/n-heptane water-in-oil microemulsion (except n-butanol as it followed *different path). All the ω values at different experimental temperature were* considered. n-alkanols used have been mentioned inside the Figure. Compensation temperature: 314K (close to the average of the experimental temperature range 303-323K, i.e., 313K).

3.2.2. Structural parameters

The results of dilution experiments could suitably be further computed in evaluating different structural parameters of the w/o microemulsion. The microemulsion droplets are approximated to have spherical shape in general, mono dispersed with a surface mono layer comprising surfactant and cosurfactant to be present at the interface. The total volume of the dispersed droplets (V_d) per unit volume (here in mL) can be expressed as follows:

$$V_d = \frac{4}{3}\pi R_e^{\,3} N_d \qquad (1.\mathbf{15})$$

R_e and N_d represents the effective diameter and total number of the droplets respectively.

The droplet surface area (A_d) of droplets per unit volume is therefore:

$$A_d = 4\pi R_e^{\,2} N_d = (n_S A_S + n_a^{\,i} A_a) N_A \qquad (1.\mathbf{16})$$

where, A_S and A_a are the cross sectional area of the surfactant and cosurfactant molecules respectively, N_A Avogadro's constant.

The equation for R_e from equation 1.15 and 1.16 can be written as:

$$R_e = 3V_d/A_d \qquad (1.17)$$

Total volume of the dispersed phase, herein the water droplet embedded by the surfactant and n-alkanols at the oil-water interface, is the sum of the volume contribution of water (V_{H_2O}), surfactant (V_S) and the interfacial n-alkanol molecules (V_a^i) at the interface respectively. Thus one could write;

$$V_d = V_{H_2O} + V_S + V_a^i \qquad (1.18)$$

One can determine the respective volumes using the values of number of moles (n_a^i), molar mass (M_a) and density of the components (ρ_a) according to the relation:

$$V_a^i = n_a^i M_a/\rho_a \qquad (1.19)$$

The total droplet surface area (A_d) can be obtained from the equation:

$$A_d = (n_S A_S + n_a^i A_a) N_A \qquad (1.20)$$

where, A_S and A_a are the polar head group area of surfactant and alkanol, respectively, and N_A is the Avogadro constant.

Putting the value of R_e in equation (1.15) we get the values of N_d

$$N_d = 3V_d/4\pi R_e^3 \qquad (1.21)$$

The average aggregation number of surfactant (N_S) and cosurfactant (N_a) in a microemulsion droplet can be expressed as:

$$N_S = \frac{n_S N_A}{N_d} \qquad (1.22)$$

$$N_a = \frac{n_o^i N_A}{N_d} \qquad (1.23)$$

Volume of a microemulsion droplet is contributed by dispersed water, surfactant and cosurfactant molecules. Thus the radius of water pool in a microemulsion droplet is related to the effective radius (i.e., the sum of pool radius and surfactant tail) according to the relation:

$$R_w = \left(\frac{V_{H_2O} + V_S{}^h + V_a{}^h}{V_d}\right)^{1/3} R_e \qquad (1.24)$$

where V_{H_2O} , $V_S{}^h$ and $V_a{}^h$ are volume of water droplet, surfactant head group, and alkanol head group, respectively. Volume contribution due to surfactant head group and cosurfactant head group could be evaluated from the following two equations:

$$V_S{}^h = \frac{4}{3\pi^{1/2}} A_S{}^{3/2} N_S \qquad (1.25)$$

$$V_a{}^h = \frac{4}{3\pi^{1/2}} A_a{}^{3/2} N_a \qquad (1.26)$$

Various structural parameters, as described in the earlier section were computed by employing the dilution data into the aforementioned equations. Variation in the number of droplets per unit volume (N_d) with [water]/[Tween 20] mole ratio and temperature is shown in Figure 6 for microemulsion comprising n-hexanol as representative. Detailed results for all the systems are also summarized in Table 1.6.

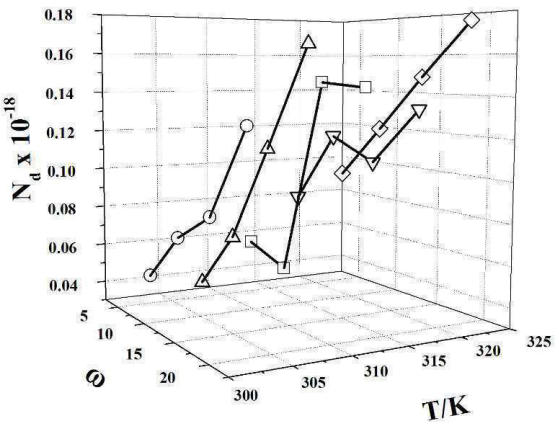

Figure 1.6. N_d - ω - T profile for water/(Tween 20 +n-hexanol)/n-heptane water-in-oil microemulsion system. A 1:1 (w/w) Tween 20: n-hexanol mixture was used.

Number of droplets per unit volume (herein mL) was found to increase with the increase in ω values. Such results apparently seem to be contradictory as one could expect an incremental effect when the volume of the added water is increased for a particular system at fixed surfactant/cosurfactant and oil and at a certain temperature.[223,228] This unusual behavior was only observed in our earlier investigations.[226,229] Such behavior was observed only for nonionic surfactants having polyoxyethylene head groups[230,231]. It is assumed that with the increase in the volume of water, newer droplets could be formed with smaller dimensions. This assumption would further be established by analyzing the other structural parameters as well as the dynamic light scattering measurements to be presented in subsequent sections. We also expect occurrence of droplet fission phenomena while the temperature of the microemulsion media were increased.

With the increase in the number of droplets through the progressive addition of water to a fixed amount of surfactant, alkanol and oil, if the number of droplet increases, one could also expect in the change of number of surfactant (N_s) and cosurfactant (N_{cs}) molecules per microemulsion droplet. ω and temperature dependence of N_s and N_{cs} for water/(Tween 20+n-hexanol)/n-heptane water-in-oil microemulsion system is shown in Figure 1.7 as representative.

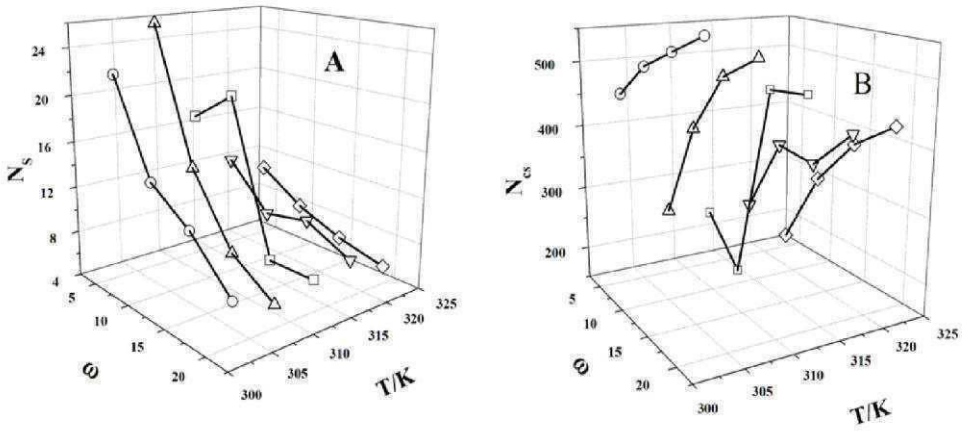

Figure 1.7. Variation in the number of A) surfactant (N_s) and B) cosurfactant (N_{cs}) per microemulsion droplet with ω and temperature in water/(Tween 20 +n-hexanol)/n-heptane water-in-oil microemulsion system.

Table 1.6. Structural parameters of Water/(Tween 20+n-alkanol)/n-Heptane water-in-oil microemulsion at at different temperatures and and [Water]/[Tween 20*] mole ratio, ω.*

n-alkanol		$10^{-18}N_d$(per mL)/N_s (per droplet)/ /N_{cs} (per droplet)				
	ω	**303**	**308**	**313**	**318**	**323**
BuOH	5	1.47/66.33/36.37	4.08/23.93/124.61	7.09/13.77/124.26	7.63/12.78/34.67	0.13/7.65/87.72
	10	2.06/47.22/186.22	3.96/24.64/154.12	5.50/17.73/101.92	8.15/11.96/90.33	0.11/8.66/83.52
	15	1.42/68.42/138.70	2.82/34.50/118.34	4.60/21.28/93.52	7.86/12.41/110.97	0.10/8.96/102.39
	20	3.43/28.38/324.36	8.97/10.87/289.03	6.55/14.90/188.84	7.76/12.60/134.29	8.83/11.05/78.45
PentOH	5	4.04/24.15/316.82	4.45/21.93/192.57	7.46/13.07/202.17	0.10/9.65/188.96	0.12/8.04/157.30
	10	6.78/14.38/396.03	8.39/11.64/336.23	9.08/10.75/271.30	0.11/8.57/243.52	0.13/7.44/208.30
	15	0.12/8.37/435.33	0.12/8.41/383.26	0.12/8.18/331.05	0.14/6.57/308.91	0.15/6.45/261.00
	20	0.12/8.49/447.06	0.15/6.64/409.31	0.17/5.75/378.31	0.16/5.87/336.19	0.19/5.17/312.85
HexOH	5	0.45/21.85/454.01	0.38/25.72/255.04	0.57/17.05/238.63	0.80/12.16/240.20	0.92/10.61/171.24
	10	0.70/13.87/509.71	0.68/14.30/411.56	0.49/19.78/172.17	0.12/8.34/366.92	0.12/8.13/300.20
	15	0.86/11.41/542.40	0.12/8.44/503.76	0.15/6.68/478.83	0.11/9.17/360.00	0.15/6.57/380.04
	20	0.13/7.56/574.27	0.16/5.97/542.21	0.14/6.75/488.09	0.13/7.28/426.23	0.18/5.54/428.05
HeptOH	5	3.33/29.33/470.23	3.96/24.66/326.04	5.76/16.96/324.30	6.68/14.62/223.63	8.48/11.51/227.21
	10	6.35/15.38/639.54	7.28/13.42/563.95	8.59/11.36/511.96	9.19/10.62/441.03	0.10/9.68/383.14
	15	7.58/12.87/679.39	9.36/10.43/628.14	0.10/9.34/577.10	0.12/8.31/536.52	0.11/9.02/435.22
	20	0.11/9.28/719.85	0.13/7.69/679.30	0.13/7.76/624.15	0.13/7.66/569.35	0.13/7.27/523.16
OctOH	5	8.47/11.53/298.14	8.57/11.39/232.62	0.11/9.04/193.72	0.14/6.93/174.43	0.16/6.28/136.21
	10	0.15/6.35/323.92	0.18/5.55/291.39	0.16/5.95/250.99	0.19/5.25/223.89	0.20/4.82/196.90
	15	0.19/5.16/333.74	0.23/4.20/307.76	0.25/3.96/283.84	0.26/3.77/260.98	0.24/4.02/228.36
	20	0.28/3.53/338.60	0.30/3.22/318.20	0.28/3.52/295.36	0.33/2.96/281.09	0.35/2.81/264.18

Results have also been detailed in Table 1.6. It is evident from the Figure and Table 1.6 that the N_s value decreased with the increase in the ω. N_s also decreased with the increase in temperature. Such behavior contradicts the earlier reports by Hait et. al where a water in oil microemulsion comprising of water/(CPC + n-alkanol)/n-heptane was used [98]. In their studies both temperature and ω tendered incremental effect on the N_s. However, in the present study as we have noticed that with a fixed number of surfactant molecules, formation of larger number of droplets would reduce the average number of surfactant molecules per microemulsion droplets. This apparent unusual behavior was made possible because of the presence of oxyethylene groups in Tween-20. In Tween-20 the oxyethylene group could 'open up' or 'uncoil' itself to provide a better coverage at the oil-water interface[229]. Ionic surfactants because of their relatively smaller head groups, could not tender such effect.

It was found that both the increase in temperature and ω values led to an increase in number of droplet per unit volume and subsequent decrease in the average aggregation number of surfactants (N_s) per droplet. For a better delineation and protection of water droplets from the oil contact, the decrease in N_s needs to be compensated by an increase in the average number of cosurfactant molecule per droplet (N_{cs}). Figure 1.7B confirms such predictions in a better way. Trend in the variation of N_s and N_{cs} followed opposite path, especially while in considering their variations with ω values.

While considering the effect of alkanol chain length on the N_{cs} value it was observed that in general the N_{cs} values increased from n-butanol to n-heptanol. However N_{cs} values for n-octanol were found to lie in between n-butanol and n-pentanol. This supports the larger involvement of cosurfactant molecule in stabilizing a microemulsion droplet. n-octanol behaved more like an oil than a cosurfactant, for which its effect was different from the other cosurfactants.

Involvement of cosurfactant as surfactant substitute and their compensation effect could further be ascertained while considering the ratio of N_{cs} and $N_{s.}$ Except n-butanol, it was found that the ratio of N_{cs}/N_s increased linearly with the increase in ω value. Interestingly, the ratio was found to be independent of temperature (data not shown to save space). These results were in conformity with the earlier observations[98,223,226].

3.3. Size of the microemulsion droplets

Results on the hydrodynamic parameters of the microemulsion droplets are summarized in Table 1.7. In this table, radius of the water pool (R_w), effective radius of the microemulsion droplets (R_e), contributory effect of water pool, surfactant/cosurfactant head group and surfactant hydrocarbon tails and hydrodynamic radius during heating (R_h) and cooling (R_c) have been presented for all the systems except n-octanol (the reason stated earlier in the experimental section).

It is to be noted that R_w and R_e were obtained by computing the results of dilution measurements while the R_h and R_c were directly obtained from the dynamic light scattering measurements. Results are found to be comparable with each other. It is also to be noted that R_h values were found to be in between the R_w and R_e values. This is also not unexpected, although such reports are not available in literature. In case of water in oil microemulsion the hydrocarbon chains, being in oil continuum, do not get involved in the scattering of light. Therefore one could, in general, expect depreciation in size corresponding to the dimension (length) of the surfactant tail. According to Tanford's formula, the critical (l_c) or effective length (l_{max}) of a saturated hydrocarbon chain having C_n number of carbon atoms will be [2]:

$$l_c \leq l_{max} \approx (0.154 + 0.1265\, C_n)\ \text{nm} \qquad (1.\mathbf{27})$$

For Tween-20 (having a dodecyl hydrocarbon chain) l_c appears to be approximately equal to 1.672 nm. Therefore one could expect a difference of ≈

1.7 nm in between R_e and R_h value. For every system the radii were found to decrease with increase in temperature. Such observations, especially in the DLS measurements finally prove our assumptions as made during the analyses of dilution measurements. When the numbers of droplets are increased without changing the number of surfactant molecules, one could expect a decrease in the size of the microemulsion droplets. Also the decrease in $R_w/R_e/R_h/R_e$ values with the increase in ω values further establishes our mechanism as proposed in analyzing the results of dilution measurements. While considering the effect of cosurfactant chain length it was found that R_e values increased with the increase in cosurfactant chain length. However, no systematic variation in the radii values were evidenced through DLS measurements. Formation of larger number of droplets along with a size decreased could be further clarified through Figure 1.8.

Figure 8 describes the temperature dependence of microemulsion size and its distribution obtained from DLS measurements. It is clear from the Figure that with increase in temperature the size distribution moves to the lower dimensions. Besides, the intensity of the distribution curves was found to be increased with the rise in temperature. It is known that the light scattering intensity is proportional to the square of droplet volume and to the droplet number [232].

Table: 1.7. Radius of water/(Tween 20+ n-alkanol)/n-heptane water-in-oil microemulsion at different temperature and [water]/[Tween 20] *mole ratio, ω.*

n-alkanol		R_w / R_e / R_h / R_c (in nm) at different temperature (in K)				
	ω	Temp. 303	308	313	318	323
BuOH	5	1.34/3.20/1.85/2.19	0.96/2.52/1.54/2.00	0.80/2.23/1.34/1.88	0.78/1.94/1.38/1.65	0.65/1.90/1.40/1.40
	10	1.51/3.14/2.70/2.40	1.21/2.63/2.15/3.21	1.09/2.34/1.85/3.02	0.96/2.11/1.80/2.72	0.86/1.96/1.75/1.75
	15	1.96/3.49/3.30/2.80	1.56/2.86/2.37/2.60	1.32/2.47/2.10/1.88	1.10/2.21/2.16/1.53	0.99/2.05/2.25/2.25
	20	1.60/3.05/3.90/3.61	1.17/2.56/3.40/2.43	1.29/2.50/2.55/2.11	1.23/2.31/2.37/1.70	1.17/2.11/2.72/2.72
PentOH	5	0.96/2.93/0.91/0.80	0.93/2.66/0.81/0.86	0.78/2.46/0.74/0.84	0.70/2.33/0.78/0.83	0.66/2.20/0.86/0.86
	10	1.01/2.90/0.84/0.73	0.94/2.73/0.80/0.76	0.92/2.58/0.73/0.77	0.85/2.45/0.77/0.75	0.81/2.33/0.79/0.79
	15	0.85/2.86/0.94/0.93	0.85/2.76/0.87/0.91	0.84/2.65/0.80/0.93	0.78/2.56/0.79/0.86	0.77/2.45/0.85/0.85
	20	0.85/2.89/0.98/0.85	0.78/2.78/0.92/0.84	0.75/2.70/0.81/0.84	0.76/2.61/0.80/0.81	0.72/2.54/0.81/0.81
HexOH	5	1.17/3.23/0.75/0.49	1.23/2.96/0.65/0.50	1.07/2.73/0.60/0.51	0.96/2.63/0.52/0.55	0.92/2.40/0.55/0.55
	10	1.00/3.18/0.82/0.54	1.01/3.02/0.76/0.55	1.13/2.65/0.70/0.52	0.84/2.82/0.64/0.55	0.84/2.70/0.59/0.59
	15	0.94/3.21/0.87/0.60	0.85/3.09/0.77/0.74	0.78/3.01/0.72/0.71	0.87/2.83/0.66/0.72	0.78/2.82/0.65/0.65
	20	0.82/3.20/0.90/0.72	0.76/3.12/0.85/0.80	0.79/3.04/0.80/0.78	0.81/2.93/0.75/0.80	0.74/2.90/0.70/0.70
HeptOH	5	1.47/3.43/0.77/0.59	1.39/3.11/0.72/0.54	1.23/2.97/0.63/0.52	1.17/2.69/0.60/0.54	1.08/2.63/0.65/0.65
	10	1.04/3.52/0.95/0.65	0.99/3.40/0.83/0.62	0.94/3.26/0.72/0.65	0.92/3.12/0.67/0.65	0.89/2.98/0.64/0.64
	15	1.12/3.56/1.00/0.65	1.04/3.44/0.83/0.61	1.00/3.34/0.68/0.63	0.97/3.26/0.63/0.62	0.99/3.08/0.68/0.68
	20	1.10/3.58/0.95/0.61	1.04/3.49/0.85/0.63	1.04/3.40/0.74/0.57	1.04/3.31/0.63/0.58	1.02/3.22/0.60/0.60
OctOH	5	0.94/2.53/1.05/0.65	0.94/2.40/0.90/0.61	0.87/2.25/0.75/0.57	0.79/2.13/0.69/0.63	0.77/1.99/0.60/0.60
	10	0.77/2.46/1.15/0.76	0.74/2.38/0.90/0.68	0.75/2.30/0.81/0.69	0.72/2.21/0.71/0.65	0.70/2.13/0.68/0.68
	15	0.82/2.46/1.30/0.70	0.77/2.38/0.98/0.63	0.75/2.32/0.88/0.60	0.74/2.26/0.70/0.61	0.76/2.20/0.62/0.62
	20	0.80/2.43 /— /—	0.77/2.38 /— /—	0.80/2.33 /— /—	0.75/2.28 /— /—	0.74/2.24 /— /—

0.2 moldm^{-3} Tween 20 with 1:1 Tween 20 : n-alkanol (w/w) in n-heptane was used. R_w / R_e / R_h / R_c represent the radius of the water pool (derived from dilution measurement), effective radius of the microemulsion droplet (derived from dilution measurement), radius of droplet measured by DLS while heating and radius of droplet measured by DLS while cooling.

In the present study the increase in the number of droplets were more significant than the decrease in size of the microemulsion droplets. Hence increase in the intensity of the distribution curve was resulted along with a decrease in the width of the distribution curves. However, further structural studies on such microemulsions using cryo-transmission electron microscopy are warranted.

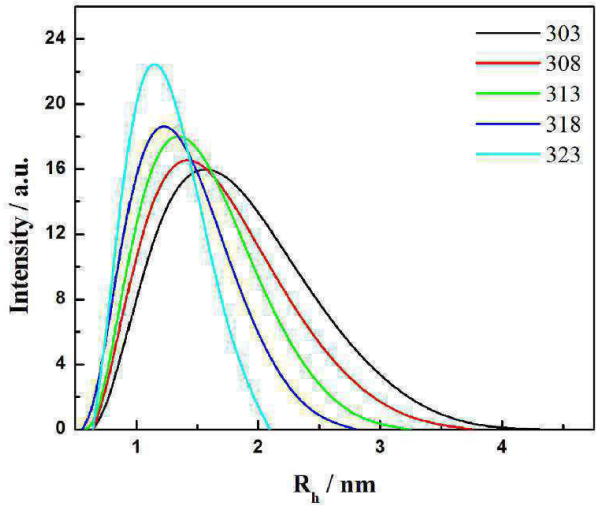

Figure 1.8. Size and size distribution of water/(Tween 20 +n-hexanol, 1:1, w/w)/n-heptane water-in-oil microemulsion at different temperatures. Temperatures (in K) have been mentioned inside the Figure [water]/[Tween 20*], ω= 10. A 0.2 moldm*$^{-3}$ Tween20 was used.

In recording the DLS data while cooling down microemulsions, it was always noted that dimensions of the droplets to follow a higher profile than the heating curves. This unusual behavior was due to the condensation effect of the droplets during the cooling [232]. However, the width of the distribution curves were not changed significantly as what was observed during the heating of the microemulsions.

3.4. Viscosity measurement

Viscosity along with viscosity derived activation parameters at 1:1 Tween20-alkanol ratio under different conditions have been summarized in Table 4. η and temperature dependency of data have been presented in Figure 1.9 for n-hexanol derived formulation as representative plot. It was generally observed that

with the rise in temperature viscosity decreased. Viscosity initially decreases with increasing ω and passes through minima at ω in the range of 10 to 15. It is known that fluidity increases with the rise in temperature for microemulsions in general[114,127,128]. However, initial decrease in viscosity of microemulsion with increase in ω could be accounted for the increase in number of droplets, and subsequent size depletion. Viscosity was found to increase with the increase in cosurfactant chain length. This is due to the stronger binding affinity of alkanol with surfactant head groups[223]. However n-octanol being more oily than other cosurfactants did not tender progressive incremental effect. Temperature dependency of viscosity was found to decrease with the increase in cosurfactant chain length. Further investigations using more sophisticated tools like small angle neutron scattering and cryo-TEM, etc., are warranted. Therefore, rheometric measurements, along with above mentioned studies on such systems could be considered as the future perspectives of the present work.

As expressed in equation (29); one can obtain ΔH^* from the slope of ln η vs T^{-1} plot. ln η was found to vary with T^{-1} in a binomial way; hence one can derive ΔH^* from it's differential with respect to temperature in the following way;

$$\ln \eta = a + bT + cT^2 \qquad \textbf{(1.30)}$$

Therefore,

$$\frac{d ln \eta}{dT} = -\frac{\Delta H^*}{RT^2} = b + 2cT \qquad \textbf{(1.31)}$$

Thus knowing the value of 'b' and 'c' one can compute ΔH^* at different temperatures.

Change in heat capacity (ΔC_p) is related to ΔH^* as;

$$\Delta C_p = \frac{d(\Delta H^*)}{dT} = -2RT(b + 3cT) \qquad \textbf{(1.32)}$$

Table: 1.8. Viscosity and viscosity derived activation parameters of water/(Tween 20+n-alkanol)/n-heptane water-in-oil microemulsion at different temperatures and [water]/[Tween 20*] mole ratio, ω.*

n-alkanol		$(\eta/cP) / \Delta H^*/kJmol^{-1}) / (\Delta G^*/kJmol^{-1}) / (\Delta S^* / J\ mol^{-1}K^{-1}) / (\Delta C_p/ kJ\ mol^{-1}K^{-1})$				
	ω	303	308	313	318	323
BuOH	5	2.88/7.17/3.52/2.36/7.10	2.56/7.53/3.54/2.44/7.33	2.34/7.90/3.58/2.52/7.58	1.80/8.30/3.57/2.60/7.82	1.34/8.68/3.55/2.69/8.07
	10	2.66/8.30/3.50/2.73/8.21	2.45/8.72/3.53/2.83/8.49	2.10/9.14/3.55/2.92/8.76	1.56/9.59/3.53/3.01/9.05	1.14/10.05/3.50/3.11/9.33
	15	2.80/5.60/3.51/1.85/5.54	2.39/5.88/3.53/1.91/5.73	1.91/6.17/3.53/1.97/5.92	1.34/6.47/3.49/2.03/6.10	1.01/6.78/3.48/2.10/6.30
	20	2.77/8.34/3.51/2.91/8.75	2.37/9.28/3.53/3.01/9.04	2.15/9.74/3.56/3.11/9.33	1.70/10.22/3.55/3.21/9.64	1.12/10.70/3.50/3.31/9.94
	5	2.80/6.73/3.51/2.22/6.66	2.58/7.07/3.55/2.29/6.88	2.44/7.42/3.59/2.37/7.11	1.86/7.78/3.58/2.44/7.34	1.49/8.15/3.58/2.52/7.57
	10	2.90/2.28/3.52/0.75/2.26	2.38/2.39/3.53/0.78/2.33	2.38/2.51/3.58/0.80/2.41	1.86/2.63/3.58/0.83/2.50	1.60/2.77/3.60/0.85/2.60
	15	2.84/1.61/3.52/0.53/1.59	2.50/1.69/3.54/0.54/1.64	2.32/1.77/3.59/0.56/1.70	1.96/1.86/3.59/0.58/1.76	1.72/1.95/3.61/0.60/1.81
	20	2.96/3.44/3.53/1.13/3.41	2.68/3.62/3.56/1.18/3.53	2.50/3.80/3.60/1.21/3.64	2.20/3.98/3.62/1.25/3.75	1.81/4.17/3.63/1.29/3.88
	5	3.17/1.03/3.54/0.34/1.02	3.01/1.09/3.59/0.35/1.05	2.81/1.13/3.63/0.36/1.09	2.60/1.19/3.67/0.37/1.12	2.40/1.25/3.70/0.39/1.16
	10	3.09/-4.40/3.53/-1.45/-4.36	2.80/-4.62/3.57/-1.50/-4.50	2.47/-4.86/3.60/-1.55/-4.65	2.30/-5.09/3.63/-1.60/-4.80	2.44/-5.33/3.71/-1.69/-4.95
	15	3.15/2.97/3.54/9.81/2.94	2.89/3.12/3.58/1.01/3.04	2.60/3.27/3.61/1.04/3.14	2.39/3.43/3.64/1.08/3.24	1.95/3.60/3.65/1.11/3.34
	20	3.30/3.00/3.55/0.99/2.98	2.90/3.15/3.58/1.02/3.07	2.70/3.31/3.62/1.05/3.18	2.27/3.47/3.63/1.09/3.28	1.89/3.64/3.64/1.12/3.38
	5	3.59/1.98/3.58/0.65/1.96	3.20/2.07/3.60/0.67/2.02	3.05/2.17/3.65/0.69/2.08	2.72/2.28/3.68/0.72/2.16	2.34/2.39/3.70/0.74/2.22
	10	3.23/0.29/3.54/0.09/0.29	2.95/0.31/3.59/0.01/0.30	2.73/0.32/3.62/0.01/0.31	2.55/0.34/3.66/0.10/0.32	2.31/0.36/3.69/0.11/0.33
	15	3.24/5.98/3.55/1.97/5.92	3.13/6.28/3.60/2.04/6.12	3.32/6.59/3.68/2.10/6.32	2.80/6.91/3.69/2.17/6.52	2.41/7.25/3.71/2.24/6.73
	20	3.54/0.55/3.73/0.18/0.54	3.31/0.58/3.61/0.18/0.56	3.04/0.60/3.65/0.19/0.58	2.82/0.63/3.69/0.20/0.60	2.59/0.67/3.72/0.20/0.62
OctOH	5	3.44/-0.80/3.56/-0.26/-0.80	3.16/-0.84/3.60/-0.27/-0.85	2.95/-0.89/3.64/-0.28/-0.85	2.68/-0.93/3.67/-0.29/-0.88	2.60/-0.98/3.73/-0.30/-0.90
	10	3.47/0.58/3.60/0.19/0.58	3.18/0.61/3.60/0.20/0.62	2.99/0.64/3.65/0.20/0.62	2.75/0.68/3.68/0.21/0.64	2.51/0.71/3.72/0.22/0.66
	15	3.60/-0.68/3.57/-0.22/-0.67	3.41/-0.71/3.62/-0.23/-0.72	3.09/-0.75/3.65/-0.24/-0.72	3.19/-0.78/3.72/-0.25/-0.74	2.92/-0.82/3.76/-0.26/-0.76

0.2 $moldm^{-3}$ Tween 20 with 1:1 Tween 20: n-alkanol (w/w) in n-heptane was used. η: viscosity; ΔH^*: Enthalpy change; ΔG^*: free energy change; ΔS^*:entropy change and ΔC_p: heat capacity change.

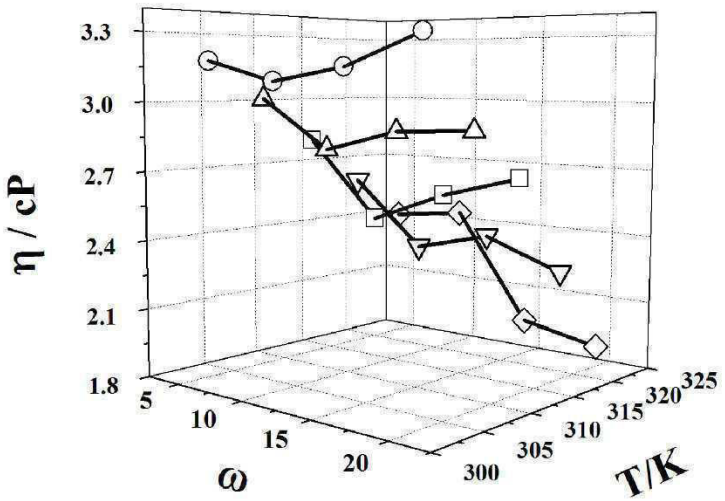

Figure 1.9. *Viscosity (η) – ω –* T profile for the microemulsion comprising of water/ (Tween 20 +n-hexanol)/n-heptane. 0.2 moldm^{-3} Tween 20 with a 1:1 (w/w) ratio of n-hexanol was used.

Therefore change in Gibb's free energy for activation could be expressed as;

$$\Delta G^* - RT\ ln\frac{\eta V}{hN} \qquad (1.\mathbf{33})$$

Once ΔH^* and ΔG^* are known, the ΔS^* value could be calculated easily according to the following expression:

$$\Delta S^* = \frac{\Delta H^* - \Delta G^*}{T} \qquad (1.\mathbf{34})$$

All the viscosity associated thermodynamic parameters have been presented in Table 1.4. The results reveal that ω dependency on ΔG^* was almost similar like its viscosity. Gibb's free energy for activation was found to increase with temperature for all the systems. The increase in ΔG^* with temperature is a consequence of shear thickening of the sample with increasing temperature. No systematic variations in the ΔC_p values were noted. Both the positive and negative ΔC_p values were in accordance with increase and decrease in ΔH^* values under various conditions[233,234]. Results also reveal the complex nature of the microemulsion droplets. The ΔG^* values were limited within the range of 3.5 to 3.8 kJ mol^{-1} whereas the ΔH^* and ΔS^* values varied significantly. Good correlation between ΔH^* and ΔS^* were found for all the compositions and

temperature as revealed from the compensation plots between ΔH^* and ΔS^* (given in Figure 10).

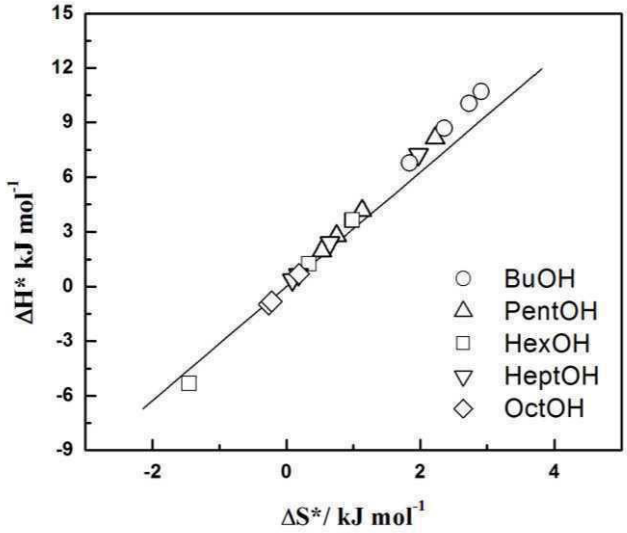

Figure 1.10. Viscosity derived activation enthalpy-entropy compensation plot for water/(Tween 20+n-alkanol)/n-heptane water-in-*oil microemulsion. All the ω values at* different experimental temperatures were considered. n-alkanols used have been mentioned inside the figure. Compensation temperatures: 313K (close to the average of the experimental temperature range 303-323K, i.e., 313K).

The compensation temperature (313K) obtained from the slope was found to be in close proximity with the average of all experimental temperatures (303, 308, 313, 318 and 323 K). Similar observations have also been reported by others[114,127,128].

4. Summary and conclusion

Physico-chemical studies on water/(Tween 20+n-alkanol)/n-heptane microemulsions were performed using different techniques, viz., phase manifestation, dilution method, DLS and viscosity measurements. Results were analyzed in the light of the above mentioned experiments. Based on the observations, the following conclusions could be made:

(1) The clarity of microemulsion formulation was reduced with the increase in cosurfactant chain length with an optimum efficacy tendered by n-hexanol.

(2) While the surfactants reside at the oil-water interface, the cosurfactants were partitioned in between the oil and oil-water interface.

(3) Spontaneity of microemulsion formation increased with increase in cosurfactant chain length, increase in temperature and decrease in the volume of the dispersed phase, water.

(4) The formation of microemulsion was found to be an enthalpy controlled process.

(5) Larger numbers of droplets were formed at the expense of size. With the increase in temperature and ω value, size reduction was also evidenced by DLS measurements.

(6) Depletion in the aggregation number of surfactant per droplet was compensated by the cosurfactant molecules. However, the compensatory effect was not affected by temperature.

(7) A symmetric variation in different physico-chemical properties were noted with the increase in the cosurfactant chain length. However, n-octanol, being oilier in nature than a cosurfactant, tendered different behavior.

CHAPTER 2

CHAPTER 2

Combined Phase Behavior, Dynamic Light Scattering, Viscosity and Spectroscopic Investigations on Pyridinium Based Ionic Liquid-in-Oil Microemulsion

Abstract

Although several studies on imidazolium based ionic liquid-in-oil microemulsion are available in the literature, however, studies on pyridinum bases ionic liquid microemulsion are not so common. Pyridinium based ionic liquids have superior yet unexplored properties when considered in the polar domain of microemulsion. 1-butyl-4-methyl pyridinium tetrafluoroborate ([b4mpy][BF_4]) / (Tween 20 + n-pentanol) / n-heptane microemulsion system has been studied by combined phase behavior, dynamic light scattering, viscosity and spectroscopic probing techniques. With the increasing amount of Tween 20/n-pentanol (S/CS) ratio, turbidity increased, although it was not possible to achieve a stable microemulsion without the cosurfactant. Dynamic light scattering and viscosity study revealed that the size of the μE droplets increased with increasing volume fraction (φ_d) of ionic liquid. Both the size and viscosity increased with φ_d. With the increasing amount of n-pentanol, the variation became less sensitive due to the better stabilizing effect induced by the alkanol. Increase in size of the microemulsion droplets was overshadowed by the increase in the fluidity of the medium, for which viscosity decreased with increasing temperature, as common for Newtonian fluids. State of the ionic liquid in the microemulsion was monitored by absorption and fluorescence spectroscopy with and without curcumin as the molecular probe. While a continuous increase in polarity of the IL domain occurred with increasing amount of IL, the fluorescence anisotropy results revealed that the rigidity of the domain passed through maxima for all S/CS ratio.

Communicated to RSC Advances, Manuscript ID: RA-ART-02-2014-001209

1. Introduction

Because of the multifaceted applications, viz., drug delivery, nanoparticle synthesis, media for organic reaction, biochemical reaction, separation, cosmetics[128], etc., studies on microemulsion (μE) have gained significant importance. A microemulsion (μE) can be defined as an optically transparent, thermodynamically stable dispersion of one liquid in otherwise immiscible second liquid, stabilized by a surfactant[34]. Sometimes, short chain alkanols and amines can assist μE formation[220]. It has been reported that ionic liquid (IL) can substitute the polar component (water) in a μE[225]. Scientific studies involving ILs have reached its credential beyond any doubt for which there has been an exponential growth in the research publication involving ILs. By definition ILs, with melting points below 100^0C, are considered as neoteric component for its specific properties, viz., non-flammability, non-corrosiveness, high ionic conductivity and inertness towards different thermal and chemical environment[185]. One of the outstanding properties of ILs lies in its use as an alternative to traditional organic solvents. ILs are also called "designer solvents" because its properties can be tuned by altering the substituent as well as the counter ions[235]. In spite of significant research contribution on ILs, the lack of complete knowledge is considered to be one of the barriers in utilizing them for practical applications. Thus more fundamental researches on ILs are warranted.

It is needless to mention that μE comprising ILs in the polar domain can have some unknown but some novel properties owing to the unique and combined features of the ILs and μEs. Thus, this domain of research has been gaining significance day by day. Ionic liquid microemulsions find application in various fields, viz., preparation and characterization of polymeric nanoparticles[236], synthesis of inorganic nanoparticles[237], renewable lubricants[238], and catalysis[239], etc.

Although most of the studies on ILs are associated with the imidazolium ion, however, there has been a current trend to search for alternate, easily available but low cost ILs other than the imidazolium ion. According Domanska et al.[240], pyridinium based ILs have specific properties, viz., broad liquidous

temperature range, inertness to air, moisture and superior solubilization capacity. These unique features of pyridinium based ILs have already been explored with special reference to antistatic thermoplastic resin[241], adhesive film[242], electrochemical probe[243], electron transfer process[244], reaction acceleration[245], organo catalysis[246], extraction process[247], etc. In spite of high possible potentials, there have been a little research on 1-butyl-4-methylpyridinium tetrafluoroborate ([b4mpy][BF_4]) comprising μE although it is one of the most reported pyridinium based IL[248]. In a very recent report of Takumi et al.[249], mutual miscibility of imidazolium and pyridinium ILs with $[BF_4]^-$ as the common counter anion have been explored. Another advantage of using this IL is that the system itself can be investigated without any molecular probe (because of the presence of the pyridinium ring) in the UV-visible region.

Curcumin is a natural polyphenolic compound isolated from the rhizome of turmeric (Curcuma longa). Researches over the last few decades have shown that curcumin possesses a great variety of beneficial biological and pharmacological activities such as anticancer, antioxidant, anti-arthritic, and anti-inflammatory agents[250]. Despite its highly promising features as a health-promoting agent, poor aqueous solubility in neutral aqueous medium of curcumin[251] is one of the major draw backs in its bioavailability, clinical efficiency and metabolism[252]. A number of attempts have been made to increase the solubility in polar medium and hence the bioavailability of curcumin through encapsulation in surfactant micelles[253,254], lipids[255], cyclodextrin[256], hydrogel[257], liposomes[258], polymeric micelles[259], nanoparticles[260], etc. Curcumin is also soluble in other polar solvents, so there is a huge scope of its bioavailability if it can be entrapped in μE with a polar phase. Once used in the IL-in-oil microemulsion, curcumin may have a possibility to reside in the inner polar core of the μE because curcumin is not soluble in n-heptane. Thus the spectroscopic investigation involving curcumin in the microemulsion will be able to probe the microenvironment of the polar domain

In the present manuscript, comprehensive studies on the IL-in-oil type microemulsion comprising 1-butyl-4-methylpyridinium tetrafluoroborate have been reported. It is expected that studies on such type of μE comprising

[b4mpy][BF_4], Tween 20 (a nonionic surfactant, S), n-pentanol (a cosurfactant, CS) and n-heptane (oil) will generate significant information in terms of its practical application as well as the view point of fundamental understanding. The effect of Tween 20(surfactant)/n-pentanol (cosurfactant) ratio, volume fraction of IL and temperature have been studied using a number of techniques, viz., phase manifestation, dynamic light scattering, viscosity, UV-visible absorption and emission spectroscopy. The detailed phase diagram studies helped in identifying the clear and turbid region. Dynamic light scattering studies provided the information about the size and its distribution at different temperature; viscosity measurements were carried out and correlated with the DLS data. μE with and without curcumin in the polar domain were investigated by UV-visible absorption spectroscopy. Fluorescence spectroscopic studies on curcumin in the polar domain helped in understanding the state of polarity and rigidity of the microenvironment.

2. Experimental section

2.1. Materials. The IL 1-butyl-4-methyl pyridinium tetrafluoroborate, [b4mpy][BF_4] was purchased from Sigma-Aldrich Chemicals Pvt. Ltd., USA. The nonionic surfactant polyoxyethylene sorbitan monolaurate (Tween 20) and the cosurfactant n-pentanol were products from Fluka, Switzerland and Lancaster, England respectively. They were stated to be more than 99.5% pure. n-heptane was obtained from E. Merck, Germany. Curcumin, [1,7-bis(4-hydroxy-3-methoxy-phenyl)-1,6-heptadiene-3,5-dione] was a product from Sigma-Aldrich Chemicals Pvt. Ltd., USA. All the chemicals were used as received.

2.2. Methods

2.2.1. Phase manifestation. In the entire work, three different ratio of Tween 20 and n-pentanol (S:CS, w/w) were used (1:0.5, 1:1 and 1:2) to explore the effect the different amount of cosurfactant in the μE system. The pseudo ternary phase diagram comprising [b4mim][BF_4]/(Tween-20+n-pentanol)/n-heptane was constructed by the method of titration and through visual inspection. Known amount of Tween 20 + n-pentanol and n-heptane or IL were taken in stoppered test tube. IL or n-heptane was then progressively added using a

Hamilton (USA) micro syringe under constant stirring[261,262]. The whole process was carried out in a controlled temperature bath (298±0.1K). The phase boundary was detected through the appearance of turbidity. The same experiment was carried out for a number of compositions by varying the amount of oil or IL as well as in different S/CS ratio.

2.2.2. Dynamic light scattering (DLS) studies. DLS measurements were carried out using a Zetasizer Nano ZS90 (ZEN3690, Malvern Instruments Ltd, U.K.). A 0.2M Tween 20 mixed with n-pentanol in n-heptane was used for such studies. Tween 20 / n-pentanol ratio (w/w) were the same as in phase manifestation studies. A He-Ne laser of 632.8 nm wavelength was used and the data were collected at 90^0 angle. Temperature was controlled by inbuilt Peltier heating-cooling device with an accuracy of ±0.05K. The instrument actually measures the diffusion coefficient (D) from which the diameter of the microemulsion droplet (d) was determined according to Stokes-Einstein's formalism[261,262]:

$$D = \frac{kT}{3\pi\eta d} \qquad \textbf{(2.1)}$$

where, k, T and η indicate the Boltzmann constant, temperature and viscosity respectively.

2.2.3. Viscosity measurement. Viscosity of μE systems were measured with an LVDV-II+PCP cone and plate type roto-viscometer (Brookfield Eng. Lab, USA). The same set of solution, as used in the DLS measurements, were employed for size analyses. Temperature was controlled by a cryogenic circulatory water bath with a precision of ±0.1K (DC-1006 M/S. Hahntech Corporation, S. Korea). Shear rate (D) was varied in the range 20 – 60 sec^{-1} with an increment of 5.0 sec^{-1} in each step. Zero shear viscosity (η) was obtained using the relation $\eta = \tau / D$ [261,262], where τ indicates the shear stress.

2.2.4. Spectral studies.

Absorption spectra. UV-visible absorption spectra of the μE systems in the absence and presence of curcumin were recorded on a UVD-2950 spectrophotometer (Labomed Inc., USA) in the range 200-400nm using a matched pair cell of 1.0cm path length. While recording the spectra of the IL comprising systems, corresponding surfactant solution without IL was used as reference. Corresponding IL-in-oil μE without the dye curcumin was used as reference for recording the spectra of curcumin comprising systems. The overall concentration of curcumin was always kept constant at 10 μM. Initially, required amount of curcumin in methanol-chloroform (1:3 v/v) was taken in a test tube. The solvent was evaporated under vacuum. μE of known composition was then added and homogenized by keeping the solution in an ultrasonic water bath. It is to be mentioned that curcumin is insoluble in n-heptane. Therefore it could be assumed that the dye molecules reside in the polar domain.

Emission spectra. Steady state fluorescence spectroscopic measurements were carried out using a bench-top spectrofluorimeter (Quantamaster-40, Photon Technology International Inc, NJ, USA). The steady state emission spectra was recorded in the range 400-650nm with an excitation of curcumin at 426nm.

To know about the microviscosity of the solvent surrounding the probe molecule, steady state anisotropy (r) values were determined using the following expressions[263]:

$$r = (I_{VV} - GI_{VH}) / (I_{VV} + 2GI_{VH}) \quad \textbf{(2.2)}$$

and,

$$G = I_{HV}/I_{HH} \quad \textbf{(2.3)}$$

where, I_{VV}, I_{VH} are the intensities obtained with the excitation polarizer oriented vertically and the emission polarizer oriented vertically and horizontally respectively; I_{HV} and I_{HH} refer to the similar parameters as above for the horizontal positions of the excitation polarizer. In case of anisotropy measurements, the fluorescence data were collected at an emission wavelength (λ_{em}) of 550 nm. Further details are available in literature[263]. Both the absorption and fluorescence spectra were recorded at ambient but controlled temperature.

3. Results and discuccions

3.1. Phase manifestation. From the application point of view, construction of the phase diagram is a primary task towards a μE formulation. Figure 2.1 describes the pseudo ternary phase diagram of [b4mpy][BF_4]/(Tween-20+n-pentanol)/n-heptane systems at different surfactant-cosurfactant ratio (w/w).

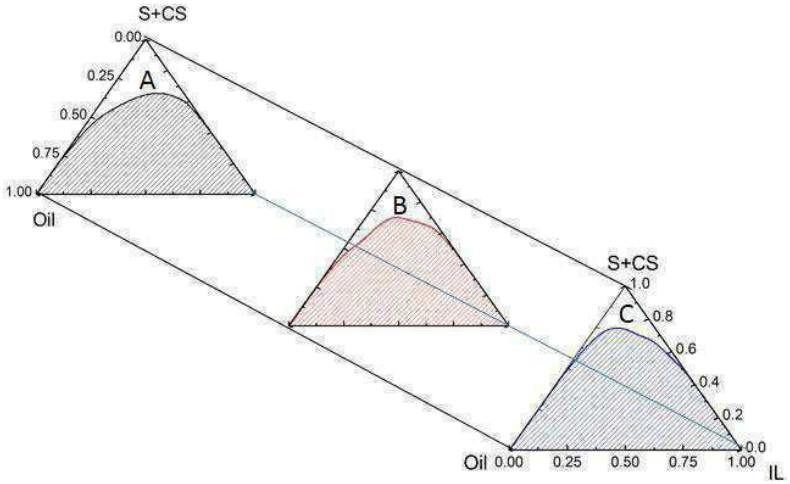

Figure 2.1. Pseudo ternary phase diagram of [b4mpy][BF_4]/(Tween-20+n-pentanol)/n-heptane at different Tween 20 (S) / n-pentanol (CS) ratio (w/w): A, 1:0.5; B, 1:1 and C, 1:2. n-heptane was used as oil (Oil) and [b4mpy][BF_4] was used as the ionic liquid (IL). Temp. 298 K.

For simplicity, only the clear single phase (1Φ, un-shaded portion) and the two phase (2 Φ, shaded portions) regions were identified. Area under the clear and turbid regions were evaluated by the method of weighing the individual areas as previously described[261]. The area under clear zone decreased with increasing amount of cosurfactant. It appeared from the results (as explained through Figure 2,) that the area under the clear zone was maximum in the absence of cosurfactant as the % area of clear zone followed a 2^0 polynomial relation with the weight% of n-pentanol (w_{cs}):

$$\% \text{ area of clear zone} = 20.34 - 8.46 \times w_{CS}\ \% + 1.61 \times (w_{CS}\ \%)^2 \qquad \textbf{(2.4)}$$

It means that in the absence of n-pentanol, % area under clear and turbid zones would be 20% and 80% respectively. However, it was impossible to obtain a stable μE without the aid of cosurfactant. Hence, unlike the other systems[211,225], use of cosurfactant was mandatory in order to achieve a stable μE. Use of cosurfactant for single tailed surfactants is not uncommon in literature[261,262]. It is known that cosurfactant can assist the surfactant molecules in a reducing

interfacial tension between two immiscible liquids. Present set of results were also comparable with the similar components where water[261] and another ionic liquid 1-butyl-3-methyl imidazolium methanesulphonate [bmim][MS][262] were used. Compared to the other systems, the %area under clear zone was less which could be due to the greater iconicity of the components in the polar domain, compared to water as well as [bmim][MS]. Although the cation $[b4mpy]^+$ was less polar, however, the BF_4^- ion played a significant role in enhancing the turbidity of the present μE.

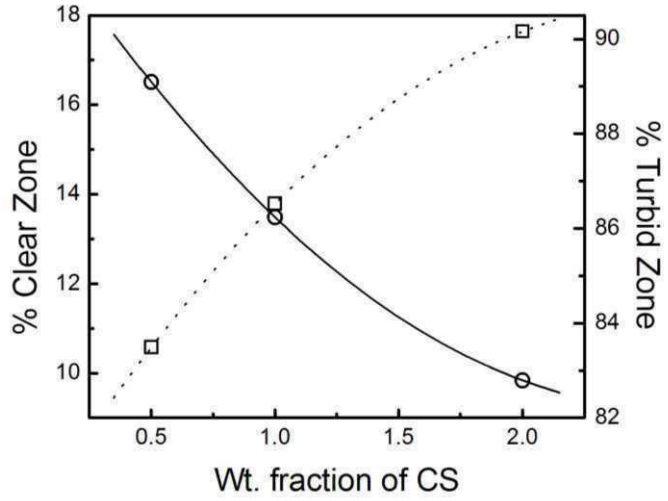

Figure 2.2. *Variation in the area under clear (O) and turbid (□) regions with the weight* fraction of n-pentanol (CS) for [b4mpy][BF_4]/(Tween-20+ n-pentanol)/n-heptane pseudo-ternary system at 298 K.

3.2. Dynamic light scattering (DLS) and viscosity studies. DLS studies on μE can provide information on its size, its distribution, and hence the polydispersity index. Variation in the diameter of [b4mpy][BF_4]/(Tween 20+n-pentanol)/n-heptane IL-in-oil μE with the volume fraction of the IL (φ_d) at 308 K have been graphically presented in Figure 2.3 at different surfactant cosurfactant ratio (panel A).

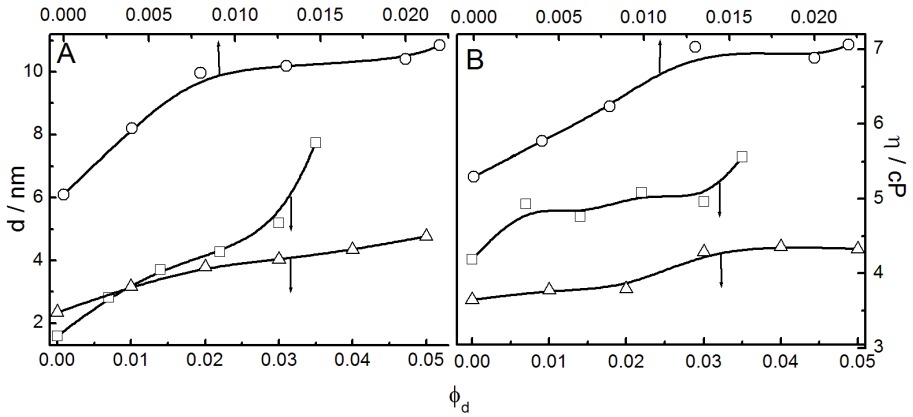

Figure 2.3. Variation in d*iameter (d) and viscosity (η) of [b4mpy][BF$_4$]*/(Tween-20+ n-pentanol)/n-heptane IL-in-*oil microemulsion system with the volume fraction (*φ_d) of [b4mpy][BF$_4$]. Temp. 308 K. Tween 20/ n-*pentanol ratio (w/w): O, 1:0.5; □, 1:1 and* Δ, 1:2.

Droplets were fairly monodispersed as revealed through its size distribution shown in Figure 2.4.

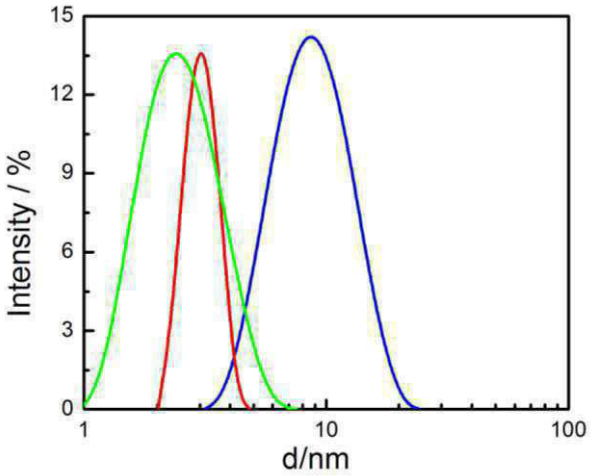

Figure 2.4. Dependence of size distribution on Tween20/n-pentanol (S/CS) ratio for [b4mpy][BF$_4$]/(Tween-20+n-pentanol)/n-heptane IL-in-oil microemulsion systems. Tween 20/ n-pentanol ratio (w/w): 1:0.5, blue line; 1:1, red line and 1:2, green line.

As under similar condition, there is a correlation between the size of droplets and viscosity, hence the viscosity (η) – φ_d profile for the similar systems were also presented in the same Figure (panel B). Experiments were carried out in the temperature range 293 – 323K and the results at 308K (intermediate temperature) have been shown as representative. Results for the other systems have been presented in the supplementary section. Size of the μE droplets increased with increasing volume fraction (φ_d) of IL. Increase in size with the

increasing volume of the dispersed phase is not an uncommon phenomena and have also been observed by others[113,176,211,225,262]. Size - φ_d profiles were found to be dependent on the S/CS ratio. Size of the μE droplet comprising Tween 20 and n-pentanol in a mass ratio of 1:0.5 was found to be larger than 1:1 which was even larger than 1:2. Results clearly indicate that cosurfactants caused size constriction. In a previous report we have shown that for the polyoxyethylene head group comprising surfactants (Tween 20), increased amount of cosurfactant can lead to the formation of larger number of droplets[261,262]. For a fixed amount of surfactants, increasing number of droplets would result only if the size is decreased. Such an observation further supports the decrease in the area under clear region with increasing amount of cosurfactant. While giving a closer look at the panel A of Figure 3 it was observed that for an S / CS ratio of 1:0.5, size of the μE droplet increased linearly up to φ_d=0. 01, after which a change in the slope of increment profile appeared. The results imply that the existence of free/unbound ILs was possible only after φ_d=0. 01. Before the said volume fraction of IL, it is mainly used up in coordinating with the polyoxyethylene head groups of Tween 20[262]. Almost twice the volume of IL was required for the attainment in the breakpoint in the μE with S/CS ratio 1:1 (φ_d=0.02). However, for such systems the slope after the threshold was higher. Such an ambiguity is beyond explanation with the present level of knowledge. Further studies are warranted to address this issue. d vs. φ_d profile for the systems with surfactant/cosurfactant ratio 1:2 was almost linear. d-φ_d profile for all the systems at different temperature have been graphically presented in Figure 2.5. It could be concluded from the results that with the increasing amount of cosurfactant (n-pentanol), size increment with the volume fraction becomes less sensitive. The viscosity profile for the similar systems followed the same trend line as in the variation of droplet size with φ_d. Thus, it could be concluded that variations in the viscosity with φ_d was a consequence of the size variation in the microemulsion droplets. In order to understand the effect of temperature, size measurements were also carried out at different temperatures (293, 298, 303, 308, 313, 318 and 323K).

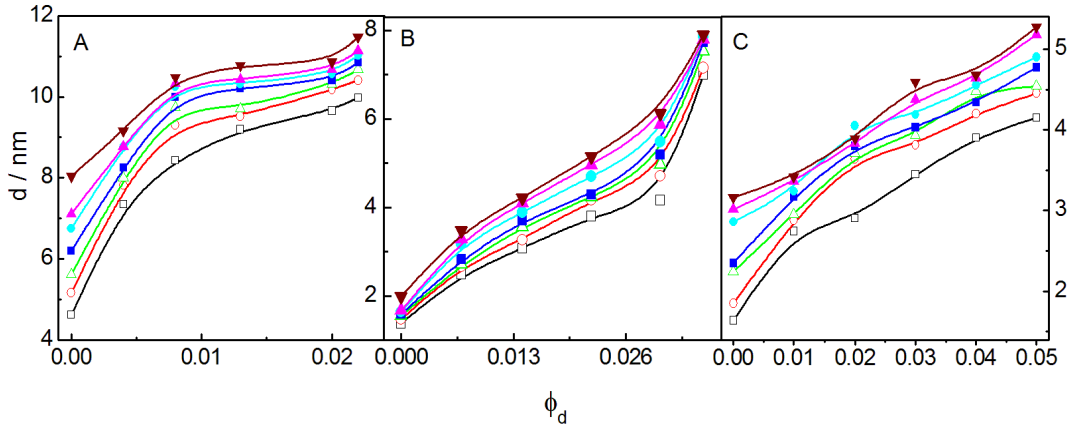

Figure 2.5. Variation in size (d) of [b4mpy][BF_4]/(Tween-20+n-pentanol)/n-heptane IL-in-*oil microemulsion systems with the volume fraction* (φ_d) of IL. Tween 20/n-pentanol *ratio (w/w): A, 1:0.5; B, 1:1 and C, 1:2. Temp. (K):* □, *293;* O, *298;* Δ, *303;* ■, *308;* ●, *313;* ▲, *318 and* ▼, *323.*

While considering the size variation (as shown in Figure 2.6 panel A), it was observed that for all the systems d vs. temperature profiles were almost linear. The parallel nature of the lines imply that the effect of temperature was independent of S/CS ratio. Although there occurred size increment with increasing temperature, however, reverse trends were recorded for the viscosity for all the systems. Results for viscosity-temperature profile for the three combinations at φ_d= 0.02 have been shown in Figure 2.6 (panel B).

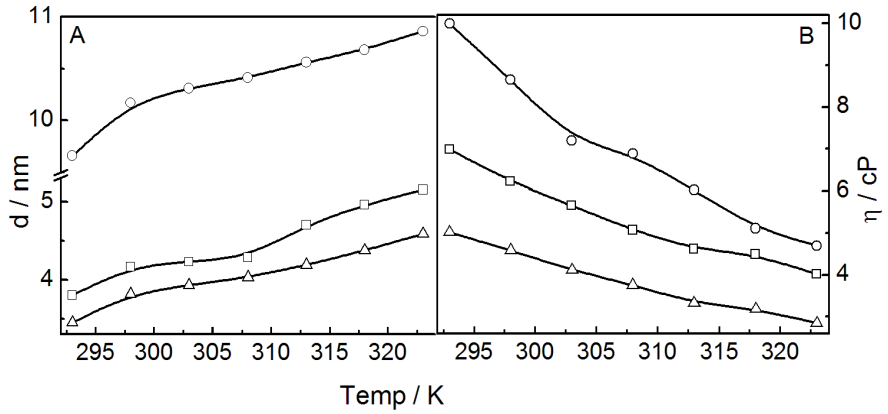

Figure 2.6. Variation in the size (A) and viscosity (B) with temperature for [b4mpy][BF_4]/(Tween-20+n-pentanol)/n-heptane IL-in-oil microemulsion at different Tween 20/n-pentanol ratio *(S/CS, w/w): O, 1:0.5;* □, *1:1 and* Δ, *1:2. 0.2 M Tween20 was used in each case where the volume fraction* (φ_d) of IL was kept constant at 0.02.

Decrease in viscosity with increase in temperature is a common phenomenon for Newtonian fluids. In the present set of studies, increase in droplet size was overshadowed by the increase in the fluidity of the medium. For

all the three systems, viscosity decreased almost linearly with increasing temperature, although the slopes were different for the different systems. Differences in the slopes were due to the differences in the rigidity of the μE droplets. Systems with larger amount of cosurfactant are expected to form more rigid structures. By suitably analyzing the viscosity data, thermodynamic parameters, viz., changes in specific heat capacity (ΔCp), activation enthalpy (ΔH*), free energy (ΔG*) and entropy (ΔS*) were evaluated. The activation enthalpy for the viscous flow and the associated entropy change could be expressed by the following equations [127]:

$$\eta = (\frac{hN}{V}) e^{\Delta H^*/RT} e^{-\Delta S^*/RT} \quad \textbf{(2.5)}$$

The logarithmic form of equation 1 could be expressed as:

$$\ln\eta = \left\{\ln\left(\frac{hN}{V}\right) - \frac{\Delta S^*}{R}\right\} + \frac{\Delta H^*}{RT} \quad \textbf{(2.6)}$$

h, N, V are Plank's constant, Avogadro's constant and molar volume respectively. R and T have their usual significances. From equation (2.2), one can obtain ΔH^* values from the slope of ln η vs T^{-1} plot. ln η was found to vary with T^{-1} in a binomial way; hence one can derive ΔH^* from it's differential with respect to temperature in the following way:

$$\ln\eta = a + bT + cT^2 \quad \textbf{(2.7)}$$

Therefore,

$$\frac{d\ln\eta}{dT} = -\frac{\Delta H^*}{RT^2} = b + 2cT \quad \textbf{(2.8)}$$

Thus, knowing the value of 'b' and 'c' one can compute ΔH^* at different temperatures.

Change in heat capacity (ΔC_p) is related to ΔH^* as:

$$\Delta C_p = \frac{d(\Delta H^*)}{dT} = -2RT(b + 3cT) \quad \textbf{(2.9)}$$

Therefore, changes in Gibb's free energy for activation could be expressed as:

$$\Delta G^* = -RT \ln\frac{\eta V}{hN} \quad \textbf{(2.10)}$$

Once ΔH^* and ΔG^* are known, the ΔS^* value could be calculated easily according to the following expression:

$$\Delta S^* = \frac{\Delta H^* - \Delta G^*}{T} \qquad \textbf{(2.11)}$$

Some of the representative results are summarized in Table 2.1. While considering the changes in the standard enthalpy (ΔH^*), it was observed that for all the systems ΔH^*decreased with increase in the volume fraction (φ_d) of the dispersed phase. For the systems comprising surfactant and cosurfactant in a ratio of 1:0.5 and 1:1 (w/w), the ΔH^*values were mostly negative, which mean that the process of flow was exothermic in nature [114,127]. On the other hand ΔH^* for the system with surfactant cosurfactant ratio 1:2 (w/w) the values were mostly positive, the difference in rigidity and subsequent viscosity attributed to such variation. While considering the variation in the ΔC_p with volume fraction, it was observed that the ΔC_p attained more negativity with increase in volume fraction. As with the increase in size droplets become less rigid, hence ΔC_p becomes more negative. The negative value of ΔS^* indicates the non-spontaneity of the flow processes.

Viscosity variation for all the systems at different volume fractions and temperature have also been graphically presented in Figure 2.7.

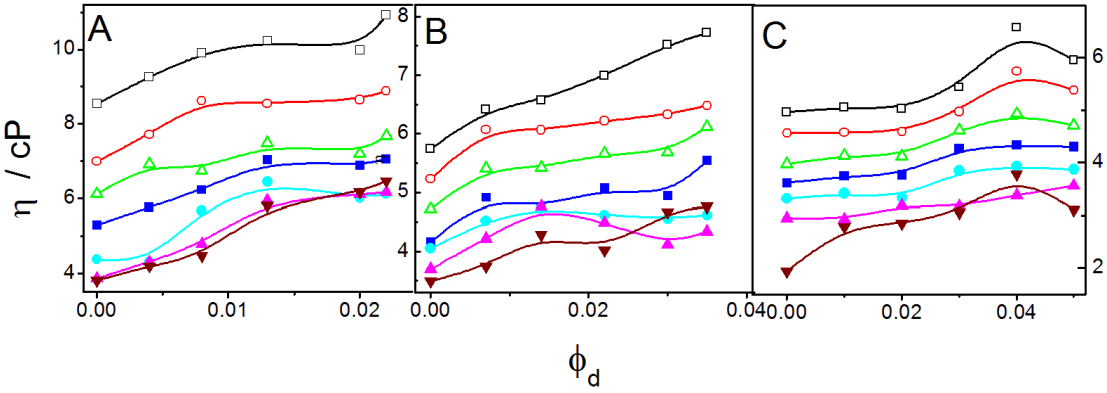

Figure 2.7. *Variation in viscosity (η) of [b4mpy][BF$_4$]*/(Tween-20+n-pentanol)/n-heptane IL-in-oil microemulsion *with the volume fraction (φ_d)* of IL. Tween 20/n-pentanol *ratio (w/w): A, 1:0.5; B, 1:1 and C, 1:2. Temp. (K): □, 293; O, 298; Δ, 303; ■, 308; ●, 313; ▲, 318 and ▼, 323.*

Table 2.1. Representative viscosity derived energetic parameters for [b4mpy][BF_4]/(Tween-20+n-pentanol)/n-heptane IL-in-oil microemulsion system.

Tween 20 / n-pentanol	**φ_d**	**ΔH^*(kJ mol^{-1})/ΔC_P(kJ mol^{-1}) / -ΔG^*(kJ mol^{-1})/ ΔS^*(J $k^{-1}mol^{-1}$) at different temperature (in K)**						
		293	**298**	**303**	**308**	**313**	**318**	**323**
1:0.5	**0.000**	-1.18/-0.95/-0.14/-3.55	-1.24/-0.99/-0.15/-4.27	-1.02/-0.17/-1.3/-1.54	-1.36/1.05/-0.19/-3.28	-1.09/-0.19/-1.43/-4.61	-1.12/-0.20/-1.50/-5.43	-1.16/-0.25/-1.58/-3.55
	0.004	-1.52/-1.20/-0.27/-3.66	-1.60/-1.25/-0.27/-4.46	-1.29/-0.27/-1.68/-1.64	-1.33/-0.27/-1.76/-3.52	-1.37/-0.27/-1.85/-4.97	-1.42/-0.27/-1.94/-5.81	-1.46/-0.28/-2.04/-3.66
	0.013	-1.56/-2.67/-0.60/-3.80	-1.65/-2.76/-0.60/-4.83	-2.85/-0.61/-1.73/-1.92	-2.95/-0.62/-1.82/-3.90	-3.04/-0.62/-1.91/-5.58	-3.14/-0.63/-2.00/-6.59	-3.24/-0.64/-2.10/-3.80
	0.022	-3.18/-3.25/-1.59/-4.09	-3.34/-3.37/-1.61/-5.25	-3.48/-1.64/-3.51/-2.17	-3.60/-1.66/-3.69/-4.31	-3.71/-1.68/-3.87/-6.26	-3.83/-1.71/-4.06/-7.39	-3.95/-1.74/-4.26/-4.09
1:1	**0.000**	-0.57/-0.50/-0.03/-1.84	-0.52/-0.06/-0.60/-1.81	-0.54/-0.08/-0.63/-1.83	-0.56/-0.08/-0.66/-1.88	-0.57/-0.09/-0.69/-1.91	-0.59/-0.09/-0.72/-1.97	-0.61/-0.11/-0.76/-2.01
	0.007	0.32/-0.58/-0.06/-1.30	-0.60/-0.07/0.34/-1.38	-0.62/-0.08/0.36/-1.47	-0.64/-0.09/0.38/-1.54	-0.66/-0.11/0.40/-1.63	-0.68/-0.14/0.41/-1.73	-0.71/-0.15/-0.43/-1.80
	0.014	-1.14/-0.80/-0.18/-3.28	-0.82/-0.21/-1.20/-3.32	-0.87/-0.23/-1.26/-3.40	-0.90/-0.26/-1.33/-3.47	-0.93/-0.31/-1.39/-3.45	-0.97/-0.33/-1.46/-3.55	-1.14/-0.36/-1.53/-3.62
	0.030	-2.65/-2.71/-0.59/-7.04	-2.80/-0.59/-2.78/-7.32	-2.90/-0.61/-2.93/-7.65	-2.99/-0.62/-3.07/-7.94	-3.09/-0.64/-3.23/-8.29	-3.19/-0.65/-3.38/-8.59	-3.29/-0.66/-3.55/-8.94
1:2	**0.000**	-0.12/-0.39/0.12/1.74	-0.12/-0.40/0.12/1.74	-0.13/-0.41/0.13/1.78	-0.13/-0.41/0.14/1.79	-0.14/-0.42/0.14/1.79	-0.14/-0.43/-0.15/1.82	-0.14/-0.44/0.16/1.86
	0.010	-0.17/-0.40/0.26/2.25	-0.17/-0.41/0.28/2.32	-0.18/-0.42//0.29/2.34	-0.18/-0.43/0.31/2.40	-0.19/-0.44/0.32/2.43	-0.19/-0.46/0.34/2.52	-0.20/-0.46/0.36/2.54
	0.030	-0.32/-0.52/-0.93/-1.40	-0.34/-0.53/-0.98/-1.51	-0.35/-0.54/-1.03/-1.62	-0.38/-0.55/-1.08/-1.72	-0.39/-0.56/-1.13/-1.82	-0.42/-0.57/-1.18/-1.92	-0.43/-0.59/-0.24/-2.01
	0.050	-0.95/-0.63/0.16/2.70	-0.98/-0.71/0.17/2.95	-1.02/-0.79/0.18/3.20	-1.05/-0.81/0.19/3.25	-1.08/-0.83/0.20/3.29	-1.12/-0.88/0.21/3.43	-1.16/-0.91/0.22/3.50

3.3. Spectral studies. Spectroscopic investigation on μE using a suitable probe can provide information on the environment, viz., polarity, fluidity, extent of aggregation of the ionic liquid in μE. Substantial reports on such aspects are available in the literature[113,176,225,262]. For the present system as the ionic liquid itself exhibits UV-visible absorption band due to the presence of pyridinium ring, the μE was studied without any probe. Figure 2.8 describes the absorption spectra of [b4mpy][BF_4] confined in the polar domain at different volume fraction. Two distinct peaks, one at 280nm and another at 335 nm were recorded for the ionic liquid. The peak at 280nm was significantly more intense than the other. Intensity of both the bands increased with the increasing volume fraction (φ_d) of ionic liquid. Absorbance vs. φ_d profile for both the peaks have been graphically shown in the inset of Figure 2.8. An increment in the absorbance values were mostly linear except for the system with Tween 20/n-pentanol in a ratio of 1:0.5 (w/w). The results indicate that distinct structured aggregates were not formed at this composition. The combined phase manifestation, dynamic light scattering and viscosity data also supported such an analogy.

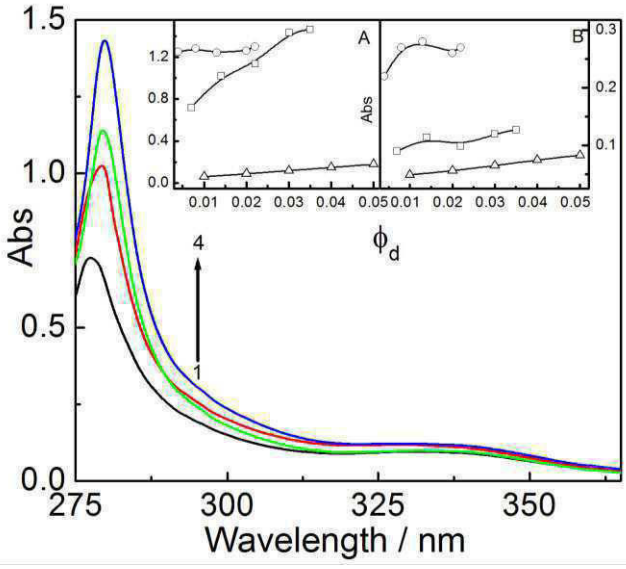

Figure 2.8. Absorption spectra of 1-butyl 4-methyl pyridinium tetrafluoroborate [b4mpy][BF_4] *confined in the polar domain at different volume fraction* (φ_d): 1, 0.007; 2, 0.014; 3, 0.022 and 4, 0.03. System without the IL was used as reference. Inset: Variation *in the absorbance at 283 nm (A) and 335 nm (B) with* φ_d.

Effect of IL was different for different Tween 20/ n-pentanol combinations; hence in order to understand the state of the IL, curcumin was used

as the fluorescent probe. Fluorescence spectra of curcumin confined in the polar domain of ionic liquid-in-oil microemulsion are shown in Figure 2.9. When excited at 426 nm, curcumin shows an emission maximum at ~500 nm. Results were found to be comparable with the previous reports[264]. A red shift in the emission maximum alongwith a decrease in fluorescence intensity with the increase in the φ_d value were noted (Inset: panel A, Figure 2.9). This was due to the localized dilution of the probe in the IL pool[113,133,205,262] . The progressive red shift (Inset: panel B, Figure2.9) in the emission maxima was due to the increased polarity of the domain with increasing volume fraction of the ionic liquid[262].

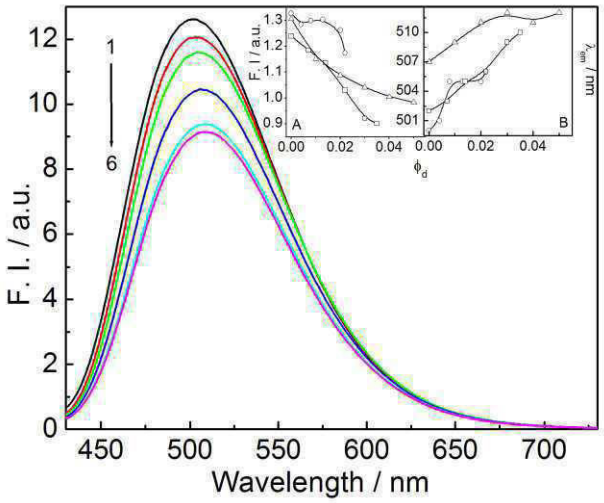

Figure 2.9. Emission spectra of 10 µM curcumin in [b4mpy][BF_4]/(Tween-20+n-pentanol)/n-heptane IL-in-*oil microemulsion at different volume fraction (φ_d) of IL.* φ_d values: 1, 0.00; 2, 0.007; 3, 0.014; 4, 0.022; 5, 0.03 and 6, 0.035. Tween 20/n-pentanol *ratio (w/w): l:1. Inset: Variation in the fluorescence intensity (panel A) and* λ_{em} (panel B) with φ_d for different Tween 20/n-*pentanol ratio (w/w): O, l:0.5; □, 1:1 and Δ, 1:2.*

To know the exact state of the solvent in the pool, fluorescence anisotropy studies on curcumin was carried out. Variation of fluorescence anisotropy value (r) with the volume fraction (φ_d) of ionic liquid have been graphically shown in Figure 2.10.

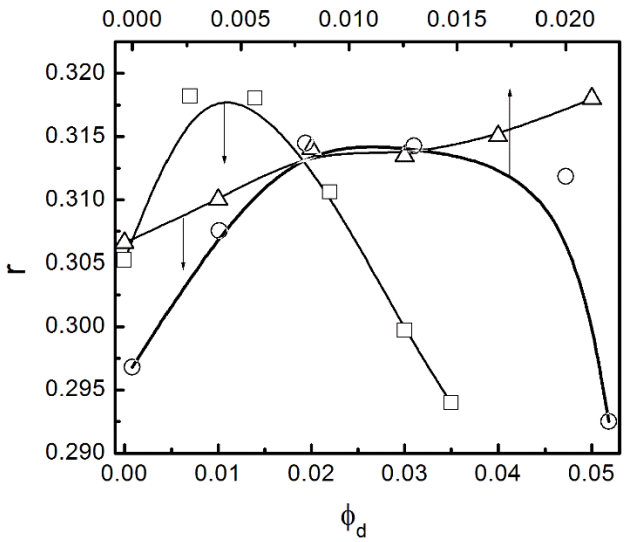

Figure 2.10. *Variation in the fluorescence anisotropy (r) for 10 μM curcumin with different volume fraction (φ_d)* of IL for [b4mpy][BF_4]/(Tween-20+ n-pentanol)/n-heptane IL-in-oil microemulsion system. Tween 20/n-*pentanol ratio (w/w): O, 1:0.5; □, 1:1 and* Δ, 1:2. Temp, 298K.

Anisotropy values passed through maxima with respect to the volume fraction of IL. Initially ILs are used up in coordinating with the oxyethylene head groups of Tween 20 for which structured entities are formed. At that stage the dye molecules did not have the freedom of movement. After the process of coordination of surfactant head group by IL cation was over, excess IL became free for which they can behave as bulk IL. Under that situation, the mobility of dye molecules became higher. This eventually led to the decrease in the fluorescence anisotropy values. A linear increase in the anisotropy value for the system comprising Tween20:n-pentanol in a 1:2 w/w ratio was due to the continued solvation of the cationic component of the ionic liquid, which was assisted by the presence of larger number of alkanols.

4. Summary and conclusion

Comprehensive studies on 1-butyl-4-methyl pyridinium tetrafluoroborate ([b4mpy][BF_4]) / (Tween 20 + n-pentanol) / n-heptane microemulsion system were carried out using a number of different physico-chemical techniques. Although the cosurfactant increased turbidity of the microemulsion, however, it was required for the attainment of stable microemulsion. Cosurfactant controlled

the curvature of the microemulsion droplets; it simultaneously also imparted better stability by solvating the cationic component of the ionic liquid. Larger number of droplet formation was aided by the cosurfactant. Sensitivity towards temperature decreased with increasing amount of cosurfactant, as revealed through the combined dynamic light scattering and viscosity measurements. Oxyethylene group of Tween 20 formed coordinate linkages with the IL cation, which resulted in the rigidity of the polar domain. The IL, in excess of the amount required for coordinating the surfactant head groups, behaved like the bulk component as revealed through the fluorescence anisotropy measurements. Electron microscopy and small angle neutron scattering studies could further shed light on the morphology of the microemulsion droplets, which are considered as the future perspective.

CHAPTER 3

CHAPTER 3

Physico-chemical investigations on the aqueous solution of an ionic liquid, 1-butyl-3-methylimidazolium methanesulfonate, [bmim] [MS], in the concentrated and dilute regime

Abstract

Physico-chemical properties of an ionic liquid (IL) 1-butyl-3-methylimidazolium methanesulfonate, ([bmim][MS]), in combination with water, were evaluated through the density, viscosity, surface tension, conductance, cyclic voltammetry, absorption and emission spectroscopic measurements. Binary mixtures were studied both in the water rich and [bmim][MS] rich regions (0.01 mM to 4.96 M). The static and dynamic properties of the binary combinations were evaluated through density and viscosity measurements. [bmim][MS] decreased the surface tension of water wherefrom the surface excess and area per molecule of the ionic liquid were determined at the air-liquid surface. Equivalent conductance of [bmim][MS] at infinite dilution was determined from the conductance data as the system obeyed Debye-Hückel-Onsager formalism. Cyclic voltammetry measurements revealed the formation of some metastable organized structures at specific compositions. Absorption and emission spectral behavior of the anionic dye eosin Y was found to be dependent on the concentration of [bmim][MS] in the water rich region. A significant change in steady state anisotropy and excited state life time of the fluorophore occurred above 1.0 M [bmim][MS] in water, which was correlated with the viscosity of the medium. It was concluded that aggregation of [bmim][MS] into micelle like aggregates above the specific concentration occurred, which significantly altered the different physiochemical parameters of [bmim][MS] binary mixture.

Colloids Surf., A **2012,** 404, 1-11

1. Introduction

Ionic liquids (IL) are neoteric and environmentally benign solvents for which they find many applications[179,265-272]. Being aprotic, less volatile and ionic in nature, ILs are used in energy production[270,273,274], process engineering[275], bioengineering[269], material engineering and sensor technology[271], electrochemical applications,[272,276] etc. As the ILs are environmentally benign solvent they act as catalyst and host for organic reactions[196,277]. Organic solvents have the limitations, viz, flammability and evaporation under warm temperature, or reactivity, which cause stability issues. That is why imidazolium based room temperature ionic liquids were mostly used for their nonvolatility, relatively high conductivity and low viscosity [278]. Because of the aforementioned applications, studies involving ILs are plenty in literature. [135,215]. Mukherjee et al. [279-281] have also studied ILs by spectroscopic techniques. Sum frequency generation studies on the ionic liquids 1-butyl-3-methylimidazolium dicyanamide ([bmim][DCA]) and 1-butyl-3-methylimidazolium methyl sulfate ([bmim][MS]) have been reported by Aliaga et al.[278], which could provide information on the interfacial behavior of ionic liquid. Use of different types of ILs have also been studied by Balducei et al.[273].

Physico-chemical investigations on the binary mixtures of ionic liquid and water have been studied by different researchers[196,270,274,282-292]. Kelkar et al. have theoretically investigated the effect of temperature and water on the viscosity behavior of 1-ethyl-3-methylimidazolium bis (trifluoromethanesulfonyl) imide [293]. Liu et al. have made a systematic investigation on the binary mixture of IL and water with the variation of both the cation and anion[294,295]. Reports are also available where different physico-chemical properties have been investigated for different ionic liquids in the aqueous dilute solutions[294-303].

Water is the ‘greenest’ solvent among all. Therefore, needless to mention that detailed investigation on IL-water binary mixtures have importance in terms of application and fundamental understanding. It is believed that evaluations of thermo-physical parameters on binary mixtures involving ILs are essential for optimally designing any industrial product[288,294,295]. Excess molar volume is an

important parameter in understanding the molecular level of interaction among the components in binary mixtures, which can be estimated by measuring the density. Viscosity is another important dynamic property of a solvent, both in its pure and mixed state with another solvent. When an IL is used as solvent, preferred viscosity is warranted in the lower range. On the other hand, a highly viscous IL mixture is preferred for lubrication and membrane preparation[293]. Therefore to tune an ionic liquid-water binary mixture, a detailed investigation on its viscosity in combination with another solvent is absolutely essential. Widegran et al.[292] have investigated the viscosity behavior of the three RTILs, where it was reported that there occurred a dramatic change in the viscosity of IL in presence of water. Conductivity of a solvent has vital importance, especially for ionic liquids as they are similar to the binary mixtures of organic solvents with an organic electrolyte[304]. Fitchett et al.[283] has found the molar conductance to be directly dependent on the viscosity of the medium. Studies on the conductance behavior of aqueous solution of IL in the dilute range are not plenty in literature. To check the validity of conventional electrochemical laws (Debye-Hückell-Onsager equation) and hence to find out the equivalent conductance of IL at infinite dilution, such studies are considered to be essential[288,294,295,305]. Similarity or difference in conductance behavior of IL with/from the conventional electrolytes can also be justified through such studies. Composition of an air-solution interface is always different from the bulk as the ILs having organic moieties, exhibit surface activity. Compared to the surface of pure IL, (IL+water)-air interface are less fairly understood[288,294,295,305,306]. As ILs have been used in many electro-chemical applications, hence cyclic voltammetric studies on the binary mixtures of ILs and water are considered to be important. Besides, such systems are advantageous to study as no carrier electrolyte is required [304,307]. Studies involving IL, interaction in the molecular level and polarity of the medium could be investigated through spectroscopic probing techniques. Solvation dynamics and subsequent characterization of solvents either in pure form or in the compartmentalized systems have been systematically investigated by different researchers[113,133,140,144,193,210,214,215,265,279,308-317]. To the best of our knowledge no systematic investigation on the absorption and emission behavior

of dye in bulk IL-water mixture over a wide concentration range has been performed using [bmim][MS].

According to Marciniak et al.[318] and Ventura et al.[291] it was proposed that the extraction capability of an ionic liquid depended on the hydrogen bond accepting strength of the anions, although detailed physico-chemical explanation behind such properties were not explained. According to Marciniak et al.[318] dearomatization can be influenced by the nature of anion in IL. Among different types of imidazolium based ionic liquids, not many works have been done with methanesulfonate anions[291,319]. Yang et al.[320] have compared the differences in the physico-chemical properties of IL comprising two different anions, viz., toluene-p-sulfonate and methanesulfonate. Khare et al.[293] has used ethyl methylimidazolium based ionic liquids with a number of anions and have found that methanesulfonate anions could act as a better stabilizing agent for in situ synthesized iron carbide nanoparticles. Rivera-Rubero[321] reported the anomalous behavior of MS containing ILs than the conventional anions. According to Fröba et al.[270,274], there could be existence of unlimited number of ILs considering the variation in the number of cation and anion and hence comprehensive physico-chemical investigations on all the ILs in their binary mixed states could not be investigated. However, to understand the structure-property relationship, such studies are warranted.

This present study focuses the investigations on the solution behavior of an ionic liquid 1-butyl-3-methylimidazolium methanesulfonate [bmim][MS] in water, over a wide concentration range, using different techniques. The investigation aims to derive the density, excess molar density and viscosity in understanding the synergistic and antagonistic behavior of all the combinations. Surface tension studies on aqueous solution of [bmim][MS] in the water rich region could evaluate the surface activity, surface excess and molecular area of the IL. Conductance measurements for all the combinations and cyclic voltammetry measurements in the IL rich region helped in understanding the states of aggregates in solution. Absorption and emission spectroscopic studies of an anionic xanthene dye eosin Y have been performed in the water rich region.

Fluorescence lifetime and anisotropy measurements could shed light on the viscosity of the media. Efforts have also been made to correlate the life time and fluorescence anisotropy with the experimentally determined viscosity. Also we intended to correlate the data of the binary mixture in the water rich region with the aggregation behavior of IL as there are several reports with conclude that [bmim] based ionic liquids can form micelle like aggregates in water after attainment of certain concentration[294,295,298,302,303,306,322]. The choice of this anion is intentional as the anion is an alkyl group containing simple inorganic ion. Our main aim is to use the binary mixture of [bmim][MS] and water in microemulsion of oil continuum. However due to relatively higher melting point, this ionic liquid, in its pure form, was thought to be not useful for practical purpose. Moreover, imidazolium based ionic liquid containing [MS] anion would be less toxic compared to the fluorine based ILs[320]. In a very recent study Stark et al.[323] has reported that 1-ethyl-3-methyl imidazolium methane sulfonate exhibits some unusual behavior in combination with water. It is reported there that this particular ionic liquid could deactivate water above a certain concentration even if water is present in high amount (upto50 mole %). In another work of Stark and Wassersch, it was reported that water molecules becomes deactivated below 50 mole % of water and in combination with [emim][MS]. The deactivation of water molecules was occured through a chemical reaction. In this reaction, 5-hydroxymethyl furfural could be obtained from an intramolecular condensation reaction of fructose; however, the reaction rate was slowed down significantly in presence of water. Nevertheless, water, when present in combination with an ionic liquid [emim][MS] at upto 50 mole %, could barely slow the reaction rate. The deactivation of water in terms of chemical reactivity was due to the formation of highly structured IL framework that physically separated water from the reactants. We also intended to check the validity of the generalization which subsequently have motivated us to undertake the physico-chemical investigations on the binary mixture of [bmim][MS] and water. Such study is believed to help in understanding the interaction between [bmim][MS] and water at the molecular level as well as the orientation of the IL at the air solution interface which, in turn, will put new physical insight into the area of IL comprising binary mixtures.

2. Experimental

2.1. Materials.

The ionic liquid (IL) 1-butyl-3-methyl-imidazolium-methanesulfonate [bmim][MS] was a product from M/S Sigma-Aldrich Chemicals Pvt. Ltd., USA. It was stated to be more than 99.5% pure. The IL was further thoroughly degassed at 333 K (60^{o}C) for a time period of 3h on a vacuum line. Double distilled water with a specific conductance of 2-4μS (at 298 K) was used to prepare the binary mixtures and also aqueous solution of [bmim][MS]. $K_4[Fe(CN)_6]$, used as an electrochemical probe, was purchased from E. Merck (India) Ltd., Mumbai, India. The dye eosinY (EY) sodium salt, was a product from E. Merck, Germany. It was used as received. The concentrated solution of dye was prepared by dissolving weighed amount in water. Working solutions were then prepared by proper dilution.

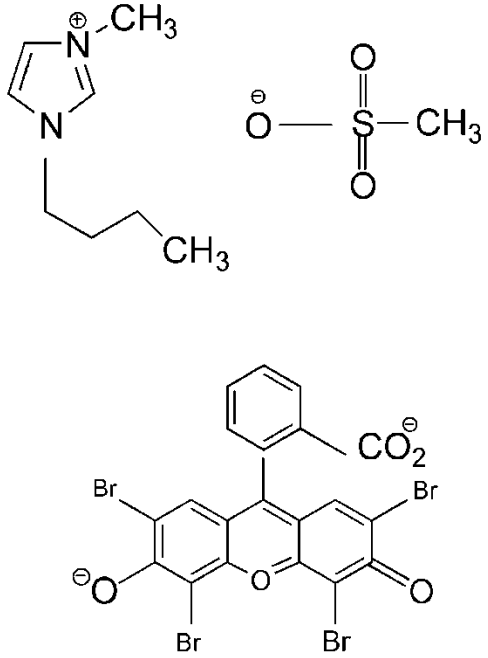

Scheme 3.1. Schematic structure of [bmim][MS] (top) and eosin Y (bottom).

2.2. Methods.

Binary mixtures of [bmim][MS] and water as well as the aqueous solution of the IL in the dilute to moderate concentration range were prepared by proper weighing. Two types of binary mixtures of [bmim][MS]+water have been used :

[bmim][MS] rich region where the mole fraction of [bmim][MS] were greater than 0.1 ($x_{[bmim][MS]}$ =0.2, 0.4, 0.5, 0.6, 0.8, 1.0). The molar concentration associated with the mole fractions are 3.69, 4.40, 4.58, 4.70, 4.86 and 4.96 M respectively. The second category was comprised of water rich regions ($x_{[bmim][MS]}$ <0.1) within a dilute concentration range of IL (0.01 M to 3.0 M). Henceforth, [bmim][MS]+water binary mixtures are categorized into two groups; (A) IL rich binary mixtures and (B) water rich IL solutions.

Density of [bmim][MS] rich binary mixtures (category A), were measured using DMA 4500-M densitometer (Anton Paar, USA), with a stated accuracy 5×10^{-5} g.mL^{-1}. Temperature during the measurements were controlled (± 0.05K) with a high precision Pt-resistance probe[274]. Densities of the binary mixtures at atmospheric pressure were recorded in the temperature range 298 to 323K with an interval of 5K. Viscosity was measured using a LVDV-II+PCP cone and plate type roto-viscometer (Brookfield Eng. Lab, USA). Temperature was controlled by a cryogenic water bath (of precision ±0.1K). Shear rates (D) was varied within the range (20 – 60 S^{-1}) and corresponding shear stress (τ) were recorded. Viscosity (η) was obtained at zero shear rates using the relation: $\eta = \tau/D$[324]. The uncertainties of the experimental density and viscosity were found to be less than 0.003 g.mL^{-1} and 0.01 mPa.s, respectively, and the deviations of V^E was less than 0.0005mL.mol^{-1} and 0.01mPa.s, respectively. Refractive indices of the binary mixtures were determined with an refractometer (Refracto 30GS, Mettler Toledo, Columbus,OH) with a stated accuracy of ±0.0005. Surface tension of the aqueous [bmim][MS] solutions were measured (measurable upto 1.0 M) with a du Noüy tensiometer (precission ± 0.1mN.m^{-1}) from Jancon, Kolkata, India. Concentrated aqueous [bmim][MS] solution was progressively added to 20 mL water kept in a thermostated double walled jacket. Solution was homogenized using magnetic stirrer and equilibrated for 15 min, prior to each measurement. Temperature was controlled at 298±0.05K by a cryogenic circulatory water bath. An average of three readings was considered. Conductance was recorded with EC-CON510/43S conductivity meter (Cyberscan, TDS/^{0}C/^{0}F, USA) at 298K. The solutions were kept in a double walled glass jacket. The cyclic voltammetric measurements were

carried out on a BAS (Bio Analytical Systems) Electrochemical Work Station, Epsilon (USA). The electrochemical measurements were conducted by using three electrode configurations which were a glassy carbon working electrode, an Ag/AgCl reference electrode and a platinum counter electrode. 1.0 mM $K_4[Fe(CN)]_6$ was used as an electrochemical probe. Scan rates were varied in the range of 50 – 100 $mV \cdot s^{-1}$. Visible absorption spectra of 10 μM aqueous solution of EY were recorded on a UVD-2950 Spectrophotometer (Labomed Inc., USA). Spectra were recorded in the range 400 to 600nm using matched pair quartz cell of 1.0cm optical path length. Water or [bmim][MS]+water solution were used as reference. Steady state and time resolved fluorescence spectroscopic measurements were performed using a bench-top spectrofluorimeter (Quantamaster-40, Photon Technology International Inc, NJ, USA). The fluorescent dye was excited at 500 nm (λ_{ex}) and emission spectra were recorded in the range 475nm to 675nm. Steady state anisotropy was determined using the following expressions[325]:

$$r = (I_{VV} - GI_{VH}) / (I_{VV} + 2GI_{VH}) \quad \textbf{(3.1)}$$

and, $$G = I_{HV}/I_{HH} \quad \textbf{(3.2)}$$

where, I_{VV}, I_{VH} are the intensities obtained with the extinction polarizer oriented vertically and the emission polarizer oriented vertically and horizontally respectively; I_{HV} and I_{HH} refer to the similar parameters as above for the horizontal positions of the extinction polarizer. Further details can be found in literature[325]. Motorized polarizers were used for such studies. Fluorescence lifetime of aqueous solution of EY in the absence and presence of the IL was determined from the fluorescence decay curve by Ströbe technique using a pulsed nano diode (Nano LED, light emitting device) as the light source at 500nm. Fluorescence decay curves were analyzed by Felix GX (version 2.0) software. Goodness of the fits were adjudged by the χ^2 values.[230,325,326]

3. Results and discussion

3.1.1. Density measurement. The density, viscosity and their derived data for the binary mixtures in the [bmim][MS] rich region are summarized in Table 3.1,

Figure 3.1 and also in the supplementary section. Figure 3.1 describes the density-composotion (concentration, C and mole fraction, x_{IL}) profile in the IL rich region, where it was found that density increased in a nonlinear fashion with increasing IL content. Initially the density increased rapidly upto 60 mole% (4.5 M) of [bmim][MS] after which the change was not so significant. Differences in the structure and packing of molecular components led to such variations[294,295,302,327]. Stark et al.[323] has proposed that in case of IL+water binary mixtures when the IL content is more than 50 mole%, highly ordered pseudo-lattice like structures are formed, as also proposed by Mendez-Morales et al.[328]. In the present case the same proposition was found to be valid.

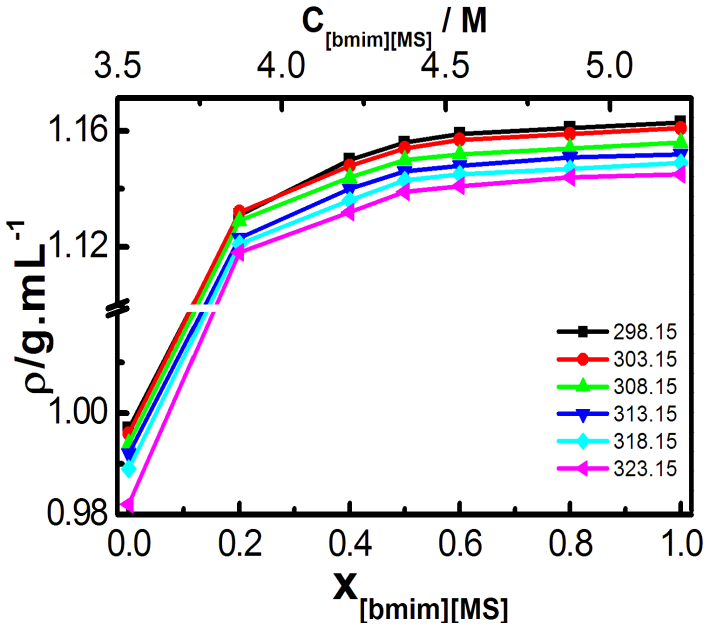

Figure 3.1. Variation of density (ρ) of [bmim][MS] +water binary mixture with the mole fraction (x) and concentration (C) of [bmim][MS] in the ionic liquid rich region. Temperatures (in K) are mentioned inside the Figure

Above 50 mole% of IL, the water molecules become less sensitive and could not perturb the pseudo-lattice like structured aggregates of IL. The variation of density with the molar concentration of [bmim][MS] was nonlinear in the entire studied concentration range as also reported previously[294,295]. Density decreased linearly with temperature obeying the following formalism:

$$\rho = \rho_0 + \rho_1 T \qquad \textbf{(3.3)}$$

The ILs were reported to be capable of forming micelle like aggregates. Above 60 mole% [bmim[MS], there will be sufficient number of such congregated species whose organizational packing would barely be perturbed by added water molecules. Additionally, the approach of Stark et al.[323] could be adapted by considering that above the stated composition, there occurred some "loosening effect" on the structure of the aggregates. We have studied mixtures at even lower concentrations. The behavior of [bmim][methyl sulphate] was also similar as ours, although the density of [bmim][methyl sulphate] were higher than that of [bmim][MS]. The temperature sensitivity on density (ρ) for [bmim][methyl sulphate] was less[329] [–(6.72± 0.0149) × 10^{-4}] g.m$L^{-1}^{o}C^{-1}$ than [bmim][MS] [–(7.263± 0.367) × 10^{-4}]g.m$L^{-1}^{o}C^{-1}$.

3.1.2. Variation of excess molar volume (V^E). The excess molar volume V^E was calculated from the experimental results according to the following equation [294,295]:

$$V^E = \frac{x_1M_1+x_2M_2}{\rho_M} - \frac{x_1M_1}{\rho_1} - \frac{x_2M_2}{\rho_2} \qquad \textbf{(3.4)}$$

where, x_1 and x_2 are the mole fractions; M_1 and M_2 are molar masses; ρ_1 and ρ_2 are the densities of pure IL and water respectively. The subscript M represents density of mixture. The deviation of V^E was approximately ±0.05% . The results are shown in Table 3.1. The V^E values at all the temperature passed through a minimum at x_{IL}=0.5, as shown in Table 3.1. Additionally, the variation of the excess molar volume with composition at different temperatures have been shown in Figure 3.2.

Table 3.1. Variation of density (ρ), excess molar volume (V^E) and viscosity (η) for the binary mixtures of [bmim][MS] and water at different temperature (T) in the [bmim][MS] rich region.

ρ / g mL^{-1} at different Temp.(in K)						
x_{IL}(Conc./M)	**298**	**303**	**308**	**313**	**318**	**323**
0.0(0.00)	0.997	0.996	0.994	0.992	0.989	0.982
0.2(3.69)	1.131	1.132	1.129	1.123	1.121	1.118
0.4(4.40)	1.150	1.148	1.144	1.140	1.136	1.132
0.5(4.58)	1.156	1.154	1.150	1.146	1.143	1.139
0.6(4.78)	1.159	1.157	1.152	1.148	1.145	1.141
0.8(4.86)	1.161	1.159	1.154	1.151	1.147	1.144
1.0(4.96)	1.163	1.161	1.156	1.152	1.149	1.145
V^E /mL.mol^{-1}						
0.2(3.69)	0.2845	0.1656	0.1033	0.2038	0.1615	0.1040
0.4(4.40)	-0.6091	-0.6007	-0.5741	-0.5569	-0.5605	-0.5875
0.5(4.58)	-0.7661	-0.6250	-0.6994	-0.6867	-0.6908	-0.7149
0.6(4.78)	-0.5922	-0.5873	-0.5711	-0.5610	-0.5644	-0.5838
0.8(4.86)	-0.2323	-0.2297	-0.3644	-0.3599	-0.2169	-0.3723
η / mPa.s(cP)						
0.0(0.00)	0.89	0.79	0.74	0.68	0.62	0.57
0.2(3.69)	10.52	8.79	7.29	6.76	3.08	2.33
0.4(4.40)	25.48	22.52	20.64	15.45	12.49	11.16
0.5(4.58)	37.18	29.48	25.01	19.99	16.75	13.91
0.6(4.78)	35.35	23.90	19.78	16.54	14.18	12.00
0.8(4.86)	63.49	49.14	38.41	31.60	25.28	20.99
1.0(4.96)	55.29	34.45	26.93	21.75	17.78	15.88

Values in the parentheses indicate the molar concentration of [bmim][MS] in water at 298K.

Table 3.2. Coefficients of density (according to eq. 3) and viscosity (according to eq. 5) for the binary mixtures of [bmim][MS]+water in the [bmim][MS] rich region.

Mole-fraction (Conc./M) of [bmim][MS]	ρ_1/ g.mL^{-1}	$10^{-3}x\,\rho_0$/ g.mL^{-1}	$10^3\,x\,\eta_0$ / mPa.s	E_a / kJ.mol^{-1}
0.0(0.00)	-(0.368 ± 0.02)	1.107		
0.2(3.69)	-(0.582 ± 0.07)	1.307		
0.4(4.40)	-(0.743 ± 0.03)	1.373	1.19	2.578
0.5(4.58)	-(0.730 ± 0.02)	1.375		
0.6(4.78)	-(0.739 ± 0.03)	1.380		
0.8(4.86)	-(0.704 ± 0.02)	1.372		
1.0(4.96)	-(0.726 ± 0.04)	1.380		

Values in the parentheses indicate the molar concentration of [bmim][MS] in water at 298K.

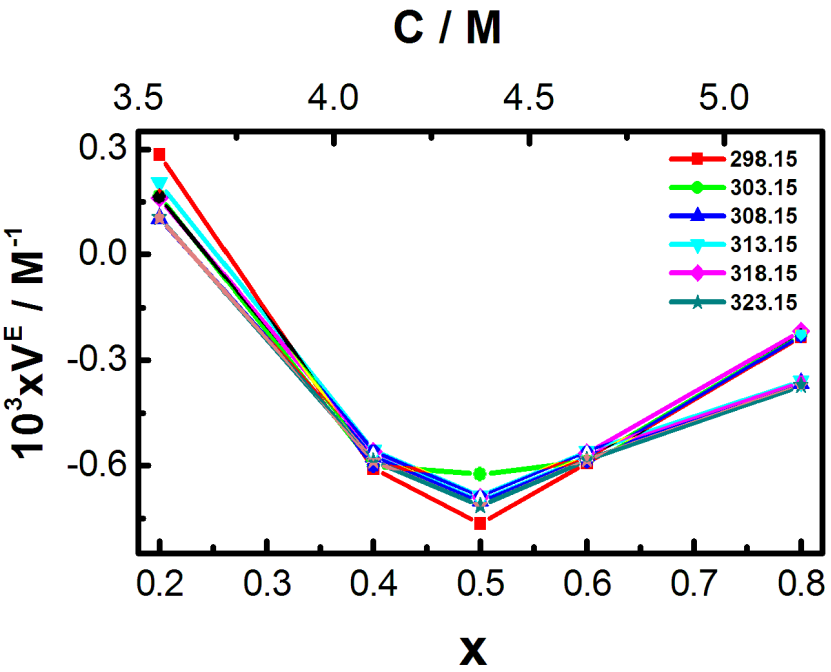

Figure 3.2. Variation of excess molar volume (V^E) of [bmim][MS] +water binary mixture with mole fraction (x) and concentration of [bmim][MS]. Temperature (in K) are mentioned inside the Figure

It was found that, at x_{IL}=0.2, the V^E for the mixture were higher than zero, which indicated a positive deviation from ideality. This finding is an indication of structural reorganization and the resulting swelling effect. The excess molar volume (V^E) was not significantly different for all the temperatures. This result indicates the quasi-ideal behavior of the binary mixture of IL+water from molar volume point of view (as the V^E values are lower than 0.5% of the ideal molar

volume value). The appearance of minima at x_{IL}=0.5 indicates formation of condensed structure. According to Rebello et al.[288] if there exist water-water and anion-cation interaction upon mixing of IL and water then there would be a significant reduction of coulumbic attraction. As a result, a size enhancement effect would occur. However, in our case, the V^E values were found to be negative for all compositions in general. This finding implies a strong associative interaction between water and [bmim][MS], except for the cases where the amount of IL is less (x_{IL}<0.2). The negative deviation from the ideality was an added contribution of the counter anion in [bmim][MS]. The methanesulfonate anion can form stronger hydrogen bond with water, compared to the other conventional anions, such as BF_4^-, halides. This unusual behavior has only recently been reported by Stark et al.[323] and Lehmann et al.[285]. A molecular organization of the components in binary mixtures have been proposed through some models[295,306,323,328].

3.2. Viscosity measurement. The $ln\ \eta$ - x_{IL} profile at different temperature are shown in the Figure 3.3. Results are also summarized in Table 3.1, 3.2 and 3.3. The measured viscosities in the studied concentration range followed Arrhenius formalism [232]:

$$\eta = \eta_0 e^{E_A/RT} \qquad \textbf{(3.5)}$$

where, E_A, R and T are the viscosity activation energy, universal gas constant and temperature in the absolute scale respectively. In a recent study of Stark et. al. it was proposed that the Arrhenius formalism for viscosity activation energy could be employed for [emim][MS]+water binary mixture. As the IL content in the system increased above 50 mole%, the micelle-like structures are stabilized and then the added water becomes deactivated, i.e., the structuredness is not perturbed due to physical separation of water from the reactants.

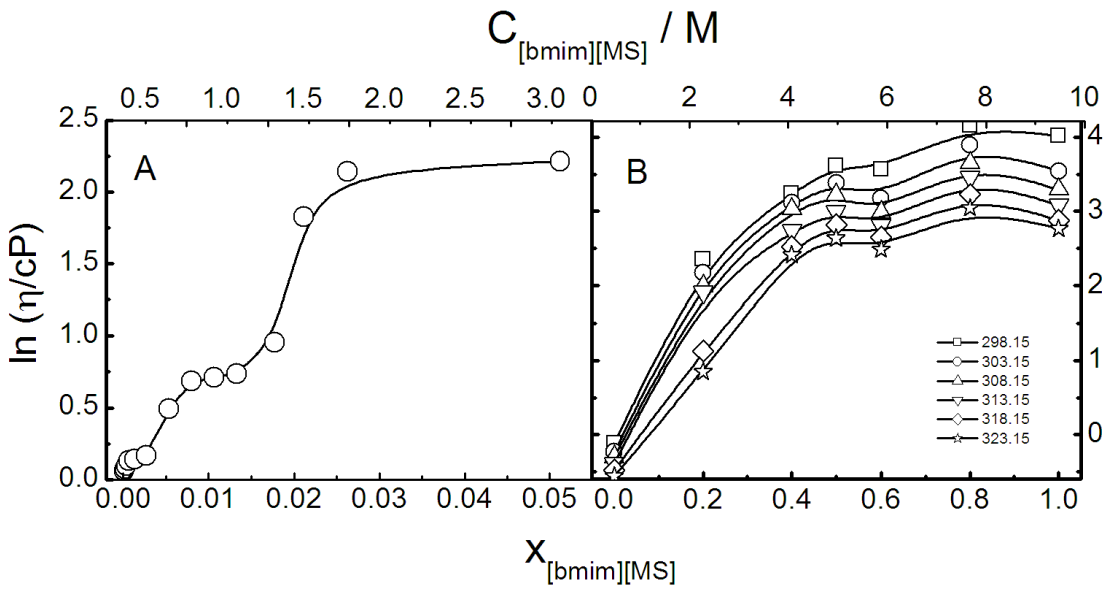

Figure 3.3. Variation of viscosity (η) of [bmim][MS] + water binary mixture with mole fraction ($x_{[bmim][MS]}$) and concentration (C) in the dilute and ionic liquid rich region. Temperatures (in K) are mentioned inside the Figure

The variation of viscosity with the molar concentration (as well as the mole fraction) was nonlinear in the entire studied concentration range. Additional viscosity and viscosity derived data are provided in the supplementary section. Similar reports are there for other binary mixtures[282]. Kelkar et al.[293] proposed that water, when present in combination with IL, could preferentially bind to more than one species and he also proposed that water preferentially associates with the anionic part of the ionic liquid. In the water rich region of the binary mixture, η – molar concentration of ionic liquid profile was found to be sigmoidal in nature indicating the formation of differently aggregated species. Viscosity initially increased mildly with the increase in concentration of ionic liquid in water. After 1.0 M, a significant rise in the viscosity occurred. According to the different available reports, it is proposed that above 1.0 M concentration, [bmim][MS] can form micelle like aggregates which are highly ordered. These aggregates could enhance the viscosity of the medium[185, 186, 188-189].

Table 3.3. Variation in different physico-chemical parameters for the aqueous solution of [bmim][MS] with its concentration in the water rich region at 298 K.

Conc. of [bmim][MS] / m M	Viscosity/ mPa.s	*Surface tension/mN.m^{-1}	Refractive index
0.16	0.88	70.6	1.350
0.316	0.97	70.5	1.351
0.63	0.98	70.3	1.351
1.25	1.03	70.2	1.352
2.50	1.03	69.7	1.352
5.00	1.06	68.9	1.352
10.00	1.08	64.5	1.352
20.00	1.10	61.7	1.352
37.50	1.14	58.2	1.353
75.00	1.15	55.8	1.354
150	1.18	48.2	1.356
300	1.64	45.3	1.360
450	1.98	44.4	1.367
600	2.04	43.8	1.370
750	2.09	43.2	1.373
1000	2.60	42.3	1.381
1200	6.20	-	1.387
1500	8.53	-	1.397
3000	9.12	-	1.435

*Surface tension of [bmim][MS] in water could not be determined at concentration higher than 1.0 M as the viscous solution interfered with the surface tension data.

Values of excess molar volume and viscosity deviations were fitted by Redlich-Kister type polynomial[232]:

$$Y = x_1 x_2 \sum_{k=0}^{m} A_k (x_1 - x_2)^k \qquad (3.6)$$

where, Y = V^E and the coefficients of A_k are parameters that were obtained by fitting the equations to the experimental values with a least square method. The correlated results for density, excess molar volume were defined by the following equation, and the results are shown in the Table 3.4 according to the following formalism[232]:

$$\sigma = \left[\frac{\sum(Y_{exp} - Y_{cal})^2}{n-p}\right]^{1/2} \qquad (3.7)$$

where, Y refers to ρ, η, V^E; the subscripts 'exp' and 'cal' represent the experimental value and the calculated value, respectively. 'n' is the number of data points; and 'p' is the number of coefficients.

Table 3.4. Fit Parameters in the Redlich-Kister Equation (eq. 6) for the density data.

Mole-fraction (Conc./M) of [bmim][MS]	a_0 / g.mL^{-1}	10^4 x a_1 / g.mL^{-1}
0.0(0.00)	1.107	-3.54
0.2(3.69)	1.307	-6.89
0.4(4.40)	1.373	-7.44
0.5(4.58)	1.375	-7.30
0.6(4.78)	1.380	-7.39
0.8(4.86)	1.372	-7.04
1.0(4.96)	1.380	-7.26

Values in the parentheses indicate the molar concentration of [bmim][MS] in water at 298K.

3.3. Refractive index. Variation of the refractive index with the molar concentration of [bmim][MS] in the water rich region has been shown in Figure 3.4. Refractive index increased linearly with the concentration of IL, like the previously reported systems [294,295]. Refractive index increased significantly above 5.0 mM [bmim][MS] in water. Change in the dielectric constant of the medium could account for such variation. The refractive index (RI) and density (ρ) obeyed the Newton's formalism:

$$\frac{RI-1}{\rho} = C \qquad \textbf{(3.8)}$$

where, C is constant, in the entire concentration range.

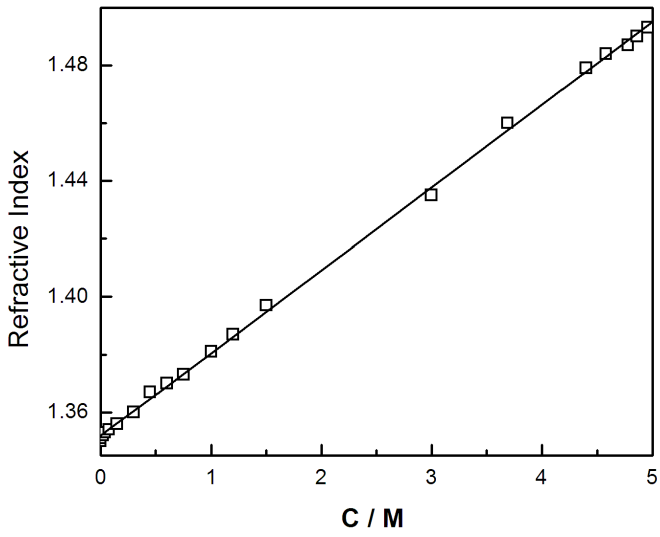

Figure 3.4. Variation in the refractive index of [bmim][MS] + water binary mixture with IL concentration (C) at 298 K.

Table 3.5. Polynomial regression coefficients for different physico-chemical parameters (according to eq. 7) of [bmim][MS]+water binary mixtures in the [bmim][MS] rich region.

Mole-fraction (Conc./M) of [bmim][MS]	σ_ρ (g.mL^{-1})/ σ_V^E(mL.mol^{-1})/σ_η (mPa.s)				
	298K				
	1^0	2^0	3^0	4^0	5^0
0.2(3.69)	0.048 / 0.127 /0.56	0.053 / 0.142/ 0.62	0.062 / 0.164 / 0.72	0.076 / 0.201 /0.88	0.107 / 0.285/ 1.25
0.4(4.40)	0.041/ 0.272/ 1.26	0.046/ 0.304/ 1.41	0.053/ 0.352/ 1.63	0.065/ 0.431/ 2.00	0.09 / 0.609/2.83
0.5(4.58)	0.036/ 0.451/ 4.06	0.040/ 0.504/ 4.45	0.046/ 0.582/ 5.25	0.057/ 0.713/ 6.43	0.080/ 1.007/ 9.09
0.6(4.78)	0.029/ 0.265/ 0.81	0.033/ 0.296/ 0.91	0.037/ 0.342/ 1.05	0.046/ 0.419/ 1.28	0.065/ 0.592/ 1.82
0.8(4.86)	0.015/ 0.104/ 8.53	0.016/ 0.116/ 9.54	0.018/ 0.134/ 11.01	0.023/ 0.164/ 13.49	0.033/ 0.232/ 19.08
	303K				
0.2(3.69)	0.048 / 0.074 / 0.57	0.054 / 0.083 /0.64	0.062 / 0.096 /0.73	0.076 / 0.117 /0.89	0.108 / 0.166 /1.27
0.4(4.40)	0.041/ 0.268/ 3.69	0.045/ 0.300/4.13	0.052/ 0.347/ 4.77	0.064/ 0.425/ 5.85	0.091/ 0.600/ 8.27
0.5(4.58)	0.035/ 0.279/ 5.30	0.039/ 0.312/ 5.93	0.045/ 0.361/ 6.85	0.055/ 0.442/ 8.38	0.078/ 0.625/ 11.86
0.6(4.78)	0.029/ 0.263/ 1.29	0.033/ 0.294/ 1.45	0.038/ 0.339/ 1.67	0.046/ 0.415/ 2.05	0.065/ 0.587/ 2.90
0.8(4.86)	0.014/ 0.103/ 9.58	0.016/ 0.115/ 10.71	0.018/ 0.133/ 12.36	0.023/ 0.162/ 15.15	0.032/ 0.229/ 21.42
	308K				
0.2(3.69)	0.047 /0.046 /0.59	0.053 / 0.052 /0.66	0.061 / 0.059 /0.76	0.075/ 0.073 /0.93	0.106 / 0.103 /1.32
0.4(4.40)	0.039 /0.257/ 4.21	0.044 / 0.287/4.71	0.051/ 0.331/ 5.43	0.062/ 0.406/ 6.66	0.087/ 0.574/ 9.42
0.5(4.58)	0.034/ 0.313/ 4.99	0.038/ 0.349/ 5.58	0.044/ 0.404/ 6.44	0.054/ 0.495/ 7.89	0.076/ 0.699/ 11.17
0.6(4.78)	0.028/ 0.255/ 1.48	0.031/ 0.286/ 1.66	0.036/ 0.329/ 1.92	0.044/ 0.404/ 2.35	0.062/ 0.571/ 3.33
0.8(4.86)	0.014/ 0.163/ 7.47	0.016/ 0.182/ 8.36	0.018/ 0.210/ 9.65	0.022/ 0.258/ 11.82	0.031/ 0.364/ 16.72
Mole-fraction (Conc./M) of [bmim][MS]	σ_ρ (g.mL^{-1})/ σ_V^E(mL.mol^{-1})/σ_η (mPa.s)				
	313K				
	1^0	2^0	3^0	4^0	5^0
0.2(3.69)	0.045/ 0.091 / 0.84	0.051 / 0.102 /0.93	0.058 / 0.117 /1.07	0.072 / 0.144 / 1.32	0.102 / 0.204 /1.87
0.4(4.40)	0.038 / 0.249/ 2.84	0.043/ 0.278/ 3.17	0.049/ 0.322/ 3.66	0.061/ 0.394/ 4.48	0.086/ 0.557/ 6.34
0.5(4.58)	0.034/ 0.307/ 3.92	0.037/ 0.343/ 4.38	0.043/ 0.396/ 5.06	0.053/ 0.486/ 6.20	0.075/ 0.687/ 8.77
0.6(4.78)	0.028/ 0.251/ 1.44	0.031/ 0.281/ 1.61	0.036/ 0.324/ 1.86	0.044/ 0.396/ 2.28	0.062/ 0.561/ 3.22
0.8(4.86)	0.014/ 0.161/ 6.28	0.016/ 0.0.179/ 7.03	0.018/ 0.207/ 8.11	0.022/ 0.254/ 9.94	0.031/ 0.359/ 14.06

			318K		
0.2(3.69)	0.044 / 0.072/0.43	0.049/ 0.081 / 0.48	0.057/ 0.093 / 0.56	0.070/ 0.114 / 0.68	0.099/ 0.161 / 0.97
0.4(4.40)	0.043/ 0.251/ 2.24	0.048/ 0.280/ 2.51	0.056/ 0.324/ 2.89	0.068/ 0.396/ 3.54	0.097/ 0.561/ 5.01
0.5(4.58)	0.033/ 0.308/ 3.37	0.036/ 0.345/ 3.77	0.042/ 0.398/ 4.36	0.052/ 0.488/ 5.34	0.074/ 0.691/ 7.55
0.6(4.78)	0.026/ 0.252/ 1.46	0.030/ 0.282/ 1.63	0.034/ 0.326/ 1.88	0.042/ 0.399/ 2.31	0.059/ 0.564/ 3.26
0.8(4.86)	0.014/ 0.097/ 4.88	0.015/ 0.108/ 5.46	0.017/ 0.125/ 6.31	0.022/ 0.153/ 7.73	0.031/ 0.217/ 10.93
			323K		
0.2(3.69)	0.043/ 0.046 /0.58	0.048/ 0.052 / 0.65	0.056/ 0.060/ 0.75	0.068/ 0.073/ 0.92	0.097/ 0.104/ 1.30
0.4(4.40)	0.036/ 0.263/ 1.99	0.040 / 0.294/ 2.24	0.046/ 0.339/ 2.58	0.057/ 0.415/ 3.16	0.081/ 0.587/ 4.47
0.5(4.58)	0.032/ 0.319/ 2.54	0.034/ 0.357/ 2.84	0.041/ 0.413/ 3.27	0.050/ 0.505/ 4.02	0.071/ 0.715/ 5.68
0.6(4.78)	0.026/ 0.261/ 1.00	0.029/ 0.292/ 1.12	0.034/ 0.337/ 1.29	0.041/ 0.413/ 1.58	0.058/ 0.584/ 2.24
0.8(4.86)	0.013/ 0.166/ 3.65	0.014/ 0.186/ 4.08	0.016/ 0.215/ 4.72	0.021/ 0.263/ 5.77	0.029/ 0.372/ 8.17

Values in the parentheses indicate the molar concentration of [bmim][MS] in water at 298K.

3.4. Surface tension. Because of the ionic liquids have organic moieties, they are expected to exhibit surface activity. The surface tension (γ) – concentration (C) profile for the binary mixture in water-rich region has been presented in Figure 3.5. It is clear from the Figure that the surface tension decreased only after 5.0mM (marked as point A in the Figure), while a second halt appeared at ~0.3 M. Similar types of variation for [bmim][BF_4] have been reported by Bowers et al.[305]. Initially, due to its high ionic nature, [bmim][MS] molecules do not spontaneously get adsorbed onto the surface. The second breakpoint confirms the changes in the structural organization through the formation of micelle like aggregates as proposed by several authors[200,284,290,294-296,298,299,301-303,305,306,322,323,330]. Stark et. al. modeled the structures of these ionic clusters in the absence and presence of water in their recent studies.

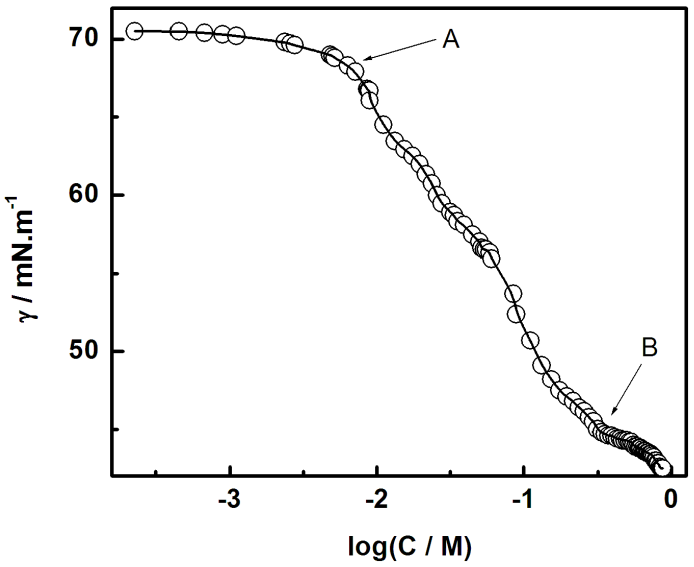

Figure 3.5. Variation of surface tension (γ) with the concentration (C) of [bmim][MS] in water at 298K. The points A and B correspond to [bmim][MS] concentration at 5.0 mM and 0.3 M respectively.

Gibbs formalism was found to be valid for aqueous ionic liquid solutions as:

$$\Gamma = -\frac{1}{2.303nRT}\left(\frac{d\gamma}{d\log a}\right) \qquad \textbf{(3.9)}$$

where, γ, a are surface tension, activity of the IL in water respectively and R, T have their usual meanings. Although strictly speaking, calculation of surface excess from the above equation needs to know the actual activity of [bmim][MS] in solution to be derived from concentration. However as in many cases activity of the specific solute solvent system cannot be accurately measured, hence in the dilute range activity was approximated as the concentration of the solute. In the present system, the surface excess was calculated by determining the slope of γ vs. log C plot (through linear regression) in the concentration range of 0.007mM to 0.20mM. The surface excess value for [bmim][MS] in the stated concentration range at the air-solution interface was found to be 1.23×10^{-6} mol.m^{-2}. This method of surface excess determination is quite reliable. However, no reported value for [bmim][MS] is available in the literature. The significant decrease after which there occurred a change in the slope of γ *vs log C* changed, was found to be (marked as point 'B' in Figure 3.4) 45mN m^{-1}. This value was found to be relatively higher than other [bmim] containing ionic liquids in their pure forms[330]. It may be mentioned that we could not measure the surface tension of [bmim][MS] in water at concentration higher 1.0 M as the stickiness of the interface interfered with the surface tension values. The surface excess value helped in determining the minimum area per ionic liquid at the surface [305]:

$$A_{min} = \frac{10^{18}}{N_A \times \Gamma_{max}} \qquad \textbf{(3.10)}$$

where, A_{min} was the minimum area per ionic liquid molecule at the air water interface, N_A was Avogadro constant and Γ_{max} was surface excess. For [bmim][MS], the A_{min} value was found to be 1.35nm^2.molecule^{-1}. The A_{min} value for [bmim][MS] was found to be higher than that from previous reports[305]. Sung et al.[290] has proposed a model depicting the orientation of 1-butyl-3-methylimidazolium tetrafluoroborate [bmim][BF_4] at the (IL+water)-air interface, where the anions are also associated with the cationic moiety. The larger size of methane sulfonate anion resulted in the larger area for the present IL. However, an additional sophisticated instrumentation technique, sum frequency generation spectroscopy, neutron reflectometry or elipsometry, etc., is warranted, and these studies are considered as future possibilities.

3.5.1. Electrical conductivity. It was found that molar conductance decreased with the increase in [bmim][MS] concentration in water (as shown in Figure 3.6). The decrease was significant up to 50 mole% of ionic liquid in combination with water; after that decrease in molar conductance was mild (panel A). It is anticipated that after 50 mole% of ionic liquid in the binary mixture, no significant structural alteration takes place. Considering the effect of temperature, it was found that the molar conductance increased with temperature. Increase in temperature results in the increase in ionic mobility. Also loss of structuredness led to the increased conductance at elevated temperature. Rise in molar conductance was significant for the binary mixtures containing lower amount ionic liquids. After 50 mole% [bmim][MS], molar conductance of the mixtures at different temperatures were not significantly higher. For ionic liquid containing 20 and 40 mole %, although there was a rise in molar conductance with temperature increase but no definite trend line was obtained. This suggests that orderedness of the structured species decreased with increase in temperature of these two systems.

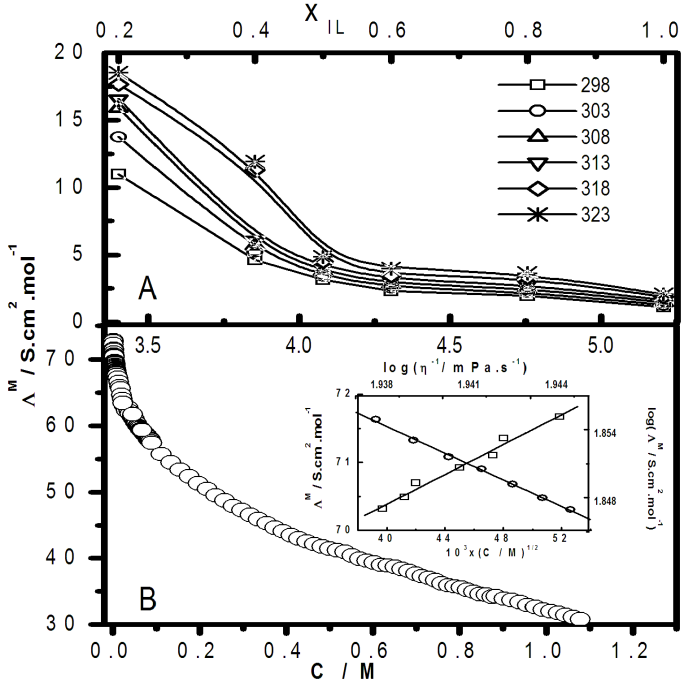

Figure 3.6. Variation of molar conductance (Λ^M) with A, mole fraction (x) in the [bmim][MS] rich region; B, concentration (C) of [bmim][MS] solution in water rich region. Inset of B: Λ^M - $C^{1/2}$ *(O) and log* Λ^M*-log* η^{-1} *(□) profile in the lower concentration* range of [bmim][MS]. Temp. 298K.

For 50, 60, 80 mole% and pure IL increase in molar conductance with temperature was more or less linear. The studies were found to be comparable with reports by other[324]. The increase in molar conductance with increase in temperature was due to increasing ionic mobility. It is to noted that the viscosity for 80 mole% [bmim][MS] containing mixture was higher than pure IL whereas the molar conductance for 80 mole% was also higher than that of pure one. This behavior was due to the formation of hydrogen bonded structures whereby a proton transfer mechanism could occur for 80 mole% ionic liquid containing mixture. We have plotted molar conductance with an intention to find out the limiting molar conductance. It may also be mentioned that conductivity-composition profile were similar as observed by others [331 332].

For aqueous dilute solution, the molar conductance decreased with the concentration and this decrease continued upto 4.2 mM [bmim[MS] (Figure 3.5B). Debye-Hückell-Onsager equation was found to be valid in the dilute concentration region upto 70mMof [bmim][MS] (as shown in the inset of panel B). The value for limiting molar conductance of [bmim][MS] was found to be 75.44 $S.cm^2.mol^{-1}$. To the best of knowledge no such reports of the limiting molar conductance of [bmim][MS] were found in the literature. According to the reports of Wang et al.[333], the limiting molar conductance of [bmim][Br] at 298K is 86.3 $S.cm^2.mol^{-1}$. Inset of Figure 3.5B ($log\ \Lambda^M$ vs $log\ \eta^{-1}$) profile has been shown, which is also known as Walden formalism [334-336]. It states that the product of the limiting molar conductance Λ^M and the viscosity η is constant for infinitely dilute electrolyte solutions and is expressed as:

$$\Lambda^M \eta = C = constant \qquad \textbf{(11)}$$

$$\log \Lambda^M = \log C + \log \eta^{-1} \qquad \textbf{(12)}$$

The Walden rule relates the ionic mobilities of the ions to the fluidity of the medium through which the ion moves [337]. The trend of the Walden plot was found to be linear which indicates the dependency of viscosity on molar conductance with a slope of 1.314 ± 0.081 and intercept of -0.700±0.158. Ion pair association is not possible at that dilute concentration range, but as concentration

goes up, the viscosity of solution increases for which the molar conductance decreased.

3.5.2. Cyclic voltammetric studies. A representative cyclic voltammogram with varied scan rate for an equimolar [bmim][MS]+water binary mixture at 298 K is shown in Figure 3.7. The electro chemical window was found to be dependent on scan rate. The peak current (i_P) varies linearly with the square root of the sweep rate (v) for a stable system[338]. However in the present case, linear variation in the i_p vs. $v^{1/2}$ profile were not observed for all the mixtures as shown in the inset of Figure 3.7. The i_p vs. $v^{1/2}$ profiles were linear for pure water and pure ionic liquid. Results clearly indicate the non-ideality in the mixing behavior of the components. Also it is evidenced from the Figure that all the combinations comprising less than 50 mole% ionic liquid were not well organized/structured. There were positive deviations from the linearity for all the mixtures (except the 1:4 mixture). As it has previously been mentioned that in case of binary mixtures, when water is present less than 50 mole%, then it cannot greatly affect the orderedness of the IL [323]. That is why the extent of deviation decreased with the increasing mole fraction of [bmim][MS].

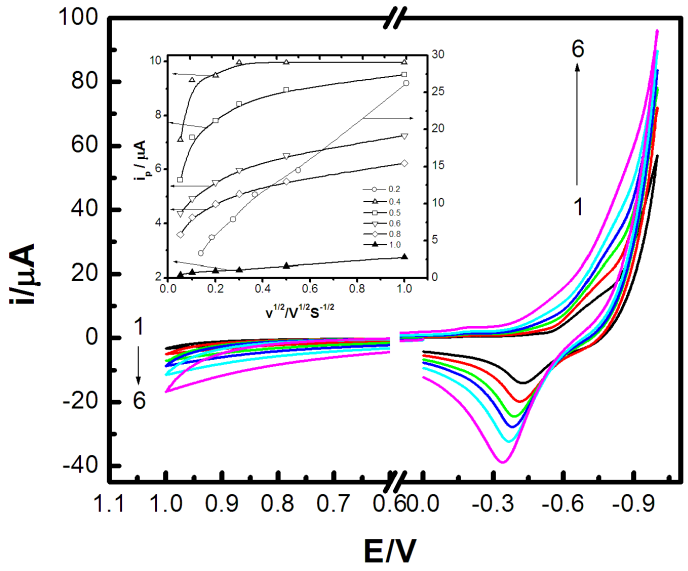

Figure 3.7. Electrochemical window for an equimolar mixture of [bmim][MS] + water at various scan rates and at 298K. Scan rates ($mV.s^{-1}$): 1, 25; 2, 50; 3, 100; 4, 200; 5, 500 and 6, 1000. 0.1 mM $K_4Fe(CN)_6$ was used as the probe. No carrier electrolyte was used as the medum was self conducting except pure water (1.0 mM KCl was used). Inset: Dependence of peak current (i_p) on the scan rate (v) for different [bmim][MS] + water mixtures. Mole fraction of [bmim][MS] are indicated inside the Figure

3.6. Effect of [bmim][MS] on the spectral behavior of eosinY (EY).

3.6.1. Absorption spectra. An aqueous solution of 10 μM EY exhibited strong absorption peak at 517nm with a faint shoulder at 495nm[230]. The band at 517nm corresponds to the monomeric form of the dye while the 495nm band was due to the formation of dimer involving the stacking of two monomers[339]. Effect of [bmim][MS] on the absorption spectra of EY has been shown in Figure 3.8(A). Absorption spectra of EY was perturbed in the presence of varying amount of [bmim][MS] in water, indicating change in the environment of the medium. With the progressive addition of [bmim][MS], a red shift occurred in the major absorption peak of EY. In the lower concentration range (<10mM) intensity of EY increased without any significant shift in the peak position. Above 10 mM [bmim][MS] concentration, a red shift in the spectra of EY was initiated. No previous studies involving the effect of ionic liquid on the absorption spectra of xanthenene dye are available. Recent studies of Adhikari et al.[225,265,308] revealed that there occurred a red shift in the absorption spectra of cumarin 480 (a solvatochromatic dye) dissolved in [bmim][BF_4] in comparison to spectra of the same in benzene. Spectral studies on some xanthene dyes were performed systematically in different solvents and in presence of different aqueous surfactant solution by De et al.[230] and Bhowmik et al.[339] and Chakraborty et al.[340] They observed a red shift in the spectra of EY and erythrosin B with the progressive addition of a cationic surfactant hexadecyltrimethylammoniumbromide (CTAB). Red shift in the absorption spectra for xanthenes dyes could also occur in less polar solvent compared to water. According to Bhowmik et al.[339] the shift in the absorption spectra was due to an additional (other than electrostatic interaction) contributory effect in the altered polarity of the media. In the present study we, therefore, believe that there occur some electrostatic attraction between [bmim] cation and EY in the ground state. Additionally, the ionic liquid, having organic moiety, alter the solvent polarity. Hence the resultant spectral shift of EY in the presence of [bmim][MS] was due to electrostatic attraction as well as altered solvent polarity. Also as Stark et al.[323] have proposed there might be a tail-tail

aggregation formation in the system which also leads to the resultant spectral shift, as what happened in case of micelles.

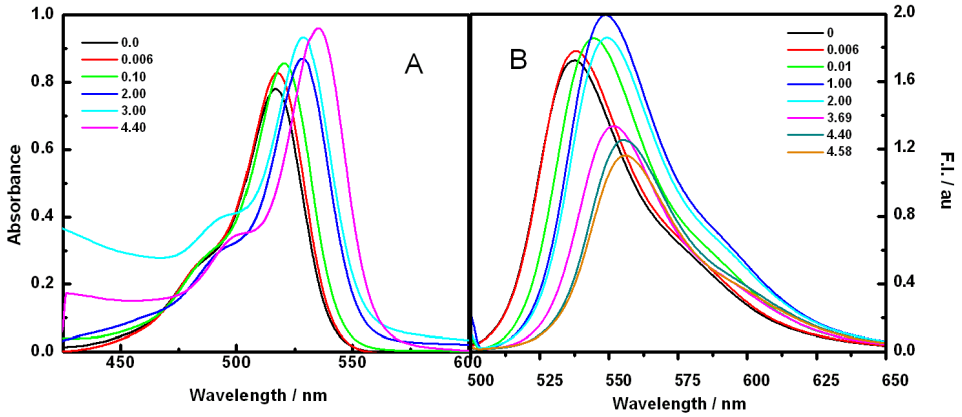

Figure 3.8. Absorption (A) and emission (B) spectra of 10 µM eosinY in presence of different amount of [bmim][MS] in water at 298 K. Molar concentration of [bmim][MS] *are mentioned inside the Figure Excitation wavelength* (λ_{ex}): 500nm.

3.6.2. Fluorescence spectra. Fluorescence spectra of EY in the presence of varying amount of aqueous solution of [bmim][MS] is presented in Figure 3.8(B). The absorption and emission pattern of EY were more or less similar up to 1.0 M [bmim][MS] in water. When the IL concentration exceeded the concentration of 1.0 M, there occurred progressive quenching of fluorescence with the increase in IL concentration. However, the red shift with increasing IL concentration was monotonous at least upto 4.58 M. Such studies reveal a different mechanism for the formation of exciplex above 1.0 M [bmim][MS]. We believe that some significant structural changes occur above this threshold concentration. Aggregation of different ILs in aqueous medium with varying alkyl chain length, cations and anions have been reported by different authors [30-32, 36, 37, 40, 41, 44, 48, 75]. According to them for [bmim] based ILs, aggregated species could form around 1.0 M concentration. Such aggregates are comprised of small clusters of 8 to 10 ionic liquid cations.

We believe that due to the formation of such clustered aggregates, there occurred a significant change in the viscosity of the medium which subsequently retarded the excitation process.

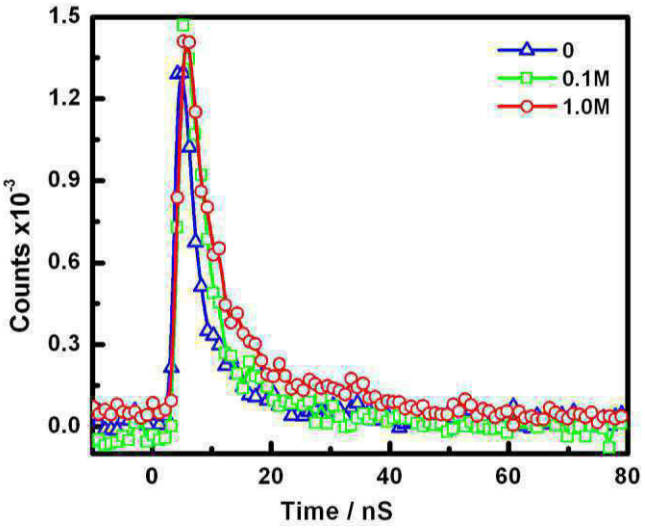

Figure 3.9. Fluorescence decay curves of 10 µM eosin Y in presence of different concentration of [bmim][MS] in water at 298 K. Concentration of [bmim][MS] have *been mentioned inside the Figure Excitation wavelength* (λ_{ex}): 500nm and emission *wavelength* (λ_{em}): 537nm.

Figure 3.9 describes the fluorescence decay profile of aqueous eosinY solution in absence and presence of [bmim][MS]. The decay profile was found to be single exponential in nature. The fluorescence lifetime was changed from 2.15 ns for EY in water to 4.8 ns in 1.0 M IL in water. Enhanced viscosity might be the causative factor to alter the excited lifetime of EY. Therefore, it could be concluded that the transition processes in the excited and ground states were affected by the viscosity of the medium. Also solvent polarity could play role in this regard[225,265,308,311].

Figure 3.10 is a combined representation for the variation of excited state life time and anisotropy with increasing concentration of [bmim][MS] in water. Both the life time and anisotropy did not change significantly upto 1.0 M [bmim][MS], above which the anisotropy value increased sharply. In the inset of Figure 3.10, variation of viscosity with concentration has been shown to compare with the anisotropy-concentration profile. Viscosity results suggest that there occurred a significant change in the viscosity of medium above 1M [bmim][MS] in water. The viscosity increase was due to the formation of aggregates [211,230,296,298,301,305,306,323,333,341-343]. As viscosity of a medium governs the

fluorescence anisotropy of a dye[326], hence fluorescence anisotropy enhancement was certainly due to enhancement in the viscosity of the media.

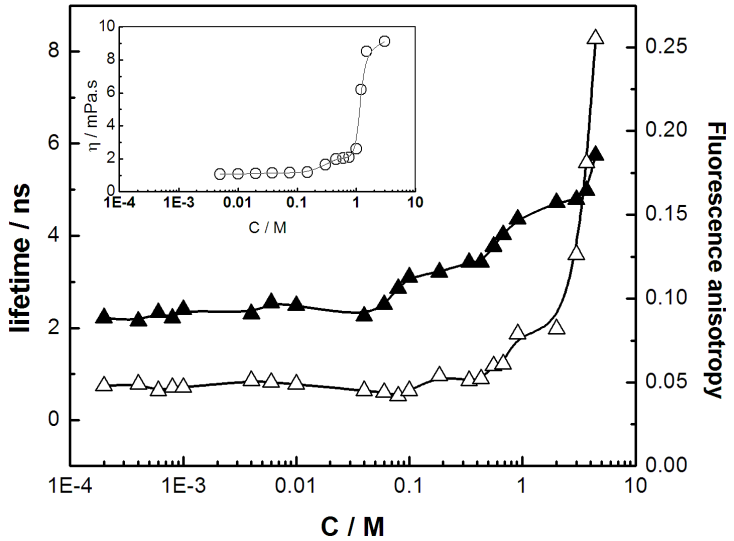

Figure 3.10. *Variation of lifetime (▲) and fluorescence anisotropy (Δ) for 10μM eosinY with concentration (C) of [bmim][MS] in water at 298K. Excitation wavelength (λ_{ex}): 500nm and emission wavelength (λ_{em}):* 537nm. Inset: viscosity (η) - [bmim][MS] concentration profile.

4. Summary and conclusion

Physico-chemical investigations on the binary mixture of [bmim][MS] + water were carried out both in the dilute and concentrated regime of [bmim][MS] using different techniques. Thereoccurred a synergistic interaction between the [bmim][MS] andwater. The surface tension decreased monotonously with a halt at0.3 M [bmim][MS]. The absorption and emission spectral behaviors were significantly different. The steady state fluorescence anisotropy and excited state lifetime were dependent on the concentration of [bmim][MS] in water. It was finally concluded that initially increasing the IL concentration led to the formation of an ion-pair, whereby the cationic component, which was surface active, was interfacially absorbed. Micelle-like aggregates were formed above a certain concentration, which was similar to ionic clusters. Above 50 mole% ionic liquid, a three dimensional quasi crystal-like network was formed which deactivates the water molecules.

CHAPTER 4

CHAPTER 4

Physico-chemical Studies on Ionic Liquid Microemulsion: Phase Manifestation, Formation Dynamics, Size, Viscosity, Percolation of Electrical Conductance and Spectroscopic Investigations on 1-butyl-3-methyl imidazolium methanesulfonate + water / Tween-20 +n-pentanol / n-heptane Pseudoternary System

Abstract

Combined phase behavior, method of dilution, viscosity, dynamic light scattering, electrical conductance and spectroscopic probing techniques were employed in understanding the physico-chemical properties of pseudo ternary microemulsion system 1-butyl-3-methyl imidazolium methanesulfonate ([bmim][MS]±water) / (Tween-20+n-pentanol) / n-heptane. Phase manifestation revealed that the area under the clear region depended on ionic liquid (IL) / water mole ratio. Thermodynamic and structural parameters for the formation of (IL+water)-in-oil μE system were evaluated employing the method of dilution at different [polar domain]/[Tween-20] mole ratio and temperature; the parameters depended on the composition of the polar domain. IL+water comprising μE behaved differently, compared to the conventional water-in-oil μE system, especially at higher mole fraction of IL. Both the size and viscosity increased with the increasing volume fraction of the dispersed phase (IL+water), while they decreased with increasing temperature. Although having IL, the μEs were less conducting due to the strong interaction between the IL cation and the oxyethylene groups of the surfactants. Formation of micelle like aggregates within the polar domain further suppressed the conductivity. Combined studies on the absorption and emission spectra of eosinY, along with the excited state lifetime and anisotropy measurements, revealed the existence of different states of IL+water in the polar domain.

Colloids Surf., A **2013,** 419, 113-124

1. Introduction

Ionic liquids (ILs) are environmentally benign materials [344] with some specific properties, viz., low melting point (less than 100^0C), ionic nature, low volatility and easy recyclability, etc., for which they have gained special pedigree as "green solvent"[191]. ILs are gaining importance for their applications, viz., as alternate solvent for chemical reaction and separation[345], in electrochemistry[346] and nanoparticle synthesis[231], etc. Advantages of using IL as media for chemical reaction have been reviewed by Hao[347] and Welton.[179] Imidazolium based ILs are used because of its tunability; tailor made ILs can be prepared using imidazolium cation. However, use of neat IL has some limitations; they are inefficient in dissolving a wide variety of compounds[204]. This could be overcome by using them in the form of microemulsion (μE). The term μE was first coined by Schülman[56] and subsequently by Lindman[60]. μE is defined as thermodynamically stable, clear and isotropic dispersion of one liquid into another immiscible liquid stabilized by a surfactant monolayer [30,34,348,349]. μEs also find various applications in the field of cosmetics, pharmaceuticals, chemical reaction in compartmentalized systems and synthesis of nanoparticles. Although a large number of articles on μE are available in the literature, however the review works of Moulik et al.[224,350,351], Gradzielsky et al.[352], Stubenrauch et al.[353], Fanun et al.[354] and Lindman et al.[219,355] are worth reading.

The limitations of ILs, in respect of their in capabilities to dissolve a wide variety of compounds, can easily be overcome through the formation of μE[211]. Research works involving IL microemulsion are ever increasing[202,210,214-216,348,356]. Han and co-workers[203] first reported the formation of μE comprising IL. Very recently Sarkar and co-workers [212] have reported a new strategy to prepare IL-in-oil μEs. Different review works on IL μEs are available in the literature[191,213,347,349,357,358]. IL based μEs in drug formulation has been explored by the research group of Moniruzzaman et al.[187] and Althanyan et al.[359] Estoe et al.[348], for the first time, have reported the characterization of IL μE using small angle neutron scattering (SANS) technique. Koetz and co-workers [213] have studied the structure of IL modified μE. Gao et al.[176,204,205] undertaken extensive

works on μEs comprising of [bmim][PF_6] and water by different techniques. While Friberg et al.[349] have reported about the works on [bmim][BF_4] based μE, the structural studies of [bmim][BF_4]-in-oil μE have been reported by Gao et al.[176]. IL-in-oil μEs have also been extensively studied by Zheng and co-workers [360] using Triton X-100 and Tween 20. In the work of Gao et al.[91] comparative studies between the properties of microemulsions comprising TX-100 and Tween 20 have been reported. In another work of Zheng et al.[361] extensive investigation were carried out on IL μE comprising Tween 80 as surfactant. It was proposed that the imidazolium cation can get coordinated with the lone pair of electrons of oxyethylene groups in Triton X-100 or Tween 20[211]. Such interactions can lead to the formation of structured/rigid/organized entities. Subsequently, the system becomes less sensitive to temperature, compared to the corresponding conventional water-in-oil μEs. Dynamic light scattering studies, combined with the viscosity measurements, can shed light on the above mentioned characteristics of IL μE (the size and its temperature sensitivity).

Studies on the microenvironment of IL-in-oil μE using different solvatochromic probes have been reported by the research groups of Bhattacharyya[133-135,216,225], Gao[140,176,203-205,211,360], Sarkar[113,144,193,212,216] and Samanta[210,214,312]. According to Gao et al.[204], with increasing amount of IL, polarity of the microenvironment increases, resulting in a red shift in the absorption spectra of dye molecule (probe). Solvent dynamics studies in reverse micelle can provide information about the different states of the polar domains[210,214-216,356]. Bhattacharya et al.[133,134] have performed solvent dynamics studies using IL μEs. Similar works have been reported by Sarkar et al.[216] where different dyes were used in the confined polar domain of μE. Samanta et al.[215] have also reported the solvent dynamic studies, both in the neat and in confined ILs. However, all those results may be considered as fragmentary in nature to completely understand the different states of IL in the μE of oil continuum.

IL based μE can be formed using any one of the three coexisting pseudo phases: the polar domain, the surfactant and the oil (non polar component). However, till date no μE is reported where all the three components are ILs[362]. IL based μEs have advantages over the pure IL, as well as the corresponding

conventional μE (comprising water). As a result, IL μEs find many applications which include colloidal crystallization[363], synthesis of nanomaterial[186], pharmaceutics[187], polymers[364], catalysis[184], chemical engineering[365,366] and energy conversion[367], etc. However, the most significant application of IL μE lies its use as alternate solvent for organic chemical reaction[179].

Although termed as environmentally benign, fluorinated ILs are toxic because they can generate HF, POF_3, etc., upon heating[193]. Hence, studies involving non-fluoridated ILs are considered to be more significant. In this aspect, 1-butyl-3-methyl imidazolium methanesulfonate [bmim][MS] is more "green" compared to the conventional fluorinated ILs. However, to the best of our knowledge no reports are available on [bmim][MS] based microemulsion.

Water is the "greenest" among all solvents. In our previous report, we showed that [bmim][MS] in combination with water exhibited some unusual behavior[368] The binary mixtures were studied using a number of techniques in the bulk condition. Different properties of the binary mixture could be tuned/altered by judicious mixing of the components. Previously, we have carried out systematic physico-chemical investigations on water / (Tween 20 + n-pentanol) / n-heptane water-in-oil μE[261]. It is, therefore, important to undertake the challenge in investigating the polar domain in oil microemulsion comprising the binary mixture of ionic liquid, [bmim][MS], in combination with water. Such studies are important in terms of their application as well as fundamental understanding point of view. However to the best our knowledge, no systematic studies have yet been carried out using a binary mixture of IL and water, which would be the novelty of the present work.

In this paper we report the results of the investigations made on pseudo ternary polar domain-in-oil μE system ([bmim][MS]+water) / (Tween 20+n-pentanol) / n-heptane. Our previously published results on water / (Tween 20+n-pentanol) / n-heptane μE[261] alongwith the binary mixture of [bmim][MS] + water[369] have been considered as the points of references. There are several reports on the microemulsions comprising TX-100[176,203,204,211]; however IL microemulsions comprising Tween 20 are not so many. Compared to TX-100, Tween 20 is less toxic. The choice of the anion in the IL is intentional as it is an

inorganic ion linked to an alkyl group. It is needless to mention that such a system will definitely be less toxic compared to the fluorinated ILs. The μE systems have been studied as functions of the composition of binary mixture of the polar domain, volume of the dispersed phase (polar domain) and temperature. μEs were characterized using a number of techniques, viz., phase behavior, method of dilution, viscosity, dynamic light scattering (DLS), electrical conductance, absorption and fluorescence spectroscopic measurements. It is believed that such a system will exhibit some unusual properties and will find different potential applications due to the unique features of the binary mixtures as well as of a μE. Usually IL-in-oil μEs are more rigid and less temperature sensitive; such limitations can be overcome provided the pure IL is replaced with a binary mixture of IL and water.

2. Experimental

2.1. Materials.

The nonionic surfactant polyoxyethylene sorbitan monolaurate (Tween 20) and the IL 1-butyl-3-methyl-imidazolium methanesulfonate, [bmim][MS] were purchased from M/S Fluka, Switzerland and M/S Sigma-Aldrich Chemicals Pvt. Ltd., USA respectively. They were stated to be more than 99.5% pure and were dried under vacuum at 60^0C for eight hours[144,193,369]. HPLC grade n-pentanol was a product from Lancaster, England while n-heptane was obtained from E. Merck, Germany. They were used as received. The dye eosinY, [2-(2, 4, 5, 7-tetrabromo-6-oxido-3-oxo-3H-xanthen-9-yl) benzoate] was a product from E. Merck, Germany. Structure of Tween 20, [bmim] cation and eosin Y are shown in Scheme 1. Double distilled water with a specific conductance of 2-4μScm^{-1} (at 298K) was used.

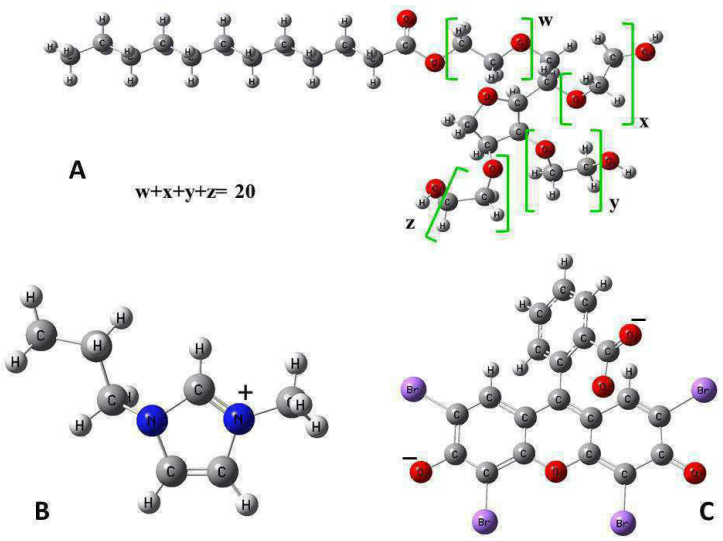

Scheme 4.1. Schematic models of A, Tween 20; B, [bmim] cation and C, eosin Y

2.2. Methods

2.2.1. Phase manifestation. The pseudo ternary phase diagram of ([bmim][MS]+water) / (Tween 20+n-pentanol) / n-heptane at different compositions of the polar domain were constructed by titrimetric method as described elsewhere[101,229,261]. Briefly, known amounts of Tween 20+n-pentanol (1:1, w/w) and n-heptane or (IL+water) were taken in a stoppered test tube. (IL+water) or n-heptane was then progressively added using a Hamilton (USA) microsyringe under constant stirring in a controlled temperature bath (298±0.1K). The phase boundary was detected through the appearance of turbidity, whereby the composition was noted. The same experiment was carried out for a number of compositions by varying the amount of oil or IL+water. Also the experiments were carried out using different combinations of IL and water.

2.2.2. Method of dilution. The simple experiment, capable of providing useful information on the thermodynamics of formation and structural parameters of μE, was also carried out titrimetrically[34,101,261]. Different binary mixtures were used as the polar domain in the oil continuum. Also experiments were carried out at different [IL+ water] / [Tween 20] mole ratio, ω (5, 10, 15, 20 and 25) and temperatures (298, 303, 308, 313, 318 and 323K). Known amount of surfactant,

polar component (IL+water) and n-heptane were taken in a stoppered test tube which, after homogenization, appeared turbid. n-pentanol was then progressively added. After saturating the oil continuum (and partly the polar domain) once excess n-pentanol became available, it behaved like cosurfactant and occupied the polar domain/oil interface whereby a clear μE was formed. The required amount of n-pentanol was then noted. Upon further addition of n-heptane, the oil continuum abstracted the cosurfactant from the interface which resulted in the destabilization of the μE. The clarity was regained again by adding cosurfactant. This method of destabilization and re-stabilization was carried out for a number of times, whereby the composition was also noted. The method basically aimed to determine the partition coefficient of n-pentanol between the oil continuum and the interface (strictly speaking, n-pentanol was partly soluble in the polar domain). The previously followed approach of Moulik et al.[98] was suitably modified in the present case as has been detailed in the supplementary section.

2.2.3. Viscosity measurements. Viscosity of μE was measured using a LVDV-II+PCP cone and plate type roto-viscometer (Brookfield Eng. Lab, USA). A 0.2M Tween20, mixed with 1:1 (w/w) n-pentanol in n-heptane was used. Unlike the dilution experiments, viscosity was measured at varied volume fraction (φ_d) of the dispersed phase. This approach was adapted because of the fact that with varying composition of the polar domain, the same molar ratio range of [IL+water] / [Tween 20] could not be maintained for all the binary mixtures. Temperature during the viscosity measurement was controlled by a cryogenic circulatory water bath with a precision of ±0.1K (DC-1006 M/S. Hahntech Corporation, S. Korea). Shear rates (D) were varied within the range 20 – 60 S^{-1} with an increment of 5.0 S^{-1} in each step. Zero shear viscosity (η) was obtained using the relation $\eta = \tau / D$[114,127,261,370], where τ is the shear stress.

2.2.4. Dynamic light scattering (DLS) studies. Size of the μE droplet was determined by dynamic light scattering (DLS) method. The same set of solution, as used in the viscosity measurements, was employed for size analyses. DLS measurements were carried out using a Zetasizer Nano ZS90 (ZEN3690, Malvern

Instruments Ltd, U.K.). A He-Ne laser of 632.8 nm wavelength was used and the data were collected at 90^0 angle. Temperature was controlled by inbuilt Peltier heating-cooling device with an accuracy of ±0.05K. The instrument actually measures the diffusion coefficient (D) from which the diameter of the microemulsion droplet (d) was determined according to Stokes–Einstein's formalism[134,136,225,261,265]:

$$D = \frac{kT}{3\pi\eta d} \qquad \textbf{(4.1)}$$

where k, T and η indicate the Boltzmann constant, temperature and viscosity respectively.

2.2.5. Conductance measurements. μE comprising IL and water in the polar domain is expected to be conducting, as reported for the conventional water-in-oil μE having ionic components in the polar domain[116]. Both the volume and temperature induced percolation studies were carried out using 0.2 M Tween20 (with 1:1 w/w n-pentanol) in n-heptane. 10 mL of Tween 20 solution was taken in a thermostated enclosure. For volume induced percolation, binary mixtures of (IL+water) was progressively added with constant stirring. Specific conductance was measured with an EC-CON510/43S conductivity meter (Cyberscan, TDS/^{0}C/^{0}F, USA). Volume induced percolation studies were conducted at four different temperatures, viz., 298, 303, 308 and 313 K. In another approach while performing the temperature induced percolation studies, a known amount of the dispersed phase (IL+water) was mixed with the surfactant solution. Conductance was then recorded in the temperature range 283-343 K with an increment of 5 K in each step.

2.2.6. Spectral studies.

2.2.6.1. Absorption spectra. Visible absorption spectra of eosin Y (EY) in the polar domain were recorded on a UVD-2950 Spectrophotometer (Labomed Inc., USA) in the range 400-600 nm using a matched pair cell of 1.0 cm path length. Corresponding (IL+water)-in-n-heptane μE without the dye was used as reference. Overall concentration of eosin Y was always kept constant at 10 μM.

Initially, required amount of eosin Y in methanol was taken in a test tube. The solvent was evaporated under vacuum. μE of known composition was then added and homogenized by vortexing the solution. It is to be mentioned that eosin Y is insoluble in n-heptane[340]. Therefore it could be assumed that the dye molecules reside in the polar domain[360].

2.2.6.2. Emission spectra. The same set of solutions, as used in absorption spectroscopic measurements, was used in the fluorescence measurements. Detail of the experimental techniques is available elsewhere [340,369]. Both the steady state and time resolved fluorescence measurements were carried out using a bench-top spectrofluorimeter (Quantamaster-40, Photon Technology International Inc, NJ, USA). For recording the steady state fluorescence spectra (500 - 650 nm), eosin Y was excited at 500 nm (λ_{ex}).

Steady state anisotropy (r), which is related to the microviscosity of the solvent surrounding the probe molecule, was determined using the following expressions[325,326]:

$$r = (I_{VV} - GI_{VH}) / (I_{VV} + 2GI_{VH}) \quad \textbf{(4.2)}$$

$$\text{and,} \quad G = I_{HV}/I_{HH} \quad \textbf{(4.3)}$$

where, I_{VV}, I_{VH} are the intensities obtained with the excitation polarizer oriented vertically and the emission polarizer oriented vertically and horizontally respectively; I_{HV} and I_{HH} refer to the similar parameters as above for the horizontal positions of the excitation polarizer. In case of anisotropy measurements, the fluorescence data were collected at an emission wavelength (λ_{em}) of 550 nm[369]. Excited state lifetime of eosin Y in the polar domain was determined by analyzing the fluorescence decay curve which was single exponential in nature. A pulsed nano diode emitting at 500nm was used as the light source[340,369]. Goodness of the fit of the curves were adjudged by χ^2 values which were in between 1 and 1.2[144]. Fluorescence decay curves were analyzed by Felix GX (version 2.0) software. Both the absorption and fluorescence data were recorded at ambient but controlled temperature.

3. Results and discussion

3.1. Phase manifestation. Although tedious, however the construction of phase diagram for ternary / pseudo ternary μE systems are essential from the fundamental as well as the application point of view[28,62]. The pseudo ternary phase diagrams for ([bmim][MS]±water)/(Tween-20+n-pentanol)/n-heptane at different [bmim][MS] / water mole fractions have been graphically presented in Figure 4.1. The phase manifestations for water containing μE system have been previously reported by the present research group[261] and this has been taken as the point of reference. Each pseudo ternary phase diagram comprise of a single phase (1Φ) clear μE region and a two phase turbid region (2Φ). The extreme corners of the polar component and oil component corresponded to oil-in-polar domain and polar domain-in-oil μE respectively. In the present system, the oil rich regions, i.e., (IL+water)-in-oil μEs were examined for other set of experiments. Area under the clear and turbid regions were calculated by weighing the individual components in the pseudoternary phase diagram as have been done previously[229,261]. The area under the turbid region was higher in each case compared to pure water. The increase in the area under turbid regions is due to the presence of the ionic components in the polar domain. However, when one analyses the results in terms of the variation of % area under the clear or turbid region with the composition of the binary mixture, it is observed that the %area under clear region for different microemulsions μE passes through a minimum at 50 mole% [bmim][MS] in combination with water (x_{IL}=0.5), as graphically presented in Figure 4.2.

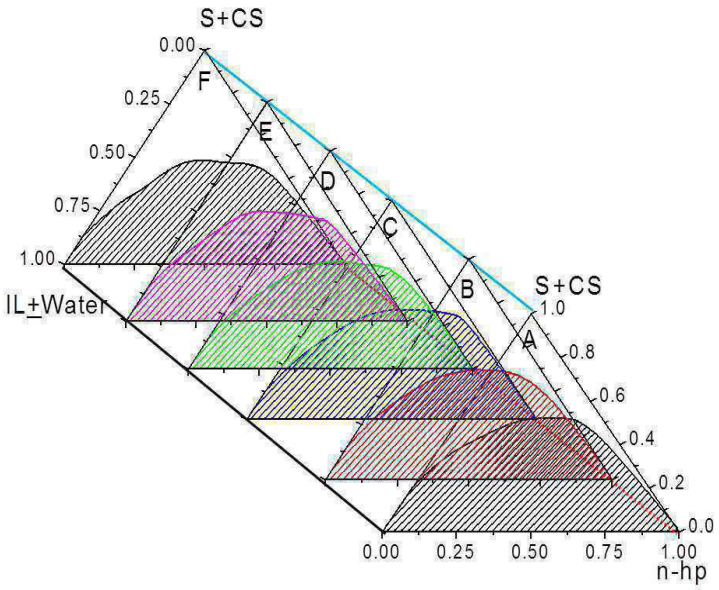

Figure 4.1. Pseudo-ternary phase diagram of ([bmim][MS]±water)/(Tween-20+n-pentanol)/n-heptane microemulsion at 298K. 1:1 (w/w) Tween-20 and n-pentanol was used. Mole fraction of [bmim][MS] in the binary mixture of [bmim][MS] and water: A, 0.2; B, 0.4; C, 0.5; D, 0.6; E, 0.8 and F, 1.0 respectively. The shaded portions represent *biphasic (2Φ) regions while the clear portions correspond to the single phase (1Φ)* regions.

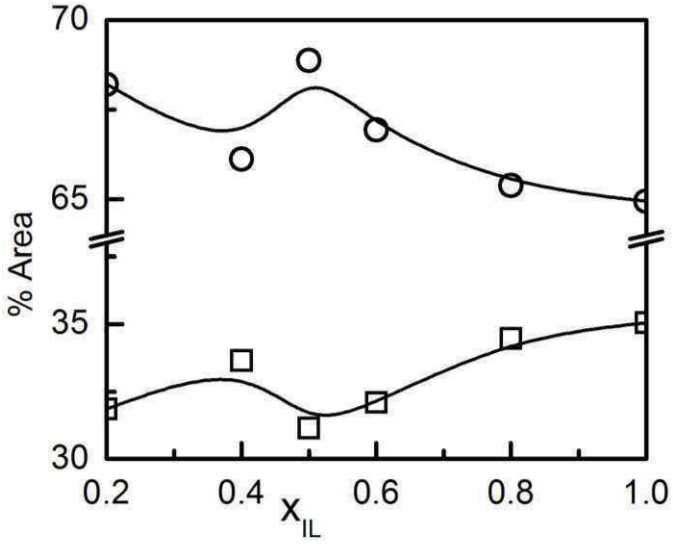

Figure 4.2. *Interdependence of the %area under clear (□) and turbid (O) regions on the* mole fraction of [bmim][MS] (x_{IL}) in the binary mixture of [bmim][MS] and water for ([bmim][MS]±water)/(Tween-20+n-pentanol)/n-heptane microemulsion system at 298K.

According to our recent study[369] as well as other available reports[294,295,323], IL can deactivate water molecules when present in excess amount in a binary mixture. The deactivation of water molecules for binary mixtures comprising of more than 50 mole% IL has recently been modeled by Stark et al.[371] and Liu et al.[294,295].

Above 50 mole% IL, the deactivated water molecules cannot significantly alter the structure of the aggregates. Also there are reports describing the formation of micelle like entities by the IL in binary mixtures[294,295,298,302,303,306]. Besides, due to amphiphilc nature, IL can also occupy the interface alongwith the surfactant and cosurfactant molecules. Subsequently, clarity of the μE increased further with increasing mole fraction of IL.

3.2. Method of dilution.

3.2.1. Evaluation of thermodynamic parameters. The method of dilution is a very simple but informative technique which can derive many useful parameters for the formation of polar domain-in-oil μE[95]. In this method, by the alternate stabilization and destabilization with the successive addition of cosurfactant and oil, one can obtain the partition coefficient of n-pentanol between oil and oil / (IL+water) interface. By suitably analyzing the distribution constant in the form of different standard thermodynamic equations, the corresponding thermodynamic parameters for the formation process can be evaluated easily[98,372,373]. In addition to the thermodynamic parameters, the structural parameters can also be computed from these experimental results[108,223,228,229]. Although several reports on the method of dilution are available in the literature involving water-in-oil μE, such studies involving ILs are not common and as per our knowledge only one recent report is available in the literature on the IL-μE system[364]. Thus the dilution studies involving the evaluation of interfacial behavior, thermodynamic and structural parameters of IL μE are considered to be significant.

For a stable μE, the alkanol is distributed in between the interface and oil; the surfactant essentially remains at the interface. In some cases the alkanol molecules may also become partly soluble in the polar domain. In the present case the alkanol molecules get distributed within the (IL+ water) mixture, interface and oil respectively. The total number of moles of n-alkanols (n_a^t) would thus follow the relation[98,108,223,364]:

$$n_a^t = n_a^p + n_a^i + n_a^o \qquad \textbf{(4.4)}$$

where, the superscripts p, i and o stand for polar phase(water+IL), interface and oil respectively.

At a constant temperature and a fixed ω , the ratio of the sum of number of moles of alkanol in the polar phase (n_a^p) and the number of moles of alkanol in oil (n_a^o) will be a constant with the total number of it in the oil (n_o) and total number of polar phase molecules (n_p) . Consequently, the mole fraction ratio of alkanol at the interface (X_a^i) and the sum of the mole fraction of alkanol in oil (X_a^o) and polar phase (X_a^p) should also be constant. Thus,

$$\frac{n_a^o + n_a^p}{n_o + n_p} = k \qquad \textbf{(5)}$$

and

$$\frac{X_a^i}{X_a^o + X_a^p} = k_d \qquad \textbf{(4.6)}$$

where, k and k_d are constant and the distribution constant respectively.

By replacing equation (4.2) in equation (4.1) one sets the following relation:

or,

$$\frac{n_a^t}{n_s} = \frac{n_a^i}{n_s} + k\left(\frac{n_o + n_p}{n_s}\right) \qquad \textbf{(4.7)}$$

where n_s represents the number of moles of surfactants.

In the dilution experiments, at a fixed n_s, n_a^t and (n_o+n_p) are varied to have a series of $\frac{n_a^t}{n_s}$ and $\frac{n_o + n_p}{n_s}$ which according to equation (4.7) can give $\frac{n_a^i}{n_s}$ and k from the linear plot between $\frac{n_a^t}{n_s}$ and $\frac{n_o + n_p}{n_s}$ as Intercept (I) and slope

(S), respectively. The plot of $\frac{n_a^t}{n_s}$ vs. $\frac{n_o+n_p}{n_s}$ for x_{IL}=0.5 at ω = 15 have been presented in Figure 4.2.

The distribution constant, k_d, can be related with the slope and intercept of equation (4.7) as:

$$k_d = \frac{X_a^i}{X_a^o + X_a^p} = \frac{\frac{n_a^i}{(n_a^i + n_s)}}{\frac{n_a^o}{(n_a^o + n_o)} + \frac{n_a^p}{(n_a^p + n_p)}} = \frac{n_a^i\left(1 + \frac{n_a^o}{n_o}\right)}{n_a^o(n_a^i + n_s)} \quad \textbf{(4.8)}$$

Or,
$$k_d = \frac{n_a^i / (n_a^i + n_s)}{(n_a^o + n_a^p) / (n_a^o + n_a^p + n_o + n_p)} \quad \textbf{(4.9)}$$

Or,
$$k_d = \frac{(n_a^o + n_a^p + n_o + n_p)}{(n_a^o + n_a^p)\left(n_a^i + n_s / n_a^i\right)} \quad \textbf{(4.10)}$$

We know, $S = \frac{n_a^o + n_a^p}{n_o + n_p}$

Thus,
$$k_d = \frac{[S(n_o + n_p) + (n_o + n_p)]}{S(n_o + n_p)\left(1 + \frac{n_s}{n_a^i}\right)} \quad \textbf{(4.11)}$$

$$k_d = \frac{I(S+1)}{S(I+1)} \quad \textbf{(4.12)}$$

Therefore, by knowing I, S one would get the value of k_d

Thus by using equations (7) and (12) one can evaluate the values of n_a^i, n_a^o and k_d for the formation of w/o microemulsion.

Changes in the standard Gibbs free energy of transfer (ΔG_t^o) of alkanol from oil to the interface (as well as into the polar domain) could be expressed as:

$$\Delta G_t^o = - RT \ln k_d \quad \textbf{(4.13)}$$

Changes in the standard enthalpy of transfer ΔH_t^o was evaluated by the van't Hoff equation:

$$[\frac{\partial(\Delta G_t^{\ o})}{\partial(1/T)}]_p = \Delta H_t^{\ o} \quad \textbf{(4.14)}$$

ΔG_t^o vs T profile was found to follow a two degree polynomial equation as:

$$\Delta G_t^o = a + bT + cT^2 \quad \textbf{(4.15)}$$

where a, b and c are the polynomial coefficients**.**

The ΔH_t^o values at the different experimental temperatures were determined using the following expression:

$$[\frac{d(\Delta G_t^{\ o}/T)}{d(1/T)}]_p = a - cT^2 = \Delta H_t^{\ o} \quad \textbf{(4.16)}$$

The standard entropy of transfer (ΔS_t^o) of the associated process was then evaluated according to the following expression:

$$\Delta S_t^o = (\Delta H_t^o - \Delta G_t^o)/ T \quad \textbf{(4.17)}$$

A representative plot of n_a^t/n_s vs. $(n_o+n_p)/n_s$ at $x_{[bmim][MS]}$=0.5 and ω=15 has been shown in Figure 4.3. Herein n_a^t, n_s, n_o, n_p stand for the total number of moles of alkanol, surfactant, oil and the polar component respectively.

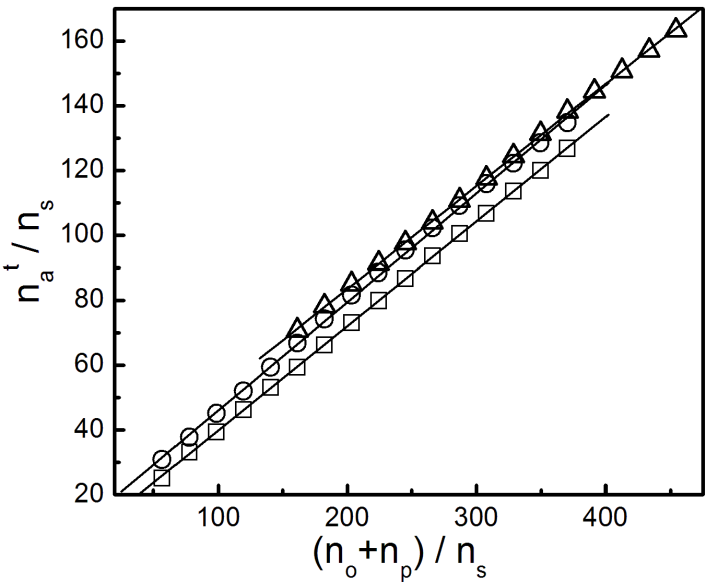

Figure 4.3. Plot of n_a^t/n_s vs. $(n_o+n_p)/n_s$ for ([bmim][MS]+water)/(Tween-20+n-pentanol)/n-heptane polar domain-in-oil microemulsion system. [bmim][MS] / [water] *mole ratio = 1:1. ([bmim][MS]+water)/Tween20 mole ratio, ω=15. Temperature (in K): O, 298; Δ, 308 and □, 318. 0.2g Tween 20 was used in each ca*se.

Results are summarized in Table 4.1 for equimolar mixture of IL and water. Other results are provided in Table 4.2.

Table 4.1. Thermodynamic parameters for the transfer of n-pentanol from oil to oil/([bmim][MS]+water) interface during the formation of [bmim][MS]±water/(Tween-20+n-pentanol)/n-heptane polar domain-in-oil microemulsion at different temperature and [IL+water]/[Tween-*20] mole ratio, ω. IL:water molar ratio = 1:1*

Parameter		**Temp. / K**					
	ω	**298**	**303**	**308**	**313**	**318**	**323**
k_d	5	3.01	3.19	2.93	4.17	3.22	3.45
	10	3.72	3.51	3.79	3.47	3.09	3.57
	15	3.69	3.88	3.97	3.56	3.62	3.90
	20	3.99	3.93	4.15	3.88	3.85	3.98
	25	4.17	4.19	4.00	3.98	3.98	4.24
$-\Delta G_t^0$ / kJ mol^{-1}	5	2.73	2.92	3.25	3.72	3.09	3.33
	10	3.25	3.16	3.41	3.24	2.98	3.42
	15	3.23	3.42	3.53	3.31	3.40	3.66
	20	3.43	3.44	3.65	3.53	3.57	3.71
	25	3.54	3.61	3.55	3.59	3.65	3.88
	5	19.79	-2.02	-24.20	-46.74	-69.65	-92.92
	10	-7.54	-4.91	-2.23	0.49	3.25	6.06

ΔH_t^0 / kJ mol^{-1}	15	-8.59	-4.65	-0.65	3.41	7.55	11.75
	20	-4.12	-2.58	-1.03	0.56	2.17	3.82
	25	-4.32	-3.05	-1.76	-0.45	0.88	2.24
ΔS_t^0 /J K^{-1} mol^{-1}	5	75.59	2.97	-69.66	-137.47	-209.30	-277.38
	10	-14.39	-5.76	3.84	11.91	19.63	29.37
	15	-17.96	-4.08	9.34	21.47	34.44	47.69
	20	-2.33	2.83	8.51	13.07	18.06	23.30
	25	-2.65	1.83	5.81	10.03	14.26	18.93

0.2g Tween-*20 was taken in each case.* φ_d = volume fraction of the dispersed phase (IL+ water).

Results revealed that increasing ω value resulted in the increase of k_d value, except in a few cases. However, while considering all the binary combinations of IL and water, the variation of k_d (and subsequently ΔG_t^0) with ω and temperature were not very straightforward. In our previous studies[228,261] for water/Tween20+n-pentanol/n-heptane water-in-oil microemulsion, we observed that with the increased volume fraction of polar domain, new droplets were formed. It was due to the capability of the polyoxyethylene groups of Tween 20 to uncoil at larger volume fraction of the polar component. Systems comprising of less than 50 mole% IL behaved similarly to water/Tween20+n-pentanol/n-heptane μE. However, for the systems comprising of more than 50 mole% IL, the variation of thermodynamic parameters was different. Microemulsions comprising more than 50 mole% IL in combination with water behaved more like the IL microemulsion. In this sense, behavior of the systems comprising less than 50 mole% IL were more like the microemulsion with water only.

Table 4.2. Thermodynamic parameters for the transfer of n-pentanol from oil to oil-(IL+water) interface in the formation of [bmim][MS]±water / (Tween-20+n-pentanol) / n-heptane polar domain-in-oil microemulsion at different temperature and [IL+water]/[Tween-*20] mole ratio, ω. IL:water = 2:4, 4:6, 6:4, 8:2 and* 1:0

IL:Wa	**k_d / $-\Delta G_t^0$** (kJ mol^{-1})/ **ΔH_t^0 (kJ mol^{-1})** / **ΔS_t^0** (J $K^{-1}mol^{-1}$) **at different temperature (in K)**					
	ω	**Temp. 298**	**303**	**308**	**313**	**318**	**323**
2:8	5	3.32/2.97/-1.62/4.54	2.88/2.67/-0.32/7.73	1.22/2.50/0.99/4.87	3.28/3.09/2.33/17.32	3.46/3.28/3.69/21.94	3.44/3.32/5.07/25.99
	10	2.70/2.84/-76.11/-	2.45/1.59/-52.06/-	2.64/2.67/-27.63/-	2.72/2.94/-2.78/-0.58	3.58/3.06/22.45/81.21	6.04/3.04/48.09/163.8
	15	3.15/ 2.84 /-0.01/9.50	1.88/1.59/-0.10/4.94	2.84/2.67/-0.19/8.05	3.09/2.94/-0.29/8.47	3.18/3.06/-0.39/8.40	3.09/3.04/-0.49/7.90
	20	2.14/1.88/33.06/117.2	2.52/2.33/25.24/91.00	0.88/2.30/17.30/55.20	1.98/2.77/9.23/35.16	3.40/3.23/1.03/13.42	3.25/3.17/-7.30/-
	25	4.45/2.69/-69.99/-	2.83/2.62/-41.60/-	2.40/2.25/-12.73/-	2.75/2.63/16.61/61.48	2.91/2.83/46.43/154.8	2.00/1.87/76.71/243.2
4:6	5	3.68/3.23/-28.54/-	3.99/3.49/-15.44/-	3.56/3.25/-2.12/3.69	3.22/3.04/11.42/46.22	3.32/3.17/25.18/89.16	4.30/3.92/39.15/133.3
	10	3.03/3.74/17.11/66.60	3.52/3.17/13.49/55.01	3.83/3.44/9.83/43.09	3.73/3.42/6.11/30.45	3.48/3.30/2.32/17.69	4.09/3.78/-1.52/6.98
	15	3.52/3.12/-10.44/-	3.42/3.10/-4.67/-5.17	3.32/3.37/1.19/13.86	3.42/3.19/7.16/33.09	3.67/3.44/13.21/52.38	3.38/3.27/19.37/70.08
	20	3.88/3.36/-6.37/-	3.70/3.29/-4.09/-2.64	3.81/3.43/-1.78/5.33	3.66/3.38/0.56/12.59	3.81/3.54/2.95/20.41	3.77/3.56/5.38/27.68
	25	3.92/3.38/-35.55/-	3.22/2.95/-17.88/-	2.40/3.24/0.08/7.54	3.93/3.56/18.34/69.96	3.85/3.57/36.89/127.2	4.97/3.31/55.73/185.8
6:4	5	2.75/2.96/29.59/107.7	3.23/3.17/13.70/54.96	3.27/3.26/-2.46/1.86	3.09/3.38/-18.88/-	3.00/3.48/-35.57/-	3.19/3.49/-52.53/-
	10	3.40/3.04/315.62/106	3.83/3.38/320.69/106	3.87/3.46/325.86/106	3.96/3.58/331.11/106	3.88/3.58/336.44/106	3.68/3.50/341.86/106
	15	4.29/3.61/-201.16/-	4.11/3.56/-204.47/-	4.15/3.65/-207.83/-	4.55/3.94/-211.24/-	4.10/3.73/-214.71/-	4.57/4.08/-218.24/-
	20	4.33/3.63/-159.76/-	4.89/3.99/-162.38/-	4.25/3.71/-165.05/-	4.69/4.02/-167.77/-	4.36/3.89/-170.52/-	4.63/4.12/-173.33/-
	25	5.14/4.05/-35.52/-	5.49/4.29/-36.07/-	5.35/4.29/-36.63/-	4.92/4.15/-37.19/-	4.89/4.19/-37.77/-	4.77/4.19/-38.35/-
8:2	5	3.22/2.90/799.82/269	3.73/3.32/812.88/269	3.25/3.02/826.18/269	3.79/3.47/839.69/269	3.25/3.12/853.41/269	2.76/2.73/867.35/269
	10	3.84/3.33/4.89/27.62	3.93/3.45/4.92/27.60	3.97/3.53/4.94/27.50	4.16/3.71/4.96/27.71	4.18/3.79/4.98/27.58	4.28/3.90/5.01/27.59
	15	4.04/3.46/-193.19/-	4.01/3.50/-196.41/-	4.31/3.74/-199.68/-	4.15/3.70/-203.01/-	4.37/3.90/-206.38/-	4.48/4.03/-209.81/-
	20	4.34/3.64/104.27/362.	4.03/3.51/105.83/360.	4.81/4.02/107.42/361.	4.43/3.88/109.03/360.	4.76/4.13/110.67/360.	4.77/4.19/112.34/360.
	25	4.76/3.87/85.92/301.3	5.24/4.17/87.29/301.8	5.56/4.39/88.68/302.2	4.89/4.13/90.11/301.0	5.02/4.27/91.55/301.3	4.97/4.31/93.01/301.3
1:0	5	5.64/4.28/-	3.61/3.24/-	3.25/3.02/28.31/29.50	5.01/4.19/97.36/27.39	4.76/4.12/167.53/25.2	3.45/3.32/238.81/22.9
	10	4.38/4.66/28.77/108.8	5.26/4.18/13.72/59.09	5.23/4.23/-1.58/8.61	4.96/4.16/-17.14/-	4.32/3.87/-32.95/-	7.28/5.33/-49.00/-
	15	5.83/4.47/-1.54/12.84	5.73/4.39/-2.21/7.24	7.05/4.58/-3.89/3.59	5.51/4.44/-5.61/-3.74	4.80/4.15/-7.36/-	5.03/4.34/-9.13/-
	20	5.89/4.39/12.14/55.47	6.24/4.61/4.23/29.19	6.49/4.78/-3.80/3.20	4.99/4.18/-11.97/-	5.19/4.35/-20.26/-	4.80/4.21/-28.69/-
	25	5.33/4.56/3.77/26.57	5.52/4.70/0.85/17.00	5.37/4.86/-2.13/7.07	5.60/4.48/-5.15/-2.12	5.10/4.31/-8.22/-	5.21/4.43/-11.34/-

The variation was similar to the conventional water-in-oil microemulsions with ionic surfactants. It has already been stated that when the amount of [bmim][MS] exceeds 50 mole% (in the binary mixture), it can deactivate water molecules. The rigidity of IL-in-oil μEs was due to strong electrostatic interaction between the imidazolium cation and oxyethylene group of Tween 20. Hence, when binary mixture comprising of more than 50 mole% IL was used as the polar domain, size of the microemulsion droplets increased with ω instead of formation of smaller droplets like water / (Tween 20+n-pentanol) / n-heptane[261] or water-in-oil μE systems comprising Tweens and Brij[228,229]. Figure 4.4 describes the variation in the changes of standard free energy (ΔG_t^0) with ω and T for x_{IL}= 0.2 and 0.8.

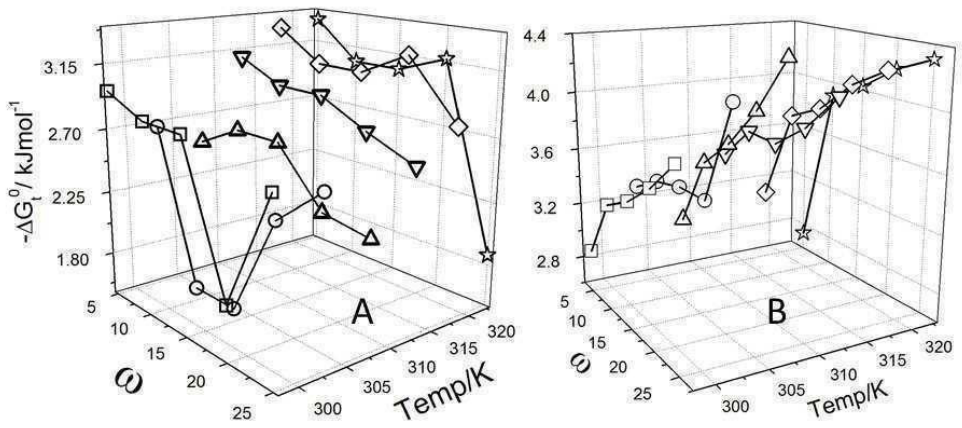

Figure 4.4. ΔG^0_t-ω-T profile for the formation of ([bmim][MS]±water)/(Tween-20+n-pentanol)/n-heptane polar domain-in-oil microemulsion system. Mole fraction of [bmim][MS] in the polar domain: A, 0.2 and B, 0.8.

Binary mixtures of different compositions (x_{IL}= 0.2, 0.4, 0.5, 0.6, 0.8 and 1.0) were used for such studies. Some representative results have been shown in Table 4.1. Other results are summarized in Table 4.2. In all the cases ΔG_t^0 values were negative which implied the spontaneity of the formation of μE. However, ΔG_t^0-ω-T profiles were found to be composition dependent. For systems comprising of lower amount of IL (less than 50 mole%) negative values of ΔG_t^0 decreased with increasing ω. This suggests the similarity of the behavior of present μE system with the corresponding water-in-oil μEs [261]. No systematic variation in ΔG_t^0 with T was observed in either case. For systems with larger amounts of IL, negative values of ΔG_t^0 increased with ω suggesting the formation of larger droplets without significantly losing their rigidity. However, to make final conclusions in

this regard some other experimental evidences like dynamic light scattering studies are warranted. While considering the formation dynamics, it was observed that behavior of the systems comprising of less than 50 mole% of IL was similar to water comprising μEs; spontaneity of μE formation decreased with increasing volume of the dispersed phase (ω or φ_d). However, for systems comprising of more than 50 mole% of IL, polarity of the dispersed phase decreased which resulted in the increased ease of μE formation. The decreased polarity was occurred due to the presence of IL molecules which themselves are amphiphilic in nature. This further supported the inferences drawn from the phase manifestation studies. With increasing ω, the curvature of μE decreased leading to more accumulation of cosurfactant at the polar domain-oil interface. While considering the enthalpy of transfer process under various conditions (as described in Table 4.1, Table 4.2 and Fig 4.5), it was found that at higher temperature ΔH_t^0 became endothermic which was initially exothermic in nature.

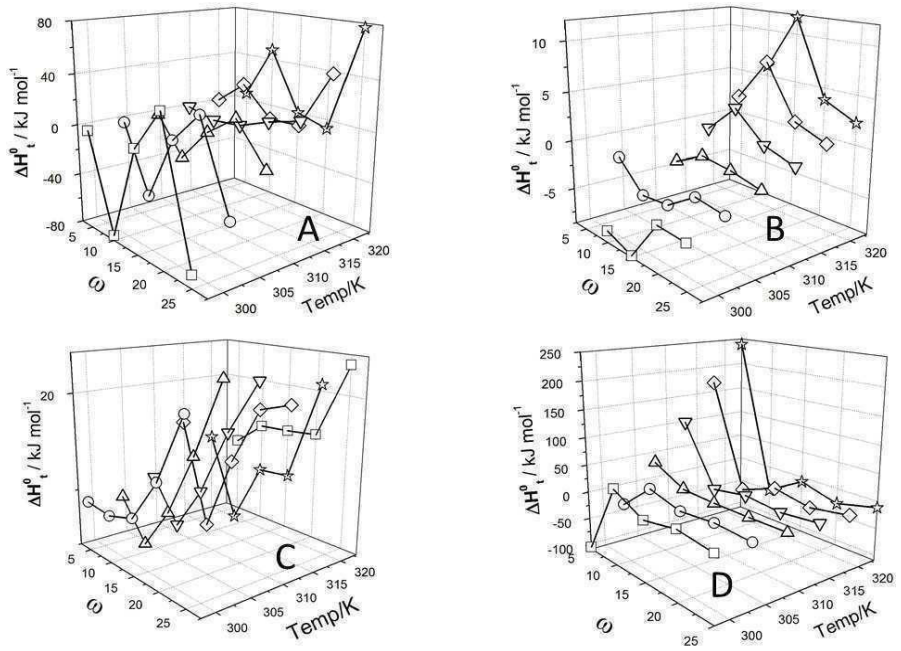

Figure 4.5. ΔH^0_t-ω-T profile for the formation of [bmim][MS]±water/(Tween-20+n-pentanol)/n-heptane polar domain in oil microemulsion system. Mole fraction of [bmim][MS] in the polar domain: A, 0.2; B, 0.5; C, 0.8 and D, 1.0

Our present set of results for the system comprising of more than 50 mole% IL showed similar behavior as in case of [bmim][BF_4] / (Brij-35+1-butanol) / toluene IL-in-oil μE system[364]. As there are possibilities for the polar components to get

dispersed into the n-heptane medium, there occured an effective increase in the area of the droplet surface. The required energy for the positive work is compensated by the absorption of heat. However, in the cases involving size increment, the negative value of ΔH_t^0 was not unexpected to decrease. To justify the similarities / dissimilarities between the behavior of conventional water-in-oil μE and IL-in-oil μE, analysis of the enthalpy-entropy profile was necessary[224]. Fig 6 describes the ΔH_t^0- ΔS_t^0 profile for all the combinations. Nice correlations were observed for all the sets of values, e.g., different x_{IL}, ω and temperature. Compensation temperature, as obtained from the slope was found to be 311 K which was in good agreement with the average of all the experimental temperatures (298, 303, 308, 313, 318 and 323 K).

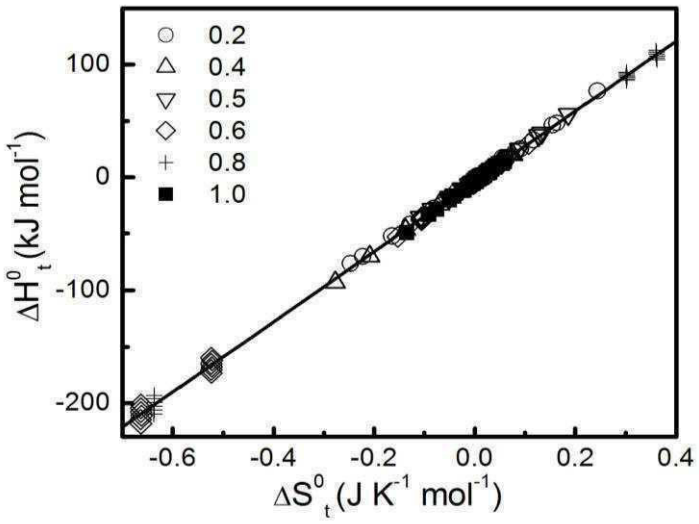

Figure 4.6. Enthalpy–entropy compensation for the formation of ([bmim][MS] + water) / (Tween-20+n-pentanol) / n-heptane polar domain-in-oil microemulsion system. Mole fraction of [bmim][MS] in the binary mixture (present in the polar domain) have been mentioned inside the Figure

3.2.2. Evaluation of structural parameters. The results of dilution experiments can be further computed to determine different structural parameters of the w/o microemulsion. For such evaluation the μE droplets are considered to be spherical, monodispersed and a monomolecular layer comprising surfactant and cosurfactant is present at the interface. The total volume of the dispersed droplets (V_d) per unit volume (here in mL) can be expressed as follows:

$$V_d = \frac{4}{3}\pi R_e^{\,3} N_d \qquad \textbf{(4.18)}$$

R_e and N_d represents the effective diameter and total number of the droplets respectively.

The droplet surface area (A_d) of droplets per unit volume is therefore:

$$A_d = 4\pi R_e^2 N_d = (n_S A_S + n_a^i A_a) N_A \qquad \textbf{(4.19)}$$

where, A_S and A_a are the cross sectional area of the surfactant and cosurfactant molecules respectively, N_A Avogadro's constant.

The equation for R_e from equation (4.18) and (14.9) can be written as:

$$R_e = 3V_d/A_d \qquad \textbf{(4.20)}$$

Total volume of the dispersed phase, herein the water droplet embedded by the surfactant and n-alkanols at the oil-water interface, is the sum of the volume contribution of water (V_{H_2O}), surfactant (V_S) and the interfacial n-alkanol molecules (V_a^i) at the interface respectively. Thus one could write;

$$V_d = V_{H_2O} + V_S + V_a^{\,i} \qquad \textbf{(4.21)}$$

One can determine the respective volumes using the values of number of moles (n_a^i), molar mass (M_a) and density of the components (ρ_a) according to the relation:

$$V_a^i = n_a^i M_a/\rho_a \qquad \textbf{(4.22)}$$

The total droplet surface area (A_d) can be obtained from the equation:

$$A_d = (n_S A_S + n_a^i A_a) N_A \qquad \textbf{(4.23)}$$

where, A_S and A_a correspond to the head group area of the surfactant and cosurfactant respectively, N_A is the Avogadro number.

Putting the value of R_e in equation (4.18) one can easily obtain the value of N_d as:

$$N_d = 3V_d/4\pi R_e^3 \quad \textbf{(4.24)}$$

Average aggregation number of surfactant (N_s) and cosurfactant (N_a) can be computed using the following formulae:

$$N_S = \frac{n_S N_A}{N_d} \quad \textbf{(4.25)}$$

$$N_a = \frac{n_o^{\,i} N_A}{N_d} \quad \textbf{(4.26)}$$

Volume of a microemulsion droplet can be considered as the additive contributions of the polar components, surfactant and cosurfactant molecules. Thus the radius of polar domain in a microemulsion droplet (R_p) and the effective radius (R_e) are related as:

$$R_P = \left(\frac{V_p + V_S^{\,h} + V_a^{\,h}}{V_d}\right)^{1/3} R_e \quad \textbf{(4.27)}$$

where, V_p , $V_S^{\,h}$ and $V_a^{\,h}$ are volume of water droplet, surfactant head group, and alkanol head group, respectively. Volume contribution due to surfactant head group and cosurfactant head group could be evaluated from the following two equations:

$$V_S^{\,h} = \frac{4}{3\pi^{1/2}} A_S^{\,3/2} N_S \quad \textbf{(4.28)}$$

$$V_a^h = \frac{4}{3\pi^{1/2}} A_a^{3/2} N_a \quad \textbf{(4.29)}$$

Results of the dilution experiments were computed using suitable mathematical formulations whereby the different structural parameters, viz., number of droplets per unit volume (N_d), number of surfactants per droplet (N_s), number of cosurfactants per droplet (N_a), effective diameter of the droplet (R_e) and radius of polar domain (R_p) could be determined[224]. While computing the structural parameters, the μE droplets were assumed to be spherical and monodispersed, stabilized by a surfactant and cosurfactant monolayer. Results are summarized in Table 4.3 and Table 4.4. N_d-ω-T profile for the systems comprising of 20 and 80 mole% of [bmim][MS] have been shown in Figure 4.7 as representative.

Table 4.3. Structural parameters of [bmim][MS]+water/(Tween-20+n-pentanol)/n-heptane polar domain-in-oil microemulsion at different temperature and [IL+water]/[Tween-*20] mole ratio, ω. Mole ratio of IL : water = 1:1*

Parameters		**Temp. / K**					
	ω	**298**	**303**	**308**	**313**	**318**	**323**
R_e / nm	5	4.74	3.75	3.35	2.83	2.63	2.42
	10	4.30	4.32	3.62	3.45	3.29	2.91
	15	5.25	4.56	3.88	3.88	3.79	3.26
	20	5.31	5.03	4.48	4.09	3.84	3.58
	25	5.65	5.09	5.09	4.35	4.22	3.79
10^{-18} N_d (per mL)	5	0.76	1.744	3.25	6.83	5.08	7.27
	10	1.89	1.56	3.11	3.13	2.93	5.28
	15	1.09	1.75	3.28	2.73	2.53	5.08
	20	1.34	1.512	2.24	3.02	3.63	4.61
	25	1.27	1.783	1.62	2.95	3.04	4.66
N_s (per droplet)	5	67.46	55.99	43.47	14.28	19.23	13.44
	10	51.56	62.63	31.40	31.21	33.35	18.46
	15	89.08	55.89	29.80	35.71	38.53	19.20
	20	72.85	64.58	43.51	32.36	26.86	21.17
	25	76.66	54.75	60.17	33.07	32.12	20.96
N_{cs} (per droplet)	5	5.27	3.67	2.07	3.06	1.29	1.26
	10	8.06	5.94	4.64	3.23	1.52	1.98
	15	11.16	7.95	6.07	4.62	2.92	3.21
	20	12.67	9.97	7.62	6.12	5.01	4.21
	25	14.74	11.25	9.46	7.35	6.10	5.24

0.2g Tween-20 was taken in *each case.* φ_d = volume fraction of the dispersed phase (Il+water).

In both the cases, the number of droplets per unit volume increased with increasing temperature. However, the extent of increase were higher for the systems comprising of lower amount of [bmim][MS]. The decrease in the number of droplet with increasing volume of the dispersed phase was not unexpected. With the increase in the volume of the dispersed phase, larger droplets were formed[364]. While considering the size of the polar domain as well as the effective size of the μE (as modeled by Wang et al.[364]), it has been noticed that both R_e and R_p decreased with the increase in temperature and ω for water rich binary mixtures (x_{IL}< 0.5). However, the size of the μE as well as the polar domain increased with increasing volume of the dispersed phase. A systems comprising of 50 mole% of IL comprising system behaved intermediately compared to water rich or IL rich binary mixtures. The reason for such unusual behavior is not certain. Compared to the corresponding water-in-oil μE systems, presently studied (IL+water) μE system was less temperature sensitive as revealed from the variation of R_e values with temperature. The rigidity was contributed by the strong electrostatic attraction between oxyethylene groups of the surfactant and the imidazolium cation.

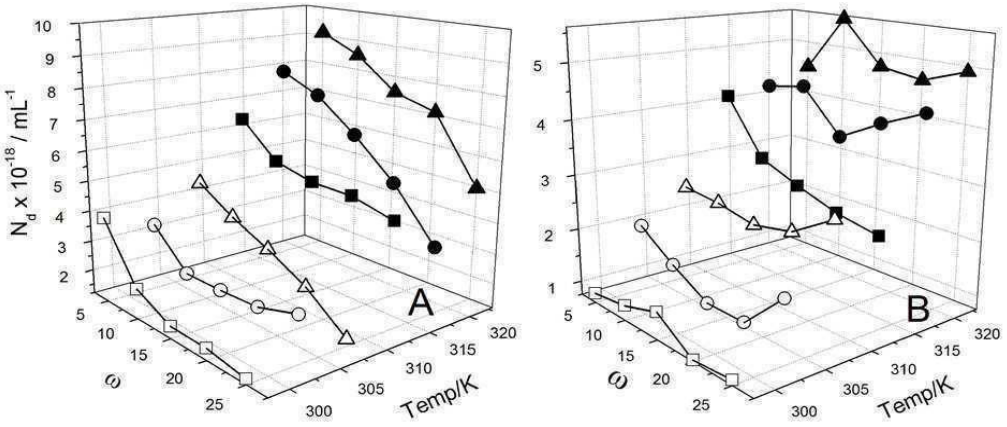

Figure 4.7. N_d-ω-T profile for the formation of ([bmim][MS]±water)/(Tween-20+n-pentanol)/n-heptane polar domain-in-oil microemulsion system. Mole fraction of *[bmim][MS] in the polar domain: A, 0.2 and B, 0.8. Temperature (in K): □, 298; O, 303; Δ, 308; ■, 313; ●, 318 and ▲, 323.*

Table 4.4. Structural parameters of [bmim][MS]±water/(Tween-20+n-hexanol)/n-heptane polar domain-in-oil microemulsion at different temperature and [IL+water]/[Tween-*20] mole ratio, ω. IL:water* = 2:4, 4:6, 6:4, 8:2 and 1:0

IL:Watere	R_e (nm)/ 10^{-18} N_d(per mL) / N_s (per droplet) / N_{cs}(per droplet) at different temperature (in K)																								
	ω	Temp. 298				303				308				313				318				323			
2:8	5	3.27	3.99	2.45	5.01	3.14	3.38	2.58	3.56	2.96	4.47	2.97	9.7	2.61	6.41	2.52	2.21	2.41	7.87	2.24	1.69	2.18	9.09	2.23	1.04
	10	3.80	2.18	3.47	5.98	3.58	2.24	3.36	4.06	3.19	3.72	3.10	2.88	2.87	5.31	2.81	2.31	2.65	7.31	2.64	2.28	2.55	8.50	2.34	2.65
	15	4.26	1.59	6.11	7.2	3.80	2.25	3.44	5.09	3.34	3.15	3.62	4.01	3.06	4.98	3.17	3.22	2.85	6.26	2.98	2.64	2.67	7.46	2.38	1.98
	20	4.47	1.58	6.18	8.26	3.97	2.32	3.89	6.03	3.58	2.46	3.84	3.18	3.23	4.96	3.36	3.88	3.22	5.03	3.19	1.96	2.85	7.08	2.35	2.73
	25	4.81	1.36	7.16	9.54	4.01	2.71	4.59	6.77	3.79	1.43	4.20	5.35	3.34	4.62	3.84	4.51	3.24	3.39	3.45	3.53	3.11	4.94	2.45	2.49
4:6	5	3.47	3.37	2.89	5.57	3.21	4.22	3.31	4.33	3.08	3.55	3.14	2.81	2.79	4.29	2.27	1.82	2.54	5.95	2.56	1.46	2.49	12.2	2.46	2.47
	10	5.01	0.85	1.14	7.78	3.85	2.33	4.18	5.46	3.21	5.62	3.54	4.53	3.11	5.34	2.83	3.57	2.99	4.43	2.78	2.13	2.73	8.87	2.54	2.7
	15	4.96	1.19	3.16	9.82	4.23	2.10	4.65	6.96	3.99	2.33	4.19	5.23	3.78	2.50	3.09	3.66	3.36	3.91	2.87	3.14	3.23	3.65	2.68	1.69
	20	4.86	1.65	5.92	10.75	4.26	2.64	4.69	8.01	3.95	3.34	4.93	6.49	4.03	2.60	3.55	5.092	3.66	3.63	3.22	4.16	3.44	4.28	2.75	3.32
	25	5.06	1.68	5.78	12.08	5.14	1.44	4.78	10.36	6.15	0.64	5.53	6.32	4.18	2.85	3.72	6.32	3.95	3.31	3.67	5.12	3.47	5.95	2.90	4.59
6:4	5	4.92	0.72	4.55	5.79	3.83	1.75	4.56	4.12	3.32	2.89	4.28	3.08	3.02	3.61	2.71	2.03	2.74	4.41	3.21	1.19	2.50	6.61	2.48	1.26
	10	5.29	0.86	5.29	9.79	4.16	2.10	4.64	6.64	3.90	2.42	4.44	4.95	3.48	3.63	2.88	3.98	3.27	4.20	3.32	3.02	3.05	4.97	2.96	2.29
	15	4.63	1.87	6.21	9.83	4.19	2.58	4.77	7.57	3.94	3.05	4.72	6.08	3.58	4.33	3.25	4.98	3.41	4.82	3.63	4.09	3.16	6.55	2.98	3.58
	20	5.18	1.47	6.62	12.31	4.37	2.81	5.17	8.79	4.54	2.11	5.13	7.66	3.83	4.25	3.59	6.08	3.80	3.84	3.74	5.05	3.46	5.70	3.17	4.42
	25	5.21	1.76	5.54	13.2	4.73	2.44	5.39	10.35	4.42	3.01	5.24	8.57	4.36	2.91	3.95	7.36	3.90	4.50	4.16	6.12	3.67	5.60	3.40	5.3
8:2	5	4.82	0.92	5.59	7.27	3.90	1.97	4.94	5.02	3.54	2.52	4.47	3.47	3.13	4.14	2.86	2.93	2.92	4.22	3.31	1.69	2.66	4.50	2.67	0.52
	10	5.35	1.02	6.56	11.33	4.71	1.52	5.43	8.04	4.11	2.45	4.98	6.07	3.79	3.12	3.13	4.77	3.46	4.35	3.54	3.97	3.23	5.54	2.76	3.35
	15	5.55	1.24	7.86	13.89	5.56	1.13	5.67	11.46	4.57	2.30	4.64	8.29	4.27	2.82	3.46	6.74	3.97	3.56	3.74	5.56	3.67	4.75	2.66	4.74
	20	6.72	0.77	7.61	19.65	5.67	1.12	6.39	14.44	4.83	2.44	4.99	10.12	4.69	2.56	3.81	8.64	4.18	3.97	3.95	7.09	3.98	4.63	2.91	6.13
	25	6.95	0.84	8.61	22.27	5.84	1.87	6.72	14.48	4.89	2.91	5.35	11.25	5.05	2.41	4.04	10.48	4.35	4.33	4.25	8.29	4.17	4.90	3.25	7.33
1:0	5	3.23	0.75	0.91	5.91	4.37	1.57	2.22	6.27	4.19	1.55	2.31	3.84	3.21	5.85	1.67	4.22	3.10	5.65	1.73	3.3	3.01	4.50	2.17	1.76
	10	5.78	1.02	1.58	14.32	4.17	3.71	2.43	8.53	4.11	3.64	2.68	7.52	3.83	4.61	2.12	6.34	3.64	5.37	1.81	5.45	3.31	5.69	2.42	4.84
	15	4.42	4.47	2.18	10.75	4.48	3.92	2.49	10.36	4.08	5.71	2.71	8.52	4.32	4.05	2.41	8.43	3.94	5.86	2.16	7.11	4.12	4.31	2.66	6.55
	20	4.78	4.15	2.36	12.67	4.59	4.68	2.58	11.32	4.21	6.62	2.47	9.44	4.58	4.22	2.71	10.06	4.19	6.01	2.32	8.47	4.32	4.94	2.97	8.13
	25	5.13	3.76	2.59	14.75	5.03	3.93	2.68	13.62	4.67	5.17	2.88	11.55	4.63	5.16	2.89	10.87	4.65	4.82	2.73	10.38	4.35	6.21	3.34	9.05

3.3. Dynamic light scattering studies. Size of the μE droplets were also determined by the dynamic light scattering experiments. As in the present study binary mixtures of [bmim][MS] and water of different compositions were used, hence size variations were considered with respect to the volume fraction of the dispersed phase. Variation in the diameter of the μE droplet with the volume fraction of polar domain has been shown in Figure 4.8 along with the viscosity data.

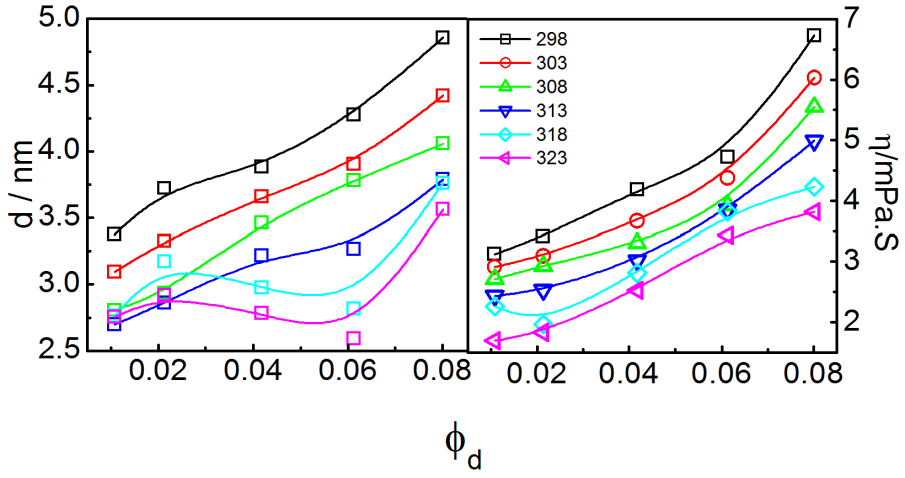

Figure 4.8. *Variation in the size (diameter, d) and viscosity (η) of the polar domain*-in-oil microemulsion of ([bmim][MS]±water)/(Tween-20+n-pentanol)/n-heptane. Mole fraction of [bmim][MS] in the polar domain: 0.5. A 0.2M Tween-20 with 1:1 (w/w) n-pentanol solution was used. Temperatures (in K) are mentioned inside the Figure

With increasing volume fraction, except at the higher temperatures (318 and 323 K), the d - φ_d profiles were nearly linear. The DLS data closely matched with the size parameters derived from the method of dilution. Size of the μE droplets decreased with increasing temperature for all the compositions, which were quite unusual. The size constriction effect was noted in both the DLS measurements as well as in the method of dilution. This kind of size variation with temperature has never been reported previously for any IL μE systems. We assume that the size constriction upon heating was due to the formation of reorganized entities. Heating of the polar domain decreased the viscosity (as shown in Figure 4.8 right panel) which allowed the IL+water to get reorganized and therefore the structured entities were formed as proposed in Scheme 4.2. Such a proposition for the formation of organized assembly of IL-in-oil μE has been reported by several

authors [191,211,364,374]. However to make final conclusion in this regard, further studies like freeze fractured electron microscopy or cryo-TEM measurements are warranted. This can be considered as the future perspectives.

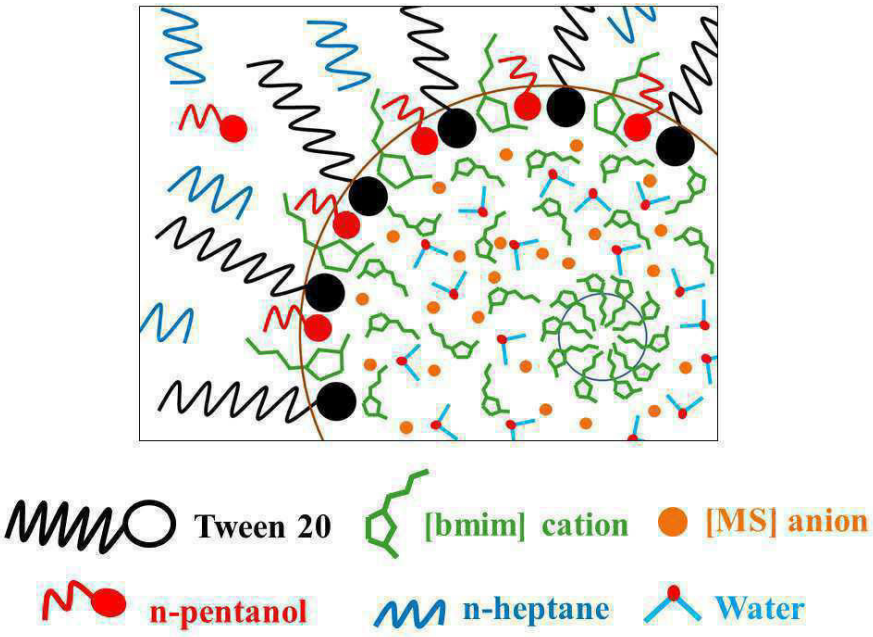

Scheme 4.2. Proposed model for the location/organization of the different components in [bmim][MS]+water/Tween 20+n-pentanol/n-heptane polar domain-in-oil microemulsion. The core of the microemulsion is comprised of micelle like aggregates of [bmim] cations.

3.4. Viscosity measurement. Viscosity of microemulsion depends on the size and number of droplets. In the present case, viscosity decreased almost linearly with temperature except a few cases. It is to be noted that in the case of pure binary mixtures in the bulk condition, viscosity variation were entirely different from the present study. Increase in viscosity with increasing volume of the dispersed phase is attributed to the increase in the size of the polar domain (the phenomenon of swelling effect). As the size of the droplets decreased with the increase in temperature hence it is not unexpected that viscosity would decrease with the increase in temperature. Additionally it is known that for all the liquids viscosity usually decreases with the increase in temperature.

3.5. Conductance measurement. Although the continuum is comprised of oil, the μEs with the ionic components in polar domain is expected to conduct electricity.

The percolation of electrical conductance for a μE in oil continuum can occur either through the "hopping mechanism" or through the mechanism of "fusion, mass transfer and fission"[28,62]. The effective mean theory with dipole-dipole interaction has been adapted in the present case. In the present set of experiment, both the volume and temperature induced conductance studies were performed. Variation in specific conductance with the volume fraction of (IL+water) at different compositions has been shown in Figure 4.9 at 298 K as representative. In the conductivity studies, ratio of surfactant, cosurfactant and oil were kept constant. Although comprised of ionic species in the polar domain, the present μE systems were found to be less conducting compared to conventional μEs comprising single tailed ionic surfactants.

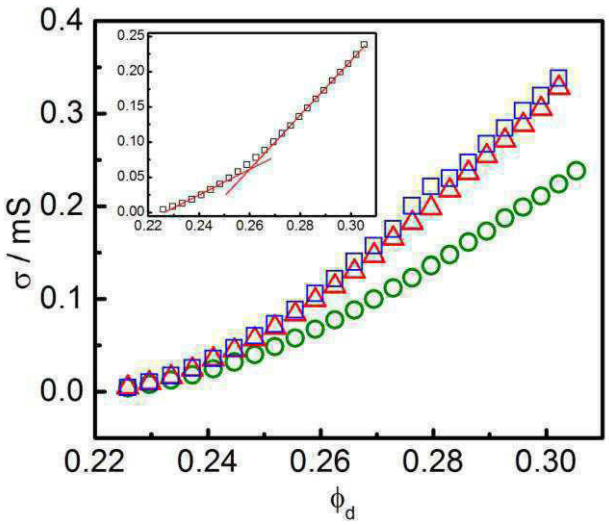

Figure 4.9. Volume induced percolation of ([bmim][MS]±water)/(Tween-20+n-pentanol)/n-heptane polar domain-in-oil microemulsion system. Mole fraction of *[bmim][MS] in the polar domain: O, 0.2; □, 0.5 and Δ, 0.8. Threshold volume fraction* (Φ_d^t) (for x_{IL}=0.2) was determined from the point of intersection of two tangents as shown in the inset. Temperature 298 K.

The depressed conductance was attributed to the dense packing of IL, the surfactant and cosurfactant at the polar domain / oil interface[113]. Besides, ILs can strongly interact with the oxyethylene group of Tween 20 [211]. These three combined factors effectively resulted in the formation of rigid entities. The threshold value for the volume induced percolation was determined from the intersection point of the two tangents as shown in the inset of Fig 9. This method of evaluation of percolation threshold (ϕ_d^t) have been previously reported [113,229].

The conductance derived results are summarized in Table 5. The conductance data were processed according to the scaling equation [226]:

$$\sigma = k (\phi_d - \phi_d^t)^m \quad \textbf{(4.30)}$$

$$\text{i.e.,} \quad \ln \sigma = \ln k + m \ln(\phi_d - \phi_d^t) \quad \textbf{(4.31)}$$

where, σ is the conductance of the microemulsion, k is a constant which depends on the conductance of the dispersed phase and m is the exponent, ϕ_d and ϕ_d^t are the post threshold and threshold volume fraction respectively. One can thus determine the value of lnk and m from the linear plot of ln σ vs $\ln(\phi_d - \phi_d^t)$ (Figure not shown to save space). According to the previously published results[51,103,115,375,376], higher ϕ_d^t corresponds to static percolation while lower ϕ_d^t indicates dynamic percolation. In the present case ϕ_d^t did not change significantly with the composition as well as the temperature. As predicted, the exponent 'm' remained constant for all the system except a few cases. The negative value of k increased with x_{IL}, which resulted from the decrease in the polarity of the binary mixtures, especially after x_{IL}> 0.5. In our previous study[368] as well as from the present results, it is known that IL, in combination with water, in polar domain can form micelle like aggregates leading to the decrease in the polarity of the dispersed phase. We failed to determine the threshold value for the temperature induced percolation, as shown in Figure 4.10. However, it was evident from Fig 10 that with increasing volume fraction of the polar domain, conductance increased. Interestingly, µEs comprising of larger proportion of IL (compared to water) were less conducting [Panel B and C of Figure 4.10]. This observation further reveals that the rigidity of the droplets is enhanced for systems comprising of high proportion of IL.

Table 4.5. Scaling law parameters for volume (IL+water) induced percolation of ([bmim][MS]±water) / (Tween-20+n-pentanol) / n-heptane polar domain-in-oil microemulsion system at different temperatures.

	ϕ_d^t / lnk / m			
IL+Water	**298K**	**303K**	**308K**	**313K**
2:8	0.276/-0.38±0.09 / 0.336±0.02	0.250 / 1.06±0.04 / 0.87±0.01	0.252 / 1.25±0.08 / 0.83±0.04	0.255 / 1.37±0.09 / 0.82±0.03
4:6	0.276 / -0.04±0.07 / 2.48±0.05	0.261/ 1.20±0.07 / 3.10±0.02	0.253 / -1.08±0.06/ 1.69±0.04	0.252/ -1.78±0.05 / 1.32±0.04
5:5	0.263 / -0.34±0.07/ 2.48±0.05	0.256 /-1.35±0.08 / 1.25±0.05	0.257/-2.01±0.01/ 0.94±0.007	0.263 /-1.94±0.04 / 1.18±0.03
6:4	0.263 / -1.04±0.05 / 1.34±0.02	0.258 /-1.79±0.02 / 1.01±0.02	0.258/-1.86±0.02 / 1.03±0.01	0.258/-2.01±0.01 / 1.00±0.008
8:2	0.263 / -1.54±0.05 / 1.46±0.04	0.257 /-1.59±0.02 / 1.39±0.02	0.258 /-2.02±0.04 / 1.21±0.04	0.259 /-2.09±0.01 / 1.38±0.02
Pure IL	0.256 /-1.25±0.04 / 1.49±0.03	0.259 /-1.44±0.04 / 1.56±0.03	0.252 /-1.78±0.03 / 1.36±0.03	0.262 /-2.06±0.04 / 1.57±0.04

A 0.2 M Tween 20 + n-pentanol (1:1, w/w) in n-heptane was used in each case.

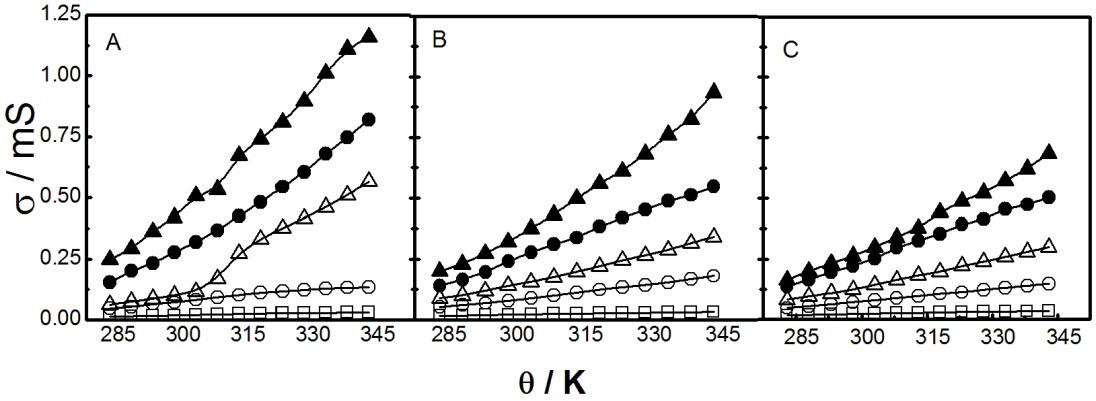

Figure 4.10. Temperature induced percolation of ([bmim][MS]±water)/(Tween-20+n-pentanol)/n-heptane polar domain-in-oil microemulsion. Mole fraction of [bmim][MS] in the polar domain: 0.2, panel A; 0.5, panel B and 0.8, panel C. Volume fraction of the *polar domain: □, 0.237; O, 0.252; Δ, 0.266; ●, 0.280 and ▲, 0.293.*

3.6. Spectroscopic studies. Absorption and emission spectroscopic probing techniques are considered to provide useful information in understanding the local environment of the polar domain-in-oil continuum. In the present study the anionic xanthene dye eosin Y was used as the probe. Our previous study involving the physico-chemical characterization of [bmim][MS]+water binary mixture was also carried out using eosin Y as the probe [369]. Such an approach has also been followed by different researchers [176,202,204,360]. Eosin Y is completely insoluble in n-heptane, therefore, it would predominantly reside in the polar domain [340,360]. Absorption and emission spectra of eosin Y in different media have been shown in Figure 4.11. While considering the absorption spectra of eosin Y in pure water, it was observed that eosin Y exhibits a strong intense peak at 517 nm with a shoulder appearing at 495 nm. For bulk IL+water mixture, the spectra was red shifted at 537 nm. The peak for eosin Y in the μE appeared at 530 nm. The red shift in the absorption maxima was due to the increasing polarity of the solvent [360,369].

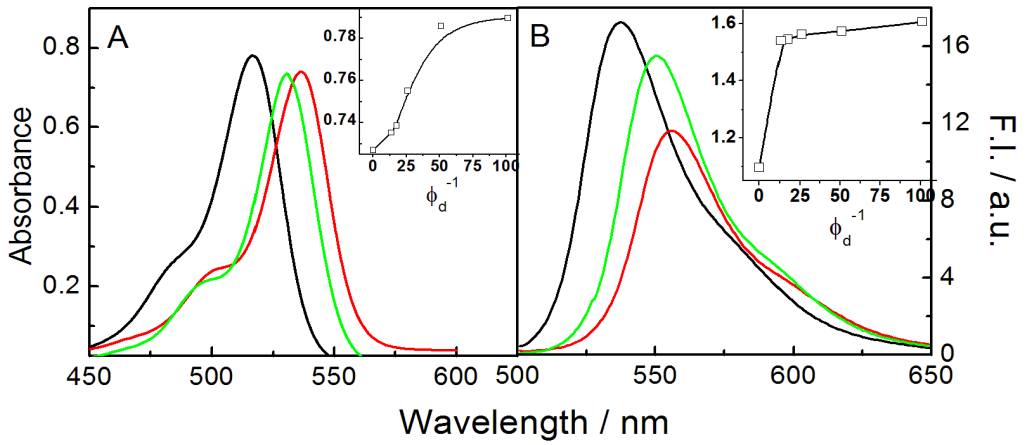

Figure 4.11. Absorption (A) and steady state emission spectra (B) of eosin Y in ([bmim][MS]±water)/(Tween-20+n-pentanol)/n-heptane polar domain-in-oil microemulsion system along with the spectra in pure water and IL + water mixture. Spectra in pure water are shown through the black lines while the green lines correspond *to the spectra in IL+water in μE comprising 50 mole% IL and* φ_d =0.057. The red lines represent the spectra of eosinY in IL + water mixture. In the insets, absorbance (at 517 nm) vs. φ_d^{-1} profile (panel A) and fluorescence intensity (at 537 nm) vs. φ_d^{-1} (panel B) *have been shown. Overall concentration of eosin Y was kept constant at 10 μM.* λ_{ex} = 500nm.

When excited at 500 nm, eosin Y in neat water showed an emission maximum at 537 nm. In the case of IL + water, the emission peak appeared at 556 nm. The results were in conformity with our previous reports [340,368]. Eosin Y in the μE exhibited intermediate behavior. Red shift in the fluorescence spectra was due to the enhanced polarity of the medium[225]. For each binary combination of [bmim][MS] and water, the spectra of eosin Y were recorded at different φ_d values for (IL+water)-in-oil μEs. All the results are not shown to save space. Compared to the absorption and emission intensity of eosin Y in water, the values decreased with increasing volume fraction of the polar domain. Simultaneously there occurred red shifts in both the absorption and emission spectra which suggests that the microenvironment around eosin Y in the μE are not the same[113]. Progressive red shift with increasing φ_d value reflects the change in the state of polar domain. Interestingly, decrease in both the absorbance and fluorescence intensity with φ_d were nonlinear in the range 0.009 - 0.07. To understand the states of the polar components in the μE system, absorbance (at 517 nm) and the fluorescence intensity (at 537 nm) were plotted against the reciprocal of the volume fraction of the dispersed phase (φ_d^{-1}). Representative plots for 50 mole% [bmim][MS] (with respect to water) have been shown in the insets of Figure 4.11.

In both the cases break points appeared around $\varphi_d^{-1} = 25$, above which, especially the fluorescence intensity, increased linearly. Results clearly indicate the change in the state of the polar component in this range. With increasing φ_d in the lower range polar components were involved in solvating the surfactant head groups whereby they resided in the palisade layer of the μE. Once the surfactant head groups were completely solvated, the polar components became free and could behave like bulk entities. Such an observation has not been reported previously and this may be considered as the novelty of the present work. To understand the solvation phenomena in further detail, both the fluorescence anisotropy and lifetime measurements were carried out for the μEs using eosin Y as the probe. Such studies helped in understanding the microviscosity of the medium as well [216,356]. Representative plots for the anisotropy and lifetime variation with φ_d^{-1} have been shown in Figure 4.12 for μE comprising of 50 mole% IL. Results for other combinations have been shown in the Figure 4.13.

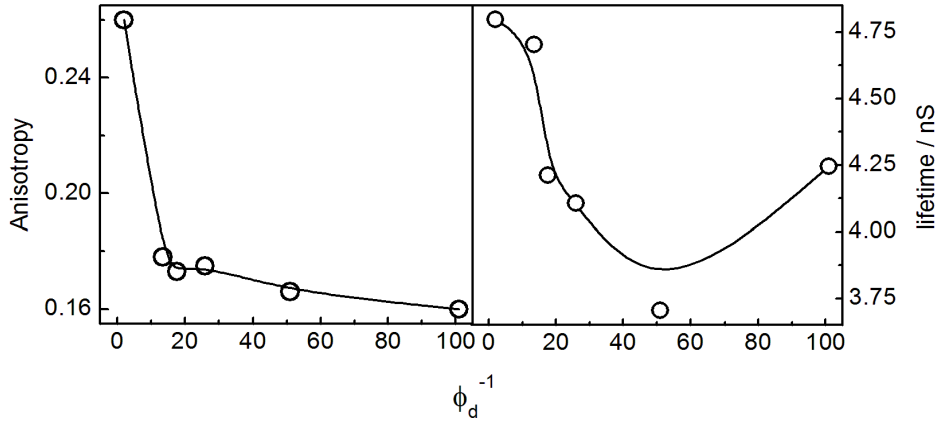

Figure 4.12. Variation in the anisotropy and lifetime for 10μM eosin Y with the inverse *of volume fraction of the polar domain* (φ_d^{-1}) for ([bmim][MS]±water)/(Tween-20+n-pentanol)/n-heptane polar domain-in-oil microemulsion system. An equimolar mixture of [bmim][MS] and water was used as the polar domain. A 10 μM *eosin Y was used.* λ_{ex}= *500nm and* λ_{em}= 537nm.

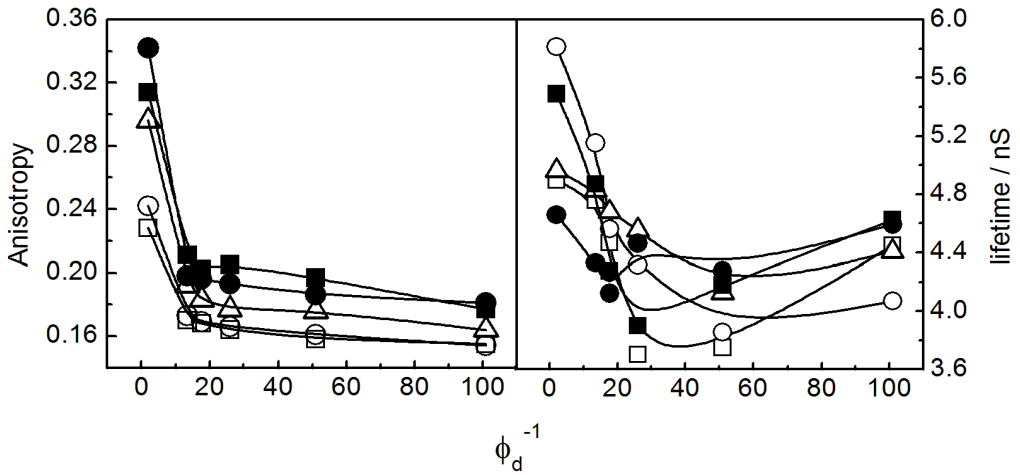

Figure 4.13. Variation in the fluorescence anisotropy and lifetime for 10µM eosinY with the inverse of *volume fraction of the polar domain* (φ_d^{-1}) for ([bmim][MS]±water)/(Tween-20+n-pentanol)/n-heptane polar domain-in-oil microemulsion system. *Mole fraction of [bmim][MS] in the polar domain: (□) 0.2; (O)0.4; (Δ) 0.6; (■)0.8 and (●) 1.0.*

Appearance of break point around φ_d^{-1} = 20 - 25 conforms the conclusion as drawn in the absorption and steady state fluorescence measurements. However, to understand such systems completely, further studies like small angle neutron scattering (SANS), transmission electron microscopy (TEM) and ultrafast solvent dynamic studies are warranted and these are considered as future perspectives.

SUMMARY AND CONCLUSION

SUMMARY AND CONCLUSION

The present dissertation describes the results on physico-chemical studies on μEs involving water, 1-butyl-4-methylpyridinium tetrafluoroborate, [b4mim][BF_4], and 1-butyl-3-methylimidazolim methanesulfonate, [bmim][MS], in the polar domain. Additionally the binary mixture of [bmim][MS] and water was studied with an intention to use them as the polar component in μE.

In **Chapter 1,** comprehensive studies on water/ (Tween-20+n-alkanol)/n-heptane microemulsions were performed using a number of techniques, viz., phase manifestation, dilution method, DLS and viscosity measurements. Results were analyzed in the light of the above mentioned experiments. Based on the observations, the following conclusions could be made:

(1) The clarity of microemulsion formulation was reduced with the increase in cosurfactant chain length with an optimum efficacy tendered by n-hexanol.

(2) While the surfactants reside at the oil-water interface, the cosurfactants were partitioned in between the oil and oil-water interface.

(3) Spontaneity of microemulsion formation increased with increase in cosurfactant chain length, increase in temperature and decrease in the volume of the dispersed phase, water.

(4) The formation of microemulsion was found to be an enthalpy controlled process.

(5) Larger numbers of droplets were formed at the expense of size. With the increase in temperature and ω value, size reduction was also evidenced by DLS measurements.

(6) Depletion in the aggregation number of surfactant per droplet was compensated by the cosurfactant molecules. However, the compensatory effect was not affected by temperature.

A symmetric variation in different physico-chemical properties were noted with the increase in the cosurfactant chain length. However, n-octanol, being oilier in nature than a cosurfactant, tendered different behavior.

Chapter 2 describes the detailed investigations on 1-butyl-4-methyl pyridinium tetrafluoroborate ([b4mpy][BF_4]) / (Tween 20 + n-pentanol) / n-heptane ionic liquid-in-oil microemulsion system. Although the cosurfactant increased turbidity of the microemulsion, however, it was essential for the attainment of stable microemulsion. Cosurfactant controlled the curvature of the microemulsion droplets; it simultaneously also imparted better stability by solvating the cationic component of the ionic liquid. Larger number of droplet formation was aided by the cosurfactant. Sensitivity towards temperature decreased with increasing amount of cosurfactant, as revealed through the combined dynamic light scattering and viscosity measurements. Oxyethylene group of Tween 20 formed coordinate linkages with the IL cation, which resulted in the rigidity of the polar domain. The IL, in excess of the amount required for coordinating the surfactant head groups, behaved like the bulk component as revealed through the fluorescence anisotropy measurements. Electron microscopy and small angle neutron scattering studies could further shed light on the morphology of the microemulsion droplets, which are considered as the future perspective.

In **Chapter 3**, physico-chemical investigations on the binary mixture of [bmim][MS] + water were carried out both in the dilute and concentrated regime of [bmim][MS] using different techniques. There occurred a synergistic interaction between the [bmim][MS] and water. The surface tension decreased monotonously with a halt at 0.3 M [bmim][MS]. The absorption and emission spectral behaviors were significantly different. The steady state fluorescence anisotropy and excited state lifetime were dependent on the concentration of [bmim][MS] in water. It was finally concluded that initially increasing the IL concentration led to the formation of an ion-pair, whereby the cationic component, which was surface active, was interfacially absorbed. Micelle-like aggregates were formed above a certain concentration, which was similar to ionic clusters. Above 50 mole% ionic liquid, a three dimensional quasi crystal-like network was formed which deactivates the water molecules.

Chapter 4 describes the studies on combined phase behavior, method of dilution, viscosity, dynamic light scattering, electrical conductance and

spectroscopic probing techniques in understanding the physicochemical properties of pseudoternary microemulsion system 1-butyl-3-methyl imidazolium methanesulfonate ([bmim][MS]±water) / (Tween-20+n-pentanol) / n-heptane. From phase manifestation it was observed that clarity of microemulsion decreases upto 50 mole % of the IL as after 50 mole %, the added water cannot disturb the structuredness of IL, thus above that said IL mole fraction, the IL become such an entity where water become inactive. For lower IL content microemulsion, spontaneity of the microemulsion decreases with increase in the volume of the dispersed phase whereas it increased above 50 mole % of the IL. Size of the microemulsion increases with increase in the volume fraction of the polar phase, this was also evidenced through the viscosity measurements. Although comprised of ionic species in the polar domain, the present microemulsion systems were found to be less conducting. Both the absorbance and fluorescence intensity decreased with increasing volume fraction of the polar phase. A red shift in the absorption and fluorescence spectra was obtained due to the increased polarity of the solvent.

BIBLIOGRAPHY

BIBLIOGRAPHY

(1) Moulik, S. P. Curr. Sci. **1996**, 71, 368.

(2) Tanford, C. J. Phys. Chem. **1972**, 76, 3020.

(3) Tanford, C.; Nozaki, Y.; Rohde, M. F. J. Phys. Chem. **1977**, 81, 1555.

(4) Evans, D. F.; Ninham, B. W. J. Phys. Chem. **1983**, 87, 5025.

(5) Evans, D. F.; Ninham, B. W. J. Phys. Chem. **1986**, 90, 226.

(6) Hardy, W. L.; Snell, F. D. Ind. Eng. Chem. **1957**, 49, 95A.

(7) Nelson, A. F. J. Chem. Edu. **1948**, 25, 379.

(8) Snell, F. D. J. Chem. Edu. **1942**, 19, 172.

(9) Menger, F. M.; Keiper, J. S. Angew. Chem. Int. Ed. **2000**, 39, 1906.

(10) Oda, R.; Huc, I.; Candau, S. J. Angew. Chem. Int. Ed. **1998**, 37, 2689.

(11) Oda, R.; J. Candau, S.; Huc, I. Chem. Commun. **1997**, 0, 2105.

(12) Abe, M.; Tsubone, K.; Koike, T.; Tsuchiya, K.; Ohkubo, T.; Sakai, H. Langmuir **2006**, 22, 8293.

(13) Bakshi, M.; Kaur, I. Colloid. Polym. Sci. **2004**, 282, 476.

(14) Pisárčik, M.; Polakovičová, M.; Pupák, M.; Devínsky, F.; Lacko, I. J. Colloid Interface Sci. **2009**, 329, 153.

(15) Chen, Y.; Liu, Y.; Guo, R. J. Colloid Interface Sci. **2009**, 336, 766.

(16) Yin, S.; Wang, C.; Song, B.; Chen, S.; Wang, Z. Langmuir **2009**, 25, 8968.

(17) Kaler, E. W.; Herrington, K. L.; Murthy, A. K.; Zasadzinski, J. A. N. J. Phys. Chem. **1992**, 96, 6698.

(18) Kaler, E. W.; Puig, J. E.; Miller, W. G. J. Phys. Chem. **1984**, 88, 2887.

(19) Kamenka, N.; El Amrani, M.; Appell, J.; Lindheimer, M. J. Colloid Interface Sci. **1991**, 143, 463.

(20) Khan, A.; Mendonca, C. J. Colloid Interface Sci. **1995**, 169, 60.

(21) Edlund, H.; Sadaghiani, A.; Khan, A. Langmuir **1997**, 13, 4953.

(22) Marques, E. F. Langmuir **2000**, 16, 4798.

(23) Tah, B.; Pal, P.; Mahato, M.; Talapatra, G. B. J. Phys. Chem. B **2011**, 115, 8493.

(24) Vold, R. D. J. Chem. Edu. **1965**, 42, 692.

(25) Griffin, W. C. J. Soc. Cosmet. Chem. **1949**, 1, 311.

(26) Griffin, W. C. J. Soc. Cosmet. Chem. **1954**, 5, 259.

(27) Israelachvili, J. N.; Mitchell, D. J.; Ninham, B. W. J. Chem. Soc. Faraday Transactions 2: Molecular and Chemical Physics **1976**, 72, 1525.

(28) Paul, B. K.; Moulik, S. P. J. Disp. Scie. Technol. **1997**, 18, 301.

(29) Scott, H. Coll. Int. Sci. **1998**, 20, 496.

(30) Shah, D. O. Micelles, Microemulsions and Monolayers; Marcel Dekker Inc.: New York, 1998.

(31) Moulik, S. P. H., M. E.; Jana, P. K.; Das, A. R. J. Phys. Chem. **1996**, 100, 701.

(32) Nagarajan, R. Langmuir **1985**, 1, 331.

(33) Nagarajan, R. Adv. Colloid Interface Sci. **1984**, 26, 205.

(34) Moulik, S. P.; Paul, B. K. Adv. Colloid Interface Sci. **1998**, 78, 99.

(35) Mitra, R. K.; Paul, B. K.; Moulik, S. P. J. Colloid Interface Sci. **2006**, 300, 755.

(36) Tanford, C. Physics of Amphiphiles: Micelles, Vesicles and Microemulsions; North Holland Physics Publishing: Amsterdam, **1985**.

(37) Shah, D. O. Marcel Dekker Inc.: New York **1998**.

(38) Acharya, A.; Sanyal, S. K.; Moulik, S. P. Curr. Sci. **2001**, 81, 362.

(39) Moulik, S. P.; Rakshit, A. K. J. Surf. Sci. Technol. **2006**, 22, 159.

(40) Töndre, C.; Hebrant, M. J. Mol. Liq. **1997**, 72, 279.

(41) Sjoblom, E.; Friberg, S. E. J. Colloid Interface Sci. **1978**, 67, 16.

(42) Safran, S. A.; Webman, I.; Grest, G. S. Phys. Rev. A **1985**, 32, 506.

(43) Safran, S. A.; Turkevich, L. A. Phys. Rev. Lett. **1983**, 1930.

(44) Peyrelasse, J.; Boned, C. Phys. Rev. A **1990**, 41, 938.

(45) Luisi, P. L.; Magid, L. J. CRC Crit. Rev. Biochem. **1986**, 20, 409.

(46) López-Quintela, M. A.; Tojo, C.; Blanco, M. C.; García Rio, L.; Leis, J. R. Curr. Opin. Colloid Interface Sci. **2004**, 9, 264.

(47) Li, Q.; Li, T.; Wu, J. J. Colloid Interface Sci. **2001**, 239, 522.

(48) Kirkpatrick, S. Rev. Mod. Phys. **1973**, 45, 574.

(49) Kabalnov, A.; Lindman, B.; Olsson, U.; Piculell, L.; Thuresson, K.; Wennerstrom, H. Colloid Polym. Sci. **1996**, 274, 297.

(50) Gupta, S.; Moulik, S. P. J. Pharm. Sci. **2008**, 97, 27.

(51) Granqvist, C. G.; Hunderi, O. Phys. Rev. B **1978**, 18, 1554.

(52) Elliott, R. J.; Krumhansl, J. A.; Leath, P. L. Rev. Mod. Phys. **1974**, 46, 465.

(53) Cametti, C.; Codastefano, P.; Tartaglia, P.; Chen, S. H.; Rouch, J. J. Phys. Rev. A **1992**, 45.

(54) Bhattacharya, S.; Stokes, J. P.; Kim, M. W.; Huang, J. S. Phys. Rev. Lett. **1985**, 55, 1884.

(55) Bernasconi, J. Phys. Rev. B **1973**, 7, 2252.

(56) Schulman, J. H.; Stoeckenius, W.; L.M. Prince J. Phys. Chem. **1959**, 63, 1677.

(57) Safarikova, M.; Roy, I.; Gupta, M. N.; Safarik, I. J. Biotechnol. **2003**, 105, 255.

(58) Prince, L. M. J. Colloid Interface Sci. **1967**, 23, 165.

(59) Ghosh, S.; Moulik, S. P. J. Colloid Interface Sci. **1998**, 208, 357.

(60) Danielsson, I.; Lindman, B. Colloids Surf. **1981**, 3, 391.

(61) Moulik, S. P.; Rakshit, A. K. J. Surf. Sci. Technol. **2006**, 22, 159.

(62) Paul, B. K.; Moulik, S. P. Curr. Sci. **2001**, 80, 990.

(63) Kotlarchyk, M.; Sheu, E. Y.; Capel, M. Phys. Rev. A **1992**, 46, 928.

(64) Kotlarchyk, M.; Chen, S. H.; Huang, J. S.; Kim, M. W. Phys. Rev. Lett. **1984**, 53, 941.

(65) Khmelnitsky, Y. L.; Hilhorst, R.; Veeger, C. Eur. J. Biochem. **1988**, 176, 265.

(66) Smith, R. E.; Luisi, P. L. Helv. Chim. Acta **1980**, 63, 2302.

(67) Kahlweit, M. Science **1988**, 240, 617.

(68) Winsor, P. A. Trans. Faraday Soc. **1948**, 44, 376.

(69) Bennett, K. E.; Davis, H. T.; Scriven, L. E. J. Phys. Chem. **1982**, 86, 3917.

(70) Gonzales, C.; Guitierrez, T.; Galan, M.; Plaja, S.; Mans, C.; Costa, J. Proc. 6th Int. Symp on Surfactants in Solution **1988**, 256.

(71) Kunieda, H.; Asaoka, H.; Shinoda, K. J. Phys. Chem. **1988**, 92, 185.

(72) Moulik, S. P.; Chakraborty, I. J. Indian Chem. Soc. **2006**, 83, 745.

(73) Shinoda, K.; Friberg, S. Adv. Colloid Interface Sci. **1975**, 4, 281.

(74) Bansal, V. K.; Chinnaswamy, K.; Ramachandran, C.; Shah, D. O. J. Colloid Interface Sci. **1979**, 72, 524.

(75) Clausse, M.; Heil, J.; Peyrelasse, J.; Boned, C. J. Colloid Interface Sci. **1982**, 87, 584.

(76) Waernheim, T.; Sjoeblom, E.; Henriksson, U.; Stilbs, P. J. Phys. Chem. **1984**, 88, 5420.

(77) Frank, S. G.; Zografi, G. J. Colloid Interface Sci. **1965**, 29, 28.

(78) Bansal, V. K.; Shah, D. O.; O'Connell, J. P. J. Colloid Interface Sci.**1980**, 75, 462.

(79) Kahlweit, M.; Strey, R.; Haase, D. J. Phys. Chem. **1985**, 89, 163.

(80) Chen, V.; Evans, D. F.; Ninham, B. W. J. Phys. Chem. **1987**, 91, 1823.

(81) Bedwell, B.; Gulari, E. J. Colloid Interface Sci. **1984**, 102, 88.

(82) Ghosh, O.; Miller, C. A. J. Phys. Chem. **1987**, 91, 4528.

(83) Hwan, R.-N.; Miller, C. A.; Fort Jr, T. J. Colloid Interface Sci. **1979**, 68, 221.

(84) Amaral, C. L. C.; Itri, R.; Politi, M. J. Langmuir **1996**, 12, 4638.

(85) Wines, T. H.; Somasundaran, P. J. Colloid Interface Sci. **2002**, 256, 183.

(86) Garcia-Rio L.; Herves P.; Mejuto J. Colloid Interface Sci. **2000**, 225, 259.

(87) Eicke, H. F.; Hofmeier, U.; Quellet, C.; Zölzer, U. In Physics of Polymer Networks; Steinkopff: **1992**; Vol. 90, p 165.

(88) Holtzscherer, C.; Candau, F. Colloids Surf. **1988**, 29, 411.

(89) Graciaa, A.; Barakat, Y.; Schechter, R. S.; Wade, W. H.; Yiv, S. J. Colloid Interface Sci. **1982**, 89, 217.

(90) Healy, R. N.; Reed, R. L.; Stenmark, D. G. Soc. Pet. Eng. AIME J. **1976**, 16, 147.

(91) Bourrel, M.; Chambu, C. Soc. Pet. Eng. J. **1983**, 23, 327.

(92) De, T. K.; Maitra, A. Adv. Colloid Interface Sci. **1995**, 59, 95.

(93) Caponetti, E.; Lizzio, A.; Triolo, R.; Griffith, W. L.; Johnson Jr, J. S. Langmuir **1992**, 8, 1554.

(94) Lagues, M. J. phys. Lett. **1979**, 40.

(95) Petit, C.; Bommarius, A. S.; Pileni, M. P.; Hatton, T. A. J. Phys. Chem. **1992**, 96, 4653.

(96) Moulik, S. P.; Das, M. L.; Bhattacharya, P. K.; Das, A. R. Langmuir **1992**, 8, 2135.

(97) Hait, S. K.; Moulik, S. P. Langmuir **2002**, 18, 6736.

(98) Hait, S. K.; Sanyal, A.; Moulik, S. P. J. Phys. Chem. B **2002**, 106, 12642.

(99) Mitra, D.; Chakraborty, I.; Bhattacharya, S. C.; Moulik, S. P.; Roy, S.; Das, D.; Das, P. K. J. Phys. Chem. B **2006**, 110, 11314.

(100) Stroud, D. Phys. Rev. B **1975**, 12, 3368.

(101) Moulik, S. P.; De, G. C.; Bhowmik, B. B.; Panda, A. K. J. Phys. Chem. B **1999**, 103, 7122.

(102) Montalvo, G.; Valiente, M.; Rodenas, E. J. Colloid Interf. Sci. **1995**, 172, 495.

(103) Kirkpatrick, S. Phys. Rev. Lett. **1971**, 27, 1722.

(104) Landauer, R. J. Appl. Phys. **1952**, 23, 779.

(105) Bruggeman, D. A. G. Ann. Phys. (Leipzig) **1935**, 24, 636.

(106) Blanc, R.; Guyon, E. Ann. Isr. Phys. Soc. **1983**, 5, 229.

(107) Scher, H.; Zallen, R. J. Chem. Phys. **1970**, 53, 3759.

(108) Moulik, S. P.; Aylward, W. M.; Palepu, R. Can. J. Chem. **2001**, 79, 1.

(109) Bisal, S.; Bhattacharya, P. K.; Moulik, S. P. J. Phys. Chem. **1990**, 94, 350.

(110) Alexandridis, P.; Holzwarth, J. F.; Hatton, T. A. J. Phys. Chem. **1995**, 99, 8222.

(111) Schrier, M. Y.; Bullock, D. A.; Schrier, E. E. J. Phys. Chem. **1980**, 84, 350.

(112) Fang, J.; Venable, R. L. J. Colloid Interface Sci. **1987**, 116, 269.

(113) Chakrabarty, D.; Seth, D.; Chakraborty, A.; Sarkar, N. J. Phys. Chem. B **2005**, 109, 5753.

(114) Acharya, A.; Sanyal, S. K.; Moulik, S. P. J. Disp. Sci. Technol. **2001**, 22, 551.

(115) Lagourette, B.; Peyrelasse, J.; Boned, C.; Clausse, M. Nature **1979**, 281, 60.

(116) Hait, S. K.; Moulik, S. P.; Rodgers, M. P.; Burke, S. E.; Palepu, R. J. Phys. Chem. B **2001**, 105, 7145.

(117) Hilfiker, R.; Eicke, H.-F.; Geiger, S.; Furler, G. J. Colloid Interface Sci. **1985**, 105, 378.

(118) Mathew, C.; Patanjali, P. K.; Nabi, A.; Maitra, A. Colloids surf. **1988**, 30, 253.

(119) Jada, A.; Lang, J.; Zana, R. J. Phys. Chem. **1989**, 93, 10.

(120) Safran, S. A.; Grest, G. S.; Bug, A. L. R. Microemulsion Systems; Marcel Decker: New York, 1987.

(121) Levashov, A. V.; Khmelnitsky, Y. L.; Klyachko, N. L.; Chernyak, V. Y.; Martinek, K. J. Colloid Interface Sci. **1982**, 88, 444.

(122) Clausse, M.; Peyrellase, J.; Boned, C.; Heil, J.; Nicolas-Morgantini, L.; Zradha, A.; Plenum Press: New York, 1983; Vol. 3, p 1583.

(123) Feldman, Y.; Kozlovich, N.; Nir, I.; Garti, N. Phys. Rev. E **1995**, 51, 478.

(124) Miteseu, C. D.; Musolf, M. J. J. Phys. Lett. (Paris) **1983**, L-679.

(125) Ray, S.; Paul, S.; Moulik, S. P. J. Colloid Interface Sci. **1996**, 183, 6.

(126) Ray, S.; Bisal, S. R.; Moulik, S. P. Proceedings of the National Conference on Physical and Chemical Aspects of Organized Biological Assemblies **1991**, 85.

(127) Acharya, A.; Moulik, S. P.; Sanyal, S. K.; Mishra, B. K.; Puri, P. M. J. Colloid Interface Sci. **2002**, 245, 163.

(128) Acharya, A.; Sanyal, S. K.; Moulik, S. P. Int. J. Pharm. **2001**, 229, 213.

(129) Chen, S. H.; Huang, J. S. Phys. Rev. Lett. **1985**, 55, 1888.

(130) Brown, D.; Clarke, J. H. R. J. Phys. Chem. **1988**, 92, 2881.

(131) Candau, S. J. Surfactant Solutions: New Methods on Investigation; Marcel Decker: New York, 1987; Vol. 22.

(132) Miller, C. C. Proceedings of the Royal Society of London. Series A, Containing Papers of a Mathematical and Physical Character **1924**, 106, 724.

(133) Adhikari, A.; Das, D. K.; Sasmal, D. K.; Bhattacharyya, K. J. Phys. Chem. A **2009**, 113, 3737.

(134) Adhikari, A.; Sahu, K.; Dey, S.; Ghosh, S.; Mandal, U.; Bhattacharyya, K. J. Phys. Chem. B **2007**, 111, 12809.

(135) Ghosh, S.; Dey, S.; Adhikari, A.; Mandal, U.; Bhattacharyya, K. J. Phys. Chem. B **2007**, 111, 7085.

(136) Panda, A. K.; Bhowmik, B. B.; Das, A. R.; Moulik, S. P. Langmuir **2001**, 17, 1811.

(137) Panda, A. K.; Moulik, S. P.; Bhowmik, B. B.; Das, A. R. J. Colloid Interface Sci. **2001**, 235, 218.

(138) Majhi, P. R.; Moulik, S. P. J. Phys. Chem. B **1999**, 103, 5977.

(139) Feng, K. I.; Schelly, Z. A. J. Phys. Chem. **1995**, , 17207.

(140) Gao, Y.; Wang, S.; Zheng, L.; Han, S.; Zhang, X.; Lu, D.; Yu, L.; Ji, Y.; Zhang, G. J. Colloid Interface Sci. **2006**, 301, 612.

(141) Chen, J.; Zhang, J.; Liu, D.; Liu, Z.; Han, B.; Yang, G. Colloids Surf. B: Biointerfaces **2004**, 33, 33.

(142) Clarke, M. J.; Harrison, K. L.; Johnston, K. P.; Howdle, S. M. J. Am. Chem. Soc. **1997**, 119, 6399.

(143) Hasegawa, M.; Sugimura, T.; Shindo, Y.; Kitahara, A. Colloids. Surf. A **1996**, 109, 305.

(144) Seth, D.; Chakraborty, A.; Setua, P.; Sarkar, N. Langmuir **2006**, 22, 7768.

(145) Biais, J.; Mercier, M.; Bothorel, P.; Clin, B.; Lalane, P.; Lamaneau, B. J. Microsc. **1981**, 121, 169.

(146) Hildebrand, E. A.; Mickinno, I. R.; MacFarlane, D. R. J. Phys. Chem. **1986**, 96, 2784.

(147) Gulik-Krzywicki, T.; Larsson, K. Chem. Phys. Lipids **1984**, 35, 127.

(148) Santhanalakshmi, J.; Parameshwari, A. Ind. J. Chem. **1992**, 31 A, 630.

(149) Dubochet, J.; Alba, C. M.; MacFarlane, D. R.; Angell, C. A.; Kadiyala, R. K.; Adrian, M.; Teixeira, J. J. Phys. Chem. **1984**, 88, 6727.

(150) Guo, J. S.; El-Aasser, M. S.; Sudol, E. D.; Yue, H. J.; Vanderhoff, J. W. J. Colloid Interface Sci. **1990**, 140, 175.

(151) Vesetova, O. V.; Nikolaev, B. P.; Shlyakov, A. M. Kolloid. Zh. **1985**, 47, 1027.

(152) Mesa, C. L.; Coppola, L.; Raniera, G. A.; Terenzi, M.; Chidichimo, G. Langmuir **1992**, 8, 26.

(153) Garti, N.; Feldenkriez, R.; Aserin, A.; Ezrahi, S.; Shapira, D. Lubr. Eng. **1993**, 49, 404.

(154) Das, K. P.; Ceglie, A.; Lindman, B. J. Phys. Chem. **1987**, 91, 2938.

(155) Das, K. P.; Ceglie, A.; Lindman, B.; Friberg, S. E. J. Colloid Interface Sci. **1987**, 116, 390.

(156) Hendrikx, Y.; Kellay, H.; Meunier, J. Europhys. Lett. **1994**, 25, 735.

(157) Jonstromer, M.; Olsson, U.; Parker Jr, W. O. Langmuir **1995**, 11, 61.

(158) Leaver, M.; Furo, I.; Olsson, U. Langmuir **1995**, 11, 1524.

(159) Olsson, U.; Schurtenberger, P. Langmuir **1993**, 9, 3389.

(160) Olsson, U.; Soderman, O.; Guering, P. J. Phys. Chem.**1986**, 90, 5223.

(161) Parker W.O, Jr.; Genova, C.; Carignano, G. Colloids. Surf. A **1993**, 72, 275.

(162) Waysbort, D.; Ezrahi, S.; Aserin, A.; Givati, R.; Garti, N. J. Colloid Interface Sci. **1997**, 188, 282.

(163) Olsson, U.; Nagai, K.; Wennerstro?m, H. J.Phys. Chem.**1988**, 92, 6675.

(164) Mackay, R. A. R. Microemulsions; 1st ed.; Plenum Press: New York, 1982.

(165) Mackay, R. A.; Myers, S. A.; Bodalbhai, L.; Brajter-Toth, A. Anal. Chem. **1990**, 62, 1084.

(166) Mo, C. Langmuir **2002**, 18, 4047.

(167) Mo, C.; Zhong, M.; Zhong, Q. J. Electroanal. Chem. **2000**, 493, 100.

(168) Rusling, J. F.; Shi, C. N.; Kumosinski, T. F. Anal. Chem. **1988**, 60, 1260.

(169) Geetha, B.; Mandal, A. B. Langmuir **1995**, 11, 1464.

(170) Mandal, A. B. Langmuir **1993**, 9, 1932.

(171) Mandal, A. B.; Nair, B. U. J. Phys. Chem. **1991**, 95, 9008.

(172) Myers, S. A.; Mackay, R. A.; Brajter-Toth, A. Anal. Chem. **1993**, 65, 3447.

(173) Mandal, A. B.; Nair, B. U.; Ramaswamy, D. Langmuir **1988**, 4, 736.

(174) Shah, D. M.; Davies, K. M.; Hussam, A. Langmuir **1997**, 13, 4729.

(175) Chokshi, K.; Qutubuddin, S.; Hussam, A. J. Colloid Interface Sci. **1989**, 129, 315.

(176) Gao, Y. a.; Li, N.; Zheng, L.; Zhao, X.; Zhang, S.; Han, B.; Hou, W.; Li, G. Green Chem. **2006**, 8, 43.

(177) Discussions of the Faraday Society **1961**, 32, 1.

(178) Sugden, S.; Wilkins, H. J. Chem. Soc. **1929**, 0, 1291.

(179) Welton, T. Chem. Rev. **1999**, 99, 2071.

(180) Gabriel, S.; Weiner, J. Berichte der deutschen chemischen Gesellschaft **1888**, 21, 2669.

(181) Plechkova, N. V.; Seddon, K. R. Chem. Soc. Rev. **2008**, 37, 123.

(182) Natalia, V. P.; Robin, D. R.; Kenneth, R. S. In Ionic Liquids: From Knowledge to Application; American Chemical Society: 2009; Vol. 1030, p xi.

(183) Rogers Robin, D.; Seddon Kenneth, R. In Ionic Liquids IIIB: Fundamentals, Progress, Challenges, and Opportunities; American Chemical Society: 2005; Vol. 902, p xiii.

(184) Xue, L.; Li, Y.; Zou, F.; Lu, L.; Zhao, Y.; Huang, X.; Qu, Y. Colloids Surf. B: Biointerfaces **2012**, 92, 360.

(185) Fischer, T.; Sethi, A.; Welton, T.; Woolf, J. Tetrahed. Lett. **1999**, 40, 793.

(186) Guo, Y.; He, D.; Xia, S.; Xie, X.; Gao, X.; Zhang, Q. J. Nanomat. **2012**, 2012.

(187) Moniruzzaman, M.; Kamiya, N.; Goto, M. J. Colloid Interface Sci. **2010**, 352, 136.

(188) Hough, W. L. R., R. D.. Bull. Chem. Soc. Jpn. **2007**, 80, 2262.

(189) Galiński, M.; Lewandowski, A.; Stępniak, I. Electrochim. Acta. **2006**, 51, 5567.

(190) Garcia, B.; Lavallée, S.; Perron, G.; Michot, C.; Armand, M. Electrochim. Acta. **2004**, 49, 4583.

(191) Qiu, Z.; Texter, J. Curr. Opin. Colloid Interface Sci. **2008**, 13, 252.

(192) Wilkes, J. S.; Zaworotko, M. J. J. Chem. Soc., Chem. Commun. **1992**, 0, 965.

(193) Seth, D.; Chakraborty, A.; Setua, P.; Sarkar, N. J. Phys. Chem. B **2007**, 111, 4781.

(194) Huddleston, J. G.; Visser, A. E.; Reichert, W. M.; Willauer, H. D.; Broker, G. A.; Rogers, R. D. Green Chem. **2001**, 3, 156.

(195) Ludwig, R. Angew. Chem. Int. Ed. **2001**, 40, 1808.

(196) Zhang, S.; Li, X.; Chen, H.; Wang, J.; Zhang, J.; Zhang, M. J. Chem. Eng. Data. **2004**, 49, 760.

(197) Schroder, U.; Wadhawan, J. D.; Compton, R. G.; Marken, F.; Suarez, P. A. Z.; Consorti, C. S.; de Souza, R. F.; Dupont, J. New J.Chem. **2000**, 24, 1009.

(198) Seddon, K. R.; Stark, A.; Torres, M. J. Pure Appl. Chem. **2000**, 72, 2275.

(199) Fletcher, K. A.; Pandey, S. Langmuir **2003**, 20, 33.

(200) Freire, M. G.; Carvalho, P. J.; Fernandes, A. M.; Marrucho, I. M.; Queimada, A. J.; Coutinho, J. A. P. J. Colloid Interface Sci. **2007**, 314, 621.

(201) Binks, B. P.; Dyab, A. K. F.; Fletcher, P. D. I. Chem. Commun. **2003**, 2540.

(202) Cheng, S.; Fu, X.; Liu, J.; Zhang, J.; Zhang, Z.; Wei, Y.; Han, B. Colloids. Surf. A **2007**, 302, 211.

(203) Gao, H.; Li, J.; Han, B.; Chen, W.; Zhang, J.; Zhang, R.; Yan, D. Phys. Chem. Chem. Phys. **2004**, 6, 2914.

(204) Gao, Y.; Han, S.; Han, B.; Li, G.; Shen, D.; Li, Z.; Du, J.; Hou, W.; Zhang, G. Langmuir **2005**, 21, 5681.

(205) Gao, Y. a.; Zhang, J.; Xu, H.; Zhao, X.; Zheng, L.; Li, X.; Yu, L. Chem. Phys. Chem. **2006**, 7, 1554.

(206) Atkin, R.; Warr, G. G. J. Phys. Chem. B **2007**, 111, 9309.

(207) Andújar-Matalobos, M.; García-Río, L.; López-García, S.; Rodríguez-Dafonte, P. J. Colloid Interface Sci. **2011**, 363, 261.

(208) Zech, O.; Thomaier, S.; Kolodziejski, A.; Touraud, D.; Grillo, I.; Kunz, W. J. Colloid Interface Sci. **2010**, 347, 227.

(209) Klee, A.; Prevost, S.; Kunz, W.; Schweins, R.; Kiefer, K.; Gradzielski, M. Phys. Chem. Chem. Phys.**2012**, 14, 15355.

(210) Bhattacharya, B.; Samanta, A. J. Phys. Chem. B **2008**, 112, 10101.

(211) Gao, Y.; Li, N.; Hilfert, L.; Zhang, S.; Zheng, L.; Yu, L. Langmuir **2009**, 25, 1360.

(212) Rao, V. G.; Ghosh, S.; Ghatak, C.; Mandal, S.; Brahmachari, U.; Sarkar, N. J. Phys. Chem. B **2012**, 116, 2850.

(213) Rojas, O.; Koetz, J.; Kosmella, S.; Tiersch, B.; Wacker, P.; Kramer, M. J. Colloid Interface Sci. **2009**, 333, 782.

(214) Samanta, A. J. Phys. Chem. B **2006**, 110, 13704.

(215) Samanta, A. J. Phys. Chem. Lett. **2010**, 1, 1557.

(216) Sarkar, N.; Das, K.; Datta, A.; Das, S.; Bhattacharyya, K. J. Phys. Chem.**1996**, 100, 10523.

(217) Myakonkaya, O.; Eastoe, J.; Mutch, K. J.; Rogers, S.; Heenan, R.; Grillo, I. Langmuir **2009**, 25, 2743.

(218) Bufe, M.; Wolff, T. Langmuir **2009**, 25, 7927.

(219) Lindman, B.; Shinoda, K.; Jonstromer, M.; Shinohara, A. J.Phys. Chem.**1988**, 92, 4702.

(220) Moulik, S. P.; Paul, B. K. Adv. Colloid Interface Sci. **1998**, 78, 99.

(221) Levinger, N. E.; Swafford, L. A. Annu. Rev. Phys. Chem. **2009**, 60, 385.

(222) Da Silva, R. C.; Loh, W.; Olofsson, G. Thermochim. Acta **2004**, 417, 295.

(223) Digout, L.; Bren, K.; Palepu, R.; Moulik, S. P. Colloid Polymer Sci. **2001**, 279, 655.

(224) Moulik, S. P.; Digout, L. G.; Aylward, W. M.; Palepu, R. Langmuir **2000**, 16, 3101.

(225) Adhikari, A.; Das, D. K.; Sasmal, D. K.; Bhattacharyya, K. J. Phys. Chem. A **2009**, 113, 3737.

(226) De, M.; Bhattacharya, S. C.; Panda, A. K.; Moulik, S. P. J. Dispersion Sci. Technol. **2009**, 30, 1262.

(227) Ninham, B. W.; Chen, S. J.; Evans, D. F. J. Phys. Chem. **1984**, 88, 5855.

(228) De, M.; Bhattacharya, S.; Moulik, S.; Panda, A. J. Surfact. Deterg. **2010**, 13, 475.

(229) De, M.; Bhattacharya, S. C.; Panda, A. K.; Moulik, S. P. J. Dispersion Sci. Technol. **2009**, 30, 277.

(230) De, S.; Das, S.; Girigoswami, A. Spectrochim. Acta, Part A **2005**, 61, 1821.

(231) Zharkouskay, A.; Lünsdorf, H.; Feldmann, C. J. Mat. Sci. **2009**, 44, 3936.

(232) Li, X.-W.; Zhang, J.; Zheng, L.-Q.; Chen, B.; Wu, L.-Z.; Lv, F.-F.; Dong, B.; Tung, C.-H. Langmuir **2009**, 25, 5484.

(233) Attwood, D.; Mallon, C.; Ktistis, G.; Taylor, C. J. Int. J. Pharm.**1992**, 88, 417.

(234) Attwood, D.; Patel, H. K. J. Colloid Interface Sci. **1989**, 129, 222.

(235) Bandres, I.; Royo, F. M.; Gascon, I.; Castro, M.; Lafuente, C. J. Phys. Chem. B **2010**, 114, 3601.

(236) Zhou, G.; Luo, Z.; Fu, X. Ind. Crops Prod. **2014**, 52, 105.

(237) Shang, W.; Kang, X.; Ning, H.; Zhang, J.; Zhang, X.; Wu, Z.; Mo, G.; Xing, X.; Han, B. Langmuir **2013**, 29, 13168.

(238) Wang, A.; Chen, L.; Jiang, D.; Yan, Z. Ind. Crops Prod. **2013**, 51, 425.

(239) Ying, A.; Xu, S.; Liu, S.; Ni, Y.; Yang, J.; Wu, C. Ind. Eng. Chem. Res. **2013**, 53, 547.

(240) Domanska, U.; Krolikowski, M.; Ramjugernath, D.; Letcher, T. M.; Tumba, K. J. Phys. Chem. B **2010**, 114, 15011.

(241) Saito, A.; Watanuki, N.; Kobayashi, S.; Toray Industries, Inc., Japan . 2010, p 18pp.

(242) Hanaki, I.; Ukei, N.; Nitto Denko Corp., Japan . 2012, p 28pp.; Chemical Indexing Equivalent to 158:13028 (WO).

(243) Pandurangachar, M.; Kumara, S. B. E.; Chandrashekar, B. N.; Gilbert, O.; Reddy, S.; Sherigara, B. S. Int. J. Electrochem. Sci. **2010**, 5, 1187.

(244) Vieira, R. C.; Falvey, D. E. J. Am. Chem. Soc. **2008**, 130, 1552.

(245) Zhao, S.-H.; Zhang, H.-R.; Feng, L.-H.; Chen, Z.-B. J. Mol. Catal. A: Chem. **2006**, 258, 251.

(246) Chinnappan, A.; Jadhav, A. H.; Kim, H.; Chung, W.-J. Chem. Eng. J. (Amsterdam, Neth.) **2014**, 237, 95.

(247) Sintra, T. E.; Cruz, R.; Ventura, S. P. M.; Coutinho, J. A. P. J. Chem. Thermodyn. **2013**, Ahead of Print.

(248) García-Mardones, M.; Osorio, H. M.; Lafuente, C.; Gascón, I. J. Chem. Eng. Data. **2013**, 58, 1613.

(249) Takumi, H.; Imai, Y.; Toh, N.; Matsubara, H.; Takiue, T.; Aratono, M. Colloids Surf., A **2014**, 441, 59.

(250) Maheshwari, R. K.; Singh, A. K.; Gaddipati, J.; Srimal, R. C. Life Sci. **2006**, 78, 2081.

(251) Kaminaga, Y.; Nagatsu, A.; Akiyama, T.; Sugimoto, N.; Yamazaki, T.; Maitani, T.; Mizukami, H. FEBS Letters **2003**, 555, 311.

(252) Ravindranath V; N., C. Toxicol. **1980**, 16, 259.

(253) Wang, Z.; Leung, M. H. M.; Kee, T. W.; English, D. S. Langmuir **2009**, 26, 5520.

(254) Iwunze, M. O. J. Mol. Liq. **2004**, 111, 161.

(255) Semalty, A.; Semalty, M.; Rawat, M. S. M.; Franceschi, F. Fitoterapia **2010**, 81, 306.

(256) Baglole, K. N.; Boland, P. G.; Wagner, B. D. J. Photochem. Photobiol., A **2005**, 173, 230.

(257) Shah, C. P. M., B.; Kumar, M.; Priyadarsini, K. Indira; Bajaj, P. N. Curr. Sci. **2010**, 95, 1426.

(258) Letchford, K.; Liggins, R.; Burt, H. J. Pharm. Sci. **2008**, 97, 1179.

(259) Takahashi, M.; Uechi, S.; Takara, K.; Asikin, Y.; Wada, K. J. Agric. Food. Chem. **2009**, 57, 9141.

(260) Yallapu, M. M.; Gupta, B. K.; Jaggi, M.; Chauhan, S. C. J. Colloid Interface Sci. **2010**, 351, 19.

(261) Paul, S.; Panda, A. J. Surfact. Deterg. **2011**, 14, 473.

(262) Paul, S.; Panda, A. K. Colloids. Surf. A **2013**, 419, 113.

(263) Jana, B.; Ghosh, S.; Chattopadhyay, N. J. Photochem. Photobiol., B **2013**, 126, 1.

(264) Banerjee, C.; Ghatak, C.; Mandal, S.; Ghosh, S.; Kuchlyan, J.; Sarkar, N. J. Phys. Chem. B **2013**, 117, 6906.

(265) Adhikari, A.; Sahu, K.; Dey, S.; Ghosh, S.; Mandal, U.; Bhattacharyya, K. J. Phys. Chem. B **2007**, 111, 12809.

(266) Kerton, F. M. Alternative Solvents for Green Chemistry; RSC: Cambridge, 2009.

(267) Ohno, H. Electrochemical Aspects of Ionic Liquids; 2nd ed.; Wiley-VCH: Verlag GmbH, 2011.

(268) Reichardt, C.; Welton, T. Solvents and Solvent Effects in Organic Chemistry; Wiley-VCH: Weinheim, 2010.

(269) Schofer, S. H.; Kaftzik, n.; Kragl, U. Chem. Commun. **2001**, null, 425.

(270) Fröba, A. P.; Wasserscheid, P.; Gerhard, D.; Kremer, H.; Leipertz, A. J Phys Chem B. **2007**, 111, 12817.

(271) Wei, D.; Ivaska, A. Anal. Chim. Acta **2008**, 607, 126.

(272) Yoo, K.; Choi, H.; Dionysiou, D. D. Chem. Commun. **2004**, 2000.

(273) Balducci, A.; Soavi, F.; Mastragostino, M. Applied Physics A: Materials Science & Processing **2006**, 82, 627.

(274) Froba, A. P.; Kremer, H.; Leipertz, A. J. Phys. Chem. B **2008**, 112, 12420.

(275) Dyson, P. J.; Ellis, D. J.; Parker, D. G.; Welton, T. Chem. Commun. **1999**, null, 25.

(276) Scurto, A. M.; Aki, S. N. V. K.; Brennecke, J. F. J. Am. Chem. Soc. **2002**, 124, 10276.

(277) Dupont, J.; de Souza, R. F.; Suarez, P. A. Z. Chem. Rev. **2002**, 102, 3667.

(278) Aliaga, C.; Baldelli, S. J. Phys. Chem. C **2008**, 112, 3064.

(279) Mukherjee, P.; Crank, J. A.; Sharma, P. S.; Wijeratne, A. B.; Adhikary, R.; Bose, S.; Armstrong, D. W.; Petrich, J. W. J. Phys. Chem. B **2008**, 112, 3390.

(280) Mukherjee, P.; Crank, J. A.; Halder, M.; Armstrong, D. W.; Petrich, J. W. J. Phys. Chem. A **2006**, 110, 10725.

(281) Halder, M.; Headley, L. S.; Mukherjee, P.; Song, X.; Petrich, J. W. J. Phys. Chem. A **2006**, 110, 8623.

(282) Carvalho, P. J.; Regueira, T.; Santos, L. M. N. B. F.; Fernandez, J.; Coutinho, J. A. P. J. Chem. Eng. Data. **2009**, 55, 645.

(283) Fitchett, B. D.; Knepp, T. N.; Conboy, J. C. J. Electrochem. Soc. **2004**, 151, E219.

(284) Lauw, Y.; Horne, M. D.; Rodopoulos, T.; Webster, N. A. S.; Minofar, B.; Nelson, A. Phys. Chem. Chem. Phys.**2009**, 11, 11507.

(285) Lehmann, J.; Rausch, M. H.; Leipertz, A.; Froba, A. P. J. Chem. Eng. Data. **2010**, 55, 4068.

(286) Martinez, I. S.; Baldelli, S. J. Phys. Chem. C **2010**, 114, 11564.

(287) Najdanovic-Visak, V.; EsperanÃ§a, J. M. S. S.; Rebelo, L. P. N.; Nunes da Ponte, M.; Guedes, H. J. R.; Seddon, K. R.; de Sousa, H. C.; Szydlowski, J. J. Phys. Chem. B **2003**, 107, 12797.

(288) Rebelo, L. P. N.; Najdanovic-Visak, V.; Visak, Z. P.; Nunes da Ponte, M.; Szydlowski, J.; Cerdeirina, C. A.; Troncoso, J.; Romani, L.; Esperanca, J. M. S. S.; Guedes, H. J. R.; de Sousa, H. C. Green Chem. **2004**, 6, 369.

(289) Sung, J.; Jeon, Y.; Kim, D.; Iwahashi, T.; Iimori, T.; Seki, K.; Ouchi, Y. Chem. Phys. Lett. **2005**, 406, 495.

(290) Sung, J.; Jeon, Y.; Kim, D.; Iwahashi, T.; Seki, K.; Iimori, T.; Ouchi, Y. Colloids. Surf. A **2006**, 284-285, 84.

(291) Ventura, S. n. P. M.; Neves, C. M. S. S.; Freire, M. G.; Marrucho, I. M.; Oliveira, J.; Coutinho, J. A. P. J. Phys. Chem. B **2009**, 113, 9304.

(292) Widegren, J. A.; Laesecke, A.; Magee, J. W. Chem. Commun. **2005**, 1610.

(293) Kelkar, M. S.; Maginn, E. J. J. Phys. Chem. B **2007**, 111, 4867.

(294) Liu, W.; Cheng, L.; Zhang, Y.; Wang, H.; Yu, M. J. Mol. Liq. **2008**, 140, 68.

(295) Liu, W.; Zhao, T.; Zhang, Y.; Wang, H.; Yu, M. J. Sol.n Chem. **2006**, 35, 1337.

(296) Cornellas, A.; Perez, L.; Comelles, F.; Ribosa, I.; Manresa, A.; Garcia, M. T. J. Colloid Interface Sci. **2011**, 355, 164.

(297) Domanska, U.; Pobudkowska, A.; Rogalski, M. J. Colloid Interface Sci. **2008**, 322, 342.

(298) Ghasemian, E.; Najafi, M.; Rafati, A. A.; Felegari, Z. J. Chem. Thermodyn. **2010**, 42, 962.

(299) Jungnickel, C.; Luczak, J.; Ranke, J.; Fernández, J. F.; Müller, A.; Thöming, J. Colloids. Surf. A **2008**, 316, 278.

(300) Amano, T.; Iseki, A.; Nitto Denko Corp., Japan . 2010, p 46pp.

(301) Modaressi, A.; Sifaoui, H.; Mielcarz, M.; Domanska, U.; Rogalski, M. Colloids. Surf. A **2007**, 302, 181.

(302) Ries, L. A. S.; do Amaral, F. A.; Matos, K.; Martini, E. M. A.; de Souza, M. O.; de Souza, R. F. Polyhedron **2008**, 27, 3287.

(303) Vaghela, N. M.; Sastry, N. V.; Aswal, V. K. Colloids. Surf. A **2011**, 373, 101.

(304) O'Mahony, A. M.; Silvester, D. S.; Aldous, L.; Hardacre, C.; Compton, R. G. J. Chem. Eng. Data. **2008**, 53, 2884.

(305) Bowers, J.; Butts, C. P.; Martin, P. J.; Vergara-Gutierrez, M. C.; Heenan, R. K. Langmuir **2004**, 20, 2191.

(306) Singh, T.; Kumar, A. J. Phys. Chem. B **2007**, 111, 7843.

(307) Silvester, D. S.; Aldous, L.; Hardacre, C.; Compton, R. G. J. Phys. Chem. B **2007**, 111, 5000.

(308) Adhikari, A.; Dey, S.; Das, D. K.; Mandal, U.; Ghosh, S.; Bhattacharyya, K. J. Phys. Chem. B **2008**, 112, 6350.

(309) Mandal, P. K.; Sarkar, M.; Samanta, A. J. Phys. Chem. A **2004**, 108, 9048.

(310) Karmakar, R.; Samanta, A. J. Phys. Chem. A **2002**, 106, 4447.

(311) Mandal, P. K.; Samanta, A. J. Phys. Chem. B **2005**, 109, 15172.

(312) Santhosh, K.; Samanta, A. J. Phys. Chem. B **2010**, 114, 9195.

(313) Paul, A.; Samanta, A. J. Phys. Chem. B **2008**, 112, 16626.

(314) Karmakar, R.; Samanta, A. J. Phys. Chem. A **2003**, 107, 7340.

(315) Paul, A.; Sarkar, M.; Khara, D. C.; Kamijo, T.; Yamaguchi, A.; Teramae, N.; Samanta, A. Chem. Phys. Lett. **2009**, 469, 71.

(316) Ray, A.; Santhosh, K.; Chattopadhyay, S.; Samanta, A.; Bhattacharya, S. J. Phys. Chem. A **2010**, 114, 5544.

(317) Paul, A.; Samanta, A. J. Phys. Chem. B **2007**, 112, 947.

(318) Marciniak, A. J. Chem. Eng. Data. **2011**, 56, 368.

(319) Santos, C. S.; Rivera-Rubero, S.; Dibrov, S.; Baldelli, S. J. Phys. Chem. C **2007**, 111, 7682.

(320) Yang, J.; Zhang, Q.; Zhu, L.; Zhang, S.; Li, J.; Zhang, X.; Deng, Y. Chem. Mat. **2007**, 19, 2544.

(321) Rivera-Rubero, S.; Baldelli, S. J. Phys. Chem. B **2006**, 110, 4756.

(322) Rilo, E.; Pico, J.; García-Garabal, S.; Varela, L. M.; Cabeza, O. Fluid Phase Equilib. **2009**, 285, 83.

(323) Stark, A.; Zidell, A. W.; Hoffmann, M. M. J. Mol. Liq. **2011**, 160, 166.

(324) Tokuda, H.; Hayamizu, K.; Ishii, K.; Susan, M. A. B. H.; Watanabe, M. J. Phys. Chem. B **2004**, 108, 16593.

(325) Chakrabarty, A.; Mallick, A.; Haldar, B.; Das, P.; Chattopadhyay, N. Biomacromol. **2007**, 8, 920.

(326) Mallick, A.; Haldar, B.; Chattopadhyay, N. J. Phys. Chem. B **2005**, 109, 14683.

(327) Zhou, Q.; Wang, L.-S.; Chen, H.-P. J. Chem. Eng. Data. **2006**, 51, 905.

(328) Méndez-Morales, T.; Carrete, J. s.; Cabeza, O. s.; Gallego, L. J.; Varela, L. M. J. Phys. Chem. B **2011**, 115, 6995.

(329) Shekaari, H.; Mousavi, S. S. Fluid Phase Equilib. **2010**, 291, 201.

(330) Law, G.; Watson, P. R. Langmuir **2001**, 17, 6138.

(331) Vila, J.; Gines, P.; Pico, J. M.; Franjo, C.; Jimenez, E.; Varela, L. M.; Cabeza, O. Fluid Phase Equilib. **2006**, 242, 141.

(332) Vila, J.; Rilo, E.; Segade, L.; Cabeza, O.; Varela, L. M. Phys. Rev. E **2005**, 71, 031201.

(333) Wang, J.; Wang, H.; Zhang, S.; Zhang, H.; Zhao, Y. J. Phys. Chem. B **2007**, 111, 6181.

(334) Schreiner, C.; Zugmann, S.; Hartl, R.; Gores, H. J. J. Chem. Eng. Data. **2009**, 55, 1784.

(335) MacFarlane, D. R.; Forsyth, M.; Izgorodina, E. I.; Abbott, A. P.; Annat, G.; Fraser, K. Phys. Chem. Chem. Phys.**2009**, 11, 4962.

(336) Zhao, C.; Burrell, G.; Torriero, A. A. J.; Separovic, F.; Dunlop, N. F.; MacFarlane, D. R.; Bond, A. M. J. Phys. Chem. B **2008**, 112, 6923.

(337) Yoshizawa, M.; Xu, W.; Angell, C. A. J. Am. Chem. Soc. **2003**, 125, 15411.

(338) Bard, A. J.; Faulkner, L. R. Electrochemical Methods: Fundamentals and Applications; 2nd ed.; John Wiley & Sons: New York, 2001.

(339) Bhowmik, B. B.; Ganguly, P. Spectrochim. Acta, Part A **2005**, 61, 1997.

(340) Chakraborty, M.; Panda, A. K. Spectrochim. Acta, Part A **2011**, 81, 458.

(341) Anouti, M.; Jones, J.; Boisset, A.; Jacquemin, J.; Caillon-Caravanier, M.; Lemordant, D. J. Colloid Interface Sci. **2009**, 340, 104.

(342) Li, X.; He, G.; Zheng, W.; Xiao, G. Colloids. Surf. A **2010**, 360, 150.

(343) Wu, J.; Li, N.; Zheng, L.; Li, X.; Gao, Y. a.; Inoue, T. Langmuir **2008**, 24, 9314.

(344) Liu, S.; Xiao, J. Journal of Molecular Catalysis A: Chemical **2007**, 270, 1.

(345) Horváth, I. T.; Anastas, P. T. Chem. Rev. **2007**, 107, 2169.

(346) Joglekar, H. G.; Rahman, I.; Kulkarni, B. D. Chem. Eng. Technol. **2007**, 30, 819.

(347) Hao, J.; Zemb, T. Curr. Opin. Colloid Interface Sci. **2007**, 12, 129.

(348) Eastoe, J.; Gold, S.; Rogers, S. E.; Paul, A.; Welton, T.; Heenan, R. K.; Grillo, I. J. Am. Chem.l Soc. **2005**, 127, 7302.

(349) Friberg, S. E. J. Colloid Interface Sci. **2007**, 307, 494.

(350) Moulik, S. P.; Paul, B. K. Trasport Processes in Microemulsion; Surfactant Sci. Ser.: New York/Basel, 1999; Vol. 78.

(351) Moulik, S. P.; Ghosh, S. J. Mol. Liq. **1997**, 72, 145.

(352) Gradzielski, M.; Hoffmann, H. Adv. Colloid Interface Sci. **1992**, 42, 149.

(353) Stubenrauch, C.; Paeplow, B.; Findenegg, G. H. Langmuir **1997**, 13, 3652.

(354) Fanun, M. J. Mol. Liq. **2008**, 139, 14.

(355) Lindman, B.; Puyal, M. C.; Kamenka, N.; Brun, B.; Gunnarsson, G. J. Phys. Chem.**1982**, 86, 1702.

(356) Bhattacharyya, K. Acc. Chem. Res. **2003**, 36, 95.

(357) Greaves, T. L.; Drummond, C. J. Chem. Soc. Rev. **2008**, 37, 1709.

(358) Mehta, S. K.; Kaur, K. Indian J. Chem. **2010**, 49A, 662.

(359) Althanyan, M. S.; Assi, K. H.; Clark, B. J.; Hanaee, J. J. Pharm. Biomed. Anal. **2011**, 55, 397.

(360) Li, N.; Gao, Y. a.; Zheng, L.; Zhang, J.; Yu, L.; Li, X. Langmuir **2006**, 23, 1091.

(361) Zheng, Y.; Eli, W.; Li, G. Colloid. Polym. Sci. **2009**, 287, 871.

(362) Kunz, W.; Zemb, T.; Harrar, A. Curr. Opin. Colloid Interface Sci. **2012**, in press.

(363) Perrin, J. Les Atomes; Felix Alcan Paris, 1913.

(364) Wang, F.; Zhang, Z.; Li, D.; Yang, J.; Chu, C.; Xu, L. J. Chem. Eng. Data. **2011**, 56, 3328.

(365) Anderson, J. L.; Armstrong, D. W.; Wei, G. T. Anal. Chem. **2007**, 79, 4247.

(366) Visser, A. E.; Swatloski, R. P.; Griffin, S. T.; Hartman, D. H.; Rogers, R. D. Sep. Sci. Technol. **2001**, 36, 785.

(367) Belieres, J.-P.; Gervasio, D.; Angell, C. A. Chem. Commun. **2006**, 4799.

(368) Paul, B. K.; Mitra, R. K.; Moulik, S. P.; Taylor & Francis: 2012, p 3927.

(369) Paul, S.; Panda, A. K. Colloids. Surf. A **2012**, 404, 1.

(370) Biswas, S.; Bhattacharya, S. C.; Moulik, S. P. Indian J. Chem., Sect A **2001**, 40, 1210.

(371) Stark, A.; Wasserscheid, P. Handbook of Green Chemistry – Green Solvents–Ionic Liquids; Wiley-VCH, 2010; Vol. 6.

(372) Gerbacia, W.; Rosano, H. L. J. Colloid Interface Sci. **1973**, 44, 242.

(373) Maiti, K.; Mitra, D.; Mitra, R. N.; Panda, A. K.; Das, P. K.; Rakshit, A. K.; Moulik, S. P. J. Phys. Chem. B **2010**, 114, 7499.

(374) Li, N.; Cao, Q.; Gao, Y.; Zhang, J.; Zheng, L.; Bai, X.; Dong, B.; Li, Z.; Zhao, M.; Yu, L. ChemPhysChem **2007**, 8, 2211.

(375) Böttcher, C. J. F. Recl. Trav. Chem. **1945**, 64, 47.

(376) Maxwell, J. C. Electrochemistry and Magnetism; Third ed., 1892; Vol. 1.

BASIC DATA

BASIC DATA
OF
CHAPTER 1

Table 1. Phase manifestation for water/(Tween 20+n-alkanol)/n-Heptane water-in-oil microemulsion at 298 K.

Zone	Oil/g	(S+CS)/g	Water/g	Wt. % of the components		
				Oil (X)	S+CS(Y)	Water (Z)
With n-butanol:						
Clear fluid-turbid boundary	1.02	0.40	0.36	1.58	11.58	86.84
	1.37	0.40	0.45	1.69	12.40	85.90
	1.71	0.40	0.32	2.30	13.48	84.22
	2.05	0.40	0.36	3.04	16.16	80.80
	2.73	0.40	0.35	6.97	38.57	54.45
	3.07	0.40	0.36	11.78	41.52	46.70
	3.42	0.40	0.38	30.18	35.35	34.47
	3.76	0.40	0.36	50.48	29.56	19.96
	4.10	0.40	0.42	57.41	22.42	20.17
	0.05	0.40	2.77	61.64	18.05	20.31
	0.07	0.40	2.50	70.34	16.48	13.18
	0.08	0.40	2.00	72.94	14.24	12.82
	0.01	0.40	1.50	75.88	12.70	11.43
	0.05	0.40	3.00	78.46	11.49	10.05
	0.35	0.40	2.90	80.17	10.43	9.39
	0.31	1.50	2.40	81.41	9.54	9.06
With n-pentanol:						
Clear fluid-turbid boundary	0.01	0.53	0.27	0.72	65.69	33.59
	0.05	0.40	0.20	8.35	61.10	30.55
	0.07	0.40	0.20	10.22	59.85	29.93
	0.35	1.50	0.77	13.30	57.29	29.41
	0.43	1.09	0.57	20.42	52.32	27.26
	0.43	0.62	0.34	30.81	44.68	24.50
	0.85	0.67	0.40	44.19	34.93	20.87
	0.68	0.40	0.27	50.48	29.56	19.96
	1.02	0.40	0.37	57.09	22.29	20.62
	1.37	0.40	0.35	64.56	18.90	16.54
	1.71	0.40	0.35	69.48	16.28	14.24
	2.39	0.40	0.37	75.64	12.66	11.71
	3.42	0.40	0.36	81.80	9.58	8.62
	4.10	0.40	0.38	84.01	8.20	7.79
	5.46	0.40	0.39	87.37	6.40	6.24
	6.83	0.20	0.45	91.31	2.67	6.02
With n-hexanol:						
Clear fluid-turbid boundary	0.28	0.53	0.01	0.71	64.88	34.41
	0.18	0.40	0.05	8.61	63.03	28.36
	0.19	0.39	0.07	10.87	60.07	29.06
	0.47	0.99	0.28	16.12	56.82	27.06
	0.27	0.40	0.34	33.76	39.55	26.69
	0.29	0.40	0.68	49.75	29.13	21.12
	0.36	0.40	1.02	57.41	22.42	20.17
	0.32	0.40	1.37	65.48	19.18	15.34
	0.37	0.40	1.71	68.92	16.15	14.93
	0.35	0.40	2.73	78.46	11.49	10.05
	0.39	0.40	5.46	87.37	6.40	6.24
	0.45	0.40	6.83	88.93	5.21	5.86

Table 1. Phase manifestation for water/(Tween 20+n-alkanol)/n-Heptane water-in-oil microemulsion at 298 K.

Zone	Oil /g	(S+CS) /g	Water /g	Wt. % of the components		
				Oil (X)	S+CS(Y)	Water (Z)
With n-heptanol:						
Clear fluid-turbid boundary	0.31	1.70	0.74	0.71	64.88	34.41
	0.35	1.50	0.64	11.19	61.88	26.94
	0.14	0.36	0.18	14.00	60.28	25.72
	0.27	0.40	0.24	20.48	52.88	26.64
	0.35	0.48	0.30	29.92	43.80	26.28
	0.34	0.40	0.26	31.16	42.29	26.55
	0.68	0.40	0.33	34.10	39.94	25.96
	0.82	0.40	0.34	48.34	28.31	23.35
	0.96	0.40	0.32	52.55	25.65	21.80
	2.05	0.60	0.36	57.05	23.86	19.09
	0.50	0.21	0.00	68.10	19.94	11.96
With n-octanol:						
Clear fluid-turbid boundary	0.11	0.45	0.22	71.95	27.26	0.79
	0.51	1.50	0.73	57.78	27.98	14.25
	0.41	0.99	0.49	54.70	26.62	18.68
	0.27	0.40	0.19	52.31	25.97	21.72
	0.34	0.40	0.14	46.34	22.01	31.65
	0.68	0.40	0.14	45.38	15.88	38.74
	0.47	0.21	0.00	32.71	11.45	55.85

Table 2. Distribution constant (k_d) of water/(Tween 20+n-alkanol)/n-Heptane water-in-oil microemulsion system by the method of dilution with 0.2 g of surfactant at different *temperatures and different ω.*

		With n-butanol	With n-pentanol	With n-hexanol	With n-heptanol	With n-octanol
ω	**T/K**	**k_d**	**k_d**	**k_d**	**k_d**	**k_d**
5	303	1.18	2.87	2.99	3.41	3.35
	308	2.83	2.70	3.08	4.09	4.22
	313	3.01	3.41	3.49	3.52	4.35
	318	2.27	3.64	4.21	3.91	4.14
	323	3.17	3.95	4.03	4.13	4.92
10	303	2.43	2.75	2.73	2.88	2.97
	308	2.47	2.98	3.18	3.16	3.50
	313	2.84	2.95	3.59	3.57	4.03
	318	2.94	3.32	3.98	3.65	4.23
	323	3.24	3.41	4.51	3.88	3.60
15	303	1.85	3.11	3.26	3.32	3.15
	308	1.88	3.37	2.97	3.11	3.12
	313	2.38	2.60	3.33	3.28	3.48
	318	2.28	3.21	3.13	3.92	3.29
	323	2.40	3.05	3.29	3.32	2.28
20	303	1.81	2.58	3.09	3.06	2.91
	308	1.91	2.36	2.82	2.91	2.70
	313	1.94	2.47	2.47	3.00	3.37
	318	2.39	2.58	2.65	3.52	3.09
	323	2.29	2.60	3.55	3.05	2.28

Table 3A. Structural parameters of water/(Tween 20+ n-butanol)/n-Heptane water-in-oil microemulsion system by the method of dilution with 0.2 g of surfactant at *different temperatures and different ω.*

	ω	V_{water} /mL	n_w X 10^{-5} /M	n_a^w X 10^4/M	n_a^i X 10^{-5}/M	V_d /m^3	V_a^i /m^3	A_d X 10^6 /m^2	V_s^h X 10^{20}/m^3	V_a^h X 10^{21}/m^3
303K	5	0.015	83.33	0.14	8.94	0.20	0.01	1.90	12.43	2.45
	10	0.030	167.00	0.29	64.27	0.27	0.06	2.56	8.85	12.53
	15	0.045	250.00	0.43	33.04	0.26	0.03	2.19	12.82	9.33
	20	0.06	333.00	0.57	186.26	0.41	0.17	4.02	5.32	21.83
308K	5	0.015	83.33	0.14	84.87	0.27	0.04	3.25	6.21	8.39
	10	0.030	167.00	0.28	101.94	0.30	0.09	3.45	6.39	10.37
	15	0.045	250.00	0.42	55.90	0.28	0.05	2.90	8.95	7.96
	20	0.06	333.00	0.55	433.25	0.63	0.39	7.42	2.82	19.45
313K	5	0.015	83.33	0.13	147.09	0.33	0.08	4.43	4.67	8.36
	10	0.030	167.00	0.27	93.69	0.30	0.09	3.79	6.01	6.86
	15	0.045	250.00	0.40	71.64	0.29	0.07	3.52	7.21	6.29
	20	0.06	333.00	0.53	206.51	0.43	0.19	5.14	5.05	12.71
318K	5	0.015	83.33	0.13	44.19	0.24	0.13	3.63	5.44	2.33
	10	0.030	167.00	0.26	123.01	0.32	0.11	4.57	5.09	6.08
	15	0.045	250.00	0.39	145.65	0.36	0.13	4.84	5.28	7.47
	20	0.06	333.00	0.52	174.04	0.40	0.16	5.18	5.35	9.04
323K	5	0.015	83.33	0.13	186.97	0.37	0.17	5.77	3.96	5.90
	10	0.030	167.00	0.26	157.31	0.35	0.14	5.42	4.48	5.62
	15	0.045	250.00	0.38	186.10	0.39	0.17	5.76	4.65	6.89
	20	0.06	333.00	0.51	115.69	0.35	0.11	4.92	5.73	5.28

Table 3A. Structural parameters of water/(Tween 20+n-pentanol)/n-Heptane water-in-oil microemulsion system by the method of dilution with 0.2 g of surfactant *at different temperatures and different ω.*

	ω	V_{water}/mL	n_w X 10^{-5}/M	n_a^i X 10^{-5}/M	V_d/m^3	V_a^i/m^3	A_d X $10^6/m^2$	V_s^h X $10^{20}/m^3$	V_a^h X $10^{21}/m^3$
303K	5	0.015	83.33	213.78	0.43	0.23	4.35	4.53	21.32
	10	0.030	167.00	448.78	0.69	0.48	7.17	2.69	26.65
	15	0.045	250.00	842.94	1.14	0.91	11.95	1.57	29.30
	20	0.06	333.00	857.63	1.16	0.92	12.07	1.59	30.09
308K	5	0.015	83.33	143.08	0.35	0.15	3.94	5.69	12.96
	10	0.030	167.00	471.01	0.72	0.51	7.87	3.02	22.63
	15	0.045	250.00	738.94	1.02	0.80	11.13	2.18	25.79
	20	0.06	333.00	1004.85	1.32	1.08	14.27	1.72	27.55
313K	5	0.015	83.33	251.98	0.47	0.27	5.68	4.43	13.61
	10	0.030	167.00	411.34	0.65	0.44	7.59	3.64	18.26
	15	0.045	250.00	655.77	0.93	0.71	10.56	2.77	22.28
	20	0.06	333.00	1071.95	1.39	1.15	15.50	1.95	25.46
318K	5	0.015	83.33	319.08	0.54	0.34	6.92	5.11	12.72
	10	0.030	167.00	463.16	0.71	0.50	8.65	3.69	16.39
	15	0.045	250.00	761.83	1.05	0.82	12.28	2.80	20.79
	20	0.06	333.00	932.79	1.24	1.00	14.27	2.50	22.63
323K	5	0.015	83.33	318.83	0.54	0.34	7.35	4.17	10.59
	10	0.030	167.00	455.97	0.70	0.49	9.00	3.86	14.02
	15	0.045	250.00	655.25	0.93	0.71	11.43	3.34	17.57
	20	0.06	333.00	985.64	1.30	1.06	15.34	2.68	21.06

Table 3A. Structural parameters of water/(Tween 20+n-hexanol)/n-Heptane water-in-oil microemulsion system by the method of dilution with 0.2 g of surfactant at different *temperatures and different ω.*

	ω	V_{water}/mL	n_w X 10^{-5}/M	n_a^i X10^{-5}/M	V_d/m^3	V_a^i/m^3	A_d X 10^6 /m^2	V_s^h X $10^{26}/m^3$	V_a^h X $10^{26}/m^3$
303K	5	0.015	83.33	336.82	0.63	0.42	5.85	4.09	30.56
	10	0.030	167.00	595.55	0.95	0.74	8.97	2.60	34.30
	15	0.045	250.00	770.67	1.19	0.96	11.08	2.14	36.50
	20	0.06	333.00	1230.82	1.77	1.53	1.66	1.42	38.65
308K	5	0.015	83.33	160.75	0.41	0.20	4.16	6.67	17.16
	10	0.030	167.00	466.89	0.79	0.58	7.85	3.71	27.70
	15	0.045	250.00	966.71	1.43	1.20	13.87	2.19	33.90
	20	0.06	333.00	1471.58	2.07	1.83	2.00	1.55	36.49
313K	5	0.015	83.33	226.89	0.49	0.28	5.40	5.78	16.06
	10	0.030	167.00	141.10	0.39	0.18	4.36	6.71	11.59
	15	0.045	250.00	1162.71	1.67	1.45	16.67	2.26	32.23
	20	0.06	333.00	1170.57	1.70	1.46	1.68	2.29	32.85
318K	5	0.015	83.33	320.05	0.61	0.40	6.95	5.18	16.17
	10	0.030	167.00	713.01	1.10	0.89	11.69	3.55	24.69
	15	0.045	250.00	636.34	1.02	0.79	10.76	3.90	24.23
	20	0.06	333.00	949.04	1.42	1.18	1.45	3.10	28.69
323K	5	0.015	83.33	261.50	0.54	0.33	6.68	5.50	11.53
	10	0.030	167.00	598.38	0.96	0.75	10.74	4.21	20.20
	15	0.045	250.00	936.92	1.39	1.17	14.82	3.41	25.58
	20	0.06	333.00	1250.34	1.80	1.56	1.86	2.87	28.81

Table 3A. Structural parameters of water/(Tween 20+n-heptanol)/n-Heptane water-in-oil microemulsion system by the method of dilution with 0.2 g of surfactant *at different temperatures and different ω.*

	ω	V_{water}/mL	n_w X 10^{-5}/M	n_a^i X 10^{-5} /M	V_d /m^3	V_a^i /m^3	A_d X 10^6 /m^2	V_s^h X 10^{26} /m^3	V_a^h X 10^{26}/m^3
303K	5	0.015	83.33	259.93	0.56	0.37	4.92	5.49	31.65
	10	0.030	167.00	673.88	1.16	0.95	9.91	2.88	43.04
	15	0.045	250.00	855.41	1.44	1.21	12.10	2.41	45.72
	20	0.06	333.00	1257.01	2.02	1.78	16.94	1.74	48.45
308K	5	0.015	83.33	214.28	0.50	0.30	4.81	6.40	21.94
	10	0.030	167.00	681.19	1.18	0.97	10.43	3.48	37.95
	15	0.045	250.00	975.79	1.61	1.38	13.98	2.71	42.27
	20	0.06	333.00	1431.13	2.27	2.03	19.47	2.00	45.72
313K	5	0.015	83.33	310.03	0.63	0.44	6.40	5.75	21.83
	10	0.030	167.00	730.55	1.25	1.04	11.46	3.85	34.46
	15	0.045	250.00	1001.84	1.64	1.42	14.73	3.17	38.84
	20	0.06	333.00	1303.88	2.09	1.85	18.37	2.63	42.01
318K	5	0.015	83.33	247.94	0.55	0.35	6.09	6.22	15.05
	10	0.030	167.00	673.04	1.16	0.95	11.21	4.52	29.68
	15	0.045	250.00	1045.89	1.71	1.48	15.70	3.54	36.11
	20	0.06	333.00	1204.27	1.95	1.71	17.61	3.26	38.32
323K	5	0.015	83.33	320.05	0.65	0.45	7.39	5.96	15.29
	10	0.030	167.00	641.83	1.12	0.91	11.26	5.01	25.79
	15	0.045	250.00	781.43	1.33	1.11	12.95	4.68	29.29
	20	0.06	333.00	1165.16	1.89	1.65	17.57	3.77	35.21

Table 3A. Structural parameters of water/(Tween 20+ n-octanol)/n-Heptane water-in-oil microemulsion system by the method of dilution with 0.2 g of surfactant *at different temperatures and different ω.*

	ω	V_{water} / mL	n_w X 10^{-5}/M	n_a^i X 10^{-5}/M	V_d /m^3	V_a^i /m^3	A_d X 10^6 / m^2	V_s^h X 10^{26} / m^3	V_a^h X 10^{26} / m^3
303K	5	0.015	83.33	419.14	0.58	0.38	6.84	2.16	20.07
	10	0.030	167.00	826.50	0.97	0.76	11.75	1.19	21.80
	15	0.045	250.00	1048.66	1.18	0.96	14.43	0.97	22.46
	20	0.06	333.00	1551.64	1.66	1.42	20.48	0.66	22.79
308K	5	0.015	83.33	330.95	0.50	0.30	6.22	2.96	15.66
	10	0.030	167.00	850.37	0.99	0.78	12.47	1.44	19.61
	15	0.045	250.00	1186.37	1.31	1.09	16.52	1.09	20.71
	20	0.06	333.00	1598.22	1.70	1.46	21.48	0.84	21.42
313K	5	0.015	83.33	347.37	0.51	0.32	6.85	3.06	13.04
	10	0.030	167.00	683.14	0.84	0.63	10.89	2.02	16.89
	15	0.045	250.00	1159.68	1.29	1.06	16.63	1.35	19.10
	20	0.06	333.00	1361.12	1.49	1.25	19.06	1.19	19.88
318K	5	0.015	83.33	408.22	0.57	0.37	8.02	2.95	11.74
	10	0.030	167.00	690.06	0.84	0.63	11.41	2.24	15.07
	15	0.045	250.00	1121.93	1.25	1.03	16.61	1.60	17.56
	20	0.06	333.00	1541.68	1.65	1.41	21.67	1.26	18.92
323K	5	0.015	83.33	351.13	0.52	0.32	7.76	3.26	9.17
	10	0.030	167.00	662.57	0.82	0.61	11.51	2.50	13.25
	15	0.045	250.00	920.18	1.07	0.84	14.62	2.08	15.37
	20	0.06	333.00	1522.28	1.63	1.39	21.87	1.46	17.78

BASIC DATA
OF
CHAPTER 2

Table 1. Pseudo ternary phase diagram of [b4mpy][BF_4]/(Tween-20+ n-pentanol)/n-heptane at different Tween 20 (S) / n-pentanol (CS) ratio (w/w). n-heptane was used as oil (Oil). Temp. 298 K.

Tween 20:n-pentanol (S:CS)	Oil /g	(S+CS) /g	IL /g	Wt. % of the components		
				Oil (X)	S+CS(Y)	IL(Z)
1:0.5						
Clear fluid-turbid boundary	0.00	0.60	1.75	0	22.22	77.78
	0.01	0.60	1.03	0.74	32.44	66.82
	0.02	0.60	0.79	1.31	38.25	60.44
	0.03	0.60	0.52	2.71	47.69	49.60
	0.07	0.60	0.37	6.14	53.94	39.92
	0.14	0.60	0.17	14.52	63.79	21.69
	0.20	0.60	0.09	22.44	65.72	11.83
	0.27	0.60	0.05	29.28	64.29	6.43
	0.34	0.60	0.03	34.94	61.38	3.68
	0.43	0.60	0.00	41.76	58.24	0.00
1:1						
Clear fluid-turbid boundary	0.00	0.80	1.87	0.00	29.94	70.06
	0.01	0.80	1.25	0.66	38.80	60.53
	0.03	0.80	0.86	2.01	47.11	50.88
	0.07	0.80	0.65	4.50	52.76	42.74
	0.08	0.80	0.55	5.72	55.79	38.49
	0.10	0.80	0.29	8.61	67.20	24.19
	0.14	0.80	0.20	11.98	70.14	17.89
	0.17	0.80	0.17	14.99	70.25	14.75
	0.34	0.80	0.07	28.14	65.93	5.93
	0.44	0.80	0.02	34.66	63.44	1.90
	0.68	0.73	0.00	48.34	51.66	0.00
1:2						
Clear fluid-turbid boundary	0.00	1.20	1.42	0	41.32	58.68
	0.01	1.20	0.78	0.64	55.82	43.54
	0.03	1.20	0.51	1.85	65.00	33.15
	0.07	1.20	0.28	4.26	74.80	20.94
	0.20	1.20	0.17	12.74	74.59	12.68
	0.34	1.20	0.14	19.98	70.20	9.83
	0.48	1.20	0.08	26.95	67.64	5.41
	0.61	1.20	0.06	32.58	63.60	3.82
	0.82	1.20	0.04	39.64	58.04	2.32
	1.02	1.20	0.00	49.49	50.51	0.00

Table 2. Absorbance data of 1-butyl 4-methyl pyridinium tetrafluoroborate [b4mpy][BF_4] *confined in the polar domain at different volume fraction (φ_d)* of [b4mpy][BF_4]/(Tween-20+ n-pentanol)/n-heptane IL-in-oil microemulsion

	Abs. of [b4mpy][BF_4] *at different volume fraction (φ_d)* Tween 20:n-pentanol (S:CS)= 1:1			
λ / nm	**φ_d**			
	0.007	**0.014**	**0.022**	**0.030**
275	0.595	0.737	0.711	0.787
280	0.642	1.030	1.141	1.453
285	0.383	0.537	0.589	0.746
290	0.257	0.340	0.339	0.424
295	0.193	0.257	0.242	0.306
300	0.151	0.201	0.181	0.236
305	0.121	0.163	0.142	0.188
310	0.102	0.137	0.115	0.152
315	0.092	0.122	0.099	0.130
320	0.090	0.116	0.093	0.121
325	0.093	0.117	0.096	0.121
330	0.096	0.118	0.099	0.121
335	0.095	0.114	0.099	0.119
340	0.090	0.108	0.095	0.114
345	0.080	0.093	0.083	0.101
350	0.065	0.075	0.067	0.083
355	0.050	0.057	0.050	0.064
360	0.038	0.042	0.037	0.050
365	0.029	0.032	0.027	0.039
370	0.016	0.014	0.008	0.019
375	0.014	0.012	0.007	0.018
380	0.012	0.011	0.008	0.018
385	0.011	0.011	0.008	0.018
390	0.010	0.011	0.009	0.019
395	0.010	0.011	0.010	0.019
400	0.009	0.011	0.010	0.019

Table 3. Emission spectra of 10 µM curcumin in [b4mpy][BF_4]/(Tween-20+n-pentanol)/n-heptane IL-in-oil microemulsion at different volume *fraction* (φ_d) of IL.

	F.I. (a.u.) *in different volume fraction* (φ_d) of the IL -in-oil µEs Tween 20:n-pentanol (S:CS)= 1:1					
λ / nm	**φ_d**					
	0.000	**0.007**	**0.014**	**0.022**	**0.030**	**0.035**
430	0.064	0.050	0.045	0.037	0.034	0.033
440	0.153	0.123	0.109	0.094	0.080	0.078
450	0.336	0.289	0.257	0.219	0.185	0.179
460	0.590	0.529	0.480	0.410	0.346	0.334
470	0.856	0.789	0.727	0.626	0.536	0.518
480	1.077	1.007	0.942	0.825	0.717	0.693
490	1.211	1.144	1.084	0.962	0.846	0.821
500	1.260	1.204	1.150	1.031	0.920	0.894
510	1.239	1.194	1.152	1.043	0.938	0.914
520	1.163	1.130	1.098	1.002	0.905	0.886
530	1.049	1.024	1.003	0.919	0.838	0.819
540	0.909	0.894	0.881	0.812	0.744	0.728
550	0.763	0.755	0.750	0.695	0.641	0.625
560	0.624	0.623	0.619	0.576	0.532	0.520
570	0.496	0.498	0.500	0.465	0.430	0.423
580	0.389	0.393	0.396	0.369	0.342	0.335
590	0.300	0.304	0.308	0.288	0.267	0.262
600	0.228	0.231	0.235	0.221	0.205	0.201
610	0.171	0.174	0.177	0.167	0.156	0.153
620	0.126	0.129	0.132	0.125	0.116	0.114
630	0.091	0.094	0.097	0.091	0.086	0.084
640	0.066	0.068	0.070	0.066	0.062	0.061
650	0.048	0.049	0.051	0.049	0.045	0.045
660	0.034	0.036	0.036	0.035	0.033	0.032
670	0.025	0.025	0.026	0.025	0.024	0.023
680	0.017	0.019	0.019	0.018	0.017	0.017
690	0.013	0.013	0.014	0.013	0.012	0.013
700	0.010	0.010	0.010	0.010	0.009	0.009
710	0.007	0.007	0.008	0.007	0.007	0.007
720	0.005	0.006	0.006	0.006	0.005	0.005
730	0.004	0.004	0.005	0.004	0.004	0.004
740	0.003	0.003	0.003	0.003	0.003	0.003
741	0.003	0.003	0.004	0.003	0.003	0.003

Table 4. *Variation in the fluorescence anisotropy (r) for 10 μM curcumin with different volume fraction (φ_d)* of IL for [b4mpy][BF_4]/(Tween-20+ n-pentanol)/n-heptane IL-in-oil microemulsion system.

Tween 20:n-pentanol (S:CS)	**Variation in the fluorescence anisotropy (r) for *10 μM curcumin with different volume fraction (φ_d)***	
	φ_d	**Anisotropy**
1:0.5	0.000	0.321
	0.004	0.323
	0.008	0.324
	0.013	0.324
	0.020	0.324
	0.022	0.320
1:1	0.000	0.305
	0.007	0.318
	0.014	0.318
	0.022	0.311
	0.030	0.300
	0.035	0.294
1:2	0.000	0.307
	0.010	0.310
	0.020	0.314
	0.030	0.313
	0.040	0.315
	0.050	0.318

BASIC DATA
OF
CHAPTER 3

Table.1 Molar conductance (Λ_M) at different concentration of [bmim][MS] solution in water rich region.

Conc. Of [bmim][MS] solution (M)	Λ_M / S.cm^2.mol^{-1}
0.001	72.63
0.002	71.04
0.003	70.617
0.004	69.469
0.005	69.200
0.006	68.611
0.007	68.282
0.008	67.961
0.009	67.597
0.011	67.230
0.020	64.656
0.026	62.996
0.035	62.682
0.046	61.122
0.053	60.413
0.060	59.806
0.067	59.400
0.073	58.713
0.079	58.429
0.085	57.980
0.111	55.710
0.196	51.316
0.277	47.868
0.354	45.289
0.429	42.980
0.500	41.454
0.552	40.419
0.618	38.974
0.682	38.097
0.744	36.684
0.804	35.587
0.861	34.495
0.921	33.674
0.992	32.257
1.044	31.419
1.078	30.804

Table 1A. M*olar conductance* (Λ_M) at different mole fraction (X) of [bmim][MS] solution in IL rich region at different temperature (T)

	Λ_M / S.cm^2.mol^{-1}					
x_{IL} (Conc / M)	**298**	**303**	**308**	**313**	**318**	**323**
0.2(3.69)	10.98	13.74	15.90	16.56	17.65	18.52
0.4(4.40)	4.62	5.22	5.66	6.07	11.29	11.91
0.5(4.58)	3.14	3.45	3.78	4.14	4.51	4.85
0.6(4.78)	2.30	2.54	2.80	3.13	3.45	3.97
0.8(4.86)	1.96	2.25	2.54	2.80	3.32	3.63
1.0(4.96)	1.13	1.27	1.46	1.64	1.87	2.06

Table 2. Absorbance data of 10 μM eosin Y at different wavelength in the presence of different amount of [bmim][MS] in water. Temp. 298 K.

λ/ nm	Absorbance in presence of different concentration (M) of [bmim][MS]					
	0.00	**0.006**	**0.10**	**2.00**	**3.00**	**4.40**
425	0.015	0.002	0.041	0.033	0.365	0.057
435	0.020	0.009	0.041	0.052	0.336	0.165
445	0.035	0.025	0.050	0.069	0.307	0.155
455	0.059	0.051	0.070	0.090	0.289	0.150
465	0.101	0.096	0.103	0.115	0.279	0.155
475	0.184	0.183	0.177	0.155	0.289	0.168
485	0.266	0.273	0.271	0.237	0.348	0.224
495	0.336	0.344	0.334	0.308	0.403	0.318
505	0.537	0.547	0.493	0.356	0.432	0.354
515	0.773	0.811	0.783	0.553	0.606	0.436
525	0.602	0.670	0.795	0.840	0.896	0.733
535	0.211	0.249	0.378	0.735	0.809	0.962
545	0.041	0.048	0.096	0.311	0.381	0.662
555	0.005	0.003	0.020	0.094	0.140	0.221
565	0.000	0.004	0.007	0.041	0.073	0.061
575	0.001	0.005	0.004	0.029	0.054	0.023

Table 3. Emission spectra of 10 μM eosin Y in the presence of different amount of [bmim][MS] in water at 298 K.

	F.I. (a.u.)							
[bmim][MS]/M / ***λ/ nm***	**0.00**	**0.006**	**0.01**	**1.00**	**2.00**	**3.69**	**4.40**	**4.58**
505	0.076	0.076	0.073	0.023	0.020	0.016	0.016	0.019
515	0.337	0.337	0.325	0.136	0.087	0.043	0.035	0.036
525	1.083	1.083	1.055	0.576	0.361	0.159	0.102	0.097
535	1.702	1.702	1.737	1.463	1.141	0.544	0.330	0.299
545	1.557	1.557	1.640	1.855	1.929	1.177	0.896	0.801
555	1.146	1.146	1.218	1.562	1.866	1.305	1.255	1.159
565	0.830	0.830	0.875	1.113	1.411	1.003	1.071	1.005
575	0.646	0.646	0.680	0.804	1.010	0.697	0.764	0.719
585	0.492	0.492	0.520	0.624	0.779	0.518	0.556	0.521
595	0.342	0.342	0.363	0.464	0.606	0.409	0.438	0.410
605	0.220	0.220	0.234	0.313	0.425	0.296	0.332	0.312
615	0.141	0.141	0.149	0.197	0.276	0.197	0.229	0.219
625	0.094	0.094	0.099	0.124	0.175	0.125	0.149	0.144
635	0.064	0.064	0.068	0.081	0.112	0.080	0.096	0.094
645	0.043	0.043	0.046	0.055	0.075	0.055	0.064	0.063

Table 4. Fluorescence lifetime of 10 µM eosin Y in the presence of different concentrations of [bmim][MS] in water at 298K.

Counts X 10^{-3}	Fluorescence lifetime / ns		
	0.00M	**0.01M**	**1.00M**
0.20	0.04	0.03	0.09
4.24	1.29	0.73	0.84
5.25	1.29	1.47	1.41
6.26	1.02	1.35	1.41
7.27	0.67	1.07	1.15
11.31	0.30	0.45	0.65
15.35	0.15	0.14	0.34
20.40	0.12	0.10	0.18
25.45	0.04	0.08	0.13
30.51	0.08	0.07	0.14
35.56	0.04	0.05	0.16
40.61	0.02	0.03	0.09
45.66	0.04	0.00	0.08
50.71	0.03	-0.01	0.08
55.76	0.03	0.00	0.06
60.81	0.07	0.01	0.00
65.86	0.01	0.02	0.03
70.91	0.05	-0.01	0.05
75.96	0.03	-0.01	0.04
78.99	0.05	0.01	0.04

BASIC DATA
OF
CHAPTER 4

Table 1. Phase diagram of ([bmim][MS] ± water)/(Tween 20 + n-pentanol)/n-heptane microemulsion at 298 K. 1:1 (w/w) Tween 20 and n-pentanol was used. Mole fraction (xIL)of [bmim][MS] in the binary mixture of [bmim][MS] and water: 0.2, 0.4, 0.5, 0.6, 0.8 and 1.0

Zone	Oil/g	(S+CS)/g	(IL+water)/g	Wt. % of the components		
				Oil (X)	S+CS(Y)	IL +water(Z)
x_{IL} 0.2:						
Clear fluid-turbid boundary	0.00	0.40	1.57	0.00	20.27	79.73
	0.03	0.40	0.88	2.59	30.37	67.04
	0.07	0.40	0.59	6.46	37.85	55.69
	0.10	0.40	0.44	10.85	42.38	46.77
	0.14	0.40	0.29	16.44	48.14	35.42
	0.17	0.40	0.20	22.05	51.65	26.31
	0.20	0.40	0.17	26.45	51.63	21.92
	0.24	0.40	0.12	31.31	52.39	16.31
	0.27	0.40	0.10	35.25	51.61	13.14
	0.34	0.40	0.03	44.04	51.58	4.38
	1.37	0.40	0.00	98.63	1.37	0.00
x_{IL} 0.4:						
Clear fluid-turbid boundary	0.00	0.40	2.53	0.00	13.64	86.36
	0.03	0.40	1.12	2.20	25.80	72.00
	0.07	0.40	0.74	5.67	33.20	61.13
	0.10	0.40	0.47	10.51	41.05	48.43
	0.14	0.40	0.32	15.90	46.57	37.52
	0.17	0.40	0.26	20.44	47.88	31.69
	0.20	0.40	0.20	25.59	49.96	24.44
	0.27	0.40	0.14	33.67	49.30	17.02
	0.41	0.40	0.02	49.21	48.03	2.76
	1.37	0.02	0.00	98.63	1.37	0.00
x_{IL} 0.5:						
Clear fluid-turbid boundary	0.00	0.53	2.96	0.00	11.90	88.10
	0.03	0.40	1.41	1.85	21.67	76.48
	0.07	0.39	0.80	5.39	31.58	63.03
	0.10	0.99	0.54	9.79	38.23	51.98
	0.14	0.40	0.30	16.31	47.77	35.92
	0.20	0.40	0.19	25.94	50.63	23.43
	0.34	0.40	0.07	42.11	49.33	8.56
	0.41	0.40	0.03	48.53	47.36	4.11
	0.44	0.40	0.01	51.89	46.76	1.35
	1.37	0.40	0.00	98.63	1.37	0.00
x_{IL} 0.6:						
Clear fluid-turbid boundary	0.00	0.40	2.50	0.00	13.78	86.22
	0.03	0.40	1.31	1.96	22.94	75.10
	0.07	0.40	0.88	5.06	29.65	65.29
	0.10	0.40	0.57	9.57	37.37	53.06
	0.14	0.40	0.34	15.65	45.83	38.51
	0.20	0.40	0.20	25.55	49.88	24.57
	0.27	0.40	0.15	33.16	48.55	18.29
	0.34	0.40	0.10	40.38	47.29	12.33
	0.44	0.40	0.01	51.89	46.75	1.35
	1.37	0.02	0.00	98.63	1.37	0.00

Table 2. Phase diagram of ([bmim][MS] ± water)/(Tween 20 + n-pentanol)/n-heptane microemulsion at 298 K. 1:1 (w/w) Tween 20 and n-pentanol was used. Mole fraction (xIL)of [bmim][MS] in the binary mixture of [bmim][MS] and water: 0.2, 0.4, 0.5, 0.6, 0.8 and 1.0

Zone	Oil /g	(S+CS) /g	(IL+water) /g	Wt. % of the components		
				Oil (X)	S+CS(Y)	IL +water(Z)
x_{IL} 0.8:						
Clear fluid-turbid boundary	0.00	0.40	2.79	0.00	12.55	87.45
	0.03	0.40	1.22	2.07	24.20	73.74
	0.07	0.40	0.89	5.01	29.36	65.62
	0.10	0.40	0.55	9.77	38.16	52.06
	0.14	0.40	0.26	17.25	50.50	32.25
	0.20	0.40	0.20	25.54	49.86	24.60
	0.27	0.40	0.14	33.62	49.23	17.15
	0.34	0.40	0.09	40.93	47.94	11.13
	0.41	0.40	0.06	47.22	46.09	6.69
	0.44	0.40	0.03	50.52	45.52	3.96
	1.37	0.02	0	98.63	1.37	0.00
x_{IL} 1.0:						
Clear fluid-turbid boundary	0.00	0.40	2.61	0.00	13.31	86.69
	0.07	0.40	0.95	4.80	28.13	67.07
	0.10	0.40	0.74	8.22	32.08	59.70
	0.12	0.40	0.59	11.02	35.84	53.14
	0.14	0.40	0.31	16.06	47.03	36.92
	0.20	0.40	0.21	25.16	49.13	25.71
	0.27	0.40	0.17	32.23	47.19	20.58
	0.34	0.40	0.10	40.36	47.27	12.37
	0.41	0.40	0.07	46.59	45.48	7.93
	0.55	0.40	0.03	55.68	40.76	3.56
	1.37	0.02	0.00	98.63	1.37	0.00

Table 3. Structural parameters for ([bmim][MS] + water)/(Tween 20 + n-pentanol)/n-heptane polar domain-in-oil microemulsion system by the method of dilution with 0.2 g of *surfactant at different temperatures and different ω.*

	With x_{IL}= 0.2								
	ω	V_{water}/mL	n_{water} X 10^{-5}/M	n_a^i X 10^{-5}/M	V_d/m^3	V_a^i/m^3	A_d X 10^6/m^2	V_s^h X 10^{20}/m^3	V_a^h X 10^{21}/m^3
298K	5	0.044	71.82	332.23	0.58	0.36	5.36	3.01	33.74
	10	0.088	143.64	216.76	0.50	0.23	3.97	5.50	40.24
	15	0.132	215.46	190.13	0.21	0.52	3.64	7.51	48.25
	20	0.176	287.28	216.54	0.59	0.23	3.96	7.60	55.58
	25	0.220	359.10	215.92	0.63	0.23	3.96	8.80	64.22
303K	5	0.044	71.82	200.09	0.44	0.22	4.20	5.40	23.96
	10	0.088	143.64	150.81	0.43	0.16	3.61	8.17	27.31
	15	0.132	215.46	190.58	0.21	0.52	4.09	8.12	34.30
	20	0.176	287.28	231.69	0.61	0.25	4.58	7.90	40.57
	25	0.220	359.10	305.20	0.73	0.33	5.47	6.74	45.58
308K	5	0.044	71.82	39.61	0.27	0.04	2.71	10.30	6.53
	10	0.088	143.64	150.58	0.43	0.16	4.04	8.05	19.40
	15	0.132	215.46	247.71	0.27	0.58	5.21	6.81	26.97
	20	0.176	287.28	75.60	0.44	0.08	3.14	17.75	21.47
	25	0.220	359.10	271.40	0.69	0.29	5.50	8.29	36.02
313K	5	0.044	71.82	235.44	0.48	0.25	5.50	5.16	14.87
	10	0.088	143.64	176.83	0.46	0.19	4.79	7.17	15.53
	15	0.132	215.46	265.50	0.29	0.60	5.86	6.67	21.70
	20	0.176	287.28	321.86	0.70	0.35	6.54	6.63	26.15
	25	0.220	359.10	397.34	0.83	0.43	7.45	6.24	30.34
318K	5	0.044	71.82	220.39	0.46	0.24	5.75	5.27	11.35
	10	0.088	143.64	276.97	0.57	0.30	6.43	5.68	15.36
	15	0.132	215.46	274.51	0.30	0.61	6.41	6.63	17.76
	20	0.176	287.28	110.29	0.48	0.12	4.43	12.23	13.16
	25	0.220	359.10	294.75	0.72	0.32	6.65	8.26	23.76
323K	5	0.044	71.82	156.61	0.39	0.17	5.42	5.56	6.98
	10	0.088	143.64	542.56	0.86	0.59	10.07	4.10	17.81
	15	0.132	215.46	233.23	0.25	0.56	6.34	7.14	13.34
	20	0.176	287.28	337.91	0.72	0.37	7.60	6.77	18.35
	25	0.220	359.10	204.69	0.62	0.22	6.00	10.23	16.78

Table 4. Structural parameters for ([bmim][MS] + water)/(Tween 20 + n-pentanol)/n-heptane polar domain-in-oil microemulsion system by the method of dilution with 0.2 g of surfactant at *different temperatures and different ω.*

	With x_{IL}= 0.4								
	ω	V_{water} /mL	n_{water} X 10^{-5} /M	n_a^i X 10^{-5}/M	V_d /m^3	V_a^i /m^3	A_d X 10^6 /m^2	V_s^h X 10^{20}/m^3	V_a^h X 10^{21}/m^3
298K	5	0.074	70.79	312.12	0.59	0.34	5.11	3.55	37.46
	10	0.148	141.60	109.77	0.45	0.12	2.68	14.13	52.37
	15	0.222	212.38	195.17	0.61	0.21	3.71	10.03	66.12
	20	0.296	283.18	294.54	0.79	0.32	4.90	7.27	72.37
	25	0.370	353.97	338.56	0.92	0.37	5.43	81.27	3.74
303K	5	0.074	70.79	303.56	0.58	0.33	5.45	4.33	29.16
	10	0.148	141.60	211.62	0.56	0.23	4.34	7.83	36.74
	15	0.222	212.38	242.64	0.66	0.26	4.72	8.71	46.81
	20	0.296	283.18	351.81	0.86	0.38	6.03	6.92	53.93
	25	0.370	353.97	247.37	0.82	0.27	4.77	69.69	3.95
308K	5	0.074	70.79	166.15	0.43	0.18	4.23	7.12	18.93
	10	0.148	141.60	422.63	0.79	0.46	7.32	4.51	30.47
	15	0.222	212.38	202.32	0.62	0.22	4.67	10.87	35.20
	20	0.296	283.18	359.49	0.87	0.39	6.56	7.60	43.69
	25	0.370	353.97	66.92	0.62	0.07	3.03	42.51	5.17
313K	5	0.074	70.79	129.91	0.39	0.14	4.23	7.71	12.26
	10	0.148	141.60	316.65	0.67	0.34	6.48	6.19	24.01
	15	0.222	212.38	151.88	0.57	0.16	4.49	13.23	24.62
	20	0.296	283.18	219.96	0.71	0.24	5.31	12.72	34.27
	25	0.370	353.97	299.17	0.87	0.32	6.27	42.52	3.14
318K	5	0.074	70.79	144.66	0.41	0.16	4.84	6.98	9.85
	10	0.148	141.60	157.17	0.50	0.17	4.99	9.37	14.37
	15	0.222	212.38	204.02	0.62	0.22	5.56	10.62	21.14
	20	0.296	283.18	251.08	0.75	0.27	6.12	11.44	28.02
	25	0.370	353.97	281.42	0.85	0.30	6.49	34.48	2.98
323K	5	0.074	70.79	500.44	0.80	0.54	9.56	4.14	16.61
	10	0.148	141.60	397.91	0.76	0.43	8.33	5.70	18.18
	15	0.222	212.38	102.77	0.51	0.11	4.77	13.86	11.42
	20	0.296	283.18	236.05	0.73	0.26	6.38	11.80	22.32
	25	0.370	353.97	453.70	1.04	0.49	9.00	30.92	2.46

Table 5. Structural parameters for ([bmim][MS] + water)/(Tween 20 + n-pentanol)/n-heptane polar domain-in-oil microemulsion system by the method of dilution with 0.2 g *of surfactant at different temperatures and different ω.*

	With x_{IL}= 0.5								
	ω	V_{water} /mL	n_{water} X 10^{-5} /M	n_a^i X 10^{-5}/M	V_d /m^3	V_a^i /m^3	A_d X 10^6 /m^2	V_s^h X 10^{20}/m^3	V_a^h X 10^{21}/m^3
298K	5	0.089	70.55	67.04	0.34	0.07	2.16	15.67	35.48
	10	0.178	141.09	253.39	0.27	0.63	4.41	6.34	54.25
	15	0.266	210.84	203.16	0.67	0.22	3.80	10.95	75.14
	20	0.356	282.18	281.92	0.84	0.31	4.75	8.95	85.27
	25	0.445	352.73	311.69	0.96	0.34	5.11	9.42	99.20
303K	5	0.089	70.55	106.44	0.38	0.12	3.08	10.49	24.74
	10	0.178	141.09	153.79	0.17	0.52	3.65	11.73	39.99
	15	0.266	210.84	230.63	0.70	0.25	4.57	10.47	53.52
	20	0.356	282.18	250.45	0.81	0.27	4.81	12.10	67.15
	25	0.445	352.73	333.17	0.99	0.36	5.81	10.26	75.74
308K	5	0.089	70.55	77.51	0.35	0.08	3.16	11.28	13.99
	10	0.178	141.09	239.89	0.26	0.62	5.12	8.15	31.28
	15	0.266	210.84	330.21	0.80	0.36	6.21	7.73	40.86
	20	0.356	282.18	284.13	0.84	0.31	5.65	11.29	51.33
	25	0.445	352.73	255.01	0.90	0.28	5.30	15.61	63.71
313K	5	0.089	70.55	347.86	0.65	0.38	6.85	4.84	20.63
	10	0.178	141.09	168.21	0.18	0.54	4.69	10.58	21.80
	15	0.266	210.84	210.09	0.67	0.23	5.19	12.11	31.15
	20	0.356	282.18	306.65	0.87	0.33	6.36	10.97	41.19
	25	0.445	352.73	360.53	1.02	0.39	7.01	11.21	49.51
318K	5	0.089	70.55	109.39	0.39	0.12	4.42	8.18	8.73
	10	0.178	141.09	74.01	0.08	0.44	3.99	14.19	10.25
	15	0.266	210.84	122.96	0.58	0.13	4.58	16.39	19.67
	20	0.356	282.18	302.30	0.86	0.33	6.74	11.43	33.71
	25	0.445	352.73	308.02	0.96	0.33	6.81	13.66	41.07
323K	5	0.089	70.55	151.98	0.43	0.16	5.36	6.96	8.48
	10	0.178	141.09	174.09	0.19	0.55	5.63	9.56	13.34
	15	0.266	210.84	271.07	0.74	0.29	6.80	9.95	21.61
	20	0.356	282.18	322.58	0.89	0.35	7.42	10.97	28.36
	25	0.445	352.73	405.21	1.06	0.44	8.41	10.86	35.25

Table 6. Structural parameters for ([bmim][MS] + water)/(Tween 20 + n-pentanol)/n-heptane polar domain-in-oil microemulsion system by the method of dilution with 0.2 g *of surfactant at different temperatures and different ω.*

	With x_{IL}= 0.6								
	ω	**V_{water} /mL**	**n_{water} X 10^{-5} /M**	**n_a^i X 10^{-5}/M**	**V_d /m^3**	**V_a^i /m^3**	**A_d X 10^6 /m^2**	**V_s^h X 10^{20}/m^3**	**V_a^h X 10^{21}/m^3**
298K	5	0.104	70.37	69.38	0.36	0.08	2.19	16.66	39.03
	10	0.208	140.74	140.51	0.54	0.15	3.05	13.89	65.91
	15	0.312	211.11	306.04	0.78	0.33	5.04	6.40	66.14
	20	0.416	281.48	301.62	0.86	0.33	4.99	8.13	82.86
	25	0.520	351.85	386.08	1.04	0.42	6.00	6.81	88.86
303K	5	0.104	70.37	120.12	0.41	0.13	3.24	10.42	27.73
	10	0.208	140.74	231.87	0.64	0.25	4.59	8.69	44.68
	15	0.312	211.11	324.90	0.80	0.35	5.71	7.08	50.95
	20	0.416	281.48	409.48	0.98	0.44	6.73	6.52	59.12
	25	0.520	351.85	420.35	1.08	0.45	6.86	7.48	69.68
308K	5	0.104	70.37	147.71	0.44	0.16	4.01	8.76	20.72
	10	0.208	140.74	198.59	0.60	0.21	4.62	10.48	33.31
	15	0.312	211.11	307.93	0.78	0.33	5.94	8.31	40.93
	20	0.416	281.48	268.49	0.83	0.29	5.46	12.00	51.57
	25	0.520	351.85	428.85	1.09	0.46	7.39	8.40	57.66
313K	5	0.104	70.37	121.78	0.42	0.13	4.13	9.18	13.69
	10	0.208	140.74	239.73	0.65	0.26	5.55	9.11	26.75
	15	0.312	211.11	358.63	0.83	0.39	6.98	7.64	33.57
	20	0.416	281.48	429.51	1.00	0.46	7.84	7.79	40.96
	25	0.520	351.85	356.00	1.01	0.39	6.95	11.37	49.56
318K	5	0.104	70.37	87.49	0.38	0.09	4.15	9.40	8.03
	10	0.208	140.74	210.90	0.61	0.23	5.64	9.88	20.34
	15	0.312	211.11	327.08	0.80	0.35	7.04	8.62	27.51
	20	0.416	281.48	322.35	0.88	0.35	6.98	10.80	33.99
	25	0.520	351.85	458.24	1.12	0.50	8.62	9.22	41.22
323K	5	0.104	70.37	138.39	0.43	0.15	5.20	7.65	8.48
	10	0.208	140.74	189.25	0.59	0.20	5.81	10.16	15.41
	15	0.312	211.11	390.47	0.87	0.42	8.24	7.72	24.16
	20	0.416	281.48	418.51	0.99	0.45	8.57	8.87	29.75
	25	0.520	351.85	493.34	1.16	0.53	9.48	9.03	35.68

Table 7. Structural parameters for ([bmim][MS] + water)/(Tween 20 + n-pentanol)/n-heptane polar domain-in-oil microemulsion system by the method of dilution with 0.2 g of surfactant at *different temperatures and different ω.*

	With x_{IL}= 0.8								
	ω	V_{water} /mL	n_{water} X 10^{-5} /M	n_a^i X 10^{-5}/M	V_d /m^3	V_a^i /m^3	A_d X 10^6 /m^2	V_s^h X 10^{20}/m^3	V_a^h X 10^{21}/m^3
298K	5	0.133	69.61	111.37	0.43	0.12	2.70	13.02	48.96
	10	0.266	139.23	192.12	0.65	0.21	3.67	11.75	76.26
	15	0.399	208.84	286.56	0.89	0.31	4.81	9.66	93.52
	20	0.532	278.45	252.49	0.99	0.27	4.40	15.50	132.24
	25	0.665	348.07	311.05	1.18	0.34	5.10	14.27	149.94
303K	5	0.133	69.61	164.86	0.49	0.18	3.78	9.25	33.79
	10	0.266	139.23	202.89	0.67	0.22	4.24	12.04	54.13
	15	0.399	208.84	214.17	0.81	0.23	4.37	16.25	77.13
	20	0.532	278.45	269.44	1.00	0.29	5.04	16.28	97.19
	25	0.665	348.07	450.04	1.33	0.49	7.21	9.77	97.44
308K	5	0.133	69.61	145.61	0.47	0.16	3.98	10.04	23.39
	10	0.266	139.23	247.40	0.71	0.27	5.21	10.32	40.87
	15	0.399	208.84	317.38	0.92	0.34	6.05	11.00	55.85
	20	0.532	278.45	410.72	1.16	0.44	7.18	10.37	68.12
	25	0.665	348.07	543.47	1.43	0.59	8.78	8.71	75.70
313K	5	0.133	69.61	201.45	0.53	0.22	5.09	8.00	19.74
	10	0.266	139.23	247.59	0.71	0.27	5.65	10.60	32.14
	15	0.399	208.84	315.50	0.92	0.34	6.46	11.74	45.35
	20	0.532	278.45	367.54	1.11	0.40	7.09	12.93	58.18
	25	0.665	348.07	420.66	1.40	0.46	7.73	13.69	70.54
318K	5	0.133	69.61	118.99	0.44	0.13	4.53	9.85	11.43
	10	0.266	139.23	286.66	0.76	0.31	6.55	9.55	26.72
	15	0.399	208.84	329.12	0.94	0.36	7.06	11.65	37.44
	20	0.532	278.45	468.74	1.22	0.51	8.74	10.44	47.75
	25	0.665	348.07	596.05	1.49	0.65	10.28	9.60	55.85
323K	5	0.133	69.61	39.21	0.36	0.03	4.01	13.02	48.96
	10	0.266	139.23	308.16	0.78	0.33	7.25	9.13	22.56
	15	0.399	208.84	373.97	0.98	0.40	8.04	10.65	31.93
	20	0.532	278.45	471.28	1.22	0.51	9.21	10.93	41.28
	25	0.665	348.07	596.47	1.49	0.65	10.72	10.32	49.32

Table 8. Structural parameters for ([bmim][MS] + water)/(Tween 20 + n-pentanol)/n-heptane polar domain-in-oil microemulsion system by the method of dilution with 0.2 g *of surfactant at different temperatures and different ω.*

	With x_{IL}= 1.0								
	ω	V_{water} /mL	n_{water} X 10^{-5} /M	n_a^i X 10^{-5}/M	V_d /m^3	V_a^i /m^3	A_d X 10^6 /m^2	V_s^h X 10^{20}/m^3	V_a^h X 10^{21}/m^3
298K	5	0.191	81.51	1054.42	1.51	1.14	14.06	1.12	39.75
	10	0.382	163.02	242.26	0.82	0.26	4.28	11.84	96.40
	15	0.573	244.54	797.69	0.86	0.86	10.97	2.70	72.39
	20	0.763	325.62	870.44	1.89	0.94	11.84	2.92	85.31
	25	0.954	407.14	920.66	2.13	1.00	12.45	3.21	99.25
303K	5	0.191	81.51	163.49	0.55	0.18	3.76	11.65	42.22
	10	0.382	163.02	525.76	1.13	0.57	8.13	4.93	57.42
	15	0.573	244.54	673.90	0.73	0.73	9.91	4.67	69.70
	20	0.763	325.62	878.70	1.89	0.95	12.38	3.91	76.16
	25	0.954	407.14	888.25	2.10	0.96	12.49	4.66	91.64
308K	5	0.191	81.51	98.71	0.48	0.11	3.42	16.38	25.87
	10	0.382	163.02	453.92	1.05	0.49	7.70	6.97	50.62
	15	0.573	244.54	807.80	0.87	0.87	11.96	4.43	57.31
	20	0.763	325.62	1037.68	2.07	1.12	14.73	3.83	63.53
	25	0.954	407.14	991.87	2.21	1.07	14.18	4.90	77.74
313K	5	0.191	81.51	410.08	0.81	0.44	7.60	5.65	28.39
	10	0.382	163.02	485.43	1.09	0.53	8.51	7.18	42.66
	15	0.573	244.54	566.37	1.37	0.61	9.49	8.18	56.73
	20	0.763	325.62	705.08	1.71	0.76	11.16	7.84	67.72
	25	0.954	407.14	931.75	2.14	1.01	13.89	6.41	73.17
318K	5	0.191	81.51	310.13	0.71	0.34	6.83	7.34	22.23
	10	0.382	163.02	487.42	1.09	0.53	8.97	7.72	36.74
	15	0.573	244.54	692.23	1.50	0.75	11.44	7.08	47.85
	20	0.763	325.62	846.00	1.86	0.92	13.29	6.91	57.06
	25	0.954	407.14	831.25	2.03	0.90	13.11	8.61	69.89
323K	5	0.191	81.51	132.00	0.51	0.14	5.12	11.23	11.88
	10	0.382	163.02	699.41	1.32	0.76	11.96	5.82	32.61
	15	0.573	244.54	469.32	1.26	0.51	9.19	11.73	44.10
	20	0.763	325.62	667.51	1.67	0.72	11.57	10.23	54.72
	25	0.954	407.14	933.83	2.14	1.01	14.78	8.14	60.94

Table 9. Volume induced percolation of ([bmim][MS]±water)/(Tween 20 + n-pentanol)/n-heptane polar domain-in-oil microemulsion system at 298K.

$V_{IL+Water}$ / mL	φ_d	σ / $\mu S\ cm^{-1}$					
		2:8	**4:6**	**5:5**	**6:4**	**8:2**	**1:0**
0.05	0.23	0.00	0.00	0.00	0.00	0.01	0.00
0.10	0.23	0.01	0.01	0.01	0.01	0.01	0.01
0.15	0.23	0.01	0.01	0.01	0.01	0.01	0.02
0.20	0.24	0.02	0.02	0.02	0.02	0.02	0.03
0.25	0.24	0.02	0.03	0.03	0.03	0.03	0.03
0.30	0.24	0.03	0.04	0.04	0.04	0.04	0.05
0.35	0.25	0.03	0.04	0.05	0.05	0.06	0.06
0.40	0.25	0.04	0.05	0.06	0.06	0.07	0.07
0.45	0.26	0.05	0.06	0.07	0.07	0.08	0.08
0.50	0.26	0.06	0.08	0.09	0.08	0.09	0.10
0.55	0.26	0.07	0.09	0.10	0.09	0.11	0.11
0.60	0.27	0.08	0.10	0.12	0.11	0.13	0.13
0.65	0.27	0.09	0.11	0.14	0.12	0.14	0.14
0.70	0.27	0.10	0.13	0.16	0.13	0.16	0.16
0.75	0.28	0.11	0.14	0.17	0.14	0.17	0.17
0.80	0.28	0.12	0.15	0.19	0.16	0.19	0.18
0.85	0.28	0.13	0.17	0.20	0.17	0.20	0.20
0.90	0.29	0.15	0.18	0.22	0.18	0.22	0.22
0.95	0.29	0.16	0.20	0.24	0.20	0.24	0.24
1.00	0.29	0.17	0.22	0.25	0.21	0.26	0.25
1.05	0.30	0.18	0.23	0.27	0.22	0.28	0.26
1.10	0.30	0.20	0.25	0.29	0.24	0.29	0.28
1.15	0.30	0.21	0.27	0.31	0.25	0.31	0.29
1.20	0.31	0.23	0.29	0.33	0.27	0.39	0.31

10mL 0.2 M Tween 20 + n-pentanol (1:1, w/w) in n-heptane was used in each case.

Table 10. Volume induced percolation of ([bmim][MS]±water)/(Tween 20 + n-pentanol)/n-heptane polar domain-in-oil microemulsion system at 303K.

$V_{IL+Water}$ / mL	φ_d	σ / $\mu S\ cm^{-1}$					
		2:8	4:6	5:5	6:4	8:2	1:0
0.05	0.23	0.00	0.00	0.00	0.01	0.00	0.01
0.10	0.23	0.01	0.01	0.01	0.01	0.01	0.01
0.15	0.23	0.01	0.02	0.02	0.02	0.02	0.02
0.20	0.24	0.02	0.02	0.02	0.03	0.03	0.03
0.25	0.24	0.02	0.03	0.04	0.04	0.04	0.04
0.30	0.24	0.03	0.04	0.04	0.05	0.05	0.05
0.35	0.25	0.04	0.06	0.06	0.06	0.06	0.06
0.40	0.25	0.05	0.07	0.07	0.07	0.07	0.08
0.45	0.26	0.06	0.08	0.08	0.09	0.09	0.10
0.50	0.26	0.07	0.10	0.10	0.11	0.11	0.11
0.55	0.26	0.08	0.11	0.11	0.12	0.12	0.13
0.60	0.27	0.09	0.13	0.13	0.14	0.14	0.14
0.65	0.27	0.10	0.14	0.15	0.16	0.16	0.16
0.70	0.27	0.11	0.16	0.17	0.17	0.17	0.18
0.75	0.28	0.12	0.18	0.18	0.19	0.20	0.20
0.80	0.28	0.14	0.19	0.20	0.21	0.22	0.21
0.85	0.28	0.15	0.21	0.22	0.23	0.23	0.23
0.90	0.29	0.16	0.23	0.24	0.25	0.25	0.25
0.95	0.29	0.17	0.25	0.25	0.27	0.27	0.27
1.00	0.29	0.19	0.26	0.27	0.29	0.28	0.28
1.05	0.30	0.20	0.28	0.29	0.31	0.30	0.30
1.10	0.30	0.21	0.30	0.30	0.33	0.32	0.32

10mL 0.2 M Tween 20 + n-pentanol (1:1, w/w) in n-heptane was used in each case.

Table 11. Volume induced percolation of ([bmim][MS]±water)/(Tween 20 + n-pentanol)/n-heptane polar domain-in-oil microemulsion system at 308K.

$V_{IL+Water}$ / mL	φ_d	σ / $\mu S\ cm^{-1}$					
		2:8	4:6	5:5	6:4	8:2	1:0
0.05	0.23	0.00	0.00	0.00	0.01	0.00	0.01
0.10	0.23	0.01	0.01	0.01	0.01	0.01	0.01
0.15	0.23	0.02	0.02	0.02	0.02	0.02	0.02
0.20	0.24	0.02	0.02	0.03	0.03	0.03	0.03
0.25	0.24	0.03	0.04	0.04	0.04	0.04	0.04
0.30	0.24	0.04	0.05	0.06	0.05	0.05	0.06
0.35	0.25	0.05	0.06	0.07	0.07	0.07	0.07
0.40	0.25	0.06	0.07	0.08	0.08	0.08	0.10
0.45	0.26	0.07	0.09	0.10	0.10	0.10	0.11
0.50	0.26	0.08	0.10	0.12	0.12	0.12	0.13
0.55	0.26	0.10	0.14	0.14	0.14	0.14	0.15
0.60	0.27	0.11	0.15	0.16	0.15	0.16	0.17
0.65	0.27	0.13	0.17	0.18	0.17	0.18	0.20
0.70	0.27	0.14	0.19	0.20	0.19	0.20	0.22
0.75	0.28	0.16	0.21	0.22	0.21	0.22	0.24
0.80	0.28	0.17	0.23	0.24	0.23	0.24	0.27
0.85	0.28	0.19	0.25	0.27	0.26	0.26	0.29
0.90	0.29	0.20	0.27	0.29	0.27	0.28	0.31
0.95	0.29	0.22	0.29	0.31	0.29	0.30	0.33
1.00	0.29	0.24	0.31	0.34	0.31	0.33	0.34
1.05	0.30	0.26	0.33	0.36	0.34	0.35	0.37
1.10	0.30	0.28	0.35	0.38	0.36	0.37	0.39
1.15	0.30		0.00	0.41	0.38	0.39	0.41
1.20	0.31		0.01	0.43	0.40	0.51	0.43

10mL 0.2 M Tween 20 + n-pentanol (1:1, w/w) in n-heptane was used in each case.

Table 12. Volume induced percolation of ([bmim][MS]±water)/(Tween 20 + n-pentanol)/n-heptane polar domain-in-oil microemulsion system at 313K.

$V_{IL+Water}$ / mL	φ_d	σ / $\mu S\ cm^{-1}$					
		2:8	4:6	5:5	6:4	8:2	1:0
0.05	0.23	0.00	0.00	0.00	0.01	0.01	0.01
0.10	0.23	0.01	0.01	0.01	0.01	0.01	0.01
0.15	0.23	0.01	0.02	0.02	0.02	0.02	0.02
0.20	0.24	0.02	0.03	0.03	0.03	0.03	0.03
0.25	0.24	0.03	0.04	0.04	0.04	0.04	0.05
0.30	0.24	0.04	0.05	0.06	0.05	0.06	0.06
0.35	0.25	0.05	0.07	0.07	0.07	0.07	0.08
0.40	0.25	0.06	0.08	0.09	0.09	0.10	0.11
0.45	0.26	0.08	0.10	0.11	0.11	0.12	0.13
0.50	0.26	0.09	0.12	0.13	0.13	0.14	0.15
0.55	0.26	0.11	0.14	0.15	0.14	0.16	0.17
0.60	0.27	0.12	0.16	0.17	0.17	0.18	0.20
0.65	0.27	0.14	0.18	0.19	0.19	0.20	0.22
0.70	0.27	0.16	0.20	0.21	0.21	0.23	0.25
0.75	0.28	0.17	0.22	0.24	0.23	0.25	0.27
0.80	0.28	0.19	0.24	0.26	0.26	0.28	0.29
0.85	0.28	0.21	0.27	0.28	0.28	0.30	0.32
0.90	0.29	0.23	0.29	0.31	0.31	0.33	0.35
0.95	0.29	0.25	0.31	0.34	0.33	0.35	0.37
1.00	0.29	0.27	0.34	0.36	0.36	0.38	0.40
1.05	0.30	0.29	0.36	0.39	0.39	0.41	0.42
1.10	0.30	0.31	0.39	0.42	0.41	0.44	0.45
1.15	0.30		0.41	0.44	0.44	0.46	0.48
1.20	0.31			0.47	0.46	0.56	0.51

10mL 0.2 M Tween 20 + n-pentanol (1:1, w/w) in n-heptane was used in each case.

Table 13. Temperature induced percolation of ([bmim][MS]±water)/Tween 20 + n-pentanol)/n-heptane polar domain-in-oil microemulsion. Volume fraction of the polar domain: 0.24, 0.25, 0.27, 0.28 and, 0.29.

	2:8					4:6					5:5					6:4				
φ_d =	0.24	0.25	0.27	0.28	0.29	0.24	0.25	0.27	0.28	0.29	0.24	0.25	0.27	0.28	0.29	0.24	0.25	0.27	0.28	0.29
T/K	σ / $\mu S\ cm^{-1}$					σ / $\mu S\ cm^{-1}$					σ / $\mu S\ cm^{-1}$					σ / $\mu S\ cm^{-1}$				
283	0.01	0.05	0.06	0.15	0.25	0.02	0.05	0.08	0.15	0.21	0.01	0.05	0.09	0.14	0.20	0.02	0.05	0.09	0.17	0.23
288	0.01	0.05	0.08	0.20	0.29	0.02	0.05	0.09	0.17	0.26	0.02	0.06	0.10	0.17	0.23	0.02	0.06	0.10	0.20	0.29
293	0.02	0.07	0.09	0.23	0.36	0.02	0.06	0.11	0.19	0.31	0.02	0.07	0.12	0.20	0.27	0.02	0.07	0.12	0.23	0.34
298	0.02	0.07	0.10	0.28	0.42	0.02	0.07	0.12	0.24	0.35	0.02	0.08	0.14	0.24	0.32	0.02	0.07	0.14	0.27	0.41
303	0.02	0.08	0.12	0.32	0.51	0.02	0.08	0.14	0.28	0.43	0.02	0.09	0.16	0.28	0.38	0.03	0.09	0.15	0.31	0.47
308	0.02	0.09	0.17	0.37	0.53	0.03	0.09	0.16	0.32	0.47	0.02	0.10	0.18	0.31	0.43	0.03	0.10	0.17	0.36	0.55
313	0.02	0.10	0.27	0.42	0.67	0.03	0.10	0.18	0.35	0.54	0.03	0.11	0.20	0.34	0.50	0.03	0.11	0.20	0.41	0.60
318	0.03	0.11	0.33	0.48	0.74	0.03	0.11	0.20	0.40	0.63	0.03	0.12	0.22	0.38	0.56	0.03	0.12	0.22	0.46	0.67
323	0.03	0.12	0.38	0.54	0.81	0.03	0.12	0.22	0.45	0.69	0.03	0.13	0.25	0.42	0.61	0.03	0.13	0.24	0.50	0.72
328	0.03	0.12	0.42	0.60	0.90	0.03	0.12	0.24	0.49	0.76	0.03	0.14	0.27	0.45	0.68	0.04	0.14	0.26	0.56	0.81
333	0.03	0.13	0.46	0.68	1.01	0.03	0.13	0.26	0.54	0.81	0.03	0.15	0.29	0.49	0.76	0.04	0.15	0.29	0.61	0.89
338	0.03	0.13	0.51	0.75	1.11	0.03	0.14	0.28	0.60	0.89	0.03	0.17	0.32	0.51	0.83	0.04	0.16	0.32	0.66	0.95
343	0.03	0.13	0.57	0.82	1.16	0.03	0.15	0.31	0.66	0.94	0.03	0.18	0.34	0.55	0.94	0.04	0.17	0.34	0.74	1.01

Table 14. Temperature induced percolation of ([bmim][MS]±water)/Tween 20 + n-pentanol)/n-heptane polar domain-in-oil microemulsion. Volume fraction of the polar domain: 0.24, 0.25, 0.27, 0.28 and, 0.29.

	8:2					**1:0**				
φ_d =	**0.24**	**0.25**	**0.27**	**0.28**	**0.29**	**0.24**	**0.25**	**0.27**	**0.28**	**0.29**
T/K	σ / $\mu S\ cm^{-1}$					σ / $\mu S\ cm^{-1}$				
283	0.02	0.05	0.08	0.14	0.16	0.02	0.05	0.08	0.13	0.20
288	0.02	0.05	0.10	0.17	0.20	0.02	0.06	0.10	0.16	0.23
293	0.02	0.06	0.11	0.20	0.23	0.02	0.07	0.11	0.18	0.28
298	0.02	0.07	0.12	0.22	0.26	0.03	0.08	0.13	0.20	0.32
303	0.02	0.08	0.14	0.25	0.30	0.03	0.10	0.14	0.24	0.36
308	0.03	0.09	0.16	0.30	0.34	0.03	0.11	0.16	0.28	0.41
313	0.03	0.10	0.18	0.33	0.38	0.03	0.12	0.18	0.31	0.46
318	0.03	0.11	0.20	0.35	0.44	0.03	0.13	0.20	0.34	0.52
323	0.03	0.11	0.22	0.39	0.49	0.04	0.14	0.22	0.38	0.57
328	0.03	0.12	0.24	0.41	0.52	0.04	0.15	0.24	0.41	0.62
333	0.03	0.13	0.26	0.46	0.57	0.04	0.16	0.26	0.45	0.67
338	0.03	0.14	0.28	0.47	0.62	0.04	0.16	0.28	0.50	0.70
343	0.03	0.15	0.30	0.50	0.69	0.04	0.17	0.29	0.55	0.75

Table 15. Absorbance data of eosin Y in ([bmim][MS]±water)/(Tween 20 + n-pentanol)/n-heptane polar domain-in-oil microemulsion system. Concentration of eosin Y was kept constant at 10 μM.

λ / nm	**Abs. of *different volume fraction* (φ_d) of the (IL + water)-in-oil μEs, x_{IL}=0.2**					
	0.01	**0.02**	**0.04**	**0.06**	**0.07**	**IL+water**
405	0.047	0.034	0.006	0.014	0.064	0.274
415	0.039	0.030	0.005	0.009	0.055	0.234
425	0.032	0.025	0.005	0.005	0.048	0.195
435	0.023	0.020	0.008	0.005	0.044	0.165
445	0.012	0.011	0.013	0.009	0.044	0.143
455	0.007	0.006	0.027	0.022	0.053	0.132
465	0.030	0.028	0.047	0.041	0.068	0.132
475	0.063	0.060	0.075	0.069	0.092	0.142
485	0.146	0.138	0.148	0.144	0.157	0.193
495	0.228	0.219	0.225	0.224	0.227	0.265
505	0.255	0.245	0.251	0.251	0.251	0.289
515	0.413	0.395	0.390	0.393	0.376	0.388
525	0.759	0.727	0.703	0.718	0.663	0.659
535	0.764	0.744	0.732	0.753	0.699	0.784
545	0.323	0.322	0.335	0.344	0.337	0.450
555	0.067	0.066	0.083	0.075	0.089	0.129
565	0.005	0.002	0.018	0.005	0.023	0.030
575	0.005	0.008	0.008	0.005	0.011	0.009
585	0.006	0.010	0.006	0.008	0.009	0.003
595	0.007	0.010	0.006	0.008	0.008	0.008

Table 16. Absorbance data of eosin Y in ([bmim][MS]±water)/(Tween 20 + n-pentanol)/n-heptane polar domain-in-oil microemulsion system. Concentration of eosin Y was kept constant at 10 μM.

λ / nm	Abs. of *different volume fraction* (φ_d) of the (IL + water)-in-oil μEs, x_{IL}=0.4					
	0.01	**0.02**	**0.04**	**0.06**	**0.07**	**IL+water**
405	0.061	-0.043	-0.015	0.009	0.040	0.057
415	0.048	-0.034	-0.012	0.007	0.032	0.006
425	0.038	-0.027	-0.009	0.005	0.026	-0.007
435	-0.027	-0.018	-0.005	0.005	0.022	-0.011
445	0.014	-0.007	0.002	0.009	0.023	-0.009
455	0.007	0.012	0.018	0.022	0.032	1E-3
465	0.033	0.037	0.039	0.042	0.049	0.017
475	0.069	0.071	0.069	0.070	0.074	0.038
485	0.155	0.154	0.144	0.144	0.141	0.088
495	0.243	0.241	0.224	0.225	0.216	0.167
505	0.272	0.270	0.251	0.252	0.241	0.202
515	0.434	0.425	0.391	0.390	0.367	0.268
525	0.791	0.776	0.713	0.713	0.670	0.501
535	0.808	0.803	0.749	0.758	0.718	0.702
545	0.358	0.362	0.345	0.354	0.341	0.481
555	0.087	0.089	0.084	0.084	0.083	0.141
565	0.017	0.019	0.014	0.011	0.012	0.019
575	0.005	0.006	0.002	-0.003	-0.002	-0.007
585	0.003	0.004	0.001	-0.005	-0.004	-0.011
595	0.003	0.003	-0.001	-0.006	-0.005	-0.012

Table 17. Absorbance data of eosin Y in ([bmim][MS]±water)/(Tween 20 + n-pentanol)/n-heptane polar domain-in-oil microemulsion system. Concentration of eosin Y was kept constant at 10 μM.

λ / nm	Abs. of *different volume fraction* (φ_d) of the (IL + water)-in-oil μEs, x_{IL}=0.5					
	0.01	**0.02**	**0.04**	**0.06**	**0.07**	**IL+water**
405	-0.090	-0.060	-0.027	0.016	0.049	0.107
415	-0.075	-0.048	-0.022	0.014	0.041	0.038
425	-0.062	-0.040	-0.018	0.012	0.034	0.029
435	-0.050	-0.030	-0.014	0.011	0.029	0.029
445	-0.035	-0.018	-0.006	0.015	0.029	0.036
455	-0.014	0.002	0.010	0.026	0.037	0.048
465	0.012	0.025	0.030	0.043	0.051	0.067
475	0.046	0.057	0.058	0.068	0.073	0.087
485	0.125	0.133	0.129	0.134	0.136	0.133
495	0.204	0.211	0.204	0.205	0.206	0.211
505	0.232	0.238	0.229	0.229	0.228	0.248
515	0.379	0.380	0.361	0.352	0.347	0.303
525	0.700	0.695	0.661	0.642	0.631	0.518
535	0.708	0.715	0.692	0.677	0.671	0.736
545	0.304	0.317	0.314	0.313	0.315	0.555
555	0.064	0.074	0.072	0.074	0.074	0.210
565	0.002	0.011	0.008	0.008	0.007	0.075
575	-0.009	0.003	-0.004	-0.004	-0.006	0.046
585	-0.010	-0.002	-0.006	-0.007	-0.009	0.040
595	-0.010	-0.002	-0.006	-0.007	-0.010	0.039

Table 18. Absorbance data of eosin Y in ([bmim][MS]±water)/(Tween 20 + n-pentanol)/n-heptane polar domain-in-oil microemulsion system. Concentration of eosin Y was kept constant at 10 μM.

λ/ nm	Abs. of *different volume fraction* (φ_d) of the (IL + water)-in-oil μEs, x_{IL}=0.6					
	0.01	**0.02**	**0.04**	**0.06**	**0.07**	**IL+water**
405	-0.082	-0.071	-0.017	-0.027	0.024	0.160
415	-0.069	-0.060	-0.015	-0.026	0.017	0.093
425	-0.058	-0.052	-0.015	-0.026	0.010	0.064
435	-0.047	-0.043	-0.012	-0.024	0.006	0.048
445	-0.033	-0.030	-0.005	-0.017	0.006	0.040
455	-0.011	-0.009	0.010	-0.002	0.016	0.037
465	0.015	0.017	0.032	0.019	0.033	0.043
475	0.051	0.052	0.062	0.050	0.058	0.053
485	0.137	0.138	0.140	0.127	0.125	0.088
495	0.225	0.228	0.225	0.212	0.202	0.158
505	0.254	0.257	0.252	0.238	0.226	0.189
515	0.414	0.416	0.396	0.381	0.352	0.229
525	0.773	0.779	0.738	0.721	0.661	0.418
535	0.796	0.813	0.789	0.775	0.724	0.655
545	0.346	0.357	0.361	0.351	0.339	0.504
555	0.075	0.076	0.081	0.071	0.073	0.168
565	0.005	0.003	0.007	-0.004	-0.004	0.036
575	-0.007	-0.009	-0.007	-0.018	-0.014	0.006
585	-0.009	-0.011	-0.009	-0.020	-0.017	0.00
595	-0.009	-0.011	-0.010	-0.020	-0.017	-0.002

Table 19. Absorbance data of eosin Y in ([bmim][MS]±water)/(Tween 20 + n-pentanol)/n-heptane polar domain-in-oil microemulsion system. Concentration of eosin Y was kept constant at 10 μM.

λ / nm	Abs. of *different volume fraction* (φ_d) of the (IL + water)-in-oil μEs, x_{IL}=0.8					
	0.01	**0.02**	**0.04**	**0.06**	**0.07**	**IL+water**
405	0.042	0.031	0.003	0.023	0.054	0.054
415	0.034	0.026	0.003	0.018	0.045	0.065
425	0.028	0.021	0.003	0.015	0.037	0.061
435	0.021	0.015	0.000	0.014	0.033	0.052
445	0.011	0.007	0.005	0.016	0.032	0.040
455	0.007	0.008	0.018	0.026	0.040	0.024
465	0.028	0.027	0.034	0.040	0.052	0.002
475	0.058	0.054	0.059	0.062	0.073	0.020
485	0.132	0.121	0.122	0.121	0.130	0.061
495	0.206	0.191	0.190	0.186	0.195	0.137
505	0.230	0.212	0.210	0.205	0.213	0.180
515	0.370	0.338	0.329	0.315	0.321	0.208
525	0.682	0.625	0.607	0.579	0.585	0.373
535	0.693	0.646	0.640	0.619	0.633	0.626
545	0.297	0.283	0.289	0.286	0.301	0.545
555	0.068	0.065	0.068	0.070	0.079	0.197
565	0.010	0.009	0.012	0.013	0.019	0.050
575	0.000	0.001	0.001	0.002	0.008	0.019
585	0.001	0.002	0.001	0.000	0.006	0.015
595	0.001	0.002	0.001	0.000	0.006	0.015

Table 20. Emission spectra of eosin Y in ([bmim][MS]±water)/(Tween 20 + n-pentanol)/n-heptane polar domain-in-oil microemulsion system. Concentration of eosin Y was kept constant at 10 μM.

λ/ nm	**F.I. (a.u.), x_{IL}=0.2**					
	0.01	**0.02**	**0.04**	**0.06**	**0.07**	**IL+water**
500	0.003	0.003	0.003	0.003	0.003	0.002
510	0.016	0.016	0.014	0.014	0.014	0.009
520	0.097	0.095	0.089	0.089	0.087	0.057
530	0.413	0.408	0.394	0.383	0.386	0.258
540	1.179	1.159	1.113	1.098	1.076	0.785
550	1.583	1.577	1.536	1.539	1.488	1.311
560	1.308	1.311	1.291	1.303	1.266	1.208
570	0.902	0.907	0.896	0.908	0.881	0.867
580	0.645	0.647	0.635	0.644	0.621	0.598
590	0.508	0.507	0.495	0.501	0.482	0.455
600	0.377	0.378	0.373	0.377	0.363	0.349
610	0.250	0.254	0.250	0.255	0.245	0.244
620	0.156	0.160	0.158	0.160	0.155	0.156
630	0.096	0.100	0.098	0.099	0.096	0.097
640	0.063	0.064	0.064	0.065	0.062	0.062
650	0.043	0.043	0.043	0.043	0.042	0.042

Table 21. Emission spectra of eosin Y in ([bmim][MS]±water)/(Tween 20 + n-pentanol)/n-heptane polar domain-in-oil microemulsion system. Concentration of eosin Y was kept constant at 10 μM.

λ / nm	F.I. (a.u.), x_{IL}=0.4					
	0.01	**0.02**	**0.04**	**0.06**	**0.07**	**IL+water**
500	0.005	0.005	0.004	0.003	0.003	0.002
510	0.018	0.017	0.016	0.015	0.014	0.005
520	0.100	0.097	0.094	0.091	0.089	0.034
530	0.421	0.415	0.408	0.393	0.392	0.163
540	1.200	1.179	1.153	1.118	1.094	0.536
550	1.603	1.589	1.549	1.530	1.490	1.011
560	1.316	1.313	1.292	1.278	1.245	1.000
570	0.907	0.907	0.893	0.882	0.860	0.737
580	0.650	0.647	0.633	0.628	0.609	0.505
590	0.512	0.509	0.496	0.498	0.475	0.379
600	0.377	0.380	0.371	0.376	0.356	0.296
610	0.251	0.253	0.248	0.250	0.240	0.212
620	0.158	0.157	0.155	0.155	0.150	0.139
630	0.099	0.098	0.097	0.097	0.094	0.088
640	0.065	0.065	0.064	0.062	0.061	0.056
650	0.045	0.044	0.043	0.043	0.041	0.038

Table 22. Emission spectra of eosin Y in ([bmim][MS]±water)/(Tween 20 + n-pentanol)/n-heptane polar domain-in-oil microemulsion system. Concentration of eosin Y was kept constant at 10 μM.

λ / nm	F.I. (a.u.), x_{IL}=0.5					
	0.01	**0.02**	**0.04**	**0.06**	**0.07**	**IL+water**
500	0.005	0.004	0.004	0.003	0.003	0.002
510	0.018	0.017	0.017	0.015	0.015	0.005
520	0.106	0.101	0.099	0.094	0.092	0.028
530	0.389	0.415	0.366	0.372	0.362	0.130
540	1.175	1.176	1.106	1.103	1.079	0.449
550	1.607	1.573	1.564	1.549	1.538	0.986
560	1.329	1.299	1.323	1.308	1.310	1.065
570	0.919	0.893	0.920	0.915	0.913	0.803
580	0.659	0.638	0.658	0.649	0.649	0.556
590	0.519	0.501	0.515	0.507	0.507	0.416
600	0.385	0.374	0.386	0.384	0.381	0.327
610	0.260	0.252	0.261	0.258	0.257	0.237
620	0.163	0.159	0.164	0.164	0.164	0.159
630	0.101	0.099	0.102	0.102	0.102	0.101
640	0.065	0.064	0.066	0.066	0.066	0.064
650	0.045	0.044	0.045	0.044	0.044	0.043

Table 23. Emission spectra of eosin Y in ([bmim][MS]±water)/(Tween 20 + n-pentanol)/n-heptane polar domain-in-oil microemulsion system. Concentration of eosin Y was kept constant at 10 μM.

λ / nm	F.I. (a.u.), x_{IL}=0.6					
	0.01	**0.02**	**0.04**	**0.06**	**0.07**	**IL+water**
500	0.005	0.004	0.004	0.003	0.003	0.002
510	0.018	0.017	0.017	0.015	0.015	0.005
520	0.106	0.101	0.099	0.094	0.092	0.028
530	0.448	0.427	0.425	0.401	0.398	0.132
540	1.249	1.211	1.189	1.136	1.107	0.453
550	1.601	1.583	1.558	1.513	1.474	0.967
560	1.290	1.286	1.271	1.243	1.209	1.003
570	0.884	0.883	0.874	0.854	0.834	0.747
580	0.637	0.635	0.627	0.612	0.590	0.510
590	0.502	0.500	0.492	0.480	0.463	0.382
600	0.373	0.371	0.366	0.356	0.346	0.302
610	0.246	0.246	0.245	0.238	0.231	0.219
620	0.153	0.152	0.153	0.149	0.145	0.145
630	0.096	0.096	0.096	0.093	0.090	0.092
640	0.064	0.062	0.064	0.060	0.058	0.059
650	0.043	0.043	0.044	0.041	0.040	0.039

Table 24. Emission spectra of eosin Y in ([bmim][MS]±water)/(Tween 20 + n-pentanol)/n-heptane polar domain-in-oil microemulsion system. Concentration of eosin Y was kept constant at 10 μM.

λ / nm	F.I. (a.u.), x_{IL}=0.8					
	0.01	**0.02**	**0.04**	**0.06**	**0.07**	**IL+water**
500	0.003	0.003	0.002	0.002	0.002	0.001
510	0.014	0.013	0.012	0.010	0.010	0.003
520	0.087	0.085	0.079	0.072	0.070	0.018
530	0.389	0.385	0.371	0.342	0.331	0.102
540	1.106	1.069	1.040	0.958	0.929	0.383
550	1.444	1.402	1.383	1.277	1.263	0.864
560	1.164	1.129	1.126	1.040	1.037	0.949
570	0.788	0.764	0.764	0.702	0.700	0.713
580	0.558	0.538	0.537	0.488	0.489	0.475
590	0.438	0.422	0.419	0.380	0.380	0.345
600	0.326	0.314	0.314	0.285	0.285	0.271
610	0.216	0.209	0.209	0.191	0.191	0.198
620	0.134	0.130	0.130	0.120	0.120	0.133
630	0.084	0.080	0.080	0.074	0.074	0.083
640	0.055	0.052	0.052	0.047	0.048	0.052
650	0.037	0.036	0.035	0.032	0.032	0.034

Table 25. Emission spectra of eosin Y in ([bmim][MS]±water)/(Tween 20 + n-pentanol)/n-heptane polar domain-in-oil microemulsion system. Concentration of eosin Y was kept constant at 10 μM.

λ / nm	F.I. (a.u.), x_{IL}=1.0					
	0.01	**0.02**	**0.04**	**0.06**	**0.07**	**IL+water**
500	0.003	0.003	0.003	0.003	0.003	0.001
510	0.015	0.014	0.014	0.012	0.012	0.002
520	0.088	0.087	0.089	0.075	0.076	0.011
530	0.381	0.383	0.390	0.339	0.342	0.063
540	1.091	1.070	1.121	0.975	1.001	0.242
550	1.403	1.371	1.502	1.316	1.391	0.640
560	1.112	1.083	1.224	1.072	1.160	0.765
570	0.750	0.728	0.837	0.724	0.795	0.592
580	0.538	0.520	0.595	0.509	0.558	0.403
590	0.425	0.410	0.469	0.399	0.437	0.300
600	0.313	0.304	0.350	0.298	0.329	0.244
610	0.206	0.200	0.233	0.199	0.221	0.182
620	0.127	0.124	0.146	0.125	0.139	0.123
630	0.079	0.077	0.091	0.077	0.086	0.080
640	0.052	0.050	0.059	0.050	0.056	0.051
650	0.035	0.034	0.040	0.034	0.039	0.035

Table 26. Variation in the anisotropy and lifetime for 10 μM eosin Y with the volume fraction of the polar domain (ϕ_d) for ([bmim][MS]±water)/(Tween 20 + n-pentanol)/n-heptane polar domain-in-oil microemulsion system.

φ_d	**0.01**	**0.02**	**0.04**	**0.06**	**0.07**	**0.50**
	Anisotropy / Lifetime(nS)	**Anisotropy / Lifetime(nS)**	**Anisotropy / Lifetime(nS)**	**Anisotropy / Lifetime(nS)**	**Anisotropy / Lifetime(nS)**	**Anisotropy / Lifetime(nS)**
2:8	0.16 / 4.45	0.16 / 3.75	0.16 / 3.70	0.17 / 4.47	0.17 / 4.76	0.23 / 4.90
4:6	0.15 / 4.07	0.16 / 3.86	0.17 / 4.32	0.17 / 4.56	0.17 / 5.15	0.24 / 5.81
5:5	0.16 / 4.25	0.17 / 3.71	0.17 / 4.11	0.17 / 4.21	0.18 / 4.70	0.26 / 4.80
6:4	0.16 / 4.41	0.18 / 4.13	0.18 / 4.56	0.18 / 4.68	0.19 / 4.83	0.30 / 4.96
8:2	0.18 / 4.62	0.20 / 4.18	0.20 / 3.90	0.20 / 4.27	0.21 / 4.87	0.31 / 5.49
1:0	0.18 / 4.59	0.19 / 4.27	0.19 / 4.46	0.20 / 4.12	0.20 / 4.33	0.34 / 4.71

BIBLIOGRAPHY

J Surfact Deterg (2011) 14:473–486
DOI 10.1007/s11743-011-1256-5

ORIGINAL ARTICLE

Physico-Chemical Studies on Microemulsion: Effect of Cosurfactant Chain Length on the Phase Behavior, Formation Dynamics, Structural Parameters and Viscosity of Water/(Polysorbate-20 + *n*-Alkanol)/*n*-Heptane Water-in-Oil Microemulsion

Sujoy Paul · Amiya Kumar Panda

Received: 16 November 2010 / Accepted: 15 February 2011 / Published online: 6 March 2011

Abstract The pseudo-ternary water-in-oil microemulsion system, comprising water/polyoxyethylene sorbitan monolaurate (Polysorbate-20) + *n*-alkanol/*n*-heptane, have been studied by phase manifestation, method of dilution, viscosity and dynamic light scattering measurements. Polysorbate-20, in combination with equal mass of cosurfactants (of varying chain length, from *n*-butanol to *n*-octanol) were used in studying the systems in the temperature range 303–323 K. Appearance of turbidity was noted visually, which indicated the attainment of immiscibility or phase separation; a clear dependence of the different phases on cosurfactant chain length was noted. By employing the method of dilution, associated thermodynamic parameters for the formation of water-in-oil microemulsion droplets were derived. Different associated structural parameters were derived through further computation of the data derived from the method of dilution. Unusual behavior of Polysorbate-20, compared to the conventional ionic surfactants, was noted. Viscosity measurements, as carried out with different compositions and temperatures, revealed the temperature and water pool size dependency of the microemulsion systems. Viscosity data did not follow the same trend during heating and the cooling process, due to the condensation effect. This phenomenon was further confirmed by dynamic light scattering measurements.

Keywords Microemulsion · Polysorbate-20 · *n*-Alkanol · Thermodynamic parameter · Viscosity · Light scattering

Introduction

Microemulsions (μEs) are thermodynamically stable, macroscopically homogeneous and isotropic dispersions of water-in-oil (w/o) or vice versa (o/w), stabilized by a surfactant monolayer [1–4]. The surfactant monolayer not only prohibits the direct contact between water and oil, but also reduces the interfacial tension between the two immiscible liquids. Beside water-in-oil or oil-in-water microemulsion, another type of microemulsion, so-called bicontinuous is also possible. A number of good review works on the use and applications of microemulsion are available in literature [2, 5–18]. Thermodynamic stability, solubilizing capacity, optical transparency and isotropicity, etc., have credited microemulsions in different fields of applications like synthesis of nanomaterial [7, 11, 12, 14, 19, 20], enhanced oil recovery [21], polymerization reaction [22], remediation of organic contaminants from soil and water [15], drug delivery [6, 13, 17, 23], etc. As microemulsions are compartmentalized entities, they could mimic biological systems too [24] for which enzymatic activities have been found to be greatly altered in microemulsion media [25]. The field of microemulsion research started when the term was first used by Schulman et al. in the year 1959 [26]. Since then, substantive investigations have been carried out and considerable amounts of published data are available, however, the available information on microemulsions is still considered to be fragmentary in nature. A water-in-oil microemulsion is topologically similar to a reverse micelle [1, 2, 7, 14, 27]. When a small amount of water is added to a surfactant

Electronic supplementary material The online version of this article (doi:10.1007/s11743-011-1256-5) contains supplementary material, which is available to authorized users.

S. Paul · A. K. Panda (✉)
Department of Chemistry, University of North Bengal, Darjeeling, West Bengal 734 013, India
e-mail: akpanda1@yahoo.com

solution in oil, droplets of water get delineated from the non-polar phase. The delineation becomes possible due to the formation of a well-defined boundary by the surfactant monolayer [5]. In most of the cases when single tailed surfactants are used as an emulsifying agent, a fourth component becomes essential to maintain the curvature of the microemulsion droplets [1, 21, 22, 25, 28]. The influence of alkanols has been explained through a concept that explains the role of alcohol near the interface as lipophilic linkers. In addition, they can promote larger curvatures and higher oil solubilization [1, 21, 22, 25, 28]. Although small chain alkyl halides and amines could be used as the fourth component (also known as a cosurfactant) the most widely used cosurfactants are short chain *n*-alkanols. Extensive studies have been done by different researchers in understanding the effect of *n*-alkanols as an additional stabilizer. Moulay et al. [1] have studied the effect of alkanol chain length during the microemulsion breakdown by a pervaporation technique. Our research group has also studied the effect of cosurfactant chain length on different physicochemical parameters of AOT-based microemulsions [29] and other ionic/nonionic surfactants [30, 31]. Moulik et al. [32, 33], Digout et al. [34] and Wang et al. [21] have systematically studied the effect of alkanol chain length on the interfacial composition and thermodynamic of formation of water-in-oil (w/o) microemulsions. The influence of primary and secondary alcohols on the partition equilibrium of phenol red has been studied by Sarma et al. [35] Enzymatic activity dependence on the cosurfactant chain length was studied by Savelli et al. [36] According to Bayrak [37], there was a direct correlation between the solubilization of water with the chain length of both the oils and *n*-alkanols. It was therefore concluded that higher water solubilization was a consequence of the partitioning of the cosurfactant at the oil water interface, although contradictory reports are also available in the literature [38]. However, besides these above mentioned references, studies on microemulsions comprising polyoxyethylene sorbitan monolaurate and *n*-alkanols (*n*-butanol to *n*-octanol) of varying chain length are not plentiful in the literature to the best of our knowledge. In most of the cases, cosurfactants used include *n*-butanol, *n*-pentanol and *n*-hexanol for their better stabilizing efficiency in microemulsion formation [1, 21, 30, 34]. However, the exact reasons for the better efficacy of these alkanols over the other homologs are still not exactly known. This has motivated us to carry out an investigation of the water-in-oil microemulsion comprised of water/(Polysorbate-20 + *n*-alkanol)/*n*-heptane where the cosurfactant (*n*-alkanol) chain lengths varied from *n*-butanol to *n*-octanol.

In this paper, we explored the effect of cosurfactant chain length on different physicochemical parameters of w/o microemulsion as mentioned above. Cosurfactant chain length was varied from *n*-butanol to *n*-octanol. Also investigations on the physicochemical properties of microemulsions have been carried out at different temperatures and different [water]/[Polysorbate-20] mole ratios, ω. The above-mentioned systems were investigated by way of phase manifestation, method of dilution, viscosity and dynamic light scattering measurements. We believe such studies provide valuable information on microemulsions with regard to their formulation, energetics, and structural parameters.

Experimental

Materials

The non-ionic surfactant Polysorbate-20 was purchased from Fluka, Switzerland. The cosurfactants *n*-butanol, *n*-pentanol, *n*-hexanol, *n*-heptanol and *n*-octanol were products from Lancaster, England. All the materials were stated to be more than 99.5% pure and were used as received. HPLC grade *n*-heptane was obtained from E. Merck, Germany. Double distilled water was used throughout the experiment.

Methods

Construction of the Phase Diagram

The pseudo ternary phase diagram comprising of water/(Polysorbate-20 + *n*-alkanol)/*n*-heptane was constructed by the method of titration and through visual inspection [39]. To investigate different regions (mainly two phase turbid, 2Φ and homogeneous single phase, 1Φ), known amounts of Polysorbate-20, mixed with *n*-alkanol in 1:1 ratio (w/w) were placed in different stoppered test tubes. Varying amounts of oil (or water) were then added. Water (or oil) was progressively added by using a Hamilton (USA) microsyringe under constant stirring and the temperature was controlled using a cryogenic circulatory water bath (of precession ±0.1 K) at 303 K. Appearance of the state of turbidity was noted visually, which indicated the onset of phase separation or immiscibility [29–31]. The solutions were allowed to attain equilibrium for at least for 30 min (we found that equilibrium was attained within this time period in most of the systems). The process was followed for all the cosurfactants (*n*-butanol to *n*-octanol).

Method of Dilution

Thermodynamics of formation of water-in-oil (w/o) microemulsion (μE) comprising water/(Polysorbate-20 + *n*-alkanol)/*n*-heptane were evaluated by the method of

dilution. In this method, besides using a series of alkanols, experiments were carried out at different [water]/[Polysorbate-20] mole ratios, ω (5, 10, 15 and 20) and at five different temperatures (303, 308, 313, 318 and 323 K). The temperature was controlled by a cryogenic circulatory water bath with an accuracy of ±0.1 K. The method of dilution also helped in evaluating different structural parameters of the microemulsion under various conditions. Briefly, in the method of dilution, a fixed amount of water, surfactant and oil were placed in a stoppered test tube. The turbid solution was then titrated with cosurfactant under constant stirring unless a clear solution appeared. Sufficient time was allowed for equilibrium to be attained. At this point of clarity, composition of the mixture was then noted. A known quantity of *n*-heptane was then further added whereby the microemulsion became destabilized [21]. Clarity of the microemulsion was regained by further addition of *n*-alkanol under constant stirring; the amount of cosurfactant required was again noted. This method of destabilization and re-stabilization was repeated to obtain several points. Experiments were then done under different conditions, viz., [water]/[Polysorbate-20] mole ratio, ω, temperature and cosurfactant chain length in order to evaluate thermodynamic and structural parameters. Each set of experiments was carried out at least four times and the average of the values were used in obtaining the final result [30, 31].

Viscosity Measurements

Viscosity measurements were performed on monophasic microemulsions of known composition where 0.2 mol dm^{-3} Polysorbate-20 in *n*-heptane, mixed with 1:1 (w/w) alkanols were used. Choice of such a composition was intended for comparative studies. Solutions of different ω were then used for viscosity measurements using a LVDV-II + PCP cone and plate type roto viscometer (Brookfield Eng. Lab, USA). A CPE-42 type spindle made by Brookfield Eng. Lab, USA was used. Viscosity of the microemulsion at different temperature was measured where the temperature was controlled by a circulatory water bath (±0.1 K). The microemulsion with *n*-octanol as cosurfactant, at $\omega = 20$ could not be studied at 0.2 mol dm^{-3} Polysorbate-20 as the solution appeared turbid. During the measurements, shear rates (D) were varied within the range 20–60 S^{-1} and the corresponding shear stress (τ) was recorded. Finally the viscosity of the solution was obtained using the zero shear rates according to the relation $\eta = \tau/D$ [40, 41].

Dynamic Light Scattering Studies

Solutions, as prepared for the viscosity measurements, were used in measuring the dimension of the microemulsion droplets by the dynamic light scattering (DLS) method under different sets of conditions (viz., cosurfactant chain length, ω and temperature). Diameters of the microemulsion droplets were determined using a Zetasizer Nano ZS90 (ZEN3690, Malvern Instruments Ltd, UK). A He–Ne laser of 632.8 nm wavelength was used and the measurements were made at a scattering angle of 90°. The temperature was controlled by an inbuilt Peltier heating–cooling device (±0.05 K). The refractive index of each solution was recorded with an ABBE type refractometer, as it was required as an input in determining the size of the μE droplet by the DLS technique. Viscosity data, as obtained from viscosity measurements, were also used in processing the DLS data. Samples were filtered three times using a Milipore™ hydrophobic membrane filter of 0.25 μm pore size. In actual DLS measurements, the diffusion coefficient (D) of a solution is measured which is related to the diameter of a droplet (d) according to the Stokes–Einstein equation [28, 42–46]:

$$D = \frac{kT}{3\pi\eta d} \tag{1}$$

where k, T and η indicate the Boltzmann constant, temperature and viscosity respectively.

Results and Discussion

Phase Manifestation

Figure 1 shows the pseudo ternary phase diagram of water/(Polysorbate-20 + *n*-alkanol)/*n*-heptane systems. The solid line indicates the boundary region between the clear, single phase (1Φ) microemulsion region (un-shaded portions in the Figure) and the two phase (2Φ) turbid region (shaded portions). From the Fig. 1 it is also noticeable that the area under the clear region was dependent on the cosurfactant chain length. Results are clarified further through Fig. 2. With the increase in cosurfactant chain length, the area under the monophasic region decreased with a small halt at *n*-hexanol. The area under the monophasic region was ~55% (*n*-butanol) which decreased progressively upto ~25% in the case of *n*-octanol. *n*-Pentanol and *n*-hexanol displayed more or less similar effects. It could be concluded, therefore, that an increase in the cosurfactant chain length (decrease in polarity) makes the homogeneous system unstable, i.e., clear microemulsion formation becomes less favorable with the increasing cosurfactant (*n*-alkanol) chain length. Although different regions (viz., gel, viscous and clear fluid) were recorded in the monophasic region, for a simple and better understanding on the effect of *n*-alkanol chain length results have been described in terms of only two phases (1Φ and 2Φ). Construction of the phase diagram is the first and foremost job to be

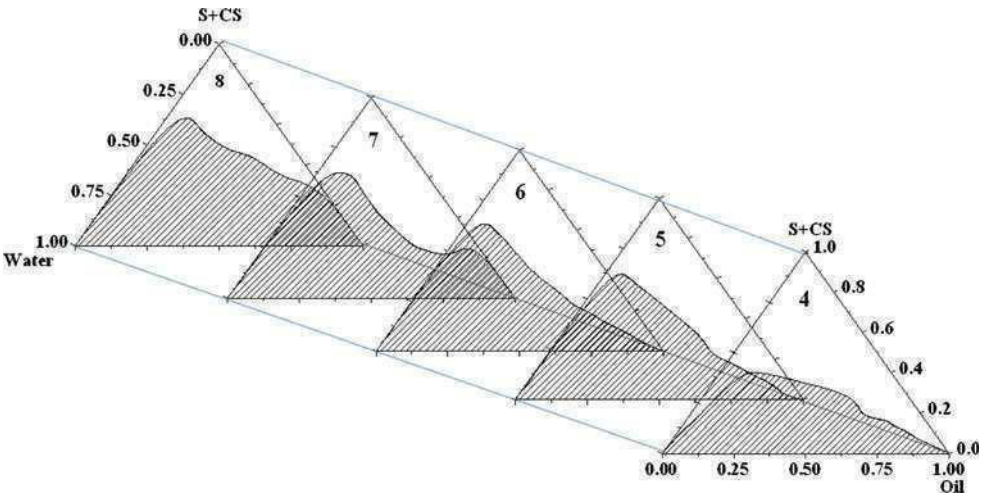

Fig. 1 Pseudo-ternary phase diagram of water/(Polysorbate-20 +*n*-alkanol)/*n*-heptane system at 303 K. Polysorbate-20 and *n*-alkanol were used in a 1:1 w/w ratio. *n*-Alkanol chain lengths are mentioned inside each plot. Scale magnitudes were reduced by 1/100 in the plot

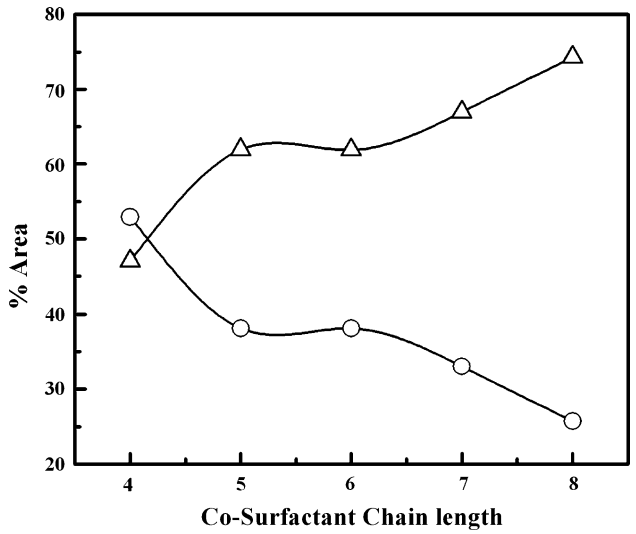

Fig. 2 Interdependence of the % area under clear (*circles*) and turbid (*triangles*) region with the cosurfactant chain length for water/(Polysorbate-20 + *n*-alkanol)/*n*-heptane pseudo-ternary system at 303 K

executed by a researcher, although the process is tedious in nature [2]. It is known that the phase behavior of a pseudo-ternary system depends on various factors, viz., nature of the polar medium (herein water), surfactant and cosurfactant used, the presence of an additive, the nature of the nonpolar medium (oil, herein *n*-heptane) and temperature, pressure, etc. [2, 47]. According to Ninham et al. [48] the compactness/ease of microemulsion formation depends on the packing symmetry between the surfactant chain length and the combined chain length of the oil and the cosurfactant used. Polysorbate-20 has a hydrocarbon tail comprised of 12 carbon atoms. It is, therefore, not unexpected that *n*-pentanol and *n*-hexanol would have a matching symmetry when combined with *n*-heptane. The appearance of a larger monophasic region in the case of *n*-butanol could be explained by its higher miscibility with water [21, 34]. Higher *n*-alkanols (>C_6) behaved more like oil than a cosurfactant.

Dilution Method

Evaluation of Thermodynamic Parameters

For a stable μE, the alkanol is distributed in the water, interface and oil; the surfactant essentially remains at the interface. The total number of moles of *n*-alkanol (n_a^i) would thus follow the relation [21, 34]:

$$n_a^t = n_a^w + n_a^i + n_a^o \tag{2}$$

where the superscripts w, i and o stand for water, interface and oil, respectively.

At a constant temperature and fixed ω, the ratio of the number of moles of alkanol to the number of moles of alkanol in oil (n_a^o) will be constant (with respect to the total number of them in the oil, n_o). Consequently, the mole fraction ratio of alkanol at the interface (X_a^i) and in oil (X_a^o) should also be constant. Thus,

$$n_a^o/n_o = k \tag{3}$$

and $$\frac{X_a^i}{X_a^o} = k_d \tag{4}$$

where k and k_d are a constant and the distribution constant, respectively.

By replacing Eq. 3 in Eq. 2 one sets the following relation:

$$\frac{n_a^t}{n_s} = \frac{n_a^w + n_a^i}{n_s} + k\frac{n_o}{n_s} \tag{5}$$

n_s represents the number of moles of surfactant.

In the dilution experiment, at a fixed n_s, n_a^t and n_o are varied to have a series of $\frac{n_a^t}{n_s}$ and $\frac{n_o}{n_s}$ which according to Eq. 5

can give $\frac{n_a^w + n_a^i}{n_s}$ and k from the linear plot between $\frac{n_a^t}{n_s}$ and $\frac{n_o}{n_s}$ as intercept (I) and slope (S), respectively. For n-butanol, which is a lower alkanol, n_a^w can be obtained from its water solubility, and by this value $\frac{n_a^i}{n_s}$ can be evaluated. Higher n-alkanols are practically insoluble in water; thus $\frac{n_a^i}{n_s}$ could directly be obtained from the intercept. The plot of $\frac{n_a^t}{n_s}$ versus $\frac{n_o}{n_s}$ for n-hexanol at $\omega = 10$ are presented in Fig. 3.

The distribution constant k_d is related to the slope and intercept of Eq. 5 as:

$$k_d = \frac{X_a^i}{X_a^o} = \frac{n_a^i/(n_a^i + n_s)}{n_a^o/(n_a^o + n_o)} = \frac{n_a^i\left(1 + \frac{n_a^o}{n_o}\right)}{n_a^o(n_a^i + n_s)} \quad (6)$$

Alternately,

$$k_d = \frac{\alpha(1+S)}{S\left[1 + \left(I - \frac{n_a^w}{n_s}\right)\right]} = \frac{\alpha(1+S)}{S(1+\alpha)} \quad (7)$$

$$\text{where } \alpha = \left(I - \frac{n_a^w}{n_s}\right) = \frac{n_a^i}{n_s} \quad (8)$$

Therefore, by knowing I, S and α, one can obtain the value of k_d. For alkanols longer than n-butanol $\alpha = I$, and Eq. 7 could be approximated as [21, 34]:

$$k_d = \frac{I(1+S)}{S(1+I)} \quad (9)$$

Thus by using Eqs. 5, 7 and 9 one can evaluate the values of n_a^i, n_a^o and k_d which are useful information for the formation of w/o microemulsions. Evaluation of the k_d value is required for obtaining the information on the thermodynamics of the process involved.

Changes in the standard Gibbs free energy of transfer (ΔG_t^o) of alkanol from oil to the interface could be expressed as:

$$\Delta G_t^o = -RT \ln k_d \quad (10)$$

Changes in the standard enthalpy of transfer ΔH_t^o was evaluated by the van't Hoff equation:

$$\left[\frac{\partial(\Delta G_t^o)}{\partial(1/T)}\right]_p = \Delta H_t^o \quad (11)$$

In the present study, ΔG_t^o versus T profile was found to follow a 2nd polynomial equation as:

$$\Delta G_t^o = a + bT + cT^2 \quad (12)$$

where a, b and c are the polynomial coefficients.

The polynomial coefficients thus helped in determining the ΔH_t^o values described in the following expression:

$$\left[\frac{d(\Delta G_t^o/T)}{d(1/T)}\right]_p = a - cT^2 = \Delta H_t^o \quad (13)$$

The standard entropy of transfer (ΔS_t^o) of the associated process was then evaluated according to the following expression:

$$\Delta S_t^o = (\Delta H_t^o - \Delta G_t^o)/T \quad (14)$$

Figure 4 describes the variation of ΔG_t^o with [water]/[Polysorbate-20] mole ratio (ω) at different temperature for water/(Polysorbate-20 + n-hexanol)/n-heptane as representative. Results are also summarized in Tables 1 and 2 and further details have been provided in the supplementary

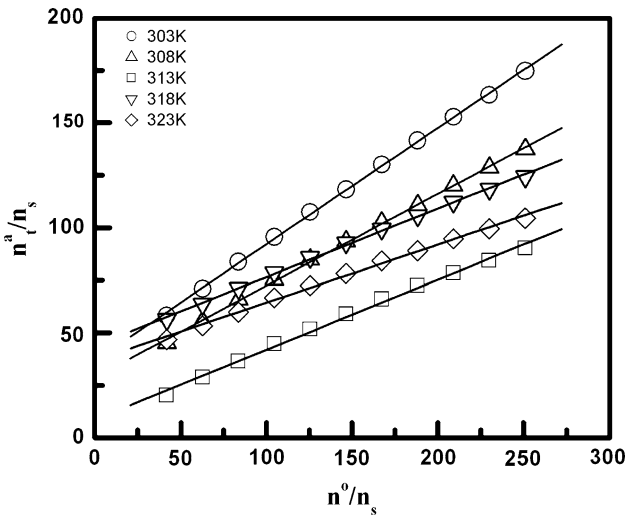

Fig. 3 Plot of n_a^t/n_s versus n_o/n_s for a water/(Polysorbate-20 + n-hexanol)/n-heptane water-in-oil microemulsion system. A 1:1 (w/w) mixture of Polysorbate-20 and n-hexanol was used at a [water]/[Polysorbate-20] mole ratio, $\omega = 10$. Temperatures are mentioned within the figure

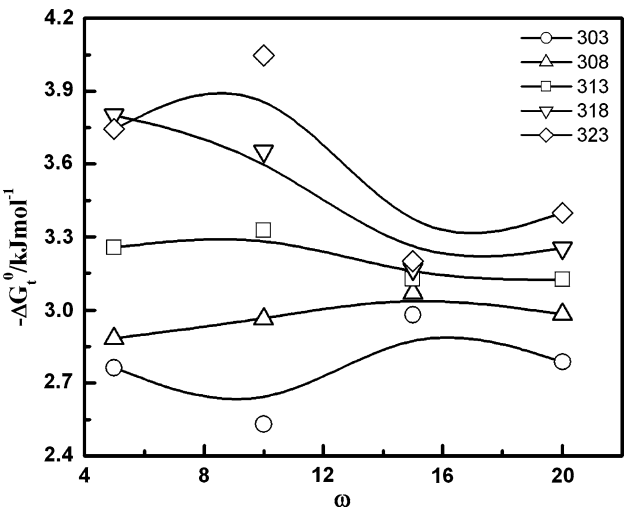

Fig. 4 ΔG_t^0 versus ω plot for water/(Polysorbate-20 + n-hexanol, 1:1, w/w)/n-heptane water-in-oil microemulsion at $\omega = 10$. Temperatures (in K) are mentioned inside the figure

section (Tables S1–S3). ΔG_t^o values were found to be negative in all the cases, which indicate the spontaneity of microemulsion formation. Polysorbate-20, along with *n*-alkanol, can tune the curvature of the water droplets, delineated from the contact of oil. It is clear from the results that with the rise in temperature for a particular alkanol, the negative value of ΔG_t^o increased. Higher negativity of ΔG_t^o represents enhanced spontaneity of the microemulsion formation process. Increases in temperature would lead to an overall increase in the kinetic energy of the system, which subsequently eases the easier formation of droplet. Increasing the temperature might lead to the opening up of the coiled surfactant head group, for which better efficacy of the system could have been achieved by Polysorbate-20 at a higher temperature [30, 31].

A decrease in the negative value of ΔG_t^o with increasing [water]/[Polysorbate-20] mole ratio ω was observed in general. An increase in the volume of the water droplet with increasing ω value requires larger coverage or delineation of water from the hydrophobic environment. At a fixed surfactant/cosurfactant composition, the spontaneity of the microemulsion formation would be limited with the progressive increase in ω values.

While considering the effect of the cosurfactant chain length, the spontaneity of the process is increased with the increase in the cosurfactant chain length. However, no significant difference was noticed between *n*-heptanol and *n*-octanol. An increase in the cosurfactant chain length leads to better accommodation of *n*-alkanol at the oil–water interface. However, the alkanols larger than *n*-heptanol behaved more like oil than a cosurfactant. Overall values of

Table 1 Thermodynamic parameters for the transfer of *n*-hexanol from oil to oil–water interface in the formation of water/(Polysorbate-20 + *n*-hexanol)/*n*-heptane water-in-oil microemulsion at different temperature and [water]/[Polysorbate-20] mole ratio, ω

Parameter	Temp. (K)					
	ω	303	308	313	318	323
k_d	5	2.99	3.08	3.40	4.21	4.03
	10	2.73	3.18	3.59	3.98	4.51
	15	3.26	2.97	3.32	3.13	3.29
	20	3.09	2.82	2.47	2.65	3.54
$(-)\Delta G_t^0$/kJmol^{-1}	5	2.76	2.88	3.25	3.80	3.74
	10	2.53	2.96	3.32	3.65	4.04
	15	2.98	3.07	3.13	3.16	3.20
	20	2.80	2.98	3.12	3.25	3.39
ΔH_t^0/kJmol^{-1}	5	17.99	16.40	14.71	13.03	11.32
	10	22.00	21.00	19.98	18.94	17.90
	15	2.48	1.36	0.23	−0.92	−2.09
	20	8.15	7.20	6.23	5.24	4.25
ΔS_t^0/JK^{-1}mol^{-1}	5	68.51	62.51	57.41	52.93	46.64
	10	81.00	77.81	74.50	71.10	67.94
	15	18.04	14.40	10.73	7.06	3.42
	20	36.12	33.07	29.90	26.73	23.67

0.2 g of Polysorbate-20 was taken in each case

Table 2 Thermodynamic parameters for the transfer of *n*-alkanol from the oil to oil–water interface in the formation of a water/(Polysorbate-20 + *n*-alkanol)/*n*-heptane water-in-oil microemulsion at 313 K and at different and [water]/[Polysorbate-20] mole ratios, ω

n-Alkanol	Parameter				
	ω	k_d	$(-)\Delta G_t^0$/kJmol^{-1}	ΔH_t^0/kJmol^{-1}	ΔS_t^0/JK^{-1} mol^{-1}
BuOH	5	3.01	2.86	27.42	96.75
	10	2.84	2.71	12.26	47.87
	15	2.38	2.08	11.56	0.043
	20	1.94	1.72	11.34	41.76
PentOH	5	3.41	3.19	13.41	53.05
	10	2.94	2.81	8.83	37.22
	15	2.60	2.50	−0.86	5.18
	20	2.47	2.35	4.30	21.29
HexOH	5	3.49	3.25	14.71	57.41
	10	3.59	3.32	19.99	74.50
	15	3.32	3.13	0.23	10.73
	20	2.47	3.12	6.23	29.90
HeptOH	5	3.52	3.43	7.67	35.47
	10	3.57	3.31	12.10	49.24
	15	3.30	3.39	6.18	30.59
	20	3.00	3.11	4.50	24.24
OctOH	5	4.34	3.82	11.76	49.78
	10	4.09	3.62	8.64	39.21
	15	3.48	3.24	2.27	17.62
	20	2.69	3.05	15.04	57.82

0.2 g of Polysorbate-20 was taken in each case

ΔG_t^o were found to be within the range of −1 to −5 kJ mol^{-1}. The lower ΔG_t^o are indicative of weak interactions between the alkanol and Polysorbate-20 at the interface [30, 31, 34].

While considering the ΔH_t^o value under various conditions (as described in Tables 1, 2 and Table S2) it was found that, except a few case, the ΔH_t^o values were positive. Positive ΔH_t^o values indicate that endothermicity is involved in the microemulsion formation process. This was as expected; with water droplets becoming dispersed into the oil continuum, due to area enhancement, there would be absorption of heat (energy). In general ΔH_t^o values decreased with the rise in the ω value. It also decreased with the increase in temperature. With the rise in temperature, overall structuredness of the system decreases, thus the energy change associated with the process becomes lower. However, ΔH_t^o values were found to decrease with the increasing *n*-alkanol chain length. With the increase in *n*-alkanol chain length, partitioning of the cosurfactant at the oil–water interface becomes easier. Entropy values were found to be positive in most of the cases. Variation in the ΔS_t^o value was not so significant compared the associated enthalpy changes. ΔS_t^o values decreased with the rise in ω values; however, ΔS_t^o values increased linearly with the rise in cosurfactant chain length.

Investigation on the enthalpy versus entropy compensation could justify the similarities in the structuredness of a reverse micelle and water-in-oil microemulsion system. Normally the compensation effect is stated to be valid for surfactant aggregates [49]. The plot of ΔH_t^o versus ΔS_t^o is shown in Fig. 5. In this plot all the compositions/conditions were taken into account except *n*-butanol. Microemulsion system comprising *n*-butanol behaved differently due to its significant solubility in water compared to its higher homologs [1, 21, 28, 34]. A nice correlation was observed for all sets of values (different *n*-alkanols, ω values and temperature). The compensation temperature, as obtained from the slope, was found to be 314 K which was in good agreement with the average over all the experimental temperature range (average temperature: 313 K; experimental temperature range: 303, 308, 313, 318 and 323 K). Although the energetic parameters were indirectly computed, they could, however, also be experimentally evaluated by calorimetric measurements. Such studies could be considered as a worthwhile study for the future.

Structural Parameters

The results of dilution experiments could suitably be further computed in evaluating different structural parameters of the w/o microemulsion. The microemulsion droplets are considered to have an approximately spherical shape

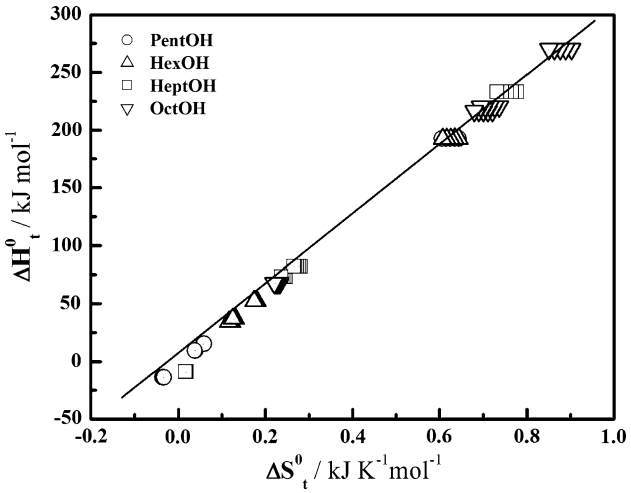

Fig. 5 Enthalpy-entropy compensation for the formation of a water/(Polysorbate-20 + *n*-alkanol)/*n*-heptane water-in-oil microemulsion (except *n*-butanol as it followed a different path). All the ω values at different experimental temperatures were considered. The *n*-alkanols used are shown inside the Figure. Compensation temperature: 314 K (close to the average of the experimental temperature range 303–323 K, i.e., 313 K)

in general, mono dispersed with a surface monolayer comprising surfactant and cosurfactant present at the interface. The total volume of the dispersed droplets (V_d) per unit volume (here in mL) can be expressed as follows:

$$V_d = \frac{4}{3}\pi R_e^3 N_d \tag{15}$$

R_e and N_d represents the effective diameter and total number of the droplets, respectively.

The droplet surface area (A_d) of droplets per unit volume is therefore:

$$A_d = 4\pi R_e^2 N_d = \left(n_S A_S + n_a^i A_a\right) N_A \tag{16}$$

where A_S and A_a are the cross sectional area of the surfactant and cosurfactant molecules, respectively, N_A Avogadro's constant.

The equation for R_e from Eqs. 15 and 16 can be written as:

$$R_e = 3V_d/A_d \tag{17}$$

Total volume of the dispersed phase, herein the water droplet embedded by the surfactant and *n*-alkanols at the oil–water interface, is the sum of the volume contribution of water (V_{H_2O}), surfactant (V_S) and the interfacial *n*-alkanol molecules (V_a^i) at the interface, respectively. Thus, one could write;

$$V_d = V_{H_2O} + V_S + V_a^i \tag{18}$$

One can determine the respective volumes using the values of number of moles (n_a^i), molar mass (M_a) and density of the components (ρ_a) according to the relation:

$$V_a^i = n_a^i M_a/\rho_a \tag{19}$$

The total droplet surface area (A_d) can be obtained from the equation:

$$A_d = \left(n_S A_S + n_a^i A_a\right) N_A \tag{20}$$

where A_S and A_a are the polar head group area of surfactant and alkanol, respectively, and N_A is the Avogadro constant.

Putting the value of R_e in Eq. 15 we get the values of N_d

$$N_d = 3V_d/4\pi R_e^3 \tag{21}$$

The average aggregation number of surfactant (N_S) and cosurfactant (N_a) in a microemulsion droplet can be expressed as:

$$N_S = \frac{n_S N_A}{N_d} \tag{22}$$

$$N_a = \frac{n_o^i N_A}{N_d} \tag{23}$$

The volume of a microemulsion droplet is contributed to by dispersed water, surfactant and cosurfactant molecules. Thus, the radius of the water pool in a microemulsion droplet is related to the effective radius (i.e., the sum of the pool radius and surfactant tail) according to the relation:

$$R_w = \left(\frac{V_{H_2O} + V_S^h + V_a^h}{V_d}\right)^{1/3} R_e \tag{24}$$

where V_{H_2O}, V_S^h and V_a^h are the volumes of the water droplet, surfactant head group, and alkanol head group, respectively. Volume contributions due to the surfactant head group and cosurfactant head group could be evaluated from the following two equations:

$$V_S^h = \frac{4}{3\pi^{1/2}} A_S^{3/2} N_S \tag{25}$$

$$V_a^h = \frac{4}{3\pi^{1/2}} A_a^{3/2} N_a \tag{26}$$

Various structural parameters, as described in the earlier section were computed by inserting the dilution data into the aforementioned equations. Variation in the number of droplets per unit volume (N_d) with [water]/[Polysorbate-20] mole ratio and temperature is shown in Fig. 6 for microemulsion containing *n*-hexanol as representative. Detailed results for all the systems are also summarized in the supplementary section (Table S4).

The number of droplets per unit volume (herein mL) was found to increase with the increase in ω values. Such results apparently seem to be contradictory as one could expect an incremental effect when the volume of the added water is increased for a particular system at fixed surfactant/cosurfactant and oil system and at a certain temperature [1, 21, 28, 30, 31, 34]. This unusual behavior was only

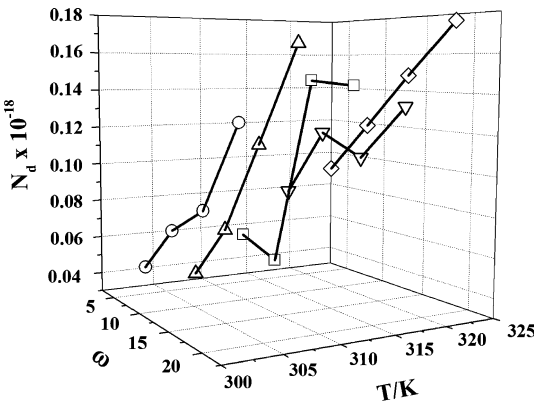

Fig. 6 N_d—ω—T profile for water/(Polysorbate-20 + *n*-hexanol)/*n*-heptane water-in-oil microemulsion system. A 1:1 (w/w) Polysorbate-20: *n*-hexanol mixture was used

observed in our earlier investigations [30, 31]. Such a behavior was observed only for nonionic surfactants having polyoxyethylene head groups [30, 31]. It is assumed that with the increase in the volume of water, newer droplets could be formed with smaller dimensions. This assumption would further be established by analyzing the other structural parameters as well as the dynamic light scattering measurements to be presented in subsequent sections. We also expect the occurrence of droplet fission phenomena when the temperature of the microemulsion media is increased.

With the increase in the number of droplets through the progressive addition of water to a fixed amount of surfactant, alkanol and oil, one could also expect a change in the number of surfactant (N_s) and cosurfactant (N_{cs}) molecules per microemulsion droplet. The ω and temperature dependence of N_s and N_{cs} for a water/(Polysorbate-20 + *n*-hexanol)/*n*-heptane water-in-oil microemulsion system is shown in Fig. 7 as representative.

Results have also been detailed in the supplementary section (Table S4). It is evident from Fig. 7 and Table S4 that the N_s value decreased with the increase in the ω. N_s also decreased with the increase in temperature. Such behavior contradicts the earlier reports by Hait et al. [50] where a water-in-oil microemulsion comprising of water/(CPC + *n*-alkanol)/*n*-heptane was used. In their studies both temperature and ω had an incremental effect on the N_s. However, in the present studywe noted that with a fixed number of surfactant molecules, the formation of a larger number of droplets would reduce the average number of surfactant molecules per microemulsion droplet. This apparent unusual behavior was made possible because of the presence of oxyethylene groups in Polysorbate-20. In Polysorbate-20, the oxyethylene group could 'open up' or 'uncoil' themselves to provide a better coverage at the oil–water interface [30, 31]. Ionic surfactants, because of

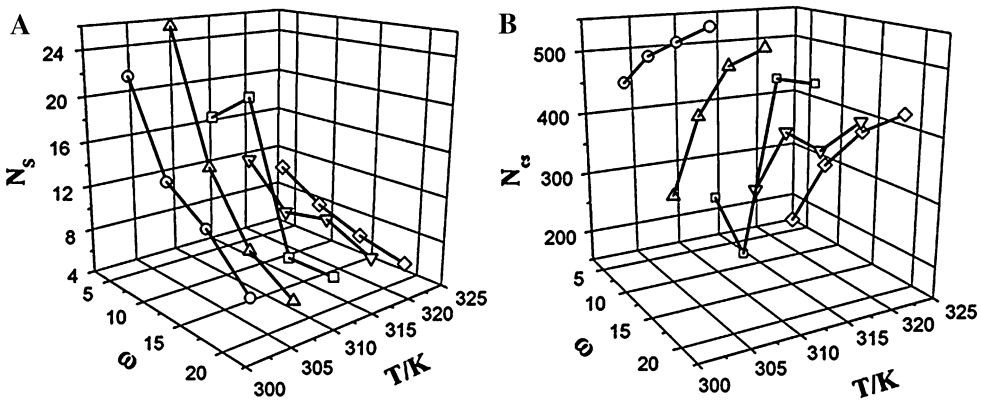

Fig. 7 Variation in the amounts of **a** surfactant (N_s) and **b** cosurfactant (N_{cs}) per microemulsion droplet with ω and temperature in the water/(Polysorbate-20 + *n*-hexanol)/*n*-heptane water-in-oil microemulsion system

their relatively smaller head groups, could not cause such an effect.

It was found that both the increases in temperature and ω values led to an increase in the number of droplets per unit volume and subsequent decrease in the average aggregation number of surfactants (N_s) per droplet. For a better delineation and protection of water droplets from the oil contact, the decrease in N_s needs to be compensated for by an increase in the average number of cosurfactant molecule per droplet (N_{cs}). Figure 7b confirms such predictions in a better way. Trends in the variation of N_s and N_{cs} followed an opposite path, especially when considering their variations with ω values.

While considering the effect of the alkanol chain length on the N_{cs} value it was observed that in general the N_{cs} values increased from *n*-butanol to *n*-heptanol. However, N_{cs} values for *n*-octanol were found to lie in between *n*-butanol and *n*-pentanol. This supports the larger involvement of the cosurfactant molecule in stabilizing a microemulsion droplet. *n*-Octanol behaved more like an oil than a cosurfactant as its effect was different from the other cosurfactants.

Involvement of a cosurfactant as a surfactant substitute and its compensation effect could further be ascertained while considering the ratio of N_{cs} and N_s. Except for *n*-butanol, it was found that the ratio of N_{cs}/N_s increased linearly with the increase in the ω value. Interestingly, the ratio was found to be independent of temperature (data not shown to save space). These results were in conformity with earlier observations [30, 31, 34, 50].

Size of the Microemulsion Droplets

Results on determining the hydrodynamic parameters of the microemulsion droplets are summarized in Table 3. In this table, the radius of the water pool (R_w), effective radius of the microemulsion droplets (R_e), contributory effect of water pool, surfactant/cosurfactant head group and surfactant hydrocarbon tails and hydrodynamic radius during heating (R_h) and cooling (R_c) have been presented for all the systems except *n*-octanol (the reason was stated earlier in the experimental section). It is to be noted that R_w and R_e were obtained by computing the results of dilution measurements while the R_h and R_c were directly obtained from the dynamic light scattering measurements. Results were found to be comparable with each other. It is also to be noted that R_h values were found to be in between the R_w and R_e values. This is also not unexpected, although such reports are not available in the literature. In the case of water-in-oil microemulsion the hydrocarbon chains, being in an oil continuum, do not get involved in the scattering of light. Therefore, one could, in general, expect depreciation in the size corresponding to the dimension (length) of the surfactant tail. According to Tanford's formula, the critical (l_c) or effective length (l_{max}) of a saturated hydrocarbon chain having a C_n number of carbon atoms will be [51]:

$$l_c \leq l_{max} \approx (0.154 + 0.1265\ C_n)\ \text{nm} \quad (27)$$

For Polysorbate-20 (having a dodecyl hydrocarbon chain) l_c appears to be approximately equal to 1.672 nm. Therefore, one could expect a difference of $\approx$1.7 nm in between R_e and R_h value. For every system, the radii were found to decrease with increases in temperature. Such observations, especially in the DLS measurements finally prove our assumptions as made during the analyses of dilution measurements. When the numbers of droplets are increased without changing the number of surfactant molecules, one could expect a decrease in the size of the microemulsion droplets. Also the decrease in $R_w/R_e/R_h/R_e$ values with the increase in ω values further establishes our mechanism as proposed in analyzing the results of dilution measurements. While considering the effect of cosurfactant chain length it was found that R_e values increased with the increase in cosurfactant chain length. However, no systematic variation in the radii values were evidenced

Table 3 Radius of a water/(Polysorbate-20 + *n*-alkanol)/*n*-heptane water-in-oil microemulsion at different temperatures and [water]/[Polysorbate-20] mole ratios, ω

n-Alkanol	$R_w/R_e/R_h/R_c$ (in nm) at different temperature (in K)					
	ω	Temp. 303	308	313	318	323
BuOH	5	1.34/3.20/1.85/2.19	0.96/2.52/1.54/2.00	0.80/2.23/1.34/1.88	0.78/1.94/1.38/1.65	0.65/1.90/1.40/1.40
	10	1.51/3.14/2.70/2.40	1.21/2.63/2.15/3.21	1.09/2.34/1.85/3.02	0.96/2.11/1.80/2.72	0.86/1.96/1.75/1.75
	15	1.96/3.49/3.30/2.80	1.56/2.86/2.37/2.60	1.32/2.47/2.10/1.88	1.10/2.21/2.16/1.53	0.99/2.05/2.25/2.25
	20	1.60/3.05/3.90/3.61	1.17/2.56/3.40/2.43	1.29/2.50/2.55/2.11	1.23/2.31/2.37/1.70	1.17/2.11/2.72/2.72
PentOH	5	0.96/2.93/0.91/0.80	0.93/2.66/0.81/0.86	0.78/2.46/0.74/0.84	0.70/2.33/0.78/0.83	0.66/2.20/0.86/0.86
	10	1.01/2.90/0.84/0.73	0.94/2.73/0.80/0.76	0.92/2.58/0.73/0.77	0.85/2.45/0.77/0.75	0.81/2.33/0.79/0.79
	15	0.85/2.86/0.94/0.93	0.85/2.76/0.87/0.91	0.84/2.65/0.80/0.93	0.78/2.56/0.79/0.86	0.77/2.45/0.85/0.85
	20	0.85/2.89/0.98/0.85	0.78/2.78/0.92/0.84	0.75/2.70/0.81/0.84	0.76/2.61/0.80/0.81	0.72/2.54/0.81/0.81
HexOH	5	1.17/3.23/0.75/0.49	1.23/2.96/0.65/0.50	1.07/2.73/0.60/0.51	0.96/2.63/0.52/0.55	0.92/2.40/0.55/0.55
	10	1.00/3.18/0.82/0.54	1.01/3.02/0.76/0.55	1.13/2.65/0.70/0.52	0.84/2.82/0.64/0.55	0.84/2.70/0.59/0.59
	15	0.94/3.21/0.87/0.60	0.85/3.09/0.77/0.74	0.78/3.01/0.72/0.71	0.87/2.83/0.66/0.72	0.78/2.82/0.65/0.65
	20	0.82/3.20/0.90/0.72	0.76/3.12/0.85/0.80	0.79/3.04/0.80/0.78	0.81/2.93/0.75/0.80	0.74/2.90/0.70/0.70
HeptOH	5	1.47/3.43/0.77/0.59	1.39/3.11/0.72/0.54	1.23/2.97/0.63/0.52	1.17/2.69/0.60/0.54	1.08/2.63/0.65/0.65
	10	1.04/3.52/0.95/0.65	0.99/3.40/0.83/0.62	0.94/3.26/0.72/0.65	0.92/3.12/0.67/0.65	0.89/2.98/0.64/0.64
	15	1.12/3.56/1.00/0.65	1.04/3.44/0.83/0.61	1.00/3.34/0.68/0.63	0.97/3.26/0.63/0.62	0.99/3.08/0.68/0.68
	20	1.10/3.58/0.95/0.61	1.04/3.49/0.85/0.63	1.04/3.40/0.74/0.57	1.04/3.31/0.63/0.58	1.02/3.22/0.60/0.60
OctOH	5	0.94/2.53/1.05/0.65	0.94/2.40/0.90/0.61	0.87/2.25/0.75/0.57	0.79/2.13/0.69/0.63	0.77/1.99/0.60/0.60
	10	0.77/2.46/1.15/0.76	0.74/2.38/0.90/0.68	0.75/2.30/0.81/0.69	0.72/2.21/0.71/0.65	0.70/2.13/0.68/0.68
	15	0.82/2.46/1.30/0.70	0.77/2.38/0.98/0.63	0.75/2.32/0.88/0.60	0.74/2.26/0.70/0.61	0.76/2.20/0.62/0.62
	20	0.80/2.43/–/–	0.77/2.38/–/–	0.80/2.33/–/–	0.75/2.28/–/–	0.74/2.24/–/–

0.2 mol dm^{-3} Polysorbate-20 with 1:1 Polysorbate-20: *n*-alkanol (w/w) in *n*-heptane was used. $R_w/R_e/R_h/R_c$ represent the radius of the water pool (derived from dilution measurement), effective radius of the microemulsion droplet (derived from dilution measurement), radius of droplet measured by DLS while heating and radius of droplet measured by DLS while cooling

through DLS measurements. Our present set of results have been found to be comparable with the reported values for different alkanols [28].

The formation of a larger number of droplets along with a size decrease can be further clarified through Fig. 8. Figure 8 describes the temperature dependence of microemulsion size and its distribution obtained from DLS measurements. It is clear from the Figure that with an increase in temperature the size distribution moves to the lower dimensions. Besides, the intensity of the distribution curves was found to be increased with the rise in temperature. It is known that the light scattering intensity is proportional to the square of the droplet volume and to the droplet number [20]. In the present study, the increase in the number of droplets was more significant than the decrease in size of the microemulsion droplets. Hence increase in the intensity of the distribution curve resulted along with a decrease in the width of the distribution curves. However, further structural studies on such microemulsions using cryo-transmission electron microscopy are warranted.

In recording the DLS data while cooling down microemulsions, it was always noted that the dimensions of the droplets followed a higher profile than the heating curves. This unusual behavior was due to the condensation effect of the droplets during the cooling [20]. However, the width

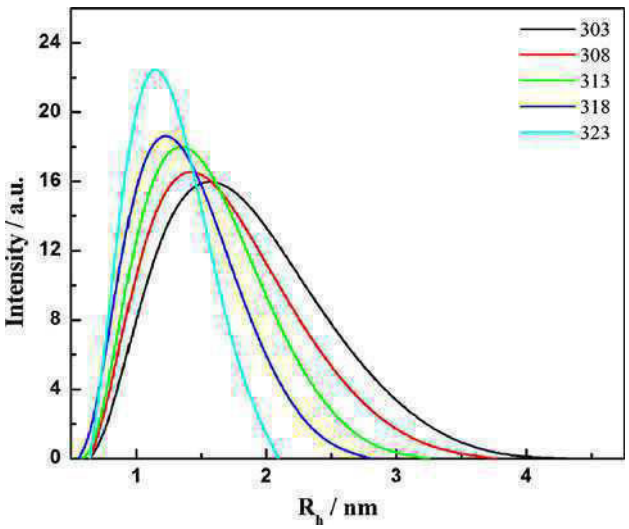

Fig. 8 Size and size distribution of a water/(Polysorbate-20 + *n*-hexanol, 1:1, w/w)/*n*-heptane water-in-oil microemulsion at different temperatures. Temperatures (in K) are within the figure [water]/[Polysorbate-20], $\omega = 10$. A 0.2 mol dm^{-3} Polysorbate-20 was used

of the distribution curves were not changed significantly as was observed during the heating of the microemulsions.

Viscosity Measurement

Viscosity along with viscosity derived activation parameters at a 1:1 Polysorbate-20/alkanol ratio under different conditions are summarized in Table 4. η and temperature dependency of data are presented in Fig. 9 for the *n*-hexanol derived formulation as a representative plot. It was generally observed that with the rise in temperature viscosity decreased. Viscosity initially decreases with increasing ω and passes through minima at ω in the range of 10–15. It is known that fluidity increases with the rise in temperature for microemulsions in general [40, 41, 52, 53]. However, initial decrease in viscosity of microemulsion with increase in ω could be accounted for the increase in the number of droplets, and the subsequent size depletion. Viscosity was found to rise with the increase in the cosurfactant chain length. This is due to the stronger binding affinity of alkanol with surfactant head groups [34]. However, *n*-octanol being more oily than other cosurfactants did not bring abpout a progressive incremental effect. The temperature dependency of viscosity was found to decrease with the increase in cosurfactant chain length. Further investigations using more sophisticated tools like small angle neutron scattering and cryo-TEM, etc., are warranted. Therefore, rheometric measurements, along with the above-mentioned studies on such systems could be considered as future perspectives of the present work.

Viscosity data were further computed and analyzed in deriving the activation enthalpy (ΔH^*), which is equivalent to the activation energy, free energy (ΔG^*), entropy change (ΔS^*) and change in specific heat capacity (ΔC_p) [40, 41, 52, 53].

The activation enthalpy for the viscous flow and the associated entropy change can be expressed by the following equation,

$$\eta = \left(\frac{hN}{V}\right) e^{\Delta H^*/RT} e^{-\Delta S^*/RT} \tag{28}$$

Its logarithmic form can be expressed as:

$$\ln \eta = \left\{ \ln\left(\frac{hN}{V}\right) - \frac{\Delta S^*}{R} \right\} + \frac{\Delta H^*}{RT} \tag{29}$$

h, N, V are Plank's constant, Avogadro's constant and molar volume, respectively. R and T have their usual significances. As expressed in Eq. 29; one can obtain ΔH^* from the slope of $ln\ \eta$ versus T^{-1} plot. ln η was found to vary with T^{-1} in a binomial way; hence one can derive ΔH^* from its differential with respect to temperature in the following way;

$$\ln \eta = a + bT + cT^2 \tag{30}$$

Therefore,

$$\frac{d \ln \eta}{dT} = -\frac{\Delta H^*}{RT^2} = b + 2cT \tag{31}$$

Thus knowing the value of 'b' and 'c' one can compute ΔH^* at different temperatures.

Change in the heat capacity (ΔC_p) is related to ΔH^* as:

$$\Delta C_p = \frac{d(\Delta H^*)}{dT} = -2RT(b + 3cT) \tag{32}$$

Therefore the change in Gibb's free energy for activation can be expressed as;

$$\Delta G^* - RT \ln \frac{\eta V}{hN} \tag{33}$$

Once ΔH^* and ΔG^* are known, the ΔS^* value can be calculated easily according to the following expression:

$$\Delta S^* = \frac{\Delta H^* - \Delta G^*}{T} \tag{34}$$

All the viscosity-associated thermodynamic parameters have been presented in Table 4. The results reveal that ω dependency on ΔG^* was almost similar to its viscosity. Gibb's free energy for activation was found to increase with increasing temperature for all the systems. The increase in ΔG^* with increasing temperature is a consequence of shear thickening of the sample with increasing temperature. No systematic variations in the ΔC_p values were noted. Both the positive and negative ΔC_p values were in accordance with the increase and decrease in ΔH^* values under various conditions [54, 55]. Results also reveal the complex nature of the microemulsion droplets. The ΔG^* values were limited to within the range of 3.5–3.8 kJ mol^{-1} whereas the ΔH^* and ΔS^* values varied significantly. A good correlation between ΔH^* and ΔS^* was found for all the compositions and temperatures as revealed from the compensation plots between ΔH^* and ΔS^* (given in supplementary data, Fig. 1S). The compensation temperature (313 K) obtained from the slope was found to be in close proximity to the average of all the experimental temperatures (303, 308, 313, 318 and 323 K). Similar observations have also been reported by others [40, 41, 52, 53].

Summary and Conclusion

Physicochemical studies on water/(Polysorbate-20 + *n*-alkanol)/*n*-heptane w/o microemulsions were performed using different techniques, viz., phase manifestation, dilution method, DLS and viscosity measurements. Results were analyzed in the light of the above-mentioned

Table 4 Viscosity and viscosity derived activation parameters of water/(Polysorbate-20 + *n*-alkanol)/*n*-heptane water-in-oil microemulsions at different temperatures and [water]/[Polysorbate-20] mole ratios, ω

n-Alkanol	(η/cP)/ΔH^*/kJ mol^{-1})/(ΔG^*/kJ mol^{-1})/(ΔS^*/J mol^{-1} K^{-1})/(ΔCp/kJ mol^{-1} K^{-1})				
	ω	303	308	313	318	323
BuOH	5	2.88/7.17/3.52/2.36/7.10	2.56/7.53/3.54/2.44/7.33	2.34/7.90/3.58/2.52/7.58	1.80/8.30/3.57/2.60/7.82	1.34/8.68/3.55/2.69/8.07
	10	2.66/8.30/3.50/2.73/8.21	2.45/8.72/3.53/2.83/8.49	2.10/9.14/3.55/2.92/8.76	1.56/9.59/3.53/3.01/9.05	1.14/10.05/3.50/3.11/9.33
	15	2.80/5.60/3.51/1.85/5.54	2.39/5.88/3.53/1.91/5.73	1.91/6.17/3.53/1.97/5.92	1.34/6.47/3.49/2.03/6.10	1.01/6.78/3.48/2.10/6.30
	20	2.77/8.34/3.51/2.91/8.75	2.37/9.28/3.53/3.01/9.04	2.15/9.74/3.56/3.11/9.33	1.70/10.22/3.55/3.21/9.64	1.12/10.70/3.50/3.31/9.94
PentOH	5	2.80/6.73/3.51/2.22/6.66	2.58/7.07/3.55/2.29/6.88	2.44/7.42/3.59/2.37/7.11	1.86/7.78/3.58/2.44/7.34	1.49/8.15/3.58/2.52/7.57
	10	2.90/2.28/3.52/0.75/2.26	2.38/2.39/3.53/0.78/2.33	2.38/2.51/3.58/0.80/2.41	1.86/2.63/3.58/0.83/2.50	1.60/2.77/3.60/0.85/2.60
	15	2.84/1.61/3.52/0.53/1.59	2.50/1.69/3.54/0.54/1.64	2.32/1.77/3.59/0.56/1.70	1.96/1.86/3.59/0.58/1.76	1.72/1.95/3.61/0.60/1.81
	20	2.96/3.44/3.53/1.13/3.41	2.68/3.62/3.56/1.18/3.53	2.50/3.80/3.60/1.21/3.64	2.20/3.98/3.62/1.25/3.75	1.81/4.17/3.63/1.29/3.88
HexOH	5	3.17/1.03/3.54/0.34/1.02	3.01/1.09/3.59/0.35/1.05	2.81/1.13/3.63/0.36/1.09	2.60/1.19/3.67/0.37/1.12	2.40/1.25/3.70/0.39/1.16
	10	3.09/−4.40/3.53/−1.45/−4.36	2.80/−4.62/3.57/−1.50/−4.50	2.47/−4.86/3.60/−1.55/−4.65	2.30/−5.09/3.63/−1.60/−4.80	2.44/−5.33/3.71/−1.69/−4.95
	15	3.15/2.97/3.54/9.81/2.94	2.89/3.12/3.58/1.01/3.04	2.60/3.27/3.61/1.04/3.14	2.39/3.43/3.64/1.08/3.24	1.95/3.60/3.65/1.11/3.34
	20	3.30/3.00/3.55/0.99/2.98	2.90/3.15/3.58/1.02/3.07	2.70/3.31/3.62/1.05/3.18	2.27/3.47/3.63/1.09/3.28	1.89/3.64/3.64/1.12/3.38
HeptOH	5	3.59/1.98/3.58/0.65/1.96	3.20/2.07/3.60/0.67/2.02	3.05/2.17/3.65/0.69/2.08	2.72/2.28/3.68/0.72/2.16	2.34/2.39/3.70/0.74/2.22
	10	3.23/0.29/3.54/0.09/0.29	2.95/0.31/3.59/0.01/0.30	2.73/0.32/3.62/0.01/0.31	2.55/0.34/3.66/0.10/0.32	2.31/0.36/3.69/0.11/0.33
	15	3.24/5.98/3.55/1.97/5.92	3.13/6.28/3.60/2.04/6.12	3.32/6.59/3.68/2.10/6.32	2.80/6.91/3.69/2.17/6.52	2.41/7.25/3.71/2.24/6.73
	20	3.54/0.55/3.73/0.18/0.54	3.31/0.58/3.61/0.18/0.56	3.04/0.60/3.65/0.19/0.58	2.82/0.63/3.69/0.20/0.60	2.59/0.67/3.72/0.20/0.62
OctOH	5	3.44/−0.80/3.56/−0.26/−0.80	3.16/−0.84/3.60/−0.27/−0.85	2.95/−0.89/3.64/−0.28/−0.85	2.68/−0.93/3.67/−0.29/−0.88	2.60/−0.98/3.73/−0.30/−0.90
	10	3.47/0.58/3.60/0.19/0.58	3.18/0.61/3.60/0.20/0.62	2.99/0.64/3.65/0.20/0.62	2.75/0.68/3.68/0.21/0.64	2.51/0.71/3.72/0.22/0.66
	15	3.60/−0.68/3.57/−0.22/−0.67	3.41/−0.71/3.62/−0.23/−0.72	3.09/−0.75/3.65/−0.24/−0.72	3.19/−0.78/3.72/−0.25/−0.74	2.92/−0.82/3.76/−0.26/−0.76

0.2 mol dm^{-3} Polysorbate-20 with 1:1 Polysorbate-20: *n*-alkanol (w/w) in *n*-heptane was used

η viscosity, ΔH^* Enthalpy change, ΔG^* free energy change, ΔS^* entropy change, ΔC_p heat capacity change

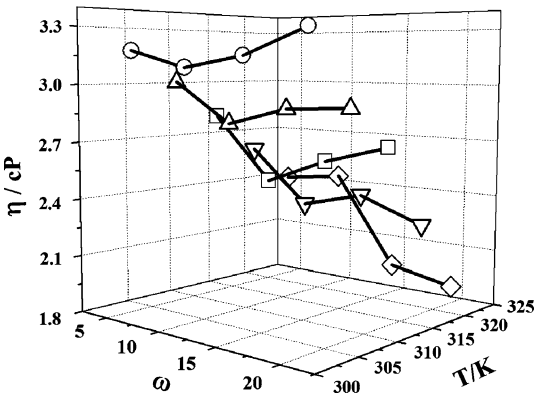

Fig. 9 Viscosity (η)—ω—T profile for the microemulsion comprising of water/(Polysorbate-20 + *n*-hexanol)/*n*-heptane. 0.2 mol dm^{-3} Polysorbate-20 with a 1:1 (w/w) ratio of *n*-hexanol was used

experiments. Based on these observations, the following conclusions can be made:

1. The clarity of w/o microemulsion system was reduced with the increase in cosurfactant chain length with an optimum efficacy given by *n*-hexanol.
2. While the surfactants reside at the oil–water interface, the cosurfactants were partitioned between the oil and oil–water interface.
3. The spontaneity of microemulsion formation increased with increasing cosurfactant chain length, increasing temperature and decreasing volume of the dispersed phase, water.
4. The formation of the microemulsion was found to be an enthalpy controlled process.
5. Larger numbers of droplets were formed at the expense of size. With the increase in temperature and ω values, size reduction was also evidenced by DLS measurements.
6. Depletion in the aggregation number of the surfactant per droplet was compensated by the cosurfactant molecules. However, the compensatory effect was not affected by temperature.
7. A symmetric variation in different physico-chemical properties was noted with the increase in the cosurfactant chain length. However, *n*-octanol, being oilier in nature than a cosurfactant, brought about a different behavior.

Acknowledgments The work was financially supported by the Department of Science and Technology, Government of India, through a research grant (Ref. No.- SR/S1/PC/24/2008, Dt.23/09/2008).

References

1. Moulay S, Hadj-Ziane AZ, Canselier JP (2007) Microemulsion breakdown by pervaporation technique: effect of the alkyl chain length of n-alkanol, a cosurfactant of the microemulsion. J Colloid Interface Sci 311:556–561
2. Moulik SP, Paul BK (1998) Structure, dynamics and transport properties of micro emulsions. Adv Colloid Interface Sci 78:99–195
3. Myakonkaya O, Eastoe J, Mutch KJ, Rogers S, Heenan R, Grillo I (2009) Control over microemulsions with solvent blends. Langmuir 25:2743–2748
4. Salager JL, Forgiarini A, Márquez L, Peña A, Pizzino A, Rodriguez MP, Rondón-González M (2004) Using emulsion inversion in industrial processes. Adv Colloid Interface Sci 108–109:259–272
5. Levinger NE, Swafford LA (2009) Ultrafast dynamics in reverse micelles. Annual Rev Phys Chem 60:385–406
6. Grampurohit N, Ravikumar P, Mallya R (2011) Microemulsions for topical use—a review. Indian J Pharm Educ Res 45:100–107
7. Uskokovi V, Drofenik M (2007) Reverse micelles: inert nanoreactors or physico-chemically active guides of the capped reactions. Adv Coll Int Sci 133:23–34
8. Shakeel F, Ramadan W, Faisal MS, Rizwan M, Faiyazuddin M, Mustafa G, Shafiq S (2010) Transdermal and topical delivery of anti-inflammatory agents using nanoemulsion/microemulsion: an updated review. Curr Nanosci 6:184–198
9. Capek I (1999) Microemulsion polymerization of styrene in the presence of anionic emulsifier. Adv Colloid Interface Sci 82:253–273
10. Förster T, Von Rybinski W, Wadle A (1995) Influence of microemulsion phases on the preparation of fine-disperse emulsions. Adv Colloid Interface Sci 58:119–149
11. Capek I (2004) Preparation of metal nanoparticles in water-in-oil (w/o) microemulsions. Adv Colloid Interface Sci 110:49–74
12. Chen Q, Shen X, Gao H (2010) Radiolytic syntheses of nanoparticles in supramolecular assemblies. Adv Colloid Interface Sci 159:32–44
13. Spernath A, Aserin A (2006) Microemulsions as carriers for drugs and nutraceuticals. Adv Colloid Interface Sci 128–130: 47–64
14. Eastoe J, Hollamby MJ, Hudson L (2006) Recent advances in nanoparticle synthesis with reversed micelles. Adv Colloid Interface Sci 128–130:5–15
15. Paria S (2008) Surfactant-enhanced remediation of organic contaminated soil and water. Adv Colloid Interface Sci 138:24–58
16. Yaghmur A, Glatter O (2009) Characterization and potential applications of nanostructured aqueous dispersions. Adv Colloid Interface Sci 147–148:333–342
17. Kreilgaard M (2002) Influence of microemulsions on cutaneous drug delivery. Adv Drug Delivery Rev 54:S77–S98
18. Talegaonkar S, Azeem A, Ahmad F, Khar R, Pathan S, Khan Z (2008) Microemulsions: a novel approach to enhanced drug delivery. Recent Pat Drug Deliv Formul 2:238–257
19. Li H, Zhao J, Ruckenstein E (2000) The preparation and characterization of amphiphilic core/shell particles. Colloids Surf A 161:489–498
20. Li XW, Zhang J, Zheng LQ, Chen B, Wu LZ, Lv FF, Dong B, Tung CH (2009) Microemulsions of N-alkylimidazolium ionic liquid and their performance as microreactors for the photocycloaddition of 9-substituted anthracenes. Langmuir 25:5484–5490
21. Wang F, Fang B, Zhang Z, Zhang S, Chen Y (2008) The effect of alkanol chain on the interfacial composition and thermodynamic properties of diesel oil microemulsion. Fuel 87:2517–2522
22. Otto DP, Vosloo HCM, Liebenberg W, de Villiers MM (2008) Effects of the cosurfactant 1-butanol and feed composition on nanoparticle properties produced by microemulsion copolymerization of styrene and methyl methacrylate. J Appl Polym Sci 107:3950–3962

23. Hathout RM, Woodman TJ, Mansour S, Mortada ND, Geneidi AS, Guy RH (2010) Microemulsion formulations for the transdermal delivery of testosterone. Eur J Pharm Sci 40:188–196
24. Bufe M, Wolff T (2009) Reversible switching of electrical conductivity in an AOT/isooctane/water microemulsion via photoisomerization of azobenzene. Langmuir 25:7927–7931
25. Lopez F, Cinelli G, Ambrosone L, Colafemmina G, Ceglie A, Palazzo G (2004) Role of the cosurfactant in water-in-oil microemulsion: interfacial properties tune the enzymatic activity of lipase. Colloids Surf A 237:49–59
26. Schulman JH, Stoeckenius W, Prince LM (1959) Mechanism of formation and structure of microemulsions by electron microscopy. J Phys Chem 63:1677–1680
27. Friberg SE (1987) Microemulsions: structure and dynamics. CRC, Boca Raton, Florida
28. Li X, He G, Zheng W, Xiao G (2010) Study on conductivity property and microstructure of TritonX-100/alkanol/n-heptane/water microemulsion. Colloids Surf A 360:150–158
29. De M, Bhattacharya SC, Panda AK, Moulik SP (2009) Physicochemistry of mixed systems of water/AOT (surfactant)/alkanol (cosurfactant)/cycloalkanone (oil): a detailed study of phase behavior, salt effect, and conductance properties. J Dispers Sci Technol 30:277–288
30. De M, Bhattacharya S, Moulik S, Panda A (2010) Interfacial composition, structural and thermodynamic parameters of water/(surfactant + n-butanol)/n-heptane water-in-oil microemulsion formation in relation to the surfactant chain length. J Surfact Deterg 13:475–484
31. De M, Bhattacharya SC, Panda AK, Moulik SP (2009) Interfacial behavior, structure, and thermodynamics of water in oil microemulsion formation in relation to the variation of surfactant head group and cosurfactant. J Dispers Sci Technol 30:1262–1272
32. Moulik SP, Aylward WM, Palepu R (2001) Phase behaviours and conductivity study of water/CPC/alkan-1-ol (C4 and C5)/1-hexane water/oil microemulsions with reference to their structure and related thermodynamics. Canadian J Chem 79:1–12
33. Moulik SP, Digout LG, Aylward WM, Palepu R (2000) Studies on the interfacial composition and thermodynamic properties of W/O microemulsions. Langmuir 16:3101–3106
34. Digout L, Bren K, Palepu R, Moulik SP (2001) Interfacial composition, structural parameters and thermodynamic properties of water-in-oil microemulsions. Colloid Polym Sci 279:655–663
35. Sarma S, Bora M, Dutta RK (2005) Effects of alcohol on partition equilibrium of phenol red in micellar solutions and o/w microemulsions of anionic surfactants. Colloids Surf A 256:105–110
36. Savelli MP, Solans C, Pons R, Clausse M, Erra P (1996) Keratin cystine reactivity in microemulsion media: influence of cosurfactant chain length. Colloids Surf A 119:155–162
37. Bayrak Y (2004) Interfacial composition and formation of w/o microemulsion with different amphiphiles and oils. Colloids Surf A 247:99–103
38. Plucinski P, Reitmeir J (1995) The influence of cosurfactants on the solubilization of phenylalanine in water-in-oil microemulsion. Colloids Surf A 97:157–167
39. Gao Y, Li N, Hilfert L, Zhang S, Zheng L, Yu L (2009) Temperature-induced microstructural changes in ionic liquid-based microemulsions. Langmuir 25:1360–1365
40. Acharya A, Moulik SP, Sanyal SK, Mishra BK, Puri PM (2002) Physicochemical investigations of microemulsification of coconut oil and water using polyoxyethylene 2-cetyl ether (Brij 52) and isopropanol or ethanol. J Colloid Interface Sci 245: 163–170
41. Acharya A, Sanyal SK, Moulik SP (2001) Physicochemical investigations on microemulsification of eucalyptol and water in presence of polyoxyethylene (4) lauryl ether (Brij-30) and ethanol. Int J Pharm 229:213–226
42. Adhikari A, Das DK, Sasmal DK, Bhattacharyya K (2009) Ultrafast FRET in a room temperature ionic liquid microemulsion: a femtosecond excitation wavelength dependence study. J Phys Chem A 113:3737–3743
43. Adhikari A, Sahu K, Dey S, Ghosh S, Mandal U, Bhattacharyya K (2007) Femtosecond solvation dynamics in a neat ionic liquid and ionic liquid microemulsion: excitation wavelength dependence. J Phys Chem B 111:12809–12816
44. Ghosh S, Dey S, Adhikari A, Mandal U, Bhattacharyya K (2007) Ultrafast fluorescence resonance energy transfer in the micelle and the gel phase of a PEO-PPO-PEO triblock copolymer: excitation wavelength dependence. J Phys Chem B 111:7085–7091
45. Panda AK, Bhowmik BB, Das AR, Moulik SP (2001) Dispersed molecular aggregates—3. Synthesis and characterization of colloidal lead chromate in water/sodium bis(2-ethylhexyl) sulfosuccinate/n-heptane water-in-oil microemulsion medium. Langmuir 17:1811–1816
46. Panda AK, Moulik SP, Bhowmik BB, Das AR (2001) Dispersed molecular aggregates: II. Synthesis and characterization of nanoparticles of tungstic acid in H2O/(TX-100 + alkanol)/n-heptane w/o microemulsion media. J Colloid Interface Sci 235:218–226
47. De TK, Maitra A (1995) Solution behavior of aerosol OT in nonpolar solvents. Adv Colloid Interface Sci 59:95–193
48. Ninham BW, Chen SJ, Evans DF (1984) Role of oils and other factors in microemulsion design. J Phyl Chem 88:5855–5857
49. Moulik SP, De GC, Bhowmik BB, Panda AK (1999) Physicochemical studies on microemulsions. 6. Phase behavior, dynamics of percolation, and energetics of droplet clustering in water/AOT/n-heptane system influenced by additives (sodium cholate and sodium salicylate). J Phys Chem B 103:7122–7129
50. Hait SK, Moulik SP (2002) Interfacial composition and thermodynamics of formation of water/isopropyl myristate water-in-oil microemulsions stabilized by butan-1-ol and surfactants like cetyl pyridinium chloride, cetyl trimethyl ammonium bromide, and sodium dodecyl sulfate. Langmuir 18:6736–6744
51. Tanford C (1972) Micelle shape and size. J Phys Chem 76:3020–3024
52. Acharya A, Sanyal SK, Moulik SP (2001) Formation and characterization of a pharmaceutically useful microemulsion derived from isopropyl myristate, polyoxyethylene (4) lauryl ether (Brij-30), isopropyl alcohol and water. Curr Sci 81:362–370
53. Acharya A, Sanyal SK, Moulik SP (2001) Formation and characterization of a useful biological microemulsion system using mixed oil (Rice bran and Isopropyl Myristate), polyoxyethylene (2) oleyl ether (Brij 92), isopropyl alcohol, and water. J Dispers Sci Technol 22:551–561
54. Attwood D, Mallon C, Ktistis G, Taylor CJ (1992) A study on factors influencing the droplet size in nonionic oil-in-water microemulsions. Int J Pharm 88:417–422
55. Attwood D, Patel HK (1989) Mixed micelles of alkyltrimethylammonium bromides and chlorhexidine digluconate in aqueous solution. J Colloid Interface Sci 129:222–230

Author Biographies

Sujoy Paul obtained his M.Sc. degree in Chemistry in 2007 from Tripura University, India. He is carrying out research at North Bengal University on different physicochemical properties of ionic liquids.

Amiya Kumar Panda obtained his M.Sc. and Ph. D. degrees in Chemistry from Tripura University, Agartala, Tripura, India. He is currently an associate professor in chemistry at the University of North Bengal. His research interests are in the fields of polymer and surface science, nanomaterials and membrane mimetic systems. He has so far published 50 papers in different journals.

RSC Advances

RSCPublishing

ARTICLE

Combined Phase Behavior, Dynamic Light Scattering, Viscosity and Spectroscopic Investigations on Pyridinium Based Ionic Liquid-in-Oil Microemulsion

Cite this: DOI: 10.1039/x0xx00000x

Received 00th January 2012,
Accepted 00th January 2012

DOI: 10.1039/x0xx00000x

www.rsc.org/

Sujoy Paul and Amiya Kumar Panda*

Although several studies on imidazolium based ionic liquid-in-oil microemulsion are available in literature, however, studies on pyridinum based ionic liquid microemulsion are uncommon. Pyridinium based ionic liquids have superior yet unexplored properties when considered in the polar domain of microemulsion. *1*-butyl-*4*-methyl pyridinium tetrafluoroborate ($[b_4mpy][BF_4]$) / (Tween 20 + n-pentanol) / n-heptane ionic liquid-in-oil microemulsion system has been studied by combined phase behavior, dynamic light scattering, viscosity and spectroscopic probing techniques. With decreasing Tween 20/n-pentanol (S/CS) ratio, turbidity increased, although it was not possible to achieve stable microemulsion without the cosurfactant. Dynamic light scattering and viscosity studies revealed that the size of the μE droplets increased with increasing volume fraction (φ_d) of ionic liquid. Both the size and viscosity increased with φ_d. With the increasing amount of n-pentanol, the variation became less sensitive due to the better stabilizing effect induced by the alkanol. Increase in size of the microemulsion droplets was overshadowed by the increase in the fluidity of the medium, for which viscosity decreased with increasing temperature, as common for Newtonian fluids. State of the ionic liquid in the microemulsion was monitored by absorption and fluorescence spectroscopy without and with curcumin as the molecular probe respectively. While a continuous increase in polarity of the IL domain occurred with increasing amount of IL, the fluorescence anisotropy results revealed that the rigidity of the domain passed through maxima for all S/CS combinations.

1. Introduction

Because of the multifaceted applications, *viz.*, drug delivery, nanoparticle synthesis, media for organic reaction, biochemical reaction, separation, cosmetics[1], *etc.*, studies on microemulsion (μE) have gained significant importance. A microemulsion (μE) can be defined as an optically transparent, thermodynamically stable dispersion of one liquid in otherwise immiscible second liquid, stabilized by a surfactant[2]. Sometimes, short chain alkanols and amines can assist μE formation[2]. It has been reported that ionic liquid (IL) can substitute the polar component (water) in a μE[3]. Scientific studies involving ILs have reached its credential beyond any doubt for which there has been an exponential growth in the research publication involving ILs. By definition ILs, with melting points below 100^0C, are considered as neoteric component for its specific properties, *viz.*, non-flammability, non-corrosiveness, high ionic conductivity and inertness towards different thermal and chemical environment[4]. One of the outstanding properties of ILs lies in its use as an alternative to traditional organic solvents. ILs are also called "designer solvents" because its properties can be tuned by altering the substituent as well as the counter ions[5]. In spite of significant research contribution on ILs, the lack of complete knowledge is considered to be one of the barriers in utilizing them for practical applications. Thus more fundamental researches on ILs are warranted.

It is needless to mention that μE comprising ILs in the polar domain can have some unknown but some novel properties owing to the unique and combined features of the ILs and μEs. Thus, this domain of research has been gaining significance day by day. Ionic liquid microemulsions find application in various fields, *viz.*, preparation and characterization of polymeric nanoparticles[6], synthesis of inorganic nanoparticles[7], renewable lubricants[8], and catalysis[9], *etc*.

Although most of the studies on ILs are associated with the imidazolium ion, however, there has been a current trend to search for alternate, easily available but low cost ILs other than the imidazolium ion. According Domanska et al.[10], pyridinium based ILs have specific properties, *viz.*, broad liquidous temperature range, inertness to air, moisture and superior solubilization capacity. These unique features of pyridinium based ILs have already been explored with special reference to antistatic thermoplastic resin[11], adhesive film[12], electrochemical probe[13], electron transfer process[14], reaction acceleration[15], organo catalysis[16], extraction process[17], *etc*. In spite of high possible potentials, there have been a little research on *1*-butyl-*4*-methylpyridinium tetrafluoroborate ($[b_4mpy][BF_4]$) comprising μE although it is one of the most reported pyridinium based IL[18]. In a very recent report of Takumi et al.[19], mutual miscibility of imidazolium and pyridinium ILs with $[BF_4]^-$ as the common counter anion have been explored. Another advantage of using this IL is that the system itself can be investigated without any molecular probe (because of the presence of the pyridinium ring) in the UV-visible region.

Curcumin is a natural polyphenolic compound isolated from the rhizome of turmeric (*Curcuma longa*). Researches over the last few decades have shown that curcumin possesses a great variety of beneficial biological and pharmacological activities such as anticancer, antioxidant, anti-arthritic, and anti-inflammatory agents[20]. Despite its highly promising features as a health-promoting agent, poor aqueous solubility in neutral aqueous medium of curcumin[21] is one of the major draw backs in its bioavailability, clinical efficiency and metabolism[22]. A number of attempts have been made to increase the solubility in polar medium and hence the bioavailability of curcumin through encapsulation in surfactant micelles[23,24], lipids[25], cyclodextrin[26], hydrogel[27], liposomes[28], polymeric micelles[29], nanoparticles[30], *etc*. Curcumin is also soluble in other polar solvents, so there is a huge scope of its bioavailability if it can be entrapped in μE with a polar phase. Once used in the IL-in-oil microemulsion, curcumin may have a possibility to reside in the inner polar core of the μE because curcumin is not soluble in n-heptane. Thus the spectroscopic investigation involving curcumin in the microemulsion will be able to probe the microenvironment of the polar domain

In the present manuscript, comprehensive studies on the IL-in-oil type microemulsion comprising *1*-butyl-*4*-methylpyridinium tetrafluoroborate have been reported. It is expected that studies on such type of μE comprising $[b_4mpy][BF_4]$, Tween 20 (a nonionic surfactant, S), n-pentanol (a cosurfactant, CS) and n-heptane (oil) will generate significant information in terms of its practical application as well as the view point of fundamental understanding. The effect of Tween 20(surfactant)/n-pentanol (cosurfactant) ratio, volume fraction of IL and temperature have been studied using a number of techniques, *viz.*, phase manifestation, dynamic light scattering, viscosity, UV-visible absorption and emission spectroscopy. The detailed phase diagram studies helped in identifying the clear and turbid region. Dynamic light scattering studies provided the information about the size and its distribution at different temperature; viscosity measurements were carried out and correlated with the DLS data. μE with and without curcumin in the polar domain were investigated by UV-visible absorption

spectroscopy. Fluorescence spectroscopic studies on curcumin in the polar domain helped in understanding the state of polarity and rigidity of the microenvironment.

2. Experimental section

2.1. Materials. The IL *1*-butyl-*4*-methyl pyridinium tetrafluoroborate, [$b_4$mpy][BF_4] was purchased from Sigma-Aldrich Chemicals Pvt. Ltd., USA. The nonionic surfactant polyoxyethylene sorbitan monolaurate (Tween 20) and the cosurfactant n-pentanol were products from Fluka, Switzerland and Lancaster, England respectively. They were stated to be more than 99.5% pure. n-heptane was obtained from E. Merck, Germany. Curcumin, [*1,7*-bis(*4*-hydroxy-*3*-methoxy-phenyl)-*1*,*6*-heptadiene-*3*,*5*-dione] was a product from Sigma-Aldrich Chemicals Pvt. Ltd., USA. All the chemicals were used as received.

2.2. Methods

2.2.1. Phase Manifestation. In the entire work, three different ratio of Tween 20 and n-pentanol (S:CS, w/w) were used (1:0.5, 1:1 and 1:2) to explore the effect the different amount of cosurfactant in the µE system. The pseudo ternary phase diagram comprising [$b_4$mim][BF_4]/(Tween-20+n-pentanol)/n-heptane was constructed by the method of titration and through visual inspection. Known amount of Tween 20 + n-pentanol and n-heptane or IL were taken in stoppered test tube. IL or n-heptane was then progressively added using a Hamilton (USA) micro syringe under constant stirring[31,32]. The whole process was carried out in a controlled temperature bath (298±0.1K). The phase boundary was detected through the appearance of turbidity. The same experiment was carried out for a number of compositions by varying the amount of oil or IL as well as in different S/CS ratio.

2.2.2. Dynamic Light Scattering (DLS) Studies. DLS measurements were carried out using a Zetasizer Nano ZS90 (ZEN3690, Malvern Instruments Ltd, U.K.). A 0.2M Tween 20 mixed with n-pentanol in n-heptane was used for such studies. Tween 20 / n-pentanol ratio (w/w) were the same as in phase manifestation studies. A He-Ne laser of 632.8 nm wavelength was used and the data were collected at 90^0 angle. Temperature was controlled by inbuilt Peltier heating-cooling device with an accuracy of ±0.05K. The instrument actually measures the diffusion coefficient (D) from which the diameter of the microemulsion droplet (d) was determined according to Stokes-Einstein's formalism[31, 32]:

$$D = \frac{kT}{3\pi\eta d} \quad (1)$$

where, k, T and η indicate the Boltzmann constant, temperature and viscosity respectively.

2.2.3. Viscosity Measurement. Viscosity of µE systems were measured with an LVDV-II+PCP cone and plate type roto-viscometer (Brookfield Eng. Lab, USA). The same set of solution, as used in the DLS measurements, were employed for size analyses. Temperature was controlled by a cryogenic circulatory water bath with a precision of ±0.1K (DC-1006 M/S. Hahntech Corporation, S. Korea). Shear rate (D) was varied in the range 20 – 60 sec^{-1} with an increment of 5.0 sec^{-1} in each step. Zero shear viscosity (η) was obtained using the relation η= τ / D [31,32], where τ indicates the shear stress.

2.2.4. Spectral Studies.

2.2.4.1. Absorption Spectra. UV-visible absorption spectra of the µE systems in the absence and presence of curcumin were recorded on a UVD-2950 spectrophotometer (Labomed Inc., USA) in the range 200-400nm using a matched pair cell of 1.0cm path length. While recording the spectra of the IL comprising systems, corresponding surfactant solution without IL was used as reference. Corresponding IL-in-oil µE without the dye curcumin was used as reference for recording the spectra of curcumin comprising systems. The overall concentration of curcumin was always kept constant at 10 µM. Initially, required amount of curcumin in methanol-chloroform (1:3 v/v) was taken in a test tube. The solvent was evaporated under vacuum. µE of known composition was then added and homogenized by keeping the solution in an ultrasonic water bath. It is to be mentioned that curcumin is insoluble in n-heptane. Therefore it could be assumed that the dye molecules reside in the polar domain.

2.2.4.2. Emission Spectra. Steady state fluorescence spectroscopic measurements were carried out using a bench-top spectrofluorimeter (Quantamaster-40, Photon Technology International Inc, NJ, USA). The steady state emission spectra was recorded in the range 400-650nm with an excitation of curcumin at 426nm.

To know about the microviscosity of the solvent surrounding the probe molecule, steady state anisotropy (r) values were determined using the following expressions[33]:

$$r = (I_{VV} - GI_{VH}) / (I_{VV} + 2GI_{VH}) \quad (2)$$

and,

$$G = I_{HV}/I_{HH} \quad (3)$$

where, I_{VV}, I_{VH} are the intensities obtained with the excitation polarizer oriented vertically and the emission polarizer oriented vertically and horizontally respectively; I_{HV} and I_{HH} refer to the similar parameters as above for the

horizontal positions of the excitation polarizer. In case of anisotropy measurements, the fluorescence data were collected at an emission wavelength (λ_{em}) of 550 nm. Further details are available in literature[33]. Both the absorption and fluorescence spectra were recorded at ambient but controlled temperature.

3. Results and discussions

3.1. Phase Manifestation. From the application point of view, construction of the phase diagram is a primary task towards a μE formulation. Figure 1 describes the pseudo ternary phase diagram of [$b_4$mpy][BF_4]/(Tween-20+n-pentanol)/n-heptane systems

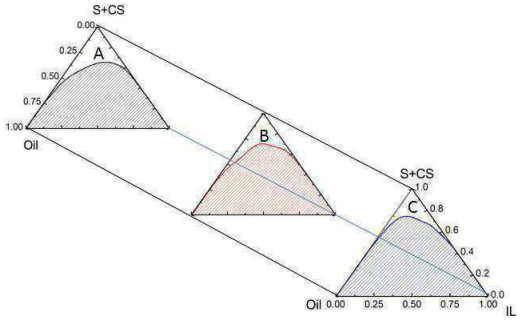

Figure 1. Pseudo ternary phase diagram of [$b_4$mpy][BF_4]/(Tween-20+n-pentanol)/n-heptane at different Tween 20 (S) / n-pentanol (CS) ratio (w/w): A, 1:0.5; B, 1:1 and C, 1:2. n-heptane was used as oil (Oil) and [$b_4$mpy][BF_4] was used as the ionic liquid (IL). Temp. 298 K.

at different surfactant-cosurfactant ratio (w/w). For simplicity, only the clear single phase (1Φ, un-shaded portion) and the two phase (2 Φ, shaded portions) regions were identified. Area under the clear and turbid regions were evaluated by the method of weighing the individual areas as previously described[31]. The area under clear zone decreased with increasing amount of cosurfactant. It appeared from the results (as explained through Figure S1, supplementary section) that the area under the clear zone was maximum in the absence of cosurfactant as the % area of clear zone followed a 2^0 polynomial relation with the weight% of n-pentanol (w_{cs}):

$$\%\ \text{area of clear zone} = 20.34 - 8.46 \times w_{CS}\ \% + 1.61 \times (w_{CS}\ \%)^2 \quad (4)$$

It means that in the absence of n-pentanol, % area under clear and turbid zones would be 20% and 80% respectively. However, it was impossible to obtain a stable μE without the aid of cosurfactant. Hence, unlike the other systems[3, 34], use of cosurfactant was mandatory in order to achieve a stable μE. Use of cosurfactant for single tailed surfactants is not uncommon in literature[31, 32]. It is known that cosurfactant can assist the surfactant molecules in a reducing interfacial tension between two immiscible liquids. Present set of results were also comparable with the similar components where water[31] and another ionic liquid *1*-butyl-*3*-methyl imidazolium methanesulphonate [bmim][MS][32] were used. Compared to the other systems, the %area under clear zone was less which could be due to the greater iconicity of the components in the polar domain, compared to water as well as [bmim][MS]. Although the cation [b4mpy]$^+$ was less polar, however, the BF_4^- ion played a significant role in enhancing the turbidity of the present μE.

3.2. Dynamic Light Scattering (DLS) and Viscosity Studies. DLS studies on μE can provide information on its size, its distribution, and hence the polydispersity index. Variation in the diameter of [$b_4$mpy][BF_4]/(Tween 20+n-pentanol)/n-heptane IL-in-oil μE with the volume fraction of the IL (φ_d) at 308 K have been graphically presented in Figure 2 at different surfactant cosurfactant ratio (panel A).

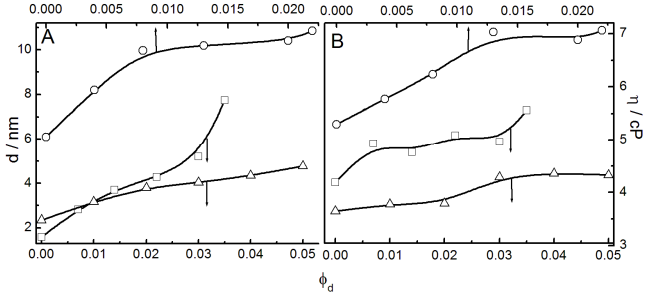

Figure 2. Variation in diameter (d) and viscosity (η) of [$b_4$mpy][BF_4]/(Tween-20+n-pentanol)/n-heptane IL-in-oil microemulsion system with the volume fraction (φ_d) of [$b_4$mpy][BF_4]. Temp. 308 K. Tween 20/ n-pentanol ratio (w/w): O, 1:0.5; □, 1:1 and Δ, 1:2.

Droplets were fairly monodispersed as revealed through its size distribution shown in Figure S2 (supplementary section). As under similar condition, there is a correlation between the size of droplets and viscosity, hence the viscosity (η) – φ_d profile for the similar systems were also presented in the same figure (panel B). Experiments were carried out in the temperature range 293 – 323K and the results at 308K (intermediate temperature) have been shown as representative. Results for the other systems have been presented in the supplementary section. Size of the μE droplets increased with increasing volume fraction (φ_d) of IL. Increase in size with the increasing volume of the dispersed phase is not an uncommon phenomena and have also been observed by others[3,32,34-36]. Size - φ_d profiles were found to be dependent on the S/CS ratio. Size of the μE

droplet comprising Tween 20 and n-pentanol in a mass ratio of 1:0.5 was found to be larger than 1:1 which was even larger than 1:2. Results clearly indicate that cosurfactants caused size constriction. In a previous report we have shown that for the polyoxyethylene head group comprising surfactants (Tween 20), increased amount of cosurfactant can lead to the formation of larger number of droplets[31,32]. For a fixed amount of surfactants, increasing number of droplets would result only if the size is decreased. Such an observation further supports the decrease in the area under clear region with increasing amount of cosurfactant. While giving a closer look at the panel A of Figure 2 it was observed that for an S / CS ratio of 1:0.5, size of the μE droplet increased linearly up to φ_d=0. 01, after which a change in the slope of increment profile appeared. The results imply that the existence of free/unbound ILs was possible only after φ_d=0. 01. Before the saud volume fraction of IL, it is mainly used up in coordinating with the polyoxyethylene head groups of Tween 20[32]. Almost twice the volume of IL was required for the attainment in the breakpoint in the μE with S/CS ratio 1:1 (φ_d=0.02). However, for such systems the slope after the threshold was higher. Such an ambiguity is beyond explanation with the present level of knowledge. Further studies are warranted to address this issue. d *vs.* φ_d profile for the systems with surfactant/cosurfactant ratio 1:2 was almost linear. d-φ_d profile for all the systems at different temperature have been graphically presented in Figure S3 (supplementary section). It could be concluded from the results that with the increasing amount of cosurfactant (n-pentanol), size increment with the volume fraction becomes less sensitive. The viscosity profile for the similar systems followed the same trend line as in the variation of droplet size with φ_d. Thus, it could be concluded that variations in the viscosity with φ_d was a consequence of the size variation in the microemulsion droplets. In order to understand the effect of temperature, size measurements were also carried out at different temperatures (293, 298, 303, 308, 313, 318 and 323K). While considering the size variation (as shown in Figure 3 panel A), it was observed that for all the systems d *vs.* temperature profiles were almost linear. The parallel nature of the lines imply that the effect of temperature was independent of S/CS ratio. Although there occurred size increment with increasing temperature, however, reverse trends were recorded for the viscosity for all the systems. Results for viscosity-temperature profile for the three combinations at φ_d= 0.02 have been shown in Figure 3 (panel B). Decrease in viscosity with increase in temperature is a common phenomenon for Newtonian fluids. In the present set of studies, increase in droplet size was overshadowed by the increase in the fluidity of the medium.

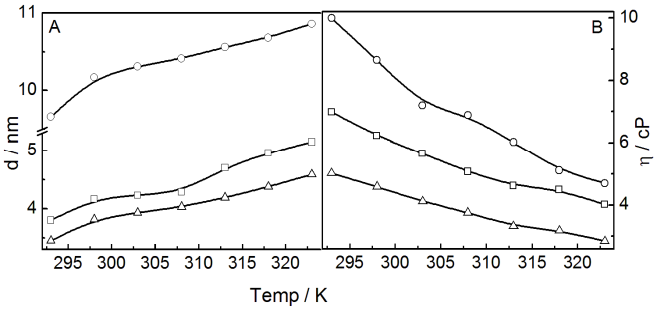

Figure 3. Variation in the size (A) and viscosity (B) with temperature for [$b_4$mpy][BF_4]/(Tween-20+n-pentanol)/n-heptane IL-in-oil microemulsion at different Tween 20/n-pentanol ratio (S/CS, w/w): O, 1:0.5; □, 1:1 and Δ, 1:2. 0.2 M Tween20 was used in each case where the volume fraction (φ_d) of IL was kept constant at 0.02.

For all the three systems, viscosity decreased almost linearly with increasing temperature, although the slopes were different for the different systems. Differences in the slopes were due to the differences in the rigidity of the μE droplets. Systems with larger amount of cosurfactant are expected to form more rigid structures. By suitably analyzing the viscosity data, thermodynamic parameters, *viz.*, changes in specific heat capacity (ΔCp), activation enthalpy (ΔH*), free energy (ΔG*) and entropy (ΔS*) were evaluated. The activation enthalpy for the viscous flow and the associated entropy change could be expressed by the following equations [37]:

$$\eta = \left(\frac{hN}{V}\right) e^{\Delta H^*/RT} e^{-\Delta S^*/RT} \quad (5)$$

The logarithmic form of equation 1 could be expressed as:

$$\ln\eta = \left\{\ln\left(\frac{hN}{V}\right) - \frac{\Delta S^*}{R}\right\} + \frac{\Delta H^*}{RT} \quad (6)$$

h, N, V are Plank's constant, Avogadro's constant and molar volume respectively. R and T have their usual significances. From equation (2), one can obtain ΔH^* values from the slope of *ln* η vs T^{-1} plot. *ln* η was found to vary with T^{-1} in a binomial way; hence one can derive ΔH^* from it's differential with respect to temperature in the following way:

$$ln\eta = a + bT + cT^2 \quad (7)$$

Therefore,

$$\frac{dln}{dT} = -\frac{\Delta H^*}{RT^2} = b + 2cT \quad (8)$$

Thus, knowing the value of 'b' and 'c' one can compute ΔH^* at different temperatures. Change in heat capacity (ΔC_p) is related to ΔH^* as:

$$\Delta C_p = \frac{d(\Delta H^*)}{dT} = -2RT(b + 3cT) \quad (9)$$

Therefore, changes in Gibb's free energy for activation could be expressed as:

$$\Delta G^* = -RT \ln \frac{V}{hN} \quad (10)$$

Once ΔH^* and ΔG^* are known, the ΔS^* value could be calculated easily according to the following expression:

$$\Delta S^* = \frac{\Delta H^* - \Delta G^*}{T} \quad (11)$$

Some of the representative results are summarized in Table 1. While considering the changes in the standard enthalpy (ΔH^*), it was observed that for all the systems ΔH^* decreased with increase in the volume fraction (φ_d) of the dispersed phase. For the systems comprising surfactant and cosurfactant in a ratio of 1:0.5 and 1:1 (w/w), the ΔH^* values were mostly negative, which mean that the process of flow was exothermic in nature [37, 38]. On the other hand ΔH^* for the system with surfactant cosurfactant ratio 1:2 (w/w) the values were mostly positive, the difference in rigidity and subsequent viscosity attributed to such variation. While considering the variation in the ΔC_p with volume fraction, it was observed that the ΔC_p attained more negativity with increase in volume fraction. As with the increase in size droplets become less rigid, hence ΔC_p becomes more negative. The negative value of ΔS^* indicates the non-spontaneity of the flow processes. Viscosity variation for all the systems at different volume fractions and temperature have also been graphically presented in Figure S4 (supplementary section).

3.3. Spectral Studies. Spectroscopic investigation on µE using a suitable probe can provide information on the environment, *viz.*, polarity, fluidity, extent of aggregation of the ionic liquid in µE. Substantial reports on such aspects are available in the literature[3,32,35,36]. For the present system as the ionic liquid itself exhibits UV-visible absorption band due to the presence of pyridinium ring, the µE was studied without any probe. Figure 4 describes the absorption spectra of [b4mpy][BF_4] confined in the polar domain at different volume fraction. Two distinct peaks, one at 280nm and another at 335 nm were recorded for the ionic liquid. The peak at 280nm was significantly more intense than the other. Intensity of both the bands increased with the increasing volume fraction (φ_d) of ionic liquid. Absorbance *vs.* φ_d profile for both the peaks have been graphically shown in the inset of Figure 4. An increment in the absorbance values were mostly linear except for the system with Tween 20/n-pentanol in a ratio of 1:0.5 (w/w). The results indicate that distinct structured aggregates were not formed at this composition. The combined phase manifestation, dynamic light scattering and viscosity data also supported such an analogy.

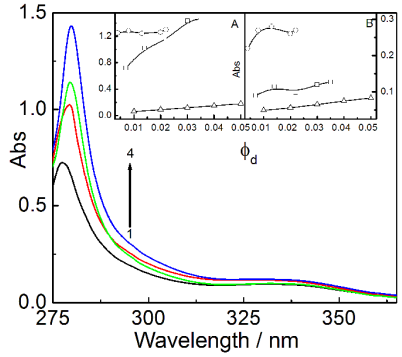

Figure 4. Absorption spectra of 1-butyl 4-methyl pyridinium tetrafluoroborate [$b_4$mpy][BF_4] confined in the polar domain at different volume fraction (φ_d): 1, 0.007; 2, 0.014; 3, 0.022 and 4, 0.03. System without the IL was used as reference. Inset: Variation in the absorbance at 283 nm (A) and 335 nm (B) with φ_d.

Effect of IL was different for different Tween 20/ n-pentanol combinations; hence in order to understand the state of the IL, curcumin was used as the fluorescent probe. Fluorescence spectra of curcumin confined in the polar domain of ionic liquid-in-oil microemulsion are shown in Figure 5.

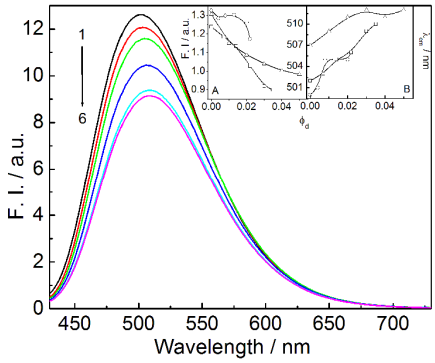

Figure 5. Emission spectra of 10 µM curcumin in [$b_4$mpy][BF_4]/(Tween-20+n-pentanol)/n-heptane IL-in-oil microemulsion at different volume fraction (φ_d) of IL. φ_d values: 1, 0.00; 2, 0.007; 3, 0.014; 4, 0.022; 5, 0.03 and 6, 0.035. Tween 20/n-pentanol ratio (w/w): l:1. Inset: Variation in the fluorescence intensity (panel A) and λ_{em} (panel B) with φ_d for different Tween 20/n-pentanol ratio (w/w): O, l:0.5; □, 1:1 and Δ, 1:2.

Table 1. Representative viscosity derived energetic parameters for $[b_4mpy][BF_4]$/(Tween-20+n-pentanol)/n-heptane IL-in-oil microemulsion system.

Tween 20 / n-pentanol	φ_d	ΔH^*(kJ mol^{-1})/ΔC_P (kJ mol^{-1}) / $-\Delta G^*$(kJ mol^{-1})/ ΔS^*(J $k^{-1}mol^{-1}$) at different temperature (in K)						
		293	298	303	308	313	318	323
1:0.5	0.000	-1.18/-0.95/-0.14/-3.55	-1.24/-0.99/-0.15/-4.27	-1.02/-0.17/-1.3/-1.54	-1.36/1.05/-0.19/-3.28	-1.09/-0.19/-1.43/-4.61	-1.12/-0.20/-1.50/-5.43	-1.16/-0.25/-1.58/-3.55
	0.004	-1.52/-1.20/-0.27/-3.66	-1.60/-1.25/-0.27/-4.46	-1.29/-0.27/-1.68/-1.64	-1.33/-0.27/-1.76/-3.52	-1.37/-0.27/-1.85/-4.97	-1.42/-0.27/-1.94/-5.81	-1.46/-0.28/-2.04/-3.66
	0.013	-1.56/-2.67/-0.60/-3.80	-1.65/-2.76/-0.60/-4.83	-2.85/-0.61/-1.73/-1.92	-2.95/-0.62/-1.82/-3.90	-3.04/-0.62/-1.91/-5.58	-3.14/-0.63/-2.00/-6.59	-3.24/-0.64/-2.10/-3.80
	0.022	-3.18/-3.25/-1.59/-4.09	-3.34/-3.37/-1.61/-5.25	-3.48/-1.64/-3.51/-2.17	-3.60/-1.66/-3.69/-4.31	-3.71/-1.68/-3.87/-6.26	-3.83/-1.71/-4.06/-7.39	-3.95/-1.74/-4.26/-4.09
1:1	0.000	-0.57/-0.50/-0.03/-1.84	-0.52/-0.06/-0.60/-1.81	-0.54/-0.08/-0.63/-1.83	-0.56/-0.08/-0.66/-1.88	-0.57/-0.09/-0.69/-1.91	-0.59/-0.09/-0.72/-1.97	-0.61/-0.11/-0.76/-2.01
	0.007	0.32/-0.58/-0.06/-1.30	-0.60/-0.07/0.34/-1.38	-0.62/-0.08/0.36/-1.47	-0.64/-0.09/0.38/-1.54	-0.66/-0.11/0.40/-1.63	-0.68/-0.14/0.41/-1.73	-0.71/-0.15/-0.43/-1.80
	0.014	-1.14/-0.80/-0.18/-3.28	-0.82/-0.21/-1.20/-3.32	-0.87/-0.23/-1.26/-3.40	-0.90/-0.26/-1.33/-3.47	-0.93/-0.31/-1.39/-3.45	-0.97/-0.33/-1.46/-3.55	-1.14/-0.36/-1.53/-3.62
	0.030	-2.65/-2.71/-0.59/-7.04	-2.80/-0.59/-2.78/-7.32	-2.90/-0.61/-2.93/-7.65	-2.99/-0.62/-3.07/-7.94	-3.09/-0.64/-3.23/-8.29	-3.19/-0.65/-3.38/-8.59	-3.29/-0.66/-3.55/-8.94
1:2	0.000	-0.12/-0.39/0.12/1.74	-0.12/-0.40/0.12/1.74	-0.13/-0.41/0.13/1.78	-0.13/-0.41/0.14/1.79	-0.14/-0.42/0.14/1.79	-0.14/-0.43/-0.15/1.82	-0.14/-0.44/0.16/1.86
	0.010	-0.17/-0.40/0.26/2.25	-0.17/-0.41/0.28/2.32	-0.18/-0.42//0.29/2.34	-0.18/-0.43/0.31/2.40	-0.19/-0.44/0.32/2.43	-0.19/-0.46/0.34/2.52	-0.20/-0.46/0.36/2.54
	0.030	-0.32/-0.52/-0.93/-1.40	-0.34/-0.53/-0.98/-1.51	-0.35/-0.54/-1.03/-1.62	-0.38/-0.55/-1.08/-1.72	-0.39/-0.56/-1.13/-1.82	-0.42/-0.57/-1.18/-1.92	-0.43/-0.59/-0.24/-2.01
	0.050	-0.95/-0.63/0.16/2.70	-0.98/-0.71/0.17/2.95	-1.02/-0.79/0.18/3.20	-1.05/-0.81/0.19/3.25	-1.08/-0.83/0.20/3.29	-1.12/-0.88/0.21/3.43	-1.16/-0.91/0.22/3.50

RSC Advances

RSCPublishing

ARTICLE

When excited at 426 nm, curcumin shows an emission maximum at ~500 nm. Results were found to be comparable with the previous reports[39]. A red shift in the emission maximum alongwith a decrease in fluorescence intensity with the increase in the φ_d value were noted (Inset: panel A, Figure 5). This was due to the localized dilution of the probe in the IL pool[3,32,35,36] . The progressive red shift (Inset: panel B, Figure 5) in the emission maxima was due to the increased polarity of the domain with increasing volume fraction of the ionic liquid[32].

To know the exact state of the solvent in the pool, fluorescence anisotropy studies on curcumin was carried out. Variation of fluorescence anisotropy value (r) with the volume fraction (φ_d) of ionic liquid have been graphically shown in Figure 6.

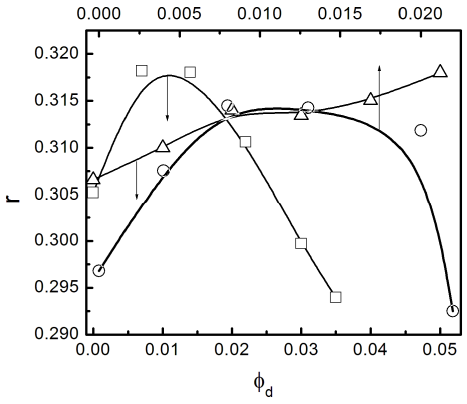

Figure 6. Variation in the fluorescence anisotropy (r) for 10 μM curcumin with different volume fraction (φ_d) of IL for [$b_4$mpy][BF_4]/(Tween-20+n-pentanol)/n-heptane IL-in-oil microemulsion system. Tween 20/n-pentanol ratio (w/w): O, 1:0.5; □, 1:1 and Δ, 1:2. Temp, 298K.

Anisotropy values passed through maxima with respect to the volume fraction of IL. Initially ILs are used up in coordinating with the oxyethylene head groups of Tween 20 for which structured entities are formed. At that stage the dye molecules did not have the freedom of movement. After the process of coordination of surfactant head group by IL cation was over, excess IL became free for which they can behave as bulk IL. Under that situation, the mobility of dye molecules became higher. This eventually led to the decrease in the fluorescence anisotropy values. A linear increase in the anisotropy value for the system comprising Tween20:n-pentanol in a 1:2 w/w ratio was due to the continued solvation of the cationic component of the ionic liquid, which was assisted by the presence of larger number of alkanols.

Conclusions

Comprehensive studies on *1*-butyl-*4*-methyl pyridinium tetrafluoroborate ([$b_4$mpy][BF_4]) / (Tween 20 + n-pentanol) / n-heptane microemulsion system were carried out using a number of different physicochemical techniques. Although the cosurfactant increased turbidity of the microemulsion, however, it was required for the attainment of stable microemulsion. Cosurfactant controlled the curvature of the microemulsion droplets; it simultaneously also imparted better stability by solvating the cationic component of the ionic liquid. Larger number of droplet formation was aided by the cosurfactant. Sensitivity towards temperature decreased with increasing amount of cosurfactant, as revealed through the combined dynamic light scattering and viscosity measurements. Oxyethylene group of Tween 20 formed coordinate linkages with the IL cation, which resulted in the rigidity of the polar domain. The IL, in excess of the amount required for coordinating the surfactant head groups, behaved like the bulk component as revealed through the fluorescence anisotropy measurements. Electron microscopy and small angle neutron scattering studies could further shed light on the morphology of the microemulsion droplets, which are considered as the future perspective.

Acknowledgements

Financial support in the form of a research grant from the Department of Science and Technology, Govt. of India (Grant Number: SR/S1/PC/24/2008) is sincerely acknowledged.

Notes and references

Department of Chemistry, University of North Bengal,
Darjeeling –734 013, West Bengal, India.
*Corresponding author: akpanda1@yahoo.com

1 D. O. Shah, *Micelles, Microemulsions and Monolayers*. Editor, Marcel Dekker Inc., New York, **1998**, pp. 1-52.

2 S. P. Moulik, B. K. Paul, *Adv. Colloid Interface Sci.* **1998**, *78*, 99-195

3 A. Adhikari, D. K. Das, D. K. Sasmal, K. Bhattacharyya, *J. Phys. Chem. A* **2009**, *113*, 3737-3743

4 T. Welton, *Chemical Reviews* **1999**, *99*, 2071-2084

5 I. Bandres, F. M. Royo, I. Gascon, M. Castro, C. Lafuente, *J. Phys. Chem. B* **2010**, *114*, 3601-3607

6 G. Zhou, Z. Luo, X. Fu, *Ind. Crops Prod.* **2014**, *52*, 105-110

7 W. Shang, X. Kang, H. Ning, J. Zhang, X. Zhang, Z. Wu, G. Mo, X. Xing, B. Han, *Langmuir* **2013**, *29*, 13168-13174

8 A. Wang, L. Chen, D. Jiang, Z. Yan, *Ind. Crops Prod.* **2013**, *51*, 425-429

9 A. Ying, S. Xu, S. Liu, Y. Ni, J. Yang, C. Wu, *Ind. Eng. Chem. Res.* **2013**, *53*, 547-552

10 U. Domanska, M. Krolikowski, D. Ramjugernath, T. M. Letcher, K. Tumba, *J. Phys. Chem. B* **2010**, *114*, 15011-15017

11 A. Saito, N. Watanuki, S. Kobayashi, Japan Patent 2010090372A, **2010**.

12 I. Hanaki, N. Ukei, Japan Patent 2012241152A, **2012**.

13 M. Pandurangachar, S. B. E. Kumara, B. N. Chandrashekar, O. Gilbert, S. Reddy, B. S. Sherigara, *Int. J. Electrochem. Sci.* **2010**, *5*, 1187-1202.

14 R. C. Vieira, D. E. Falvey, *J. Am. Chem. Soc.* **2008**, *130*, 1552-1553

15 S.-H. Zhao, H.-R. Zhang, L.-H. Feng, Z.-B. Chen, *J. Mol. Catal. A: Chem.* **2006**, *258*, 251-256

16 A. Chinnappan, A. H. Jadhav, H. Kim, W.-J. Chung, *Chem. Eng. J. (Amsterdam, Neth.)* **2014**, *237*, 95-100

17 T. E. Sintra, R. Cruz, S. P. M. Ventura, J. A. P. Coutinho, *J. Chem. Thermodyn.* **2013**, Ahead of Print 10.1016/j.jct.2013.10.024.

18 M. García-Mardones, H. M. Osorio, C. Lafuente, I. Gascón, *J. Chem. Eng. Data* **2013**, *58*, 1613-1620

19 H. Takumi, Y. Imai, N. Toh, H. Matsubara, T. Takiue, M. Aratono, *Colloids Surf., A* **2014**, *441*, 59-65

20 R. K. Maheshwari, A. K. Singh, J. Gaddipati, R. C. Srimal, *Life Sci.* **2006**, *78*, 2081-2087

21 Y. Kaminaga, A. Nagatsu, T. Akiyama, N. Sugimoto, T. Yamazaki, T. Maitani, H. Mizukami, *FEBS Letters* **2003**, *555*, 311-316

22 Ravindranath V, C. N., *Toxicology* **1980**, *16*, 259-265.

23 Z. Wang, M. H. M. Leung, T. W. Kee, D. S. English, *Langmuir* **2009**, *26*, 5520-5526

24 M. O. Iwunze, *J. Mol. Liq.* **2004**, *111*, 161-165

25 A. Semalty, M. Semalty, M. S. M. Rawat, F. Franceschi, *Fitoterapia* **2010**, *81*, 306-314

26 K. N. Baglole, P. G. Boland, B. D. Wagner, *J. Photochem. Photobiol. A: Chem.* **2005**, *173*, 230-237

27 C. P. M. Shah, B.; Kumar, M.; Priyadarsini, K. Indira; Bajaj, P. N., *Current Science* **2010**, *95*, 1426-1432.

28 K. Letchford, R. Liggins, H. Burt, *J. Pharm. Sci.* **2008**, *97*, 1179-1190

29 M. Takahashi, S. Uechi, K. Takara, Y. Asikin, K. Wada, *J. Agric. Food Chem.* **2009**, *57*, 9141-9146

30 M. M. Yallapu, B. K. Gupta, M. Jaggi, S. C. Chauhan, *J. Colloid Interface Sci.* **2010**, *351*, 19-29

31 S. Paul, A. Panda, *Journal of Surfactants and Detergents* **2011**, *14*, 473-486

32 S. Paul, A. K. Panda, *Colloids Surf. A:* **2013**, *419*, 113-124

33 B. Jana, S. Ghosh, N. Chattopadhyay, *J. Photochem. Photobiol., B* **2013**, *126*, 1-10

34 Y. Gao, N. Li, L. Hilfert, S. Zhang, L. Zheng, L. Yu, *Langmuir* **2009**, *25*, 1360-1365.

35 D. Chakrabarty, D. Seth, A. Chakraborty, N. Sarkar, *J. Phys. Chem. B* **2005**, *109*, 5753-5758

36 Y. a. Gao, J. Zhang, H. Xu, X. Zhao, L. Zheng, X. Li, L. Yu, *Chem. Phys. Chem.* **2006**, *7*, 1554-1561 .

37 A. Acharya, S. P. Moulik, S. K. Sanyal, B. K. Mishra, P. M. Puri, *J. Colloid Interface Sci.* **2002**, *245*, 163-170.

38 A. Acharya, S. K. Sanyal, S. P. Moulik, *Int.. J. Pharm.* **2001**, *229*, 213-226.

39 C. Banerjee, C. Ghatak, S. Mandal, S. Ghosh, J. Kuchlyan, N. Sarkar, *J. Phys. Chem. B* **2013**, *117*, 6906-6916

Colloids and Surfaces A: Physicochem. Eng. Aspects 404 (2012) 1–11

Contents lists available at SciVerse ScienceDirect

Colloids and Surfaces A: Physicochemical and Engineering Aspects

journal homepage: www.elsevier.com/locate/colsurfa

Physicochemical investigations on the aqueous solution of an ionic liquid, 1-butyl-3-methylimidazolium methanesulfonate, [bmim][MS], in a concentrated and dilute regime

S. Paul, A.K. Panda*

Department of Chemistry, University of North Bengal, Darjeeling 734 013, West Bengal, India

ARTICLE INFO

Article history:
Received 10 October 2011
Received in revised form 24 January 2012
Accepted 27 January 2012
Available online 7 February 2012

The paper is dedicated to Prof. Satya Priya Moulik, INSA Senior Scientist and Professor of Chemistry, Jadavpur University, Kolkata, India, on his 75th birthday.

Keywords:
[bmim][MS]
Aggregation
Viscosity
Density
Surface tension
Spectroscopy

ABSTRACT

The physicochemical properties of the ionic liquid (IL) 1-butyl-3-methylimidazolium methanesulfonate ([bmim][MS]) in combination with water were evaluated through density, viscosity, surface tension, conductance, cyclic voltammetry, absorption and emission spectroscopic measurements. Binary mixtures were studied both in the water-rich and [bmim][MS]-rich regions (0.01 mM–4.96 M). The static and dynamic properties of the binary combinations were evaluated through density and viscosity measurements. The [bmim][MS] decreased the surface tension of the water, from which the surface excess and area per molecule of the ionic liquid were determined at the air–liquid surface. The equivalent conductance of [bmim][MS] at an infinite dilution was determined from the conductance data because the system obeyed the Debye–Hückel–Onsager formalism. Cyclic voltammetry measurements revealed the formation of some metastable organized structures at specific compositions. The absorption and emission spectral behavior of the anionic dye eosin Y were found to be dependent on the concentration of [bmim][MS] in the water-rich region. A significant change in the steady state anisotropy and excited state lifetime of the fluorophore occurred above 1.0 M [bmim][MS] in water, which correlated with the viscosity of the medium. It was concluded that the aggregation of [bmim][MS] into micelle-like aggregates occurred above the specific concentration, which significantly altered the different physiochemical parameters of the [bmim][MS] binary mixture.

1. Introduction

Ionic liquids (ILs) are neoteric and environmentally benign solvents for which there are many applications for their use [1–9]. Being aprotic, less volatile and ionic in nature, ILs are used in energy production [10–12], process engineering [13], bioengineering [14], material engineering and sensor technology [7] and electrochemical applications [9,15]. Because ILs are environmentally benign solvents, they act as catalysts and hosts for organic reactions [16,17]. Organic solvents have limitations, such as flammability and evaporation under warm temperatures and reactivity, which cause stability issues. Therefore, imidazolium-based room temperature ionic liquids are mostly used for their non-volatility, relatively high conductivity and low viscosity [18]. Because of the aforementioned applications, studies involving ILs are plenty in literature [1,19]. Mukherjee et al. [20–23] also studied ILs by spectroscopic techniques. Sum frequency generation studies on the ionic liquids 1-butyl-3-methylimidazolium dicyanamide ([bmim][DCA]) and 1-butyl-3-methylimidazolium methylsulfate ([bmim][MS]) have been reported by Aliaga et al. [18], which could provide information on the interfacial behavior of ionic liquids. The use of different types of ILs has also been studied by Balducci et al. [10].

Physicochemical investigations on binary mixtures of an ionic liquid and water have been studied by different researchers [11,12,16,24–34]. Kelkar et al. theoretically investigated the effect of temperature and water on the viscosity behavior of 1-ethyl-3-methylimidazolium bis (trifluoromethanesulfonyl) imide [35]. Liu et al. made a systematic investigation on the binary mixture of an IL and water with variations of both the cation and anion

* Corresponding author. Tel.: +91 3532699425; fax: +91 3532699001.
E-mail address: akpanda1@yahoo.com (A.K. Panda).

0927-7757/$ – see front matter © 2012 Elsevier B.V. All rights reserved.
doi:10.1016/j.colsurfa.2012.01.034

[36,37]. Reports are also available on the different physicochemical properties of different ionic liquids in aqueous dilute solutions [36–45].

Water is the 'greenest' solvent. Therefore, detailed investigations on IL–water binary mixtures are important for applications and for a fundamental understanding. It is believed that evaluating the thermo-physical parameters of binary mixtures that involve ILs is essential to optimally design any industrial product [30,36,37]. An excess molar volume is an important parameter for understanding the interaction among the components of binary mixtures at a molecular level, which can be estimated by measuring the density. Viscosity is another important dynamic property of a solvent, both in its pure state and in a mixed state with another solvent. When an IL is used as the solvent, the preferred viscosity is within a lower range. However, a highly viscous IL mixture is preferred for lubrication and membrane preparations [35]. Therefore, to optimize an ionic liquid–water binary mixture, a detailed investigation on its viscosity in combination with another solvent is absolutely essential. Widegren et al. [34] have investigated the viscosity behavior of the three RTILs, and it was reported that a dramatic change in the viscosity of the IL occurred in the presence of water. The conductivity of a solvent has a vital importance, especially for ionic liquids because they are similar to the binary mixtures of organic solvents with an organic electrolyte [46]. Fitchett et al. [25] found that the molar conductance is directly dependent on the viscosity of the medium. Studies on the conductance behavior of an aqueous solution of IL in the dilute range are not abundant in the literature. Such studies are considered essential to check the validity of conventional electrochemical laws (Debye–Hückell–Onsager equation) and hence to determine the equivalent conductance of an IL at an infinite dilution [30,36,37,47]. Similarities or differences in the conductance behavior of an IL with respect to the conventional electrolytes can also be justified through such studies. The composition of an air-solution interface is always different from the bulk because ILs exhibit a surface activity due to their organic moieties. Compared to the surface of a pure IL, the (IL + water)–air interface is less understood [30,36,37,47,48]. Because ILs are used in many electrochemical applications, cyclic voltammetric studies on binary mixtures of the ILs and water are considered important. Additionally, such systems are advantageous for study because a carrier electrolyte is not required [46,49]. For studies involving an IL, the interaction at the molecular level and polarity of the medium could be investigated through spectroscopic probing techniques. Solvation dynamics and a subsequent characterization of the solvents in either the pure form or the compartmentalized systems have been systematically investigated by different researchers [1,19,20,50–69]. To the best of our knowledge, no systematic investigation on the absorption and emission behavior of a dye in a bulk IL–water mixture over a wide concentration range has been performed using [bmim][MS].

According to Marciniak [70] and Ventura et al. [33], the extraction capability of an ionic liquid was proposed to be dependent on the hydrogen bond-accepting strength of the anions, although the detailed physicochemical explanation behind such properties were not explained. According to Marciniak [70], dearomatization can be influenced by the nature of an anion in an IL. Among the different types of imidazolium-based ionic liquids, little work has been performed with methanesulfonate anions [33,71]. Yang et al. [72] compared the differences in the physicochemical properties of IL that comprised two different anions, toluene-*p*-sulfonate and methanesulfonate. Kelkar and Maginn [35] used ethyl methylimidazolium-based ionic liquids with a number of anions and found that methanesulfonate anions could act as a better stabilizing agent for iron carbide nanoparticles that were synthesized in situ. Rivera-Rubero and Baldelli [73] reported on the anomalous behavior of MS that contained ILs rather than the conventional anions. According to Fröba et al. [11,12], there could be the existence of an unlimited number of ILs considering the variations in the number of cations and anions; therefore, comprehensive physicochemical investigations on all of the ILs in their binary mixed states could not be investigated. However, to understand the structure–property relationship, such studies are warranted.

This present study focuses the investigations on the solution behavior of the ionic liquid 1-butyl-3-methylimidazolium methanesulfonate [bmim][MS] in water over a wide concentration range by using different techniques. The investigation aims to derive the density, excess molar density and viscosity to understand the synergistic and antagonistic behavior of all of the combinations. Surface tension studies on an aqueous solution of [bmim][MS] in the water-rich region evaluated the surface activity, surface excess and molecular area of the IL. Conductance measurements for all of the combinations and cyclic voltammetry measurements in the IL-rich region helped in understanding the states of aggregates in solution. Absorption and emission spectroscopic studies of the anionic xanthene dye eosin Y have been performed in the water-rich region. Fluorescence lifetime and anisotropy measurements could shed light on the viscosity of the media. Efforts have also been made to correlate the lifetime and fluorescence anisotropy with the experimentally determined viscosity. Additionally, we intended to correlate the data of the binary mixture in the water-rich region with the aggregation behavior of IL because there are several reports that conclude that [bmim]-based ionic liquids can form micelle-like aggregates in water after attaining a certain concentration [36,37,40,44,45,48,74]. The choice of this anion is intentional because it is an alkyl group-containing simple inorganic ion. Our main aim was to use the binary mixture of [bmim][MS] and water in a microemulsion of oil continuum. However, due to its relatively higher melting point, this ionic liquid was not thought to be useful for practical purposes in its pure form. Moreover, an imidazolium-based ionic liquid-containing [MS] anion would be less toxic compared to the fluorine-based ILs [72]. In a recent study, Stark et al. [75] reported that 1-ethyl-3-methylimidazolium methanesulfonate ([emim][MS]) exhibits some unusual behaviors in combination with water. It was reported that this particular ionic liquid could deactivate water above a certain concentration even if water is present in high amounts (up to 50 mole%). In another work by Stark and Wasserscheid [76], it was reported that water molecules becomes deactivated below 50 mole% of water and in combination with [emim][MS]. The deactivation of water molecules occurred through a chemical reaction. In this reaction, 5-hydroxymethyl furfural could be obtained from an intramolecular condensation reaction of fructose; however, the reaction rate was slowed down significantly in the presence of water. Nevertheless, water, when present in combination with an ionic liquid [emim][MS] at up to 50 mole%, could barely slow the reaction rate. The deactivation of water in terms of chemical reactivity was due to the formation of a highly structured IL framework that physically separated the water from the reactants. We also intended to check the validity of the generalization that subsequently motivated us to undertake the physicochemical investigations on the binary mixture of [bmim][MS] and water. Such a study is believed to help understanding the interaction between [bmim][MS] and water at the molecular level and the orientation of the IL at the air solution interface, which will then provide new insight into the area of IL-comprising binary mixtures.

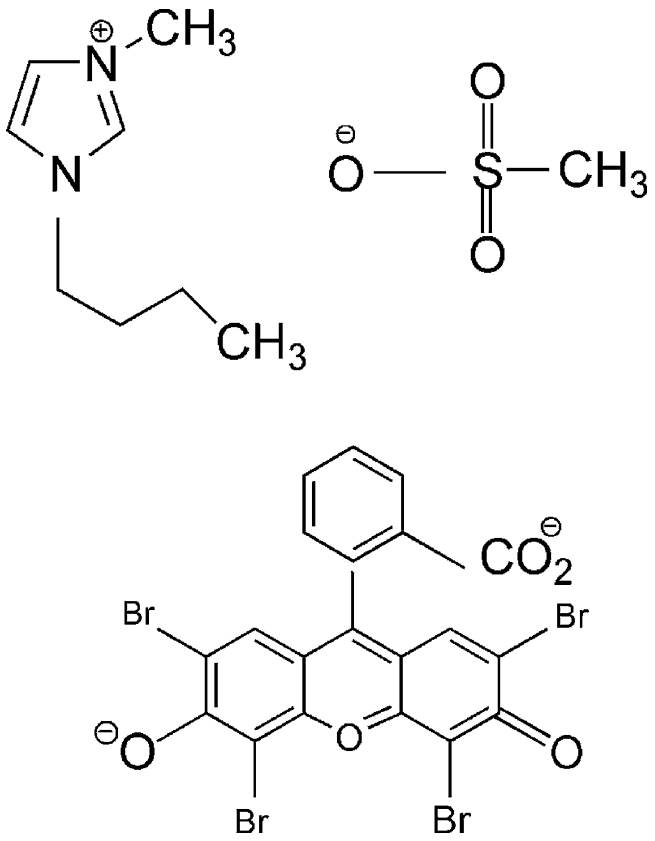

Schematic structure of [bmim][MS] (top) and eosin Y (bottom).

2. Experimental

2.1. Materials

The ionic liquid (IL) 1-butyl-3-methyl-imidazolium–methanesulfonate [bmim][MS] was a product from M/S Sigma–Aldrich Chemicals Pvt. Ltd. (USA). It was stated to be more than 99.5% pure. The IL was thoroughly degassed at 333 K (60 °C) for a time period of 3 h on a vacuum line. Double distilled water with a specific conductance of 2–4 μS (at 298.15 K) was used to prepare the binary mixtures and the aqueous solution of [bmim][MS]. $K_4[Fe(CN)_6]$, which was used as an electrochemical probe, was purchased from E. Merck (India) Ltd. (Mumbai, India). The dye eosin Y (EY) sodium salt was a product from E. Merck (Germany), and it was used as received. The concentrated solution of dye was prepared by dissolving a weighed amount in water. Working solutions were then prepared by proper dilutions.

2.2. Methods

Binary mixtures of [bmim][MS] and water and aqueous solutions of the IL in the dilute to moderate concentration range were prepared by proper weighing. Two types of binary mixtures of [bmim][MS] + water have been used. The first was the [bmim][MS]-rich region where the mole fraction of [bmim][MS] was greater than 0.1 ($x_{[bmim][MS]}$ = 0.2, 0.4, 0.5, 0.6, 0.8 and 1.0); the molar concentrations associated with the mole fractions are 3.69, 4.40, 4.58, 4.70, 4.86 and 4.96 M, respectively. The second category was comprised of water-rich regions ($x_{[bmim][MS]} < 0.1$) within a dilute concentration range of the IL (0.01–3.0 M). Therefore, the [bmim][MS] + water binary mixtures were categorized into two groups: (A) IL-rich binary mixtures and (B) water-rich IL solutions.

2.3. Instrumentation

The densities of the [bmim][MS]-rich binary mixtures (category A) were measured using a DMA 4500-M densitometer (Anton Paar, USA), which had a stated accuracy of 5×10^{-5} g mL^{-1}. The temperature during the measurements was controlled (±0.05 K) with a high precision Pt-resistance probe [11]. The densities of the binary mixtures at atmospheric pressure were recorded in the temperature range of 298.15–323.15 K with an interval of 5 K. The viscosity was measured using an LVDV-II + PCP cone and a plate-type roto-viscometer (Brookfield Eng. Lab, USA). The temperature was controlled by a cryogenic water bath (of precision ± 0.1 K). The shear rates (D) varied within the range (20–60 S^{-1}), and the corresponding shear stress (τ) was recorded. The viscosity (η) was obtained at zero shear rates using the following formula: $\eta = \tau/D$ [77]. The uncertainties of the experimental density and viscosity were found to be less than 0.003 g mL^{-1} and 0.01 mPa s, respectively, and the deviations of V^E were less than 0.0005 mL mol^{-1} and 0.01 mPa s, respectively. The refractive indices of the binary mixtures were determined with a refractometer (Refracto 30GS; Mettler Toledo, Columbus, OH) with a stated accuracy of ±0.0005. The surface tension of the aqueous [bmim][MS] solutions was measured (measurable up to 1.0 M) with a du Noüy tensiometer (precision ± 0.1 mN m^{-1}) from Jancon (Kolkata, India). A concentrated aqueous [bmim][MS] solution was progressively added to 20 mL of water that was kept in a thermostated double-walled jacket. Prior to each measurement, the solution was homogenized using a magnetic stirrer and equilibrated for 15 min. The temperature was maintained at 298 ± 0.05 K by a cryogenic circulatory water bath. An average of three readings was considered. The conductance was recorded with an EC-CON510/43S conductivity meter (Cyberscan, TDS/^{0}C/^{0}F, USA) at 298 K. The solutions were kept in a double-walled glass jacket. The cyclic voltammetric measurements were carried out on a BAS (Bioanalytical Systems) Electrochemical Work Station, Epsilon (USA). The electrochemical measurements were conducted by using three electrode configurations, which were a glassy carbon working electrode, an Ag/AgCl reference electrode and a platinum counter electrode. In addition, 1.0 mM $K_4[Fe(CN)]_6$ was used as an electrochemical probe. The scan rates were varied in the range of 50–100 mV s^{-1}. The visible absorption spectra of a 10 μM aqueous solution of EY were recorded on a UVD-2950 Spectrophotometer (Labomed Inc., USA). The spectra were recorded in the range of 400–600 nm using a matched pair of quartz cells with a 1.0-cm optical path length. Water or a [bmim][MS] + water solution was used as a reference. The steady state and time-resolved fluorescence spectroscopic measurements were performed using a bench-top spectrofluorimeter (Quantamaster-40; Photon Technology International Inc, NJ, USA). The fluorescent dye was excited at 500 nm (λ_{ex}), and the emission spectra were recorded in the range of 475–675 nm. The steady state anisotropy was determined using the following equations [78]:

$$r = \frac{I_{VV} - GI_{VH}}{I_{VV} + 2GI_{VH}} \quad (1)$$

and

$$G = \frac{I_{HV}}{I_{HH}} \quad (2)$$

where I_{VV} and I_{VH} are the intensities obtained with the extinction polarizer oriented vertically and the emission polarizer oriented vertically and horizontally, respectively. Additionally, I_{HV} and I_{HH} refer to similar parameters as above but for the horizontal positions of the extinction polarizer. Further details can be found in the literature [78]. Motorized polarizers were used for these studies. The fluorescence lifetime of an aqueous solution of EY in the absence and presence of the IL was determined from the fluorescence decay

Table 1
The variation of density (ρ), excess molar volume (V^E) and viscosity (η) for the binary mixtures of [bmim][MS] and water at different temperatures (T) in the [bmim][MS]-rich region.

x_{IL} (conc./M)	298.15	303.15	308.15	313.15	318.15	323.15
ρ/g mL^{-1} at different temp. (in K)						
0.0 (0.00)	0.997	0.996	0.994	0.992	0.989	0.982
0.2 (3.69)	1.131	1.132	1.129	1.123	1.121	1.118
0.4 (4.40)	1.150	1.148	1.144	1.140	1.136	1.132
0.5 (4.58)	1.156	1.154	1.150	1.146	1.143	1.139
0.6 (4.78)	1.159	1.157	1.152	1.148	1.145	1.141
0.8 (4.86)	1.161	1.159	1.154	1.151	1.147	1.144
1.0 (4.96)	1.163	1.161	1.156	1.152	1.149	1.145
V^E/mL mol^{-1}						
0.2 (3.69)	0.2845	0.1656	0.1033	0.2038	0.1615	0.1040
0.4 (4.40)	−0.6091	−0.6007	−0.5741	−0.5569	−0.5605	−0.5875
0.5 (4.58)	−0.7661	−0.6250	−0.6994	−0.6867	−0.6908	−0.7149
0.6 (4.78)	−0.5922	−0.5873	−0.5711	−0.5610	−0.5644	−0.5838
0.8 (4.86)	−0.2323	−0.2297	−0.3644	−0.3599	−0.2169	−0.3723
η/mPa s (cP)						
0.0 (0.00)	0.89	0.79	0.74	0.68	0.62	0.57
0.2 (3.69)	10.52	8.79	7.29	6.76	3.08	2.33
0.4 (4.40)	25.48	22.52	20.64	15.45	12.49	11.16
0.5 (4.58)	37.18	29.48	25.01	19.99	16.75	13.91
0.6 (4.78)	35.35	23.90	19.78	16.54	14.18	12.00
0.8 (4.86)	63.49	49.14	38.41	31.60	25.28	20.99
1.0 (4.96)	55.29	34.45	26.93	21.75	17.78	15.88

Values in the parentheses indicate the molar concentration of [bmim][MS] in water at 298.15 K.

curve by the Ströbe technique using a pulsed nano diode (Nano LED light-emitting device) as the light source at 500 nm. Fluorescence decay curves were analyzed by the Felix GX (version 2.0) software. The goodness of fit was adjudged by the χ^2 values [78–80].

3. Results and discussion

3.1. Density measurement

The density, viscosity and their derived data for the binary mixtures in the [bmim][MS]-rich region are summarized in Table 1, Fig. 1 and also in Supplementary section. Fig. 1 describes the density–composition (concentration, C and mole fraction, x_{IL}) profile in the IL-rich region, where it was found that the density increased in a nonlinear fashion with increasing IL content. Initially, the density increased rapidly up to 60 mole% (4.5 M) of [bmim][MS] after that the change was not as significant. Differences in the structure and packing of molecular components led to similar variations [36,37,44,81]. Stark et al. [75] proposed that for IL + water binary

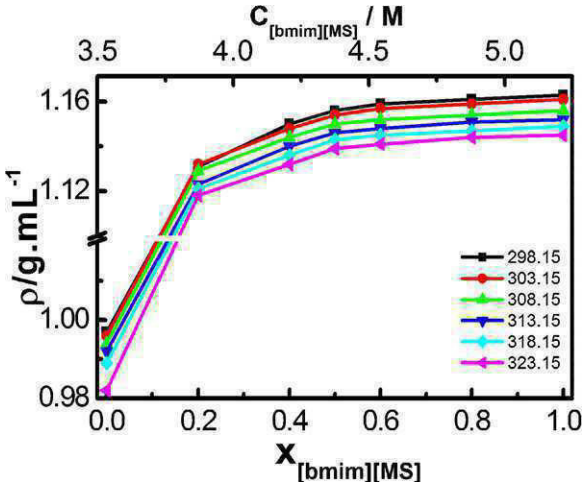

Fig. 1. The variation of the density (ρ) of a [bmim][MS] + water binary mixture with the mole fraction (x) and concentration (C) of [bmim][MS] in the ionic liquid-rich region. The temperatures (in K) are indicated in the figure.

mixtures that, when the IL content is more than 50 mole%, highly ordered pseudo-lattice-like structures are formed, which was also proposed by Méndez-Morales et al. [82]. In the present case, the same proposition was found to be valid. Above 50 mole% of the IL, the water molecules become less sensitive and could not perturb the pseudo-lattice-like structured aggregates of the IL. The variation in density with the molar concentration of [bmim][MS] was nonlinear in the entire studied concentration range, as was reported previously [36,37]. The density decreased linearly with the temperature obeying the following formalism:

$$\rho = \rho_0 + \rho_1 T \tag{3}$$

The ILs were reported to be capable of forming micelle-like aggregates. Above 60 mole% [bmim][MS], there would be a sufficient number of such congregated species whose organizational packing would barely be perturbed by the added water molecules. Additionally, the approach of Stark et al. [75] could be adapted by considering that above the stated composition, there occurred some "loosening effect" on the structure of the aggregates. We have studied mixtures at even lower concentrations. The behavior of [bmim][methylsulphate] was also similar to ours, although the density of [bmim][methylsulphate] was higher than that of [bmim][MS]. The temperature sensitivity on density (ρ) for [bmim][methylsulphate] was less [83] ($-(6.72 \pm 0.0149) \times 10^{-4}$ g mL^{-1} °C^{-1}) than for [bmim][MS] ($-(7.263 \pm 0.367) \times 10^{-4}$ g mL^{-1} °C^{-1}).

3.2. Variations of excess molar volume (V^E)

The excess molar volume V^E was calculated from the experimental results according to the following equation [36,37]:

$$V^E = \frac{x_1 M_1 + x_2 M_2}{\rho_M} - \frac{x_1 M_1}{\rho_1} - \frac{x_2 M_2}{\rho_2} \tag{4}$$

where x_1 and x_2 are the mole fractions; M_1 and M_2 are molar masses; and ρ_1 and ρ_2 are the densities of pure IL and water, respectively. The subscript M represents the density of the mixture. The deviation of V^E was approximately ±0.05%. The results are shown in Table 1. The V^E values at all of the temperatures passed through a minimum of $x_{IL} = 0.5$, as shown in Table 1. Additionally, the variation of the excess molar volume with the composition at different

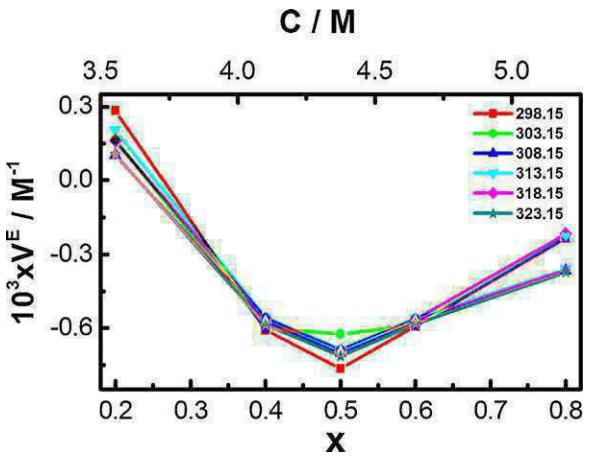

Fig. 2. The variation of an excess molar volume (V^E) of the [bmim][MS] + water binary mixture with the mole fraction (x) and concentration of [bmim][MS]. The temperatures (in K) are indicated in the figure.

temperatures is shown in Fig. 2. It was found that, at $x_{IL} = 0.2$, the V^E for the mixture was higher than zero, which indicated a positive deviation from the ideality. This finding is an indication of a structural reorganization and the resultant swelling effect. The excess molar volume (V^E) was not significantly different for all of the temperatures. This result indicates the quasi-ideal behavior of the binary mixture of IL + water from the molar volume point-of-view (as the V^E values are lower than 0.5% of the ideal molar volume value). The appearance of the minima at $x_{IL} = 0.5$ indicates the formation of a condensed structure. According to Rebello et al. [30], if there exists a water–water and anion–cation interaction upon the mixing of IL and water, then there would be a significant reduction of coulombic attraction. As a result, a size-enhancing effect would occur. However, in our case, the V^E values were found to be negative for all of the compositions in general. This finding implies a strong associative interaction between water and [bmim][MS], except for the cases where the amount of IL is less ($x_{IL} < 0.2$). The negative deviation from the ideality was an added contribution of the counter anion in [bmim][MS]. The methanesulfonate anion can form a stronger hydrogen bond with water, compared to the other conventional anions, such as BF_4^- and halides. This unusual behavior has only recently been reported by Stark et al. [75] and Lehmann et al. [27]. A molecular organization of the components in binary mixtures has been proposed through some models [37,48,75,82].

3.3. Viscosity measurement

The $\ln \eta - x_{IL}$ profile at different temperatures is shown in Fig. 3. The results are also summarized in Table 1 and in the supplementary section (Tables S1 and S2).

The measured viscosities in the studied concentration range followed the Arrhenius formalism [84]:

$$\eta = \eta_0 e^{E_A/RT} \tag{5}$$

where E_A, R and T are the viscosity activation energy, universal gas constant and temperature in the absolute scale, respectively. In a recent study by Stark et al. [75], it was proposed that the Arrhenius formalism for the viscosity activation energy could be employed for an [emim][MS] + water binary mixture. As the IL content in the system increased above 50 mole%, the micelle-like structures are stabilized and then the added water becomes deactivated, i.e., the structuredness is not perturbed due to physical separation of water from the reactants.

The variation of viscosity with the molar concentration (and the mole fraction) was non-linear in the entire studied concentration range. Additional viscosity and viscosity-derived data are provided in Supplementary section. Similar reports have been shown for other binary mixtures [24]. Kelkar and Maginn [35] proposed that water, when present in combination with IL, could preferentially bind to more than one species. These authors also proposed that water preferentially associates with the anionic part of the ionic liquid. In the water-rich region of the binary mixture, η – molar concentration of the ionic liquid profile was found to be bisigmoidal in nature, which indicated the formation of differently aggregated species. The viscosity initially increased mildly with the increase in concentration of ionic liquid in water. After 1.0 M, a significant rise in the viscosity occurred. The different available reports have proposed that [bmim][MS], above 1.0 M concentration, can form highly ordered micelle-like aggregates. These aggregates could enhance the viscosity of the medium [36,37,44,47,48].

The values of an excess molar volume and viscosity deviations were fitted by Redlich–Kister type polynomial [84]:

$$Y = x_1 x_2 \sum_{k=0}^{m} A_k (x_1 - x_2)^k \tag{6}$$

where $Y = V^E$ and the coefficients of A_k are parameters that were obtained by fitting the equations to the experimental values with a least square method. The correlated results for the density and excess molar volume were defined by the following equation, and

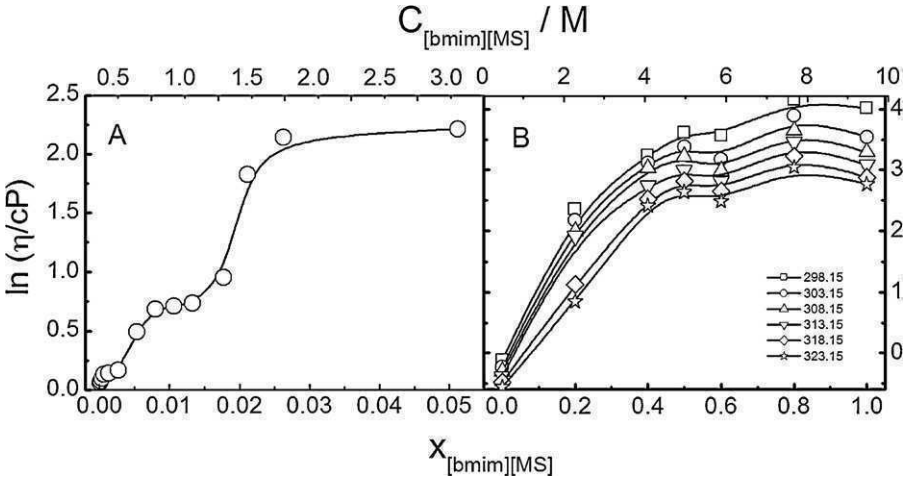

Fig. 3. The variation of viscosity (η) of [bmim][MS] + water binary mixture with mole fraction ($x_{[bmim][MS]}$) and concentration (C) in the dilute and ionic liquid-rich region. Temperatures (in K) are indicated in the figure.

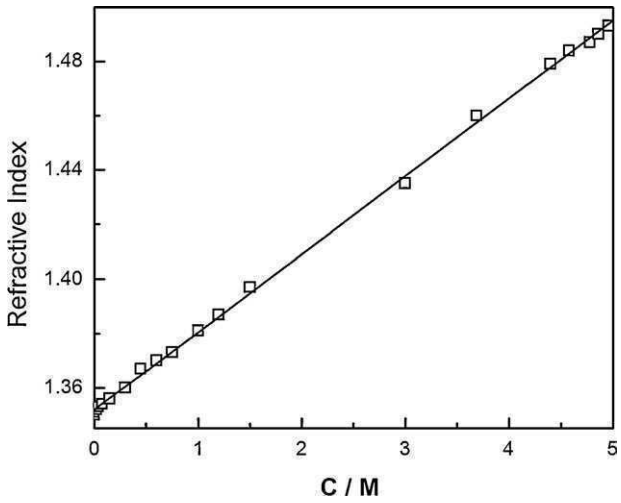

Fig. 4. The variation in the refractive index of [bmim][MS] + water binary mixture with an IL concentration (C) at 298.15 K.

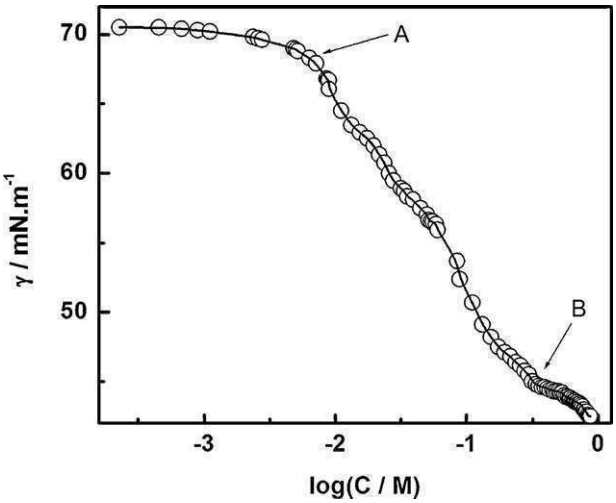

Fig. 5. The variation of surface tension (γ) with the concentration (C) of [bmim][MS] in water at 298.15 K. Points A and B correspond to the [bmim][MS] concentration at 5.0 mM and 0.3 M, respectively.

the results are shown in the supplementary section (Table S3) according to the following formalism [84]:

$$\sigma = \left[\frac{\sum (Y_{\exp} - Y_{cal})^2}{n-p}\right]^{1/2} \quad (7)$$

where Y refers to ρ, η, V^E and the subscripts '*exp*' and '*cal*' represent the experimental value and the calculated value, respectively. The number of data points is represented by '*n*', and '*p*' is the number of coefficients.

3.4. Refractive index

Variations of the refractive index with the molar concentration of [bmim][MS] in the water-rich region is shown in Fig. 4. The refractive index increased linearly with the concentration of IL, like the previously reported systems [36,37]. The refractive index increased significantly above 5.0 mM [bmim][MS] in water. A change in the dielectric constant of the medium could account for this variation. The refractive index (RI) and density (ρ) obeyed Newton's formalism:

$$\frac{RI - 1}{\rho} = C \quad (8)$$

where C is constant in the entire concentration range.

3.5. Surface tension

Because the ionic liquids have organic moieties, they are expected to exhibit surface activity. The surface tension (γ) – concentration (C) profile for the binary mixture in the water-rich region is presented in Fig. 5. It is clear from the figure that the surface tension decreased only after 5.0 mM (marked as point A in the figure), while a second halt appeared at ~0.3 M. Similar types of variations for [bmim][BF_4] have been reported by Bowers et al. [47]. Initially, due to its high ionic nature, [bmim][MS] molecules do not spontaneously get adsorbed onto the surface. The second breakpoint confirms the changes in the structural organization through the formation of micelle-like aggregates, which has been proposed by several authors [26,31,32,36–38,40,41,43–45,47,48,74,75,85,86]. Stark et al. [75] modeled the structures of these ionic clusters in the absence and presence of water in their recent studies.

Gibbs formalism was found to be valid for aqueous ionic liquid solutions as follows:

$$\Gamma = -\frac{1}{2.303\, nRT}\left(\frac{d\gamma}{d\,\log\, a}\right) \quad (9)$$

where γ and a are the surface tension and activity of the IL in water, respectively, and R and T have their typical meanings. Although strictly speaking, a calculation of the surface excess using the above equation requires the actual activity of [bmim][MS] in solution to be derived from the concentration. However, as in many cases, the activity of the specific solute solvent system cannot be accurately measured; therefore, activity was approximated as the concentration of the solute in the dilute range [87]. In the present system, the surface excess was calculated by determining the slope of γ vs. log C plot (through linear regression) in the concentration range of 0.007–0.20 mM. The surface excess value for [bmim][MS] in the stated concentration range at the air–solution interface was found to be 1.23×10^{-6} mol m^{-2}. This method of surface excess determination is quite reliable. However, no reported value for [bmim][MS] was available in the literature. The significant decrease, after which there occurred a change in the slope of γ vs. log C, was found to be 45 mN m^{-1} (marked as point 'B' in Fig. 5). This value was found to be relatively higher than other [bmim]-containing ionic liquids in their pure forms [86]. It should be mentioned that we could not measure the surface tension of [bmim][MS] in water at a concentration higher than 1.0 M because the stickiness of the interface interfered with the surface tension values. The surface excess value helped in determining the minimum area per ionic liquid at the surface [47]:

$$A_{\min} = \frac{10^{18}}{N_A \times \Gamma_{\max}} \quad (10)$$

where A_{min} was the minimum area per ionic liquid molecule at the air water interface, N_A was Avogadro's constant and Γ_{max} was the surface excess. For [bmim][MS], the A_{min} value was found to be 1.35 nm^2 molecule^{-1}. The A_{min} value for [bmim][MS] was found to be higher than that from previous reports [47]. Sung et al. [32] proposed a model depicting the orientation of 1-butyl-3-methylimidazolium tetrafluoroborate [bmim][BF_4] at the (IL + water)–air interface, where the anions are also associated with the cationic moiety. The larger size of the methane sulfonate anion resulted in the larger area for the present IL. However, an additional sophisticated instrumentation technique, such as sum frequency generation spectroscopy, neutron reflectometry or ellipsometry, is

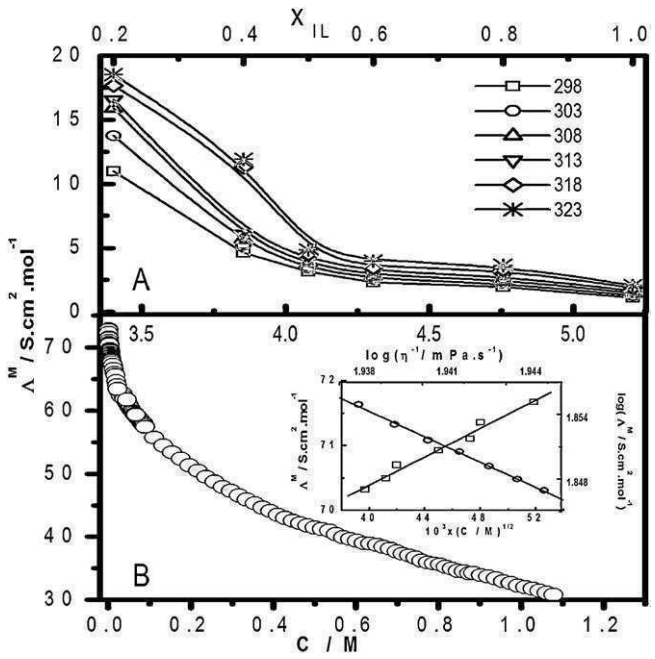

Fig. 6. The variation of molar conductance (Λ^M) with A, mole fraction (x) in the [bmim][MS]-rich region and B, concentration (C) of [bmim][MS] solution in water-rich region. Inset of B: $\Lambda^M - C^{1/2}$ (○) and $\log \Lambda^M - \log \eta^{-1}$ (□) profiles in the lower concentration range of [bmim][MS]. Temp: 298 K.

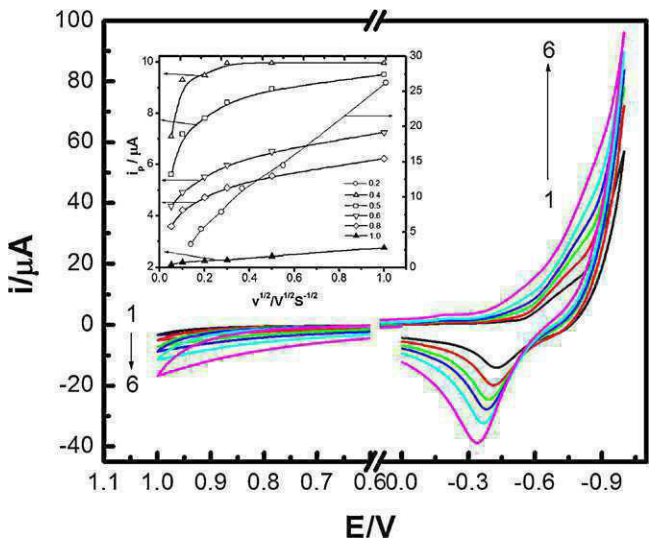

Fig. 7. The electrochemical window for an equimolar mixture of [bmim][MS] + water at various scan rates and at 298.15 K. Scan rates (mV s^{-1}): 1, 25; 2, 50; 3, 100; 4, 200; 5, 500 and 6, 1000. Here, 0.1 mM $K_4Fe(CN)_6$ was used as the probe. No carrier electrolyte was used as the medium was self-conducting, except for pure water where 1.0 mM KCl was used. Inset: dependence of peak current (i_p) on the scan rate (v) for different [bmim][MS] + water mixtures. Mole fractions of [bmim][MS] are indicated in the figure.

warranted, and these studies are considered to be future possibilities.

3.5.1. Electrical conductivity

The molar conductance was found to decrease with the increase in the [bmim][MS] concentration in water (as shown in Fig. 6). The decrease was significant up to 50 mole% of ionic liquid in combination with water, after which the decrease in the molar conductance was mild (panel A). It was anticipated that after 50 mole% of the ionic liquid in the binary mixture, no significant structural alteration takes place. Considering the effect of temperature, it was found that the molar conductance increased with the temperature. Increases in the temperature resulted in the increase in ionic mobility. Additionally, a loss of structuredness led to the increased conductance at elevated temperatures. A rise in the molar conductance was significant for the binary mixtures that contained lower amounts of ionic liquids. After 50 mole% [bmim][MS], the molar conductance of the mixtures at different temperatures was not significantly higher. For ionic liquid containing 20 and 40 mole%, there was a rise in the molar conductance with the increased temperature, but no definite trend line was obtained. This finding suggests that the orderedness of the structured species decreased with the increase in temperature for these two systems. For 50, 60 and 80 mole% and pure IL, the increase in the molar conductance with temperature was more or less linear. The studies were found to be comparable with another report [77]. The increase in the molar conductance with the increase in temperature was due to an increased ionic mobility. Notably, the viscosity for the 80 mole% [bmim][MS]-containing mixture was higher than the pure IL, although the molar conductance for the 80 mole% mixture was also higher than that of the pure one. This behavior was due to the formation of hydrogen-bonded structures, whereby a proton transfer mechanism could occur for 80 mole% ionic liquid-containing mixture. We have plotted the molar conductance with the intention to determine the limiting molar conductance. Additionally, the conductivity–composition profile was similar to that observed by other researchers [88,89].

For an aqueous dilute solution, the molar conductance decreased with the increase in [bmim][MS] concentration, and this decrease continued up to 4.2 mM [bmim][MS] (Fig. 5B). The Debye–Hückell–Onsager equation was found to be valid in the dilute concentration region at up to 70 mM of [bmim][MS] (as shown in the inset of panel B). The value of the limiting molar conductance of [bmim][MS] was found to be 75.44 S cm^2 mol^{-1}. To the best of our knowledge, no reports on the limiting molar conductance of [bmim][MS] are present in the literature. According to the report by Wang et al. [90], the limiting molar conductance of [bmim][Br] at 298.15 K is 86.3 S cm^2 mol^{-1}. Inset of Fig. 5B shows the ($\log \Lambda^M$ vs. $\log \eta^{-1}$) profile, which is also known as the Walden formalism [91–93]. It states that the product of the limiting molar conductance Λ^M and the viscosity η is constant for infinitely dilute electrolyte solutions and is expressed as:

$$\Lambda^M \eta = C = \text{constant} \tag{11}$$

$$\log\ \Lambda^M = \log\ C + \log\ \eta^{-1} \tag{12}$$

The Walden rule relates the ionic mobilities of the ions to the fluidity of the medium through which the ion moves [94]. The trend of the Walden plot was found to be linear, which indicates the dependency of the viscosity on the molar conductance, with a slope of 1.314 ± 0.081 and an intercept of -0.700 ± 0.158. An ion pair association is not possible at that dilute concentration range, but as the concentration goes up, the viscosity of the solution increases and the molar conductance decreases.

3.5.2. Cyclic voltammetric studies

A representative cyclic voltammogram with a varied scan rate for an equimolar [bmim][MS] + water binary mixture at 298.15 K is shown in Fig. 7. The electrochemical window was found to be dependent on the scan rate. The peak current (i_p) varies linearly with the square root of the sweep rate (v) for a stable system [95]. However, in the present case, linear variations in the i_p vs. $v^{1/2}$ profile were not observed for all of the mixtures, as shown in the inset of Fig. 7. The i_p vs. $v^{1/2}$ profiles were linear for pure water and the pure ionic liquid. The results clearly indicate the non-ideality in the mixing behavior of the components. Additionally, it is evident

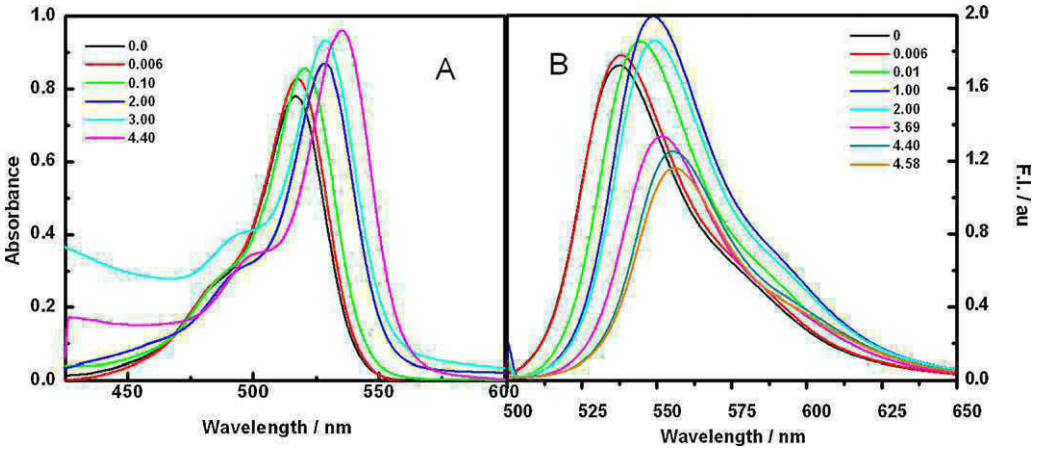

Fig. 8. Absorption (A) and emission (B) spectra of 10 μM eosin Y in the presence of different amount of [bmim][MS] in water at 298.15 K. The molar concentration of [bmim][MS] is indicated in the figure. Excitation wavelength (λ_{ex}): 500 nm.

from the figure that all of the combinations that comprise less than 50 mole% ionic liquid were not well organized/structured. There were positive deviations from the linearity for all of the mixtures (except the 1:4 mixture). As it has been previously mentioned for binary mixtures, water that is present at less than 50 mole% cannot greatly affect the orderedness of the IL [75]. That is why the extent of the deviation decreased with the increasing mole fraction of [bmim][MS].

3.6. Effect of [bmim][MS] on the spectral behavior of eosin Y (EY)

3.6.1. Absorption spectra

An aqueous solution of 10 μM EY exhibited a strong absorption peak at 517 nm with a faint shoulder at 495 nm [80]. The band at 517 nm corresponds to the monomeric form of the dye, while the 495-nm band was due to the formation of a dimer involving the stacking of two monomers [96]. The effect of [bmim][MS] on the absorption spectra of EY is shown in Fig. 8(A). The absorption spectra of EY were perturbed in the presence of varying amounts of [bmim][MS] in water, which indicated a change in the environment of the medium. With the progressive addition of [bmim][MS], a red shift occurred in the major absorption peak of EY. In the lower concentration range (<10 mM), the intensity of EY increased without any significant shift in the peak position. Above 10 mM [bmim][MS], a red shift in the spectra of EY was initiated. No previous studies involving the effect of an ionic liquid on the absorption spectra of the xanthene dye are available. Recent studies of Adhikari et al. [1,50,51] revealed that a red shift in the absorption spectra of coumarin 480 (a solvatochromic dye) that was dissolved in [bmim][BF_4] occurred compared to its spectra in benzene. Spectral studies on some xanthene dyes were performed systematically in different solvents and in the presence of different aqueous surfactant solutions by De et al. [80], Bhowmik and Ganguly [96] and Chakraborty and Panda [97]. They observed a red shift in the spectra of EY and erythrosin B with the progressive addition of a cationic surfactant hexadecyltrimethylammonium bromide (CTAB). A red shift in the absorption spectra for the xanthenes dyes could also occur in less polar solvent compared to water. According to Bhowmik and Ganguly [96], the shift in the absorption spectra was due to an additional (other than electrostatic interaction) contributory effect in the altered polarity of the media. Therefore, we believe that an electrostatic attraction occurs between the [bmim] cation and EY in the ground state. Additionally, the ionic liquid, having an organic moiety, alters the solvent polarity. Hence, the resultant spectral shift of EY in the presence of [bmim][MS] was due to an electrostatic attraction and altered solvent polarity. Additionally, as Stark et al. [75] have proposed, there might be a tail–tail aggregation formation in the system that also leads to the resultant spectral shift, which is similar to what happened in case of the micelles.

3.6.2. Fluorescence spectra

The fluorescence spectra of EY in the presence of varying amounts of an aqueous solution of [bmim][MS] are presented in Fig. 8(B). The absorption and emission pattern of EY were more or less similar upto 1.0 M [bmim][MS] in water. When the IL concentration exceeded the concentration of 1.0 M, a progressive quenching of fluorescence occurred with the increase in the IL concentration. However, the red shift with the increasing IL concentration was monotonous up to at least 4.58 M. These studies reveal a different mechanism for the formation of exciplex above 1.0 M [bmim][MS]. We believe that some significant structural changes occur above this threshold concentration. The aggregation of different ILs in an aqueous medium with varying alkyl chain length, cations and anions has been reported by different authors [30–32,36,37,40,41,44,48,75]. According to them, aggregated species could form around the 1.0 M concentration for [bmim]-based ILs. These aggregates are comprised of small clusters of 8–10 ionic liquid cations. We believe that, due to the formation of these clustered aggregates, a significant change in the viscosity of the medium, which subsequently retarded the excitation process.

Fig. 9 describes the fluorescence decay profile of the aqueous eosin Y solution in the absence and presence of [bmim][MS]. The decay profile was found to be single exponential in nature. The fluorescence lifetime changed from 2.15 ns for EY in water to 4.8 ns in 1.0 M IL in water. An enhanced viscosity might be the causative factor that altered the excited lifetime of EY. Therefore, it could be concluded that the transition processes in the excited and ground states were affected by the viscosity of the medium. The solvent polarity could also play a role [1,50,51,59]. Fig. 10 shows combined representation for the variation of excited state lifetime and anisotropy with the increasing concentration of [bmim][MS] in water. Both the lifetime and anisotropy did not change significantly up to 1.0 M [bmim][MS] aqueous solution. When the IL concentration, the anisotropy value increased sharply. In the inset of Fig. 10, the variation of the viscosity with the concentration is shown to allow a comparison with the anisotropy–concentration profile. The results suggest that there occurred a significant change in the viscosity of medium above 1 M [bmim][MS] in water. The increased viscosity was due to the formation of such clustered aggregates [38,40,42,43,47,48,75,80,90,98–100]. As viscosity of a medium governs the fluorescence anisotropy of a dye [79], the fluorescence

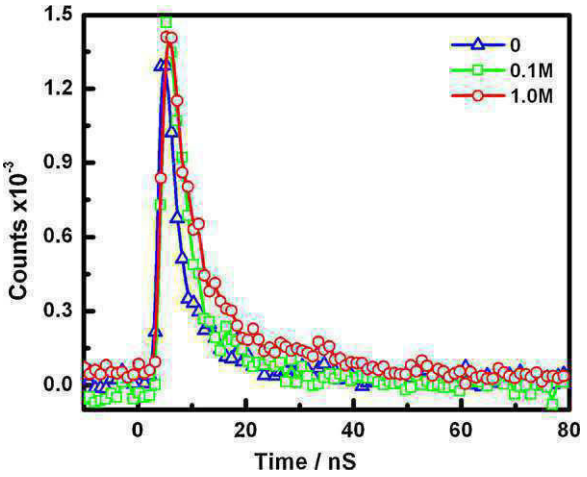

Fig. 9. Fluorescence decay curves of 10 μM eosin Y in the presence of different concentrations of [bmim][MS] in water at 298.15 K. The concentrations of [bmim][MS] are indicated in the figure. Excitation wavelength (λ_{ex}): 500 nm and emission wavelength (λ_{em}): 537 nm.

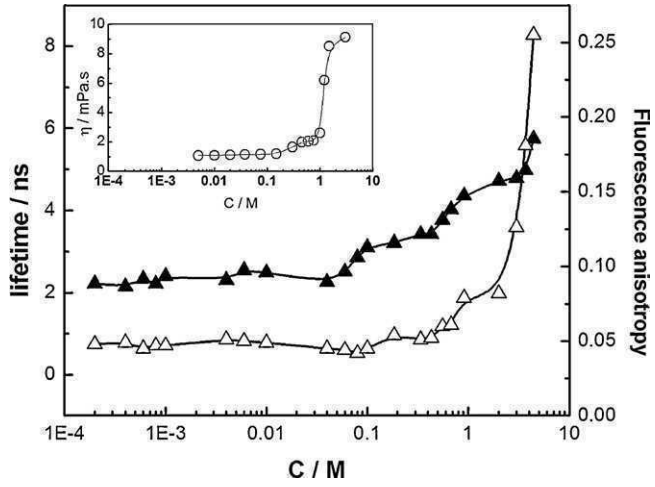

Fig. 10. Variation of lifetime (▲) and fluorescence anisotropy (△) for 10 μM eosin Y with concentration (C) of [bmim][MS] in water at 298 K. Excitation wavelength (λ_{ex}): 500 nm and emission wavelength (λ_{em}): 537 nm. Inset: viscosity (η) – [bmim][MS] concentration profile.

anisotropy enhancement was certainly due to the enhanced viscosity of the media.

4. Summary and conclusion

Physicochemical investigations on the binary mixture of [bmim][MS] + water were carried out both in the dilute and concentrated regime of [bmim][MS] using different techniques. There occurred a synergistic interaction between the [bmim][MS] and water. The surface tension decreased monotonously with a halt at 0.3 M [bmim][MS]. The absorption and emission spectral behaviors were significantly different. The steady state fluorescence anisotropy and excited state lifetime were dependent on the concentration of [bmim][MS] in water. It was finally concluded that initially increasing the IL concentration led to the formation of an ion-pair, whereby the cationic component, which was surface active, was interfacially absorbed. Micelle-like aggregates were formed above a certain concentration, which was similar to ionic clusters. Above 50 mole% ionic liquid, a three dimensional quasi crystal-like network was formed which deactivates the water molecules.

Acknowledgments

The work has been financially supported by the Department of Science and Technology (DST), Govt. of India, through a research grant (No. SR/S1/PC/24/2008). S. Paul sincerely acknowledges the receipt of a Junior Research Fellowship from the DST. We sincerely acknowledge Dr. Gautam Patra from the Department of Chemistry, Bijaygarh Jyotish Roy College, Kolkata for his kind help regarding the electrochemical measurement.

Appendix A. Supplementary data

Supplementary data associated with this article can be found, in the online version, at doi:10.1016/j.colsurfa.2012.01.034.

References

[1] A. Adhikari, K. Sahu, S. Dey, S. Ghosh, U. Mandal, K. Bhattacharyya, Femtosecond solvation dynamics in a neat ionic liquid and ionic liquid microemulsion: excitation wavelength dependence, J. Phys. Chem. B 111 (2007) 12809–12816.
[2] F.M. Kerton, Alternative Solvents for Green Chemistry, RSC, Cambridge, 2009.
[3] H. Ohno, Electrochemical Aspects of Ionic Liquids, 2nd ed., Wiley-VCH, Verlag GmbH, 2011.
[4] C. Reichardt, T. Welton, Solvents and Solvent Effects in Organic Chemistry, Wiley-VCH, Weinheim, 2010.
[5] S.H. Schofer, N. Kaftzik, P. Wasserscheid, U. Kragl, Enzyme catalysis in ionic liquids: lipase catalysed kinetic resolution of 1-phenylethanol with improved enantioselectivity, Chem. Commun. (2001) 425–426.
[6] P. Wasserscheid, T. Welton, Ionic Liquids in Synthesis, 2nd ed., Wiley-VCH, Weinheim, 2007.
[7] D. Wei, A. Ivaska, Applications of ionic liquids in electrochemical sensors, Anal. Chim. Acta 607 (2008) 126–135.
[8] T. Welton, Room-temperature ionic liquids. Solvents for synthesis and catalysis, Chem. Rev. 99 (1999) 2071–2084.
[9] K. Yoo, H. Choi, D.D. Dionysiou, Ionic liquid assisted preparation of nanostructured TiO_2 particles, Chem. Commun. (2004) 2000–2001.
[10] A. Balducci, F. Soavi, M. Mastragostino, The use of ionic liquids as solvent-free green electrolytes for hybrid supercapacitors, Appl. Phys. A: Mater. Sci. Process. 82 (2006) 627–632.
[11] A.P. Fröba, H. Kremer, A. Leipertz, Density, refractive index, interfacial tension and viscosity of ionic liquids [EMIM][$EtSO_4$], [EMIM][NTf_2], [EMIM][$N(CN)_2$], and [OMA][NTf_2] in dependence on temperature at atmospheric pressure, J. Phys. Chem. B 112 (2008) 12420–12430.
[12] A.P. Fröba, P. Wasserscheid, D. Gerhard, H. Kremer, A. Leipertz, Revealing the influence of the strength of coulomb interactions on the viscosity and interfacial tension of ionic liquid cosolvent mixtures, J. Phys. Chem. B 111 (2007) 12817–12822.
[13] T. Welton, Room temperature ionic liquids: solvents for synthesis and catalysis, Chem. Rev. 99 (1999) 2071.
[14] S.H. Schofer, N. Kaftzik, P. Wasserschied, U. Kragl, Enzyme catalysis in ionic liquids: lipase catalyzed kinetic resolution of 1-phenylthenol with improved enantioselectivity, Chem. Commun. (2001) 425.
[15] A.M. Scurto, S.N.V.K. Aki, J.F. Brennecke, CO_2 as a separation switch for ionic liquid/organic mixtures, J. Am. Chem. Soc. 124 (2002) 10276–10277.
[16] S. Zhang, X. Li, H. Chen, J. Wang, J. Zhang, M. Zhang, Determination of physical properties for the binary system of 1-ethyl-3-methylimidazolium tetrafluoroborate + H_2O, J. Chem. Eng. Data 49 (2004) 760–764.
[17] J. Dupont, R.F. de Souza, P.A.Z. Suarez, Ionic Liquid, (Molten salt) phase organometallic catalysis, Chem. Rev. 102 (2002) 3667–3692.
[18] C. Aliaga, S. Baldelli, A sum frequency generation study of the room-temperature ionic liquid–titanium dioxide interface, J. Phys. Chem. C 112 (2008) 3064–3072.
[19] A. Samanta, Solvation dynamics in ionic liquids: what we have learned from the dynamic fluorescence stokes shift studies, J. Phys. Chem. Lett. 1 (2010) 1557–1562.
[20] P. Mukherjee, J.A. Crank, P.S. Sharma, A.B. Wijeratne, R. Adhikary, S. Bose, D.W. Armstrong, J.W. Petrich, Dynamic solvation in phosphonium ionic liquids: comparison of bulk and micellar systems and considerations for the construction of the solvation correlation function $C(t)$, J. Phys. Chem. B 112 (2008) 3390–3396.
[21] P. Mukherjee, J.A. Crank, M. Halder, D.W. Armstrong, J.W. Petrich, Assessing the roles of the constituents of ionic liquids in dynamic solvation:comparison of an ionic liquid in micellar and bulk form, J. Phys. Chem. A 110 (2006) 10725–10730.
[22] M. Halder, L.S. Headley, P. Mukherjee, X. Song, J.W. Petrich, Experimental and theoretical investigations of solvation dynamics of ionic fluids: appropriateness of dielectric theory and the role of DC conductivity, J. Phys. Chem. A 110 (2006) 8623–8626.
[23] L.S. Headley, P. Mukherjee, J.L. Anderson, R. Ding, M. Halder, D.W. Armstrong, X. Song, J.W. Petrich, Dynamic solvation in imidazolium-based ionic liquids on short time scales, J. Phys. Chem. A 110 (2006) 9549–9554.

[24] P.J. Carvalho, T. Regueira, L.M.N.B.F. Santos, J. Fernandez, J.A.P. Coutinho, Effect of water on the viscosities and densities of 1-butyl-3-methylimidazolium dicyanamide and 1-butyl-3-methylimidazolium tricyanomethane at atmospheric pressure, J. Chem. Eng. Data 55 (2009) 645–652.
[25] B.D. Fitchett, T.N. Knepp, J.C. Conboy, 1-Alkyl-3-methylimidazolium *bis*(perfluoroalkylsulfonyl)imide water-immiscible ionic liquids, J. Electrochem. Soc. 151 (2004) E219–E225.
[26] Y. Lauw, M.D. Horne, T. Rodopoulos, N.A.S. Webster, B. Minofar, A. Nelson, X-ray reflectometry studies on the effect of water on the surface structure of $[C_4mpyr][NTf_2]$ ionic liquid, Phys. Chem. Chem. Phys. 11 (2009) 11507–11514.
[27] J. Lehmann, M.H. Rausch, A. Leipertz, A.P. Fröba, Densities and excess molar volumes for binary mixtures of ionic liquid 1-ethyl-3-methylimidazolium ethylsulfate with solvents, J. Chem. Eng. Data 55 (2010) 4068–4074.
[28] I.S. Martinez, S. Baldelli, On the arrangement of ions in imidazolium-based room temperature ionic liquids at the gas–liquid interface, using sum frequency generation, surface potential, and surface tension measurements, J. Phys. Chem. C 114 (2010) 11564–11575.
[29] V. Najdanovic-Visak, J.M.S.S. Esperana, L. s.P.N. Rebelo, M. Nunes da Ponte, H.J.R. Guedes, K.R. Seddon, H.N.C. de Sousa, J. Szydlowski, Pressure, isotope and water co-solvent effects in liquid–liquid equilibria of (ionic liquid + alcohol) systems, J. Phys. Chem. B 107 (2003) 12797–12807.
[30] L.P.N. Rebelo, V. Najdanovic-Visak, Z.P. Visak, M. Nunes da Ponte, J. Szydlowski, C.A. Cerdeirina, J. Troncoso, L. Romani, J.M.S.S. Esperanca, H.J.R. Guedes, H.C. de Sousa, A detailed thermodynamic analysis of $[C_4mim][BF_4]$ + water as a case study to model ionic liquid aqueous solutions, Green Chem. 6 (2004) 369–381.
[31] J. Sung, Y. Jeon, D. Kim, T. Iwahashi, T. Iimori, K. Seki, Y. Ouchi, Air–liquid interface of ionic liquid + H_2O binary system studied by surface tension measurement and sum-frequency generation spectroscopy, Chem. Phys. Lett. 406 (2005) 495–500.
[32] J. Sung, Y. Jeon, D. Kim, T. Iwahashi, K. Seki, T. Iimori, Y. Ouchi, Gibbs monolayer of ionic liquid + H_2O mixtures studied by surface tension measurement and sum-frequency generation spectroscopy, Colloids Surf. A: Physicochem. Eng. Aspects 284–285 (2006) 84–88.
[33] S.N.P.M. Ventura, C.M.S.S. Neves, M.G. Freire, I.M. Marrucho, J. Oliveira, J.A.P. Coutinho, Evaluation of anion influence on the formation and extraction capacity of ionic-liquid-based aqueous biphasic systems, J. Phys. Chem. B 113 (2009) 9304–9310.
[34] J.A. Widegren, A. Laesecke, J.W. Magee, The effect of dissolved water on the viscosities of hydrophobic room-temperature ionic liquids, Chem. Commun. (2005) 1610–1612.
[35] M.S. Kelkar, E.J. Maginn, Effect of temperature and water content on the shear viscosity of the ionic liquid 1-ethyl-3-methylimidazolium bis(trifluoromethanesulfonyl)imide as studied by atomistic simulations, J. Phys. Chem. B 111 (2007) 4867–4876.
[36] W. Liu, L. Cheng, Y. Zhang, H. Wang, M. Yu, The physical properties of aqueous solution of room-temperature ionic liquids based on imidazolium: database and evaluation, J. Mol. Liq. 140 (2008) 68–72.
[37] W. Liu, T. Zhao, Y. Zhang, H. Wang, M. Yu, The physical properties of aqueous solutions of the ionic liquid $[BMIM][BF_4]$, J. Sol. Chem. 35 (2006) 1337–1346.
[38] A. Cornellas, L. Perez, F. Comelles, I. Ribosa, A. Manresa, M.T. Garcia, Self-aggregation and antimicrobial activity of imidazolium and pyridinium based ionic liquids in aqueous solution, J. Colloid Interface Sci. 355 (2011) 164–171.
[39] U. Domanska, A. Pobudkowska, M. Rogalski, Surface tension of binary mixtures of imidazolium and ammonium based ionic liquids with alcohols, or water: cation anion effect, J. Colloid Interface Sci. 322 (2008) 342–350.
[40] E. Ghasemian, M. Najafi, A.A. Rafati, Z. Felegari, Effect of electrolytes on surface tension and surface adsorption of 1-hexyl-3-methylimidazolium chloride ionic liquid in aqueous solution, J. Chem. Thermodyn. 42 (2010) 962–966.
[41] C. Jungnickel, J. Luczak, J. Ranke, J.F. Fernández, A. Müller, J. Thöming, Micelle formation of imidazolium ionic liquids in aqueous solution, Colloids Surf. A: Physicochem. Eng. Aspects 316 (2008) 278–284.
[42] X.-W. Li, Y.-A. Gao, J. Liu, L.-Q. Zheng, B. Chen, L.-Z. Wu, C.-H. Tung, Aggregation behavior of a chiral long-chain ionic liquid in aqueous solution, J. Colloid Interface Sci. 343 (2010) 94–101.
[43] A. Modaressi, H. Sifaoui, M. Mielcarz, U. Domanska, M. Rogalski, Influence of the molecular structure on the aggregation of imidazolium ionic liquids in aqueous solutions, Colloids Surf. A: Physicochem. Eng. Aspects 302 (2007) 181–185.
[44] L.A.S. Ries, F.A. do Amaral, K. Matos, E.M.A. Martini, M.O. de Souza, R.F. de Souza, Evidence of change in the molecular organization of 1-n-butyl-3-methylimidazolium tetrafluoroborate ionic liquid solutions with the addition of water, Polyhedron 27 (2008) 3287–3293.
[45] N.M. Vaghela, N.V. Sastry, V.K. Aswal, Effect of additives on the surface active and morphological features of 1-octyl-3-methylimidazolium halide aggregates in aqueous media, Colloids Surf. A: Physicochem. Eng. Aspects 373 (2011) 101–109.
[46] A.M. O'Mahony, D.S. Silvester, L. Aldous, C. Hardacre, R.G. Compton, Effect of water on the electrochemical window and potential limits of room-temperature ionic liquids, J. Chem. Eng. Data 53 (2008) 2884–2891.
[47] J. Bowers, C.P. Butts, P.J. Martin, M.C. Vergara-Gutierrez, R.K. Heenan, Aggregation behavior of aqueous solutions of ionic liquids, Langmuir 20 (2004) 2191–2198.
[48] T. Singh, A. Kumar, Aggregation behavior of ionic liquids in aqueous solutions: effect of alkyl chain length, cations, and anions, J. Phys. Chem. B 111 (2007) 7843–7851.
[49] D.S. Silvester, L. Aldous, C. Hardacre, R.G. Compton, An electrochemical study of the oxidation of hydrogen at platinum electrodes in several room temperature ionic liquids, J. Phys. Chem. B 111 (2007) 5000–5007.
[50] A. Adhikari, S. Dey, D.K. Das, U. Mandal, S. Ghosh, K. Bhattacharyya, Solvation dynamics in ionic liquid swollen P123 triblock copolymer micelle: a femtosecond excitation wavelength dependence study, J. Phys. Chem. B 112 (2008) 6350–6357.
[51] A. Adhikari, D.K. Das, D.K. Sasmal, K. Bhattacharyya, Ultrafast fret in a room temperature ionic liquid microemulsion: a femtosecond excitation wavelength dependence study, J. Phys. Chem. A 113 (2009) 3737–3743.
[52] D. Seth, A. Chakraborty, P. Setua, N. Sarkar, Dynamics of solvent and rotational relaxation of coumarin-153 in room-temperature ionic liquid 1-butyl-3-methyl imidazolium tetrafluoroborate confined in poly(oxyethylene glycol) ethers containing micelles, J. Phys. Chem. B 111 (2007) 4781–4787.
[53] D. Seth, A. Chakraborty, P. Setua, N. Sarkar, Interaction of ionic liquid with water in ternary microemulsions (Triton X-100/Water/1-Butyl-3-methylimidazolium hexafluorophosphate) probed by solvent and rotational relaxation of coumarin 153 and coumarin 151, Langmuir 22 (2006) 7768–7775.
[54] D. Chakrabarty, D. Seth, A. Chakraborty, N. Sarkar, Dynamics of solvation and rotational relaxation of coumarin 153 in ionic liquid confined nanometer-sized microemulsions, J. Phys. Chem. B 109 (2005) 5753–5758.
[55] P.K. Mandal, M. Sarkar, A. Samanta, Excitation-wavelength-dependent fluorescence behavior of some dipolar molecules in room-temperature ionic liquids, J. Phys. Chem. A 108 (2004) 9048–9053.
[56] D. Seth, P. Setua, A. Chakraborty, N. Sarkar, Solvent relaxation of a room-temperature ionic liquid $[bmim][PF_6]$ confined in a ternary microemulsion, J. Chem. Sci. 119 (2007) 105–111.
[57] D. Seth, A. Chakraborty, P. Setua, N. Sarkar, Interaction of ionic liquid with water with variation of water content in 1-butyl-3-methyl-imidazolium hexafluorophosphate ($[bmim][PF_6]$)/TX-100/water ternary microemulsions monitored by solvent and rotational relaxation of coumarin 153 and coumarin 490, J. Chem. Phys. 126 (2007) 224512–224523.
[58] R. Karmakar, A. Samanta, Solvation dynamics of coumarin-153 in a room-temperature ionic liquid, J. Phys. Chem. A 106 (2002) 4447–4452.
[59] P.K. Mandal, A. Samanta, Fluorescence studies in a pyrrolidinium ionic liquid: polarity of the medium and solvation dynamics, J. Phys. Chem. B 109 (2005) 15172–15177.
[60] A. Samanta, Dynamic stokes shift and excitation wavelength dependent fluorescence of dipolar molecules in room temperature ionic liquids, J. Phys. Chem. B 110 (2006) 13704–13716.
[61] K. Santhosh, A. Samanta, Modulation of the excited state intramolecular electron transfer reaction and dual fluorescence of crystal violet lactone in room temperature ionic liquids, J. Phys. Chem. B 114 (2010) 9195–9200.
[62] R. Karmakar, A. Samanta, Steady-State, time-resolved fluorescence behavior of C153 and PRODAN in room-temperature ionic liquids, J. Phys. Chem. A 106 (2002) 6670–6675.
[63] B. Bhattacharya, A. Samanta, Excited-state proton-transfer dynamics of 7-hydroxyquinoline in room temperature ionic liquids, J. Phys. Chem. B 112 (2008) 10101–10106.
[64] A. Paul, A. Samanta, Free volume dependence of the internal rotation of a molecular rotor probe in room temperature ionic liquids, J. Phys. Chem. B 112 (2008) 16626–16632.
[65] R. Karmakar, A. Samanta, Dynamics of solvation of the fluorescent state of some electron donor–acceptor molecules in room temperature ionic liquids, $[BMIM][(CF_3SO_2)_2N]$ and $[EMIM][(CF_3SO_2)_2N]$, J. Phys. Chem. A 107 (2003) 7340–7346.
[66] A. Paul, M. Sarkar, D.C. Khara, T. Kamijo, A. Yamaguchi, N. Teramae, A. Samanta, Solvation dynamics of a surfactant probe in mesostructured silica-surfactant nanocomposites, Chem. Phys. Lett. 469 (2009) 71–75.
[67] A. Ray, K. Santhosh, S. Chattopadhyay, A. Samanta, S. Bhattacharya, Spectroscopic, theoretical investigations on effective and selective interaction of fullerenes C60 and C70 with a derivatized Zn–phthalocyanine: stabilization of charge-recombined state by side-on approach of C70, J. Phys. Chem. A 114 (2010) 5544–5550.
[68] A. Paul, A. Samanta, Effect of nonpolar solvents on the solute rotation and solvation dynamics in an imidazolium ionic liquid, J. Phys. Chem. B 112 (2007) 947–953.
[69] Y. a. Gao, N. Li, L. Zheng, X. Zhao, S. Zhang, B. Han, W. Hou, G. Li, A cyclic voltammetric technique for the detection of micro-regions of $[bmim][PF_6]$/Tween 20/H_2O microemulsions and their performance characterization by UV–vis spectroscopy, Green Chem. 8 (2006) 43–49.
[70] A. Marciniak, Influence of anion structure on the liquid–liquid equilibria of 1-ethyl-3-methyl-imidazolium cation based ionic liquid-hydrocarbon binary systems, J. Chem. Eng. Data 56 (2011) 368–374.
[71] C.S. Santos, S. Rivera-Rubero, S. Dibrov, S. Baldelli, Ions at the surface of a room-temperature ionic liquid, J. Phys. Chem. C 111 (2007) 7682–7691.
[72] J. Yang, Q. Zhang, L. Zhu, S. Zhang, J. Li, X. Zhang, Y. Deng, Novel ionic liquid crystals based on n-alkylcaprolactam as cations, Chem. Mater. 19 (2007) 2544–2550.
[73] S. Rivera-Rubero, S. Baldelli, Surface characterization of 1-butyl-3-methylimidazolium Br^-, I^-, PF_6^-, BF_4^-, $(CF_3SO_2)_2N^-$, SCN^-, $CH_3SO_3^-$,

$CH_3SO_4^-$, and $(CN)_2N^-$ ionic liquids by sum frequency generation, J. Phys. Chem. B 110 (2006) 4756–4765.
[74] E. Rilo, J. Pico, S. García-Garabal, L.M. Varela, O. Cabeza, Density and surface tension in binary mixtures of C_nMIM-BF_4 ionic liquids with water and ethanol, Fluid Phase Equilib. 285 (2009) 83–89.
[75] A. Stark, A.W. Zidell, M.M. Hoffmann, Is the ionic liquid 1-ethyl-3-methylimidazolium methanesulfonate [emim][$MeSO_3$] capable of rigidly binding water, J. Mol. Liq. 160 (2011) 166–179.
[76] A. Stark, P. Wasserscheid, Handbook of Green Chemistry – Green Solvents–Ionic Liquids, vol. 6, Wiley-VCH, 2010, pp. 85–113.
[77] H. Tokuda, K. Hayamizu, K. Ishii, M.A.B.H. Susan, M. Watanabe, Physicochemical properties and structures of room temperature ionic liquids. 1. Variation of anionic species, J. Phys. Chem. B 108 (2004) 16593–16600.
[78] A. Chakrabarty, A. Mallick, B. Haldar, P. Das, N. Chattopadhyay, Binding interaction of a biological photosensitizer with serum albumins: a biophysical study, Biomacromolecules 8 (2007) 920–927.
[79] A. Mallick, B. Haldar, N. Chattopadhyay, Spectroscopic investigation on the interaction of ICT probe 3-acetyl-4-oxo-6,7-dihydro-12h indolo-[2,3] quinolizine with serum albumins, J. Phys. Chem. B 109 (2005) 14683–14690.
[80] S. De, S. Das, A. Girigoswami, Environmental effects on the aggregation of some xanthene dyes used in lasers, Spectrochim. Acta A 61 (2005) 1821–1833.
[81] Q. Zhou, L.-S. Wang, H.-P. Chen, Densities and viscosities of 1-butyl-3-methylimidazolium tetrafluoroborate + H_2O binary mixtures from (303.15 to 353.15) K, J. Chem. Eng. Data 51 (2006) 905–908.
[82] T. Méndez-Morales, J.S. Carrete, O.S. Cabeza, L.J. Gallego, L.M. Varela, Molecular dynamics simulation of the structure and dynamics of water–1-alkyl-3-methylimidazolium ionic liquid mixtures, J. Phys. Chem. B 115 (2011) 6995–7008.
[83] H. Shekaari, S.S. Mousavi, Volumetric properties of ionic liquid 1,3-dimethylimidazolium methyl sulfate + molecular solvents at T = (298.15–328.15) K, Fluid Phase Equilib. 291 (2010) 201–207.
[84] X.-X. Li, Y.-J. Hu, G. Liu, Density and viscosity of the binary mixture of triethylene glycol monobutyl ether + water from (293.15 to 333.15) K at atmospheric pressure, J. Chem. Eng. Data 55 (2009) 1045–1048.
[85] M.G. Freire, P.J. Carvalho, A.M. Fernandes, I.M. Marrucho, A.J. Queimada, J.A.P. Coutinho, Surface tensions of imidazolium based ionic liquids: anion, cation, temperature and water effect, J. Colloid Interface Sci. 314 (2007) 621–630.
[86] G. Law, P.R. Watson, Surface tension measurements of n-alkylimidazolium ionic liquids, Langmuir 17 (2001) 6138–6141.
[87] A.W. Adamson, A.P. Gast, Physical Chemistry of Surfaces, 6th ed., Wiley, New York, 1997.
[88] J. Vila, P. Ginés, E. Rilo, O. Cabeza, L.M. Varela, Great increase of the electrical conductivity of ionic liquids in aqueous solutions, Fluid Phase Equilib. 247 (2006) 32–39.
[89] J. Vila, E. Rilo, L. Segade, O. Cabeza, L.M. Varela, Electrical conductivity of aqueous solutions of aluminum salts, Phys. Rev. E 71 (2005) 031201.
[90] J. Wang, H. Wang, S. Zhang, H. Zhang, Y. Zhao, Conductivities, volumes, fluorescenceand aggregation behavior of ionic liquids [C_4mim][BF_4] and [$C_n$mim]Br (n = 4, 6, 8, 10, 12) in aqueous solutions, J. Phys. Chem. B 111 (2007) 6181–6188.
[91] C. Schreiner, S. Zugmann, R. Hartl, H.J. Gores, Fractional Walden rule for ionic liquids: examples from recent measurements and a critique of the so-called ideal KCl line for the Walden plot, J. Chem. Eng. Data 55 (2009) 1784–1788.
[92] D.R. MacFarlane, M. Forsyth, E.I. Izgorodina, A.P. Abbott, G. Annat, K. Fraser, On the concept of ionicity in ionic liquids, Phys. Chem. Chem. Phys. 11 (2009) 4962–4967.
[93] C. Zhao, G. Burrell, A.A.J. Torriero, F. Separovic, N.F. Dunlop, D.R. MacFarlane, A.M. Bond, Electrochemistry of room temperature protic ionic liquids, J. Phys. Chem. B 112 (2008) 6923–6936.
[94] M. Yoshizawa, W. Xu, C.A. Angell, Ionic liquids by proton transfer: vapor pressure, conductivity, and the relevance of (pKa from aqueous solutions, J. Am. Chem. Soc. 125 (2003) 15411–15419.
[95] A.J. Bard, L.R. Faulkner, Electrochemical Methods: Fundamentals and Applications, 2nd ed., John Wiley & Sons, New York, 2001.
[96] B.B. Bhowmik, P. Ganguly, Photophysics of xanthene dyes in surfactant solution, Spectrochim. Acta A 61 (2005) 1997–2003.
[97] M. Chakraborty, A.K. Panda, Spectral behaviour of eosin Y in different solvents and aqueous surfactant media, Spectrochim. Acta A 81 (2011) 458–465.
[98] M. Anouti, J. Jones, A. Boisset, J. Jacquemin, M. Caillon-Caravanier, D. Lemordant, Aggregation behavior in water of new imidazolium and pyrrolidinium alkycarboxylates protic ionic liquids, J. Colloid Interface Sci. 340 (2009) 104–111.
[99] Y. Gao, N. Li, S. Zhang, L. Zheng, X. Li, B. Dong, L. Yu, Organic solvents induce the formation of oil-in-ionic liquid microemulsion aggregations, J. Phys. Chem. B 113 (2009) 1389–1395.
[100] J. Wu, N. Li, L. Zheng, X. Li, Y.a. Gao, T. Inoue, Aggregation behavior of polyoxyethylene (20) sorbitan monolaurate (Tween 20) in imidazolium based ionic liquids, Langmuir 24 (2008) 9314–9322.

Colloids and Surfaces A: Physicochem. Eng. Aspects 419 (2013) 113–124

Contents lists available at SciVerse ScienceDirect

Colloids and Surfaces A: Physicochemical and Engineering Aspects

journal homepage: www.elsevier.com/locate/colsurfa

Physico-chemical studies on ionic liquid microemulsion: Phase manifestation, formation dynamics, size, viscosity, percolation of electrical conductance and spectroscopic investigations on 1-butyl-3-methyl imidazolium methanesulfonate + water/Tween 20 + n-pentanol/n-heptane pseudoternary system

Sujoy Paul, Amiya Kumar Panda*

Department of Chemistry, University of North Bengal, Darjeeling - 734 013, West Bengal, India

HIGHLIGHTS

- [bmim][MS] + water/Tween 20 + n-pentanol/n-heptane microemulsion was studied.
- Phase diagram, dilution, DLS, viscosity, conductance, spectral studies were done.
- Properties were found to be dependent on the composition of IL and water.
- Studies using IL + Water in polar domain of the microemulsion are not common.

GRAPHICAL ABSTRACT

Variation in the different physicochemical properties alongwith the proposed model for the formation of ([bmim][MS] + water)/Tween 20 + n-pentanol)/nheptane polar domain-in-oil microemulsion system.

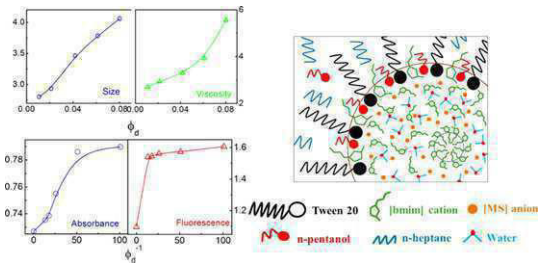

ARTICLE INFO

Article history:
Received 22 August 2012
Received in revised form
11 November 2012
Accepted 25 November 2012
Available online xxx

Keywords:
Microemulsion
Ionic liquid
Polar domain
Structural parameter
Spectroscopy

ABSTRACT

Combined phase behavior, method of dilution, viscosity, dynamic light scattering, electrical conductance and spectroscopic probing techniques were employed in understanding the physicochemical properties of pseudo ternary microemulsion system 1-butyl-3-methyl imidazolium methanesulfonate ([bmim][MS] ± water)/(Tween 20 + n-pentanol)/n-heptane. Phase manifestation revealed that the area under the clear region depended on ionic liquid (IL)/water mole ratio. Thermodynamic and structural parameters for the formation of (IL + water)-in-oil μE system were evaluated employing the method of dilution at different [polar domain]/[Tween 20] mole ratio and temperature; the parameters depended on the composition of the polar domain. IL + water comprising μE behaved differently, compared to the conventional water-in-oil μE system, especially at higher mole fraction of IL. Both the size and viscosity increased with the increasing volume fraction of the dispersed phase (IL + water), while they decreased with increasing temperature. Although having IL, the μEs were less conducting due to the strong interaction between the IL cation and the oxyethylene groups of the surfactants. Formation of micelle like aggregates within the polar domain further suppressed the conductivity. Combined studies on the absorption and emission spectra of eosinY, along with the excited state lifetime and anisotropy measurements, revealed the existence of different states of IL + water in the polar domain.

* Corresponding author. Tel.: +91 9433347210; fax: +91 353 2699001.
E-mail address: akpanda1@yahoo.com (A.K. Panda).

0927-7757/$ – see front matter © 2012 Elsevier B.V. All rights reserved.
http://dx.doi.org/10.1016/j.colsurfa.2012.11.061

1. Introduction

Ionic liquids (ILs) are environmentally benign substances [1] with some specific properties, viz., low melting point (less than 100 °C, ionic nature, low volatility and easy recyclability, etc., for which they have gained special pedigree as "green solvent" [2]. ILs are gaining importance for their applications, *viz.*, as alternate solvent for chemical reaction and separation [3], in electrochemistry [4] and nanoparticle synthesis [5], etc. Advantages of using IL as media for chemical reaction have been reviewed by Hao [6] and Welton [7]. Imidazolium based ILs are used because of its tunability; tailor made ILs can be prepared using imidazolium cation. However, use of neat IL has some limitations; they are inefficient in dissolving a wide variety of compounds [8]. This could be overcome by using them in the form of microemulsion (μE). The term μE was first coined by Schülman [9] and subsequently by Lindman and Danielsson [10]. μE is defined as thermodynamically stable, clear and isotropic dispersion of one liquid into another immiscible liquid stabilized by a surfactant monolayer [11–14]. μEs also find various applications in the field of cosmetics, pharmaceuticals, chemical reaction in compartmentalized systems and synthesis of nanoparticles. Although a large number of articles on μE are available in the literature, however the review works of Moulik et al. [15–17], Gradzielsky et al. [18], Stubenrauch et al. [19], Fanun et al. [20] and Lindman et al. [21,22] are worth reading.

The limitations of ILs, with respect to their capabilities in dissolving a wide variety of compounds, can easily be overcome through the formation of μE [23]. Research works involving IL microemulsion are ever increasing [11,24–30]. Han and co-workers [31] first reported the formation of μE comprising IL. Very recently Sarkar and co-workers [32] have reported a new strategy to prepare IL-in-oil μEs. Different review works on IL μEs are available in the literature [2,6,12,33–35]. IL based μEs in drug formulation has been explored by the research group of Moniruzzaman et al. [36] and Althanyan et al. [37]. Eastoe et al. [11], for the first time, have reported the characterization of IL μE using small angle neutron scattering (SANS) technique. Koetz and co-workers [33] have studied the structure of IL modified μE. Gao et al. [8,38,39] undertaken extensive works on μEs comprising [bmim][PF_6] and water by different techniques. While Friberg et al. [12] have reported about the works on [bmim][BF_4] based μE, the structural studies of [bmim][BF_4]-in-oil μE have been reported by Gao et al. [40]. IL-in-oil μEs have also been extensively studied by Zheng and co-workers [41] using Triton X-100 and Tween 20. In the work of Gao et al. [39] comparative studies between the properties of microemulsions comprising TX-100 and Tween 20 have been reported. In another work of Zheng et al. [42] extensive investigation were carried out on IL μE comprising Tween 80 as surfactant. It was proposed that the imidazolium cation can get coordinated with the lone pair of electrons of oxyethylene groups in Triton X-100 or Tween 20 [23]. Such interactions can lead to the formation of structured/rigid/organized entities. Subsequently, the system becomes less sensitive to temperature, compared to the corresponding conventional water-in-oil μEs. Dynamic light scattering studies, combined with the viscosity measurements, can shed light on the above mentioned characteristics of IL μE (the size and its temperature sensitivity).

Studies on the microenvironment of IL-in-oil μE using different solvatochromic probes have been reported by the research groups of Bhattacharyya and co-workers [30,43–46], Gao et al.[8,23,31,38,40], Sarkar and co-workers [30,32,47–49] and Samanta [24,28,29]. According to Gao et al. [8], with increasing amount of IL, polarity of the microenvironment increases, resulting in a red shift in the absorption spectra of dye molecule (probe). Solvent dynamics studies in reverse micelle can provide information about the different states of the polar domains [24–26,28–30]. Bhattacharya et al. have performed solvent dynamics studies using IL μEs[43,44]. Similar works have been reported by Sarkar et al. [30] where different dyes were used in the confined polar domain of μE. Samanta et al. [29] have also reported the solvent dynamic studies, both in the neat and in confined ILs. However, all those results may be considered as fragmentary in nature to completely understand the different states of IL in the μE of oil continuum.

IL based μE can be formed using any one of the three coexisting pseudo phases: the polar domain, the surfactant and the oil (non polar component). However, till date no μE is reported where all the three components are ILs [50]. IL based μEs have advantages over the pure IL, as well as the corresponding conventional μE (comprising water). As a result, IL μEs find many applications which include colloidal crystallization [51], synthesis of nanomaterial [52], pharmaceutics [36], polymers [53], catalysis [54], chemical engineering[55,56] and energy conversion [57], etc. However, the most significant application of IL μE lies its use as alternate solvent for organic chemical reaction [7].

Although termed as environmentally benign, fluorinated ILs are toxic because they can generate HF, POF_3, etc., upon heating [49]. Hence, studies involving non-fluoridated ILs are considered to be more significant. In this aspect, 1-butyl-3-methyl imidazolium methanesulfonate [bmim][MS] is more "green" compared to the conventional fluorinated ILs. However, to the best of our knowledge no reports are available on [bmim][MS] based microemulsion.

Water is the "greenest" among all solvents. In our previous report, we showed that [bmim][MS] in combination with water exhibited some unusual behavior [58]. The binary mixtures were studied using a number of techniques in the bulk condition. Different properties of the binary mixture could be tuned/altered by judicious mixing of the components. Previously, we have carried out systematic physicochemical investigations on water/(Tween 20 + n-pentanol)/n-heptane water-in-oil μE [59]. It is, therefore, important to undertake the challenge in investigating the polar domain in oil microemulsion comprising the binary mixture of ionic liquid[bmim][MS], in combination with water. Such studies are important in terms of their application as well as fundamental understanding point of view. However to the best our knowledge, no systematic studies have yet been carried out using a binary mixture of IL and water, which would be the novelty of the present work.

In this paper we report the results of the investigations made on pseudo ternary polar domain-in-oil μE system ([bmim][MS] + water)/(Tween 20 + n-pentanol)/n-heptane. Our previously published results on water/(Tween 20 + n-pentanol)/n-heptane μE [59] alongwith the binary mixture of [bmim][MS] + water [58] have been considered as the points of references. There are several reports on the microemulsions comprising TX-100 [8,23,31,38,40]; however IL microemulsions comprising Tween 20 are not so many. Compared to TX-100, Tween 20 is less toxic. The choice of the anion in the IL is intentional as it is an inorganic ion linked to an alkyl group. It is needless to mention that such a system will definitely be less toxic compared to the fluorinated ILs. The μE systems have been studied as functions of the composition of binary mixture of the polar domain, volume of the dispersed phase (polar domain) and temperature. μEs were characterized using a number of techniques, *viz.*, phase behavior, method of dilution, viscosity, dynamic light scattering (DLS), electrical conductance, absorption and fluorescence spectroscopic measurements. It is believed that such a system will exhibit some unusual properties and will find different potential applications due to the unique features of the binary mixtures as well as of a μE. Usually IL-in-oil μEs are more rigid and less temperature sensitive; such limitations can be overcome provided the pure IL is replaced with a binary mixture of IL and water.

2. Experimental

2.1. Materials

The nonionic surfactant polyoxyethylene sorbitan monolaurate (Tween 20) and the IL *1*-butyl-*3*-methyl-imidazolium methanesulfonate[bmim][MS] were purchased from M/S Fluka, Switzerland and M/S Sigma–Aldrich Chemicals Pvt. Ltd., USA, respectively. They were stated to be more than 99.5% pure and were dried under vacuum at 60 °C for 8 h [47,49,58]. HPLC grade n-pentanol was a product from Lancaster, England while n-heptane was obtained from E. Merck, Germany. They were used as received. The dye eosinY[2-(2,4,5,7-tetrabromo-6-oxido-3-oxo-3*H*-xanthen-9-yl) benzoate] was a product from E. Merck, Germany. Structure of Tween 20[bmim] cation and eosin Y are shown in Scheme 1. Double distilled water with a specific conductance of 2–4 μS cm^{-1} (at 298 K) was used.

2.2. Methods

2.2.1. Phase manifestation

The pseudo ternary phase diagram of ([bmim][MS] + water)/(Tween 20 + n-pentanol)/n-heptane at different compositions of the polar domain were constructed by titrimetric method as described elsewhere [15,59,60]. Briefly, known amounts of Tween 20 + n-pentanol (1:1, w/w) and n-heptane or (IL + water) were taken in a stoppered test tube(IL + water) or n-heptane was then progressively added using a Hamilton (USA) microsyringe under constant stirring in a controlled temperature bath (298 ± 0.1K). The phase boundary was detected through the appearance of turbidity, whereby the composition was noted. The same experiment was carried out for a number of compositions by varying the amount of oil or IL + water. Also the experiments were carried out using different combinations of IL and water.

2.2.2. Method of dilution

The simple experiment, capable of providing useful information on the thermodynamics of formation and structural parameters of μE, was also carried out titrimetrically [14,15,59]. Different binary mixtures were used as the polar domain in the oil continuum. Also experiments were carried out at different [IL + water]/[Tween 20] mole ratio, ω (5, 10, 15, 20 and 25) and temperatures (298, 303, 308, 313, 318 and 323 K). Known amount of surfactant, polar component (IL + water) and n-heptane were taken in a stoppered test tube which, after homogenization, appeared turbid. n-Pentanol was then progressively added. After saturating the oil continuum (and partly the polar domain) once excess n-pentanol became available, it behaved like cosurfactant and occupied the polar domain/oil interface whereby a clear μE was formed. The required amount of n-pentanol was then noted. Upon further addition of n-heptane, the oil continuum abstracted the cosurfactant from the interface which resulted in the destabilization of the μE. The clarity was regained again by adding cosurfactant. This method of destabilization and re-stabilization was carried out for a number of times, whereby the composition was also noted. The method basically aimed to determine the partition coefficient of n-pentanol between the oil continuum and the interface (strictly speaking, n-pentanol was partly soluble in the polar domain). The previously followed approach of Hait and Moulik [61] was suitably modified in the present case as has been detailed in the supplementary section.

2.2.3. Viscosity measurements

Viscosity of μE was measured using a LVDV-II + PCP cone and plate type roto-viscometer (Brookfield Eng. Lab, USA). A 0.2 M Tween 20, mixed with 1:1 (w/w) n-pentanol in n-heptane was used. Unlike the dilution experiments, viscosity was measured at varied volume fraction (ϕ_d) of the dispersed phase. This approach was adapted because of the fact that with varying composition of the polar domain, the same molar ratio range of [IL + water]/[Tween 20] could not be maintained for all the binary mixtures. Temperature during the viscosity measurement was controlled by a cryogenic circulatory water bath with a precision of ±0.1 K (DC-1006 M/S. Hahntech Corporation, S. Korea). Shear rates (D) were varied within the range 20–60 S^{-1} with an increment of 5.0 S^{-1} in each step. Zero shear viscosity (η) was obtained using the relation $\eta = \tau/D$ [59,62–64], where τ is the shear stress.

2.2.4. Dynamic light scattering (DLS) studies

Size of the μE droplet was determined by DLS method. The same set of solution, as used in the viscosity measurements, was employed for size analyses. DLS measurements were carried out using a Zetasizer Nano ZS90 (ZEN3690, Malvern Instruments Ltd, U.K.). A He–Ne laser of 632.8 nm wavelength was used and the data were collected at 90° angle. Temperature was controlled by inbuilt Peltier heating-cooling device with an accuracy of ±0.05 K. The instrument actually measures the diffusion coefficient (D) from which the diameter of the microemulsion droplet (d) was determined according to Stokes–Einstein's formalism [44–46,59,65,66]:

$$D = \frac{kT}{3\pi\eta d} \quad (1)$$

where k, T and η indicate the Boltzmann constant, temperature and viscosity respectively.

2.2.5. Conductance measurements

μE comprising IL and water in the polar domain is expected to be conducting, as reported for the conventional water-in-oil μE having ionic components in the polar domain [67]. Both the volume and temperature induced percolation studies were carried out using 0.2 M Tween 20 (with 1:1 w/w n-pentanol) in n-heptane. 10 mL of Tween 20 solution was taken in a thermostated enclosure. For volume induced percolation, binary mixtures of (IL + water) was progressively added with constant stirring. Specific conductance was measured with an EC-CON510/43S conductivity meter (Cyberscan, TDS/°C/°F, USA). Volume induced percolation studies were conducted at four different temperatures, *viz*., 298, 303, 308 and 313 K. In another approach while performing the temperature induced percolation studies, a known amount of the dispersed phase (IL + water) was mixed with the surfactant solution. Conductance was then recorded in the temperature range 283–343 K with an increment of 5 K in each step.

2.2.6. Spectral studies

2.2.6.1. Absorption spectra. Visible absorption spectra of eosin Y (EY) in the polar domain were recorded on a UVD-2950 Spectrophotometer (Labomed Inc., USA) in the range 400–600 nm using a matched pair cell of 1.0 cm path length. Corresponding (IL + water)-in-n-heptane μE without the dye was used as reference. Overall concentration of eosin Y was always kept constant at 10 μM. Initially, required amount of eosin Y in methanol was taken in a test tube. The solvent was evaporated under vacuum. μE of known composition was then added and homogenized by vortexing the solution. It is to be mentioned that eosin Y is insoluble in n-heptane [68]. Therefore it could be assumed that the dye molecules reside in the polar domain [41].

2.2.6.2. Emission spectra. The same set of solutions, as used in absorption spectroscopic measurements, was used in the fluorescence measurements. Detail of the experimental techniques is available elsewhere [58,68]. Both the steady state and time resolved

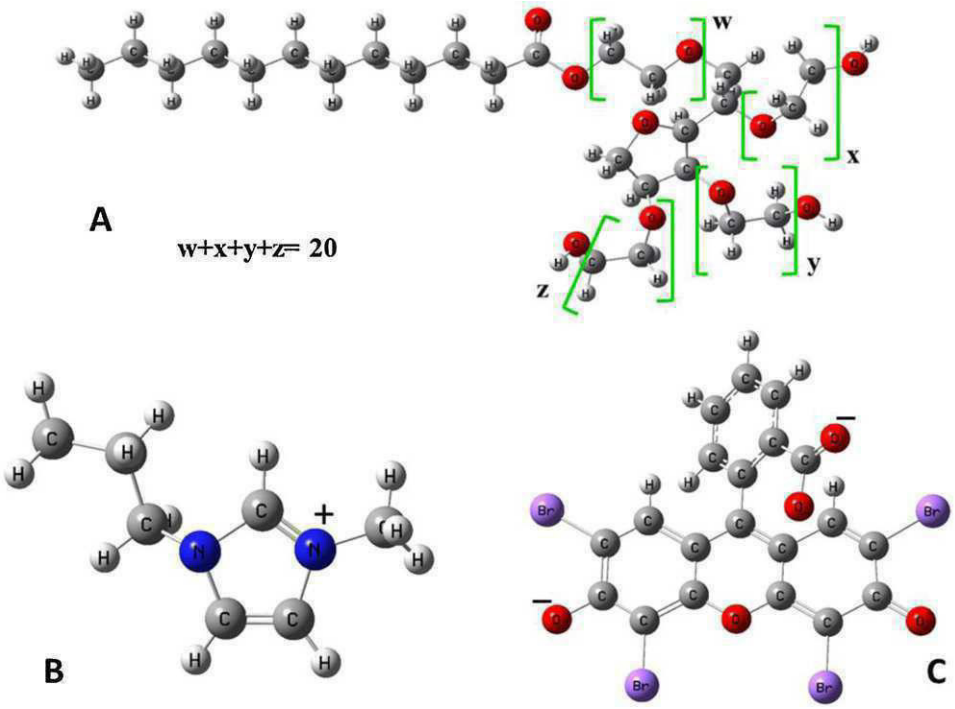

Scheme 1. Schematic models of A, Tween 20; B[bmim] cation and C, eosin Y

fluorescence measurements were carried out using a bench-top spectrofluorimeter (Quantamaster-40, Photon Technology International Inc, NJ, USA). For recording the steady state fluorescence spectra (500–650 nm), eosin Y was excited at 500 nm (λ_{ex}).

Steady state anisotropy (r), which is related to the microviscosity of the solvent surrounding the probe molecule, was determined using the following expressions [69,70]:

$$r = \frac{I_{VV} - GI_{VH}}{I_{VV} + 2GI_{VH}} \quad (2)$$

and,

$$G = \frac{I_{HV}}{I_{HH}} \quad (3)$$

where, I_{VV} and I_{VH} are the intensities obtained with the excitation polarizer oriented vertically and the emission polarizer oriented vertically and horizontally respectively; I_{HV} and I_{HH} refer to the similar parameters as above for the horizontal positions of the excitation polarizer. In case of anisotropy measurements, the fluorescence data were collected at an emission wavelength (λ_{em}) of 550 nm [58]. Excited state lifetime of eosin Y in the polar domain was determined by analyzing the fluorescence decay curve which was single exponential in nature. A pulsed nano diode emitting at 500 nm was used as the light source [58,68]. Goodness of the fit of the curves were adjudged by χ^2 values which were in between 1 and 1.2 [47]. Fluorescence decay curves were analyzed by Felix GX (version 2.0) software. Both the absorption and fluorescence data were recorded at ambient but controlled temperature.

3. Results and discussion

3.1. Phase manifestation

Although tedious, however the construction of phase diagram for ternary/pseudo ternary μE systems are essential from the fundamental as well as the application point of view [71,72]. The pseudo ternary phase diagrams for ([bmim][MS] ± water)/(Tween 20 + n-pentanol)/n-heptane at different [bmim][MS]/water mole fractions have been graphically presented in Fig. 1. The phase manifestations for water containing μE system have been previously reported by the present research group [59] and this has been taken as the point of reference. Each pseudo ternary phase diagram comprises of a single phase (1Φ) clear μE region and a two phase turbid region (2Φ). The extreme corners of the polar component and oil component correspond to oil-in-polar domain and polar domain-in-oil μE respectively. In the present system, the oil rich regions, *i.e.*(IL + water)-in-oil μEs were examined for the other set of experiments. Area under the clear and turbid regions were calculated by weighing the individual components in the

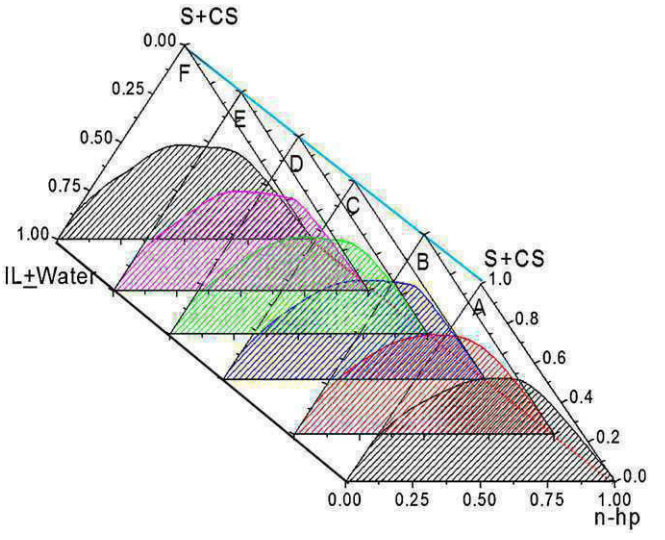

Fig. 1. Pseudo-ternary phase diagram of ([bmim][MS] ± water)/(Tween 20 + n-pentanol)/n-heptane microemulsion at 298 K. 1:1 (w/w) Tween 20 and n-pentanol was used. Mole fraction of [bmim][MS] in the binary mixture of [bmim][MS] and water: A, 0.2; B, 0.4; C, 0.5; D, 0.6; E, 0.8 and F, 1.0 respectively. The shaded portions represent biphasic (2Φ) regions while the clear portions correspond to the single phase (1Φ) regions.

pseudoternary phase diagram as were done previously [59,73]. The area under the turbid region was higher in each case compared to pure water. The increase in the area under turbid regions is due to the presence of the ionic components in the polar domain. However, when one analyses the results in terms of the variation of % area under the clear or turbid region with the composition of the binary mixture, it is observed that the %area under clear region for different microemulsions μE passes through a minimum at 50 mol% [bmim][MS] in combination with water (x_{IL} = 0.5), as graphically presented in Fig. S1 (supplementary section). According to our recent study [58] as well as other available reports [74–76], IL can deactivate water molecules when present in excess amount in a binary mixture. The deactivation of water molecules for binary mixtures comprising more than 50 mol% IL has recently been modeled by Stark and Wassercheid [77] and Liu et al. [75,76]. Above 50 mol% IL, the deactivated water molecules cannot significantly alter the structure of the aggregates. Also there are reports describing the formation of micelle like entities by the IL in binary mixtures [75,76,78–81]. Besides, due to amphiphilic nature, IL can also occupy the interface alongwith the surfactant and cosurfactant molecules. Subsequently, area under the clear regions for different combinations of μEs increased further with increasing mole fraction of IL.

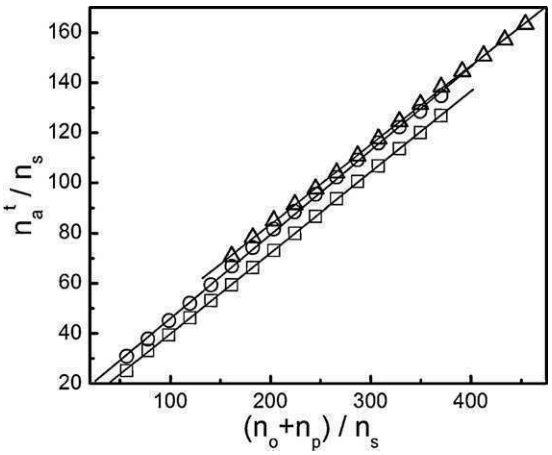

Fig. 2. Plot of n_a^t/n_s vs $(n_o + n_p)/n_s$ for ([bmim][MS] + water)/(Tween 20 + n-pentanol)/n-heptane polar domain-in-oil microemulsion system[bmim][MS]/[water] mole ratio = 1:1([bmim][MS] + water)/Tween 20 mole ratio, ω = 15. Temperature (in K): O, 298; Δ, 308 and □, 318. 0.2 g Tween 20 was used in each case.

3.2. Dilution method

3.2.1. Evaluation of thermodynamic parameters

The method of dilution is a very simple but informative technique which can derive many useful parameters for the formation of polar domain-in-oil μE [82]. In this method, by the alternate stabilization and destabilization with the successive addition of cosurfactant and oil, one can obtain the partition coefficient of n-pentanol between oil and oil/(IL + water) interface. By suitably analyzing the distribution constant in the form of different standard thermodynamic equations, the corresponding thermodynamic parameters for the formation process can easily be evaluated [61,83,84]. Besides, the structural parameters can also be computed from these experimental results [73,85–87]. Several reports on the method of dilution are available in literature involving water-in-oil μE. However, similar studies involving ILs are not common, except only one recent report of Wang et al. [88]. Thus the dilution studies involving the evaluation of interfacial behavior, thermodynamic and structural parameters of IL μE are considered to be significant. The basic mathematical formalism to determine the thermodynamics of μE formation and evaluation of structural parameters for the presently studied (IL + water)-in-oil μE systems have been presented in the supplementary section. A representative plot of n_a^t/n_s vs$(n_o + n_p)/n_s$ at $x_{[bmim][MS]}$ = 0.5 and ω = 15 has been shown in Fig. 2. Herein n_a^t, n_s, n_o, n_p stand for the total number of moles of alkanol, surfactant, oil and the polar component, respectively. Results are summarized in Table 1 for equimolar mixture of IL and water. Other results are provided in the supplementary section (Table S1). Studies revealed that increasing ω value resulted in the increase in k_d value, except in a few cases. However, while considering all the binary combinations of IL and water, the variation of k_d (and subsequently ΔG_t^0) with ω and temperature were not very straightforward. In our previous studies [59,85] for water/Tween 20 + n-pentanol/n-heptane water-in-oil microemulsion, we observed that with increasing volume fraction of the polar domain, newer droplets were formed. It was due to the capability of the polyoxyethylene groups of Tween 20 to get uncoiled at larger volume fraction of the polar component. Systems comprising less than 50 mol% IL behaved similarly to water/Tween 20 + n-pentanol/n-heptane μE. However, for the systems comprising more than 50 mol% IL, the variation in the thermodynamic parameters was different. Microemulsions comprising more than 50 mol% IL in combination with water behaved more like the IL microemulsion. In other words, behavior of the systems comprising less than 50 mol% IL were more like the microemulsion comprising only water in the polar domain. Variation was similar to the conventional water-in-oil microemulsions with ionic surfactants. It has already been stated that when the amount of [bmim][MS] exceeds 50 mol% (in the binary mixture), it can deactivate water molecules. The rigidity of IL-in-oil μEs was due to strong electrostatic interaction between the imidazolium cation and oxyethylene group of Tween 20. Hence, when binary mixture comprising more than 50 mol% IL was used as the polar domain, size of the microemulsion droplets increased with ω instead of formation of smaller droplets like water/(Tween 20 + n-pentanol)/n-heptane [59] or water-in-oil μE systems comprising Tweens and Brij [73,85]. Fig. 3 describes the variation in the changes of standard free energy (ΔG_t^0) with ω and T for x_{IL} = 0.2 and 0.8. Binary mixtures of different compositions (x_{IL} = 0.2, 0.4, 0.5, 0.6, 0.8 and 1.0) were used for such studies. Some representative results have been shown in Table 1. Other results are summarized in Table S1 in the supplementary section. In all the cases ΔG_t^0 values were negative which implied the spontaneity of the formation of μE. However, ΔG_t^0-ω-T profiles were found to be composition dependent. For systems comprising lower amount of IL (less than 50 mol%) negative values of ΔG_t^0 decreased with increasing ω. This suggests the similarity of the behavior of present μE system with the corresponding water-in-oil μEs [59]. No systematic variation in ΔG_t^0 with T was observed in either case. For systems with larger amounts of IL, negative values of ΔG_t^0 increased with ω suggesting the formation of larger droplets without significantly losing their rigidity. However, to make final conclusions in this regard some other experimental evidences like dynamic light scattering studies are warranted. While considering the formation dynamics, it was observed that behavior of the systems comprising less than 50 mol% of IL was similar to water comprising μEs; spontaneity of μE formation decreased with increasing volume of the dispersed phase (ω or ϕ_d). However, for systems comprising more than 50 mol% of IL, polarity of the dispersed phase decreased which resulted in the increased ease of μE formation. The decreased polarity was due to the presence of IL molecules which themselves were amphiphilic in nature. This further supported the inferences drawn from the phase manifestation studies. With increasing ω, the curvature of μE decreased leading to more accumulation of cosurfactants at the polar domain–oil interface. While considering the enthalpy of transfer process under various conditions (as

Table 1
Thermodynamic parameters for the transfer of n-pentanol from oil to oil/([bmim][MS] + water) interface during the formation of [bmim][MS] ± water/(Tween 20 + n-pentanol)/n-heptane polar domain-in-oil microemulsion at different temperature and [IL + water]/[Tween 20] mole ratio, ω. IL: water molar ratio = 1:1.

Parameter		Temp. (K)					
	ω	298	303	308	313	318	323
k_d	5	3.01	3.19	2.93	4.17	3.22	3.45
	10	3.72	3.51	3.79	3.47	3.09	3.57
	15	3.69	3.88	3.97	3.56	3.62	3.90
	20	3.99	3.93	4.15	3.88	3.85	3.98
	25	4.17	4.19	4.00	3.98	3.98	4.24
$-\Delta G_t^0$ (kJ mol^{-1})	5	2.73	2.92	3.25	3.72	3.09	3.33
	10	3.25	3.16	3.41	3.24	2.98	3.42
	15	3.23	3.42	3.53	3.31	3.40	3.66
	20	3.43	3.44	3.65	3.53	3.57	3.71
	25	3.54	3.61	3.55	3.59	3.65	3.88
ΔH_t^0(kJ mol^{-1})	5	19.79	−2.02	−24.20	−46.74	−69.65	−92.92
	10	−7.54	−4.91	−2.23	0.49	3.25	6.06
	15	−8.59	−4.65	−0.65	3.41	7.55	11.75
	20	−4.12	−2.58	−1.03	0.56	2.17	3.82
	25	−4.32	−3.05	−1.76	−0.45	0.88	2.24
ΔS_t^0(J K^{-1} mol^{-1})	5	75.59	2.97	−69.66	−137.47	−209.30	−277.38
	10	−14.39	−5.76	3.84	11.91	19.63	29.37
	15	−17.96	−4.08	9.34	21.47	34.44	47.69
	20	−2.33	2.83	8.51	13.07	18.06	23.30
	25	−2.65	1.83	5.81	10.03	14.26	18.93

0.2 g Tween 20 was taken in each case. ϕ_d = volume fraction of the dispersed phase (IL + water).

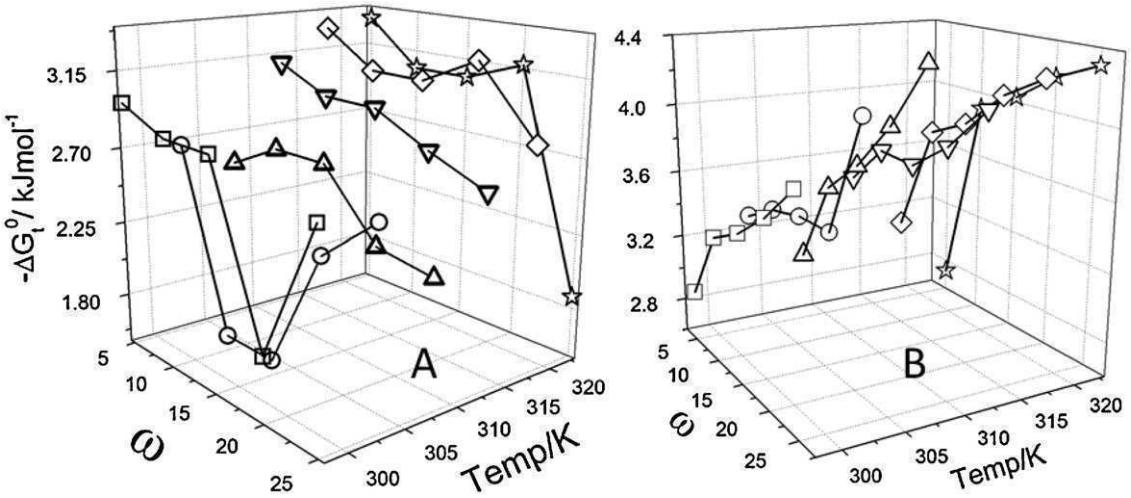

Fig. 3. ΔG_t^0-ω-T profile for the formation of ([bmim][MS] ± water)/(Tween 20 + n-pentanol)/n-heptane polar domain-in-oil microemulsion system. Mole fraction of [bmim][MS] in the polar domain: A, 0.2 and B, 0.8.

described in Table 1, Table S1 and Fig. S2), it was found that at higher temperature ΔH_t^0 became endothermic which was initially exothermic in nature. Our present set of results for the system comprising more than 50 mol% IL showed similar behavior as in case of [bmim][BF_4]/(Brij-35 + 1-butanol)/toluene IL-in-oil μE system [88]. As there are possibilities for the polar components to get dispersed into the n-heptane medium, there occurred an effective increase in the area of the droplet surface. The required energy for the positive work is compensated by the absorption of heat. However, in the cases involving size increment, the negative value of ΔH_t^0 was not unexpected to decrease. To justify the similarities/dissimilarities between the behavior of conventional water-in-oil μE and IL-in-oil μE, analysis of the enthalpy–entropy profile was necessary [16]. Fig. 4 describes the ΔH_t^0- ΔS_t^0 profile for all the combinations. Nice correlations were observed for all the sets of values, *e.g.*, different x_{IL}, ω and temperature. Compensation temperature, as obtained from the slope was found to be 311 K which was in good agreement with the average of all the experimental temperatures (298, 303, 308, 313, 318 and 323 K).

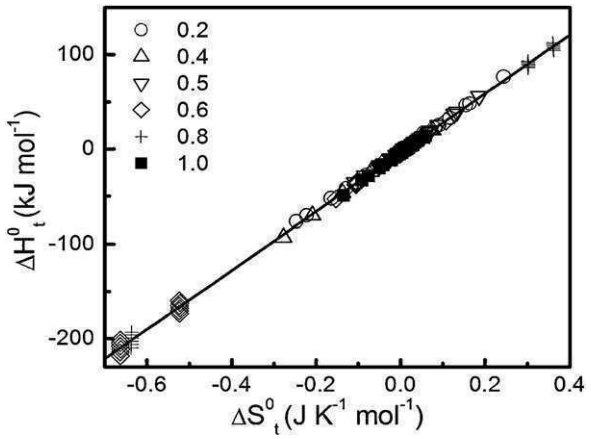

Fig. 4. Enthalpy–entropy compensation for the formation of ([bmim][MS] + water)/(Tween 20 + n-pentanol)/n-heptane polar domain-in-oil microemulsion system. Mole fraction of [bmim][MS] in the binary mixture (present in the polar domain) have been mentioned inside the figure.

Table 2
Structural parameters of [bmim][MS] + water/(Tween 20 + n-pentanol)/n-heptane polar domain-in-oil microemulsion at different temperature and [IL+water]/[Tween 20] mole ratio, ω. Mole ratio of IL: water = 1:1.

Parameter		Temp. (K)					
	ω	298	303	308	313	318	323
R_e (nm)	5	4.74	3.75	3.35	2.83	2.63	2.42
	10	4.30	4.32	3.62	3.45	3.29	2.91
	15	5.25	4.56	3.88	3.88	3.79	3.26
	20	5.31	5.03	4.48	4.09	3.84	3.58
	25	5.65	5.09	5.09	4.35	4.22	3.79
10^{-18} N_d	5	0.76	1.744	3.25	6.83	5.08	7.27
(per mL)	10	1.89	1.56	3.11	3.13	2.93	5.28
	15	1.09	1.75	3.28	2.73	2.53	5.08
	20	1.34	1.512	2.24	3.02	3.63	4.61
	25	1.27	1.783	1.62	2.95	3.04	4.66
N_s	5	67.46	55.99	43.47	14.28	19.23	13.44
(per droplet)	10	51.56	62.63	31.40	31.21	33.35	18.46
	15	89.08	55.89	29.80	35.71	38.53	19.20
	20	72.85	64.58	43.51	32.36	26.86	21.17
	25	76.66	54.75	60.17	33.07	32.12	20.96
N_{cs}	5	5.27	3.67	2.07	3.06	1.29	1.26
(per droplet)	10	8.06	5.94	4.64	3.23	1.52	1.98
	15	11.16	7.95	6.07	4.62	2.92	3.21
	20	12.67	9.97	7.62	6.12	5.01	4.21
	25	14.74	11.25	9.46	7.35	6.10	5.24

0.2g Tween 20 was taken in each case. ϕ_d = volume fraction of the dispersed phase (IL + water).

3.2.2. Evaluation of structural parameters

Results on the dilution experiments were computed using suitable mathematical formulations whereby the different structural parameters, *viz.*, number of droplets per unit volume (N_d), number of surfactants per droplet (N_s), number of cosurfactants per droplet (N_a), effective diameter of the droplet (R_e) and radius of polar domain (R_p) could be determined [16]. The detailed mathematical derivations have been presented in the supplementary section. While computing the structural parameters, the μE droplets were assumed to be spherical and monodispersed, stabilized by a surfactant and cosurfactant monolayer. Additionally, it is assumed that due to amphiphilic nature of IL, some IL molecules also occupy the interfacial region. Results are summarized in Table 2 and Table S2. N_d-ω-T profile for the systems comprising 20 and 80 mol% of [bmim][MS] have been shown in Fig. 5 as representative. In both the cases, the number of droplets per unit volume increased with increasing temperature. However, the extent of increase were higher for the systems comprising lower amount of [bmim][MS]. The decrease in the number of droplet with increasing volume of the dispersed phase was not unexpected. With the increase in the volume of the dispersed phase, larger droplets were formed [88]. While considering the size of the polar domain as well as the effective size of the μE (as modeled by Wang et al. [88]), it has been noticed that both R_e and R_p decreased with increasing temperature and ω for water rich binary mixtures ($x_{IL} < 0.5$). However, the size of the μE as well as the polar domain increased with increasing volume of the dispersed phase. Systems comprising 50 mol% of IL behaved intermediately compared to water rich or IL rich binary mixtures. The reason for such unusual behavior is not certain. Compared to the corresponding water-in-oil μE systems, presently studied (IL + water) μE system was found to be less temperature sensitive as revealed from the variation of R_e values with temperature. The rigidity was contributed by the strong electrostatic attraction between oxyethylene groups of the surfactant and the imidazolium cation.

3.3. Dynamic light scattering studies

Size of the μE droplets were also directly evidenced by the dynamic light scattering experiments. As in the present study binary mixtures of [bmim][MS] and water of different compositions were used, hence size variations were considered with respect to the volume fraction of the dispersed phase. Variation in the diameter of the μE droplet with volume fraction of the polar domain has

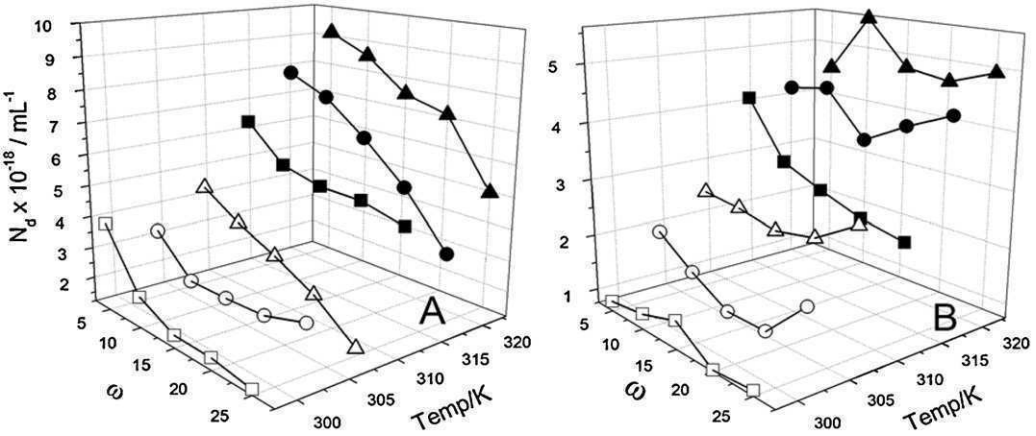

Fig. 5. N_d-ω-T profile for the formation of ([bmim][MS] ± water)/(Tween 20 + n-pentanol)/n-heptane polar domain-in-oil microemulsion system. Mole fraction of [bmim][MS] in the polar domain: A, 0.2 and B, 0.8. Temperature (in K): □, 298; O, 303; Δ, 308; ■, 313; ●, 318 and ▲, 323.

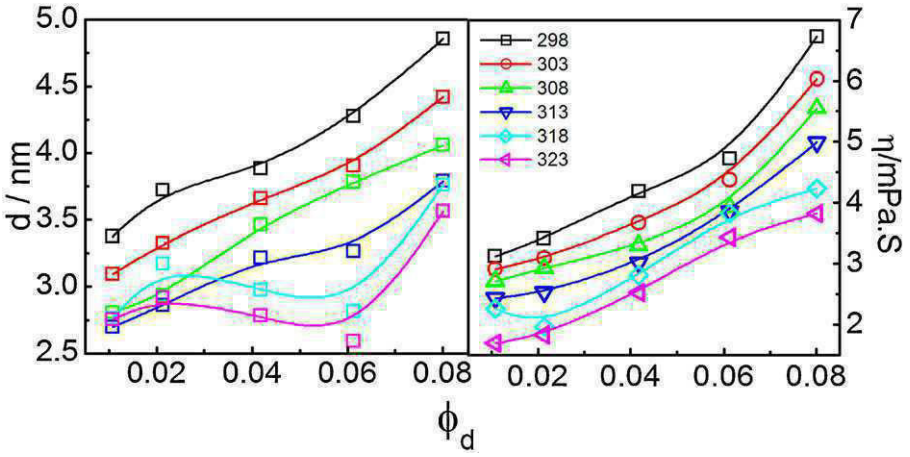

Fig. 6. Variation in the size (diameter, d) and viscosity (η) of the polar domain-in-oil microemulsion of ([bmim][MS] ± water)/(Tween 20 + n-pentanol)/n-heptane. Mole fraction of [bmim][MS] in the polar domain: 0.5. A 0.2 M Tween 20 with 1:1 (w/w) n-pentanol solution was used. Temperatures (in K) are mentioned inside the figure.

been shown in Fig. 6 along with the viscosity data. With increasing volume fraction, except at the higher temperatures (318 and 323 K), the d-ϕ_d profiles were nearly linear. The DLS data closely matched with the size parameters derived from the method of dilution. Size of the μE droplets decreased with increasing temperature for all the compositions, which were quite unusual. The size constriction effect was noted in both the DLS measurements as well as in the method of dilution. This kind of size variation with temperature has never been reported previously for any IL μE systems. We assume that the size constriction upon heating was due to the formation of reorganized entities. Temperature increased caused the decrease in viscosity (as shown in Fig. 6 right panel) which allowed the IL + water to get reorganized and therefore the structured entities were formed as proposed in Scheme 2. Such a proposition for the formation of organized assembly of IL-in-oil μE has been reported by different authors [2,23,88,89]. However to make final conclusion in this regard, further studies like freeze fractured electron microscopy or *cryo*-TEM measurements are warranted. This can be considered as the future perspectives.

3.4. Viscosity measurement

Viscosity of microemulsion depends on the size and number of droplets. In the present case, viscosity decreased almost linearly with temperature except in a few cases. It is to be noted that in the case of pure binary mixtures in the bulk condition, viscosity variation were entirely different from the present study. Increase in viscosity with increasing volume of the dispersed phase is attributed to the increase in the size of the polar domain (the phenomenon of swelling effect). As the size of the droplets decreased with the increase in temperature hence it is not unexpected that viscosity would decrease with the increase in temperature. Additionally it is known that for all the liquids viscosity usually decreases with the increase in temperature.

3.5. Conductance measurement

Although the continuum is comprised of oil, the μEs with the ionic components in polar domain is expected to conduct electricity. The percolation of electrical conductance for a μE in oil continuum can occur either through the "hopping mechanism" or through the mechanism of "fusion, mass transfer and fission" [71,72]. The effective mean theory with dipole–dipole interaction has been adapted in the present case. In the present set of experiment, both the volume and temperature induced conductance studies were performed. Variation in specific conductance with the volume fraction of (IL + water) at different compositions have

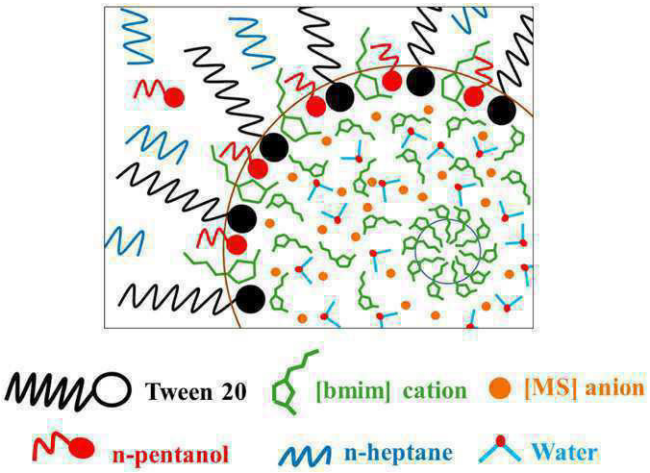

Scheme 2. Proposed model for the location/organization of the different components in [bmim][MS] + water/Tween 20 + n-pentanol/n-heptane polar domain-in-oil microemulsion. The core of the microemulsion is comprised of micelle like aggregates of [bmim] cations.

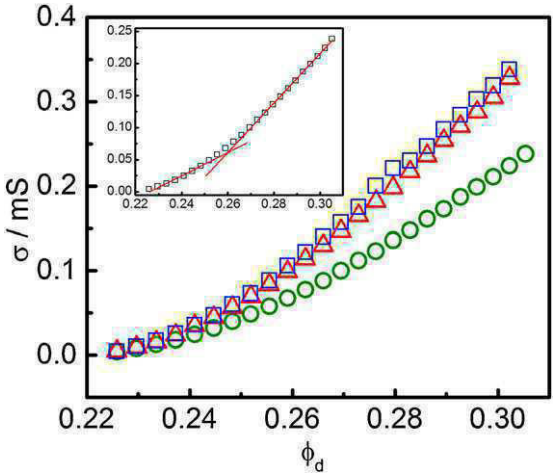

Fig. 7. Volume induced percolation of ([bmim][MS] ± water)/(Tween 20 + n-pentanol)/n-heptane polar domain-in-oil microemulsion system. Mole fraction of [bmim][MS] in the polar domain: O, 0.2; □, 0.5 and Δ, 0.8. Threshold volume fraction (Φ_d^t) (for $x_{IL} = 0.2$) was determined from the point of intersection of two tangents as shown in the inset. Temperature 298 K.

Table 3
Scaling law parameters for volume (IL + water) induced percolation of ([bmim][MS] ± water)/ (Tween 20 + n-pentanol)/n-heptane polar domain-in-oil microemulsion system at different temperatures.

/ ln k/m				
IL + water	298 K	303 K	308 K	313 K
2:8	0.276/−0.38 ± 0.09/0.336 ± 0.02	0.250/1.06 ± 0.04/0.87 ± 0.01	0.252/1.25 ± 0.08/0.83 ± 0.04	0.255/1.37 ± 0.09/0.82 ± 0.03
4:6	0.276/−0.04 ± 0.07/2.48 ± 0.05	0.261/1.20 ± 0.07/3.10 ± 0.02	0.253/−1.08 ± 0.06/1.69 ± 0.04	0.252/−1.78 ± 0.05/1.32 ± 0.04
5:5	0.263/−0.34 ± 0.07/ 2.48 ± 0.05	0.256/−1.35 ± 0.08/1.25 ± 0.05	0.257/−2.01 ± 0.01/0.94 ± 0.007	0.263/−1.94 ± 0.04/1.18 ± 0.03
6:4	0.263/−1.04 ± 0.05/1.34 ± 0.02	0.258/−1.79 ± 0.02/1.01 ± 0.02	0.258/−1.86 ± 0.02/1.03 ± 0.01	0.258/−2.01 ± 0.01/1.00 ± 0.008
8:2	0.263/−1.54 ± 0.05/1.46 ± 0.04	0.257/−1.59 ± 0.02/1.39 ± 0.02	0.258/−2.02 ± 0.04/1.21 ± 0.04	0.259/−2.09 ± 0.01/1.38 ± 0.02
Pure IL	0.256/−1.25 ± 0.04/1.49 ± 0.03	0.259/−1.44 ± 0.04/1.56 ± 0.03	0.252/−1.78 ± 0.03/1.36 ± 0.03	0.262/−2.06 ± 0.04/1.57 ± 0.04

A 0.2 M Tween 20 + n-pentanol (1:1, w/w) in n-heptane was used in each case.

been shown in Fig. 7 at 298 K as representative. In the conductivity studies, ratio of surfactant, cosurfactant and oil were kept constant. Although comprised of ionic species in the polar domain, the present μE systems were found to be less conducting compared to conventional μEs comprising ionic components in its polar domain [15]. The depressed conductance was attributed to the dense packing of IL, the surfactant and cosurfactant at the polar domain/oil interface [90]. Besides, ILs can strongly interact with the oxyethylene group of Tween 20 [23]. These three combined factors effectively resulted in the formation of rigid entities. The threshold value for the volume induced percolation was determined from the intersection point of the two tangents as shown in the inset of Fig. 7. This method of evaluation of percolation threshold (ϕ_d^t) have been previously reported [73,90]. The conductance derived results are summarized in Table 3. The conductance data were processed according to the scaling equation [60]:

$$\sigma = k(\phi_d - \phi_d^t)^m \quad (4)$$

$$i.e.,\ \ln\sigma = \ln k + m \quad \ln(\phi_d - \phi_d^t) \quad (5)$$

where σ is the conductance of the microemulsion, k is a constant which depends on the conductance of the dispersed phase and m is the exponent, ϕ_d and ϕ_d^t are the post threshold and threshold volume fraction respectively. One can thus determine the value of $\ln k$ and m from the linear plot of $\ln\sigma$ vs $\ln(\phi_d - \phi_d^t)$ (figure not shown to save space). According to the previously published results [91–95], higher ϕ_d^t corresponds to static percolation while lower ϕ_d^t indicates dynamic percolation. In the present case ϕ_d^t did not change significantly with the composition as well as the temperature. As predicted, the exponent 'm' remained constant for all the system except a few cases. The negative value of k increased with x_{IL},which resulted from the decrease in the polarity of the binary mixtures, especially after $x_{IL} > 0.5$. In our previous study [58] as well as from the present results, it is known that IL, in combination with water, in polar domain can form micelle like aggregates leading to the decrease in the polarity of the dispersed phase. We failed to determine the threshold value for the temperature induced percolation, as shown in Fig. 8. However, it was evident from Fig. 8 that with increasing volume fraction of the polar domain, conductance increased. Interestingly, μEs comprising larger proportion of IL (compared to water) were less conducting [Panel B and C of Fig. 8]. This observation further reveals that the rigidity of the droplets is enhanced for systems comprising high proportion of IL.

3.6. Spectroscopic studies

Absorption and emission spectroscopic probing techniques are considered to provide useful information in understanding the local environment of the polar domain-in-oil continuum. In the present study the anionic xanthene dye eosin Y was used as the probe. Our previous study involving the physicochemical characterization of [bmim][MS] + water binary mixture was also carried out using eosin Y as the probe [58]. Such an approach has also been followed by different researchers [8,27,40,96]. Eosin Y is completely insoluble in n-heptane, therefore, it would predominantly reside in the polar domain [41,68]. Absorption and emission spectra of eosin Y in different media have been shown in Fig. 9. While considering the absorption spectra of eosin Y in pure water, it was observed that eosin Y exhibits a strong intense peak at 517 nm with a shoulder appearing at 495 nm. For bulk IL + water mixture, the spectra was red shifted at 537 nm. The peak for eosin Y in the μE appeared at 530 nm. The red shift in the absorption maxima was due to the increasing polarity of the solvent [41,58].

When excited at 500 nm, eosin Y in neat water showed an emission maximum at 537 nm. In the case of IL + water, the emission peak appeared at 556 nm. The results were in conformity with our previous reports [58,68]. Eosin Y in the μE exhibited intermediate behavior. Red shift in the fluorescence spectra was due to the

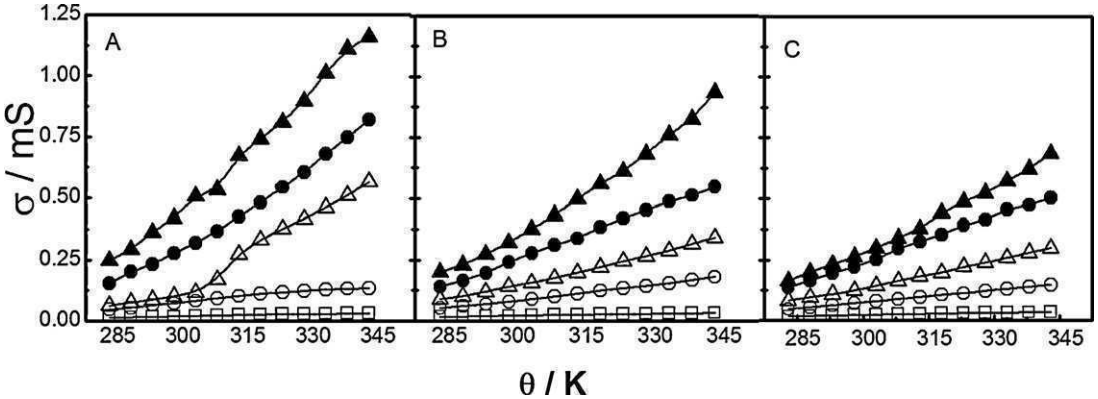

Fig. 8. Temperature induced percolation of ([bmim][MS] ± water)/(Tween 20 + n-pentanol)/n-heptane polar domain-in-oil microemulsion. Mole fraction of [bmim][MS] in the polar domain: 0.2, panel A; 0.5, panel B and 0.8, panel C. Volume fraction of the polar domain: □, 0.237; O, 0.252; △, 0.266; ●, 0.280 and ▲, 0.293.

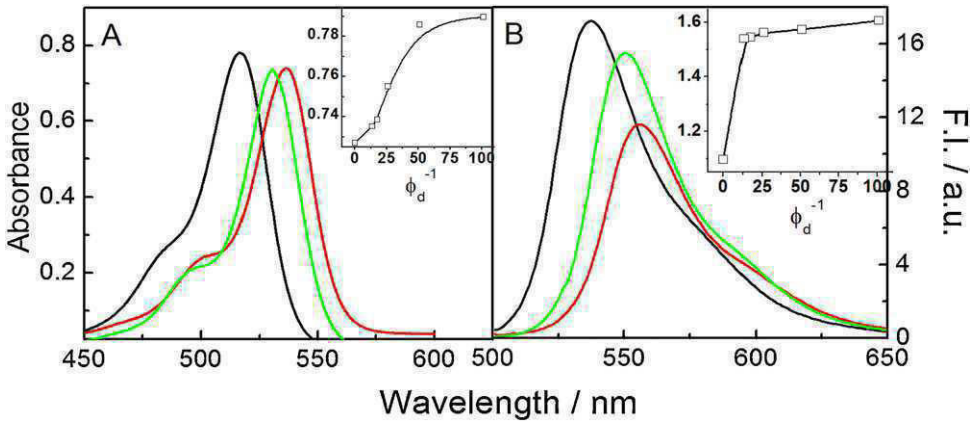

Fig. 9. Absorption (A) and steady state emission spectra (B) of eosin Y in ([bmim][MS] ± water)/(Tween 20 + n-pentanol)/n-heptane polar domain-in-oil microemulsion system along with the spectra in pure water and IL + water mixture. Spectra in pure water are shown through the black lines while the green lines correspond to the spectra in IL + water in μE comprising 50 mol% IL and $\phi_d = 0.057$. The red lines represent the spectra of eosinY in IL + water mixture. In the insets, absorbance (at 517 nm) vs. ϕ_d^{-1} profile (panel A) and fluorescence intensity (at 537 nm) vs. ϕ_d^{-1} (panel B) have been shown. Overall concentration of eosin Y was kept constant at 10 μM. $\lambda_{ex} = 500$ nm.

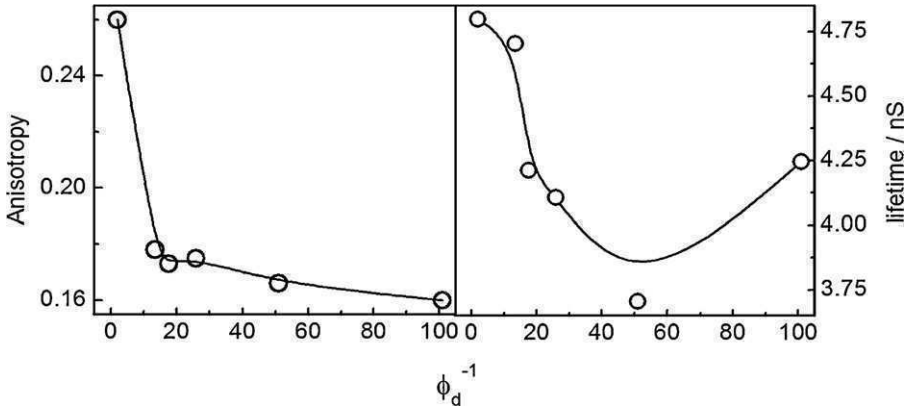

Fig. 10. Variation in the anisotropy and lifetime for 10 μM eosin Y with the inverse of volume fraction of the polar domain (φ_d^{-1}) for ([bmim][MS] ± water)/(Tween 20 + n-pentanol)/n-heptane polar domain-in-oil microemulsion system. An equimolar mixture of [bmim][MS] and water was used as the polar domain. A 10 μM eosin Y was used. $\lambda_{ex} = 500$ nm and $\lambda_{em} = 537$ nm.

enhanced polarity of the medium [43]. For each binary combination of [bmim][MS] and water, the spectra of eosin Y were recorded at different ϕ_d values for (IL + water)-in-oil μEs. All the results are not shown to save space. Compared to the absorption and emission intensity of eosin Y in water, the values decreased with increasing volume fraction of the polar domain. Simultaneously there occurred red shifts in both the absorption and emission spectra which suggests that the microenvironment around eosin Y in the μE are not the same [48]. Progressive red shift with increasing ϕ_d value reflects the change in the state of polar domain. Interestingly, decrease in both the absorbance and fluorescence intensity with ϕ_d were nonlinear in the range 0.009–0.07. To understand the states of the polar components in the μE system, absorbance (at 517 nm) and the fluorescence intensity (at 537 nm) were plotted against the reciprocal of the volume fraction of the dispersed phase (ϕ_d^{-1}). Representative plots for 50 mol% [bmim][MS] (with respect to water) have been shown in the insets of Fig. 9. In both the cases break points appeared around $\phi_d^{-1} = 25$, above which, especially the fluorescence intensity, increased linearly. Results clearly indicate the change in the state of the polar component in this range. With increasing ϕ_d in the lower range polar components were involved in solvating the surfactant head groups whereby they resided in the palisade layer of the μE. Once the surfactant head groups were completely solvated, the polar components became free and could behave like bulk entities. Such an observation has not been reported previously and this may be considered as the novelty of the present work. To understand the solvation phenomena in further detail, both the fluorescence anisotropy and lifetime measurements were carried out for the μEs using eosin Y as the probe. Such studies helped in understanding the microviscosity of the medium as well [25,30]. Representative plots for the anisotropy and lifetime variation with ϕ_d^{-1} have been shown in Fig. 10 for μE comprising 50 mol% IL. Results for other combinations have been shown in the supplementary section (Fig. S4). Appearance of break point around $\phi_d^{-1} = 20 - 25$ conforms the conclusion as drawn in the absorption and steady state fluorescence measurements. However, to understand such systems completely, further studies like small angle neutron scattering (SANS), transmission electron microscopy (TEM) and ultrafast solvent dynamic studies are warranted and these are considered as future perspectives.

Acknowledgements

Financial support from the Department of Science and Technology, Govt. of India, New Delhi in the form of a research grant (SR/S1/PC/24/2008) is gratefully acknowledged. Fluorescence spectroscopic measurement facility was made available at the Department of Chemistry, University of North Bengal under the Special Assistance Programme of University Grants Commission, New Delhi, India.

Appendix A. Supplementary data

Supplementary data associated with this article can be found, in the online version, at http://dx.doi.org/10.1016/j.colsurfa.2012.11.061.

References

[1] S. Liu, J. Xiao, Toward green catalytic synthesis—transition metal-catalyzed reactions in non-conventional media, J. Mol. Catal. A 270 (2007) 1–43.
[2] Z. Qiu, J. Texter, Ionic liquids in microemulsions, Curr. Opin. Colloid Interface Sci. 13 (2008) 252–262.
[3] I.T. Horváth, P.T. Anastas, Innovations and Green Chemistry, Chem. Rev. 107 (2007) 2169–2173.
[4] H.G. Joglekar, I. Rahman, B.D. Kulkarni, The path ahead for ionic liquids, Chem. Eng. Technol. 30 (2007) 819–828.
[5] A. Zharkouskay, H. Lünsdorf, C. Feldmann, Ionic liquid-based synthesis of luminescent and nanocrystals, J. Mater. Sci. 44 (2009) 3936–3942.
[6] J. Hao, T. Zemb, Self-assembled structures and chemical reactions in room-temperature ionic liquids, Curr. Opin. Colloid Interface Sci. 12 (2007) 129–137.
[7] T. Welton, Room-temperature ionic liquids. Solvents for synthesis and catalysis, Chem. Rev. 99 (1999) 2071–2084.
[8] Y. Gao, S. Han, B. Han, G. Li, D. Shen, Z. Li, J. Du, W. Hou, G. Zhang, TX-100/water/1-butyl-3-methylimidazolium hexafluorophosphate microemulsions, Langmuir 21 (2005) 5681–5684.
[9] J.H. Schulman, W. Stoeckenius, L.M. Prince, Mechanism of formation and structure of micro emulsions by electron microscopy, J. Phys. Chem. 63 (1959) 1677–1680.
[10] I. Danielsson, B. Lindman, The definition of microemulsion, Colloids Surf. 3 (1981) 391–392.
[11] J. Eastoe, S. Gold, S.E. Rogers, A. Paul, T. Welton, R.K. Heenan, I. Grillo, Ionic liquid-in-oil microemulsions, J. Am. Chem. Soc. 127 (2005) 7302–7303.
[12] S.E. Friberg, Evaporation from an ionic liquid emulsion, J. Colloid Interface Sci. 307 (2007) 494–499.
[13] D.O. Shah, in: Micelles, Microemulsions and Monolayers, Marcel Dekker Inc, New York, 1998.
[14] S.P. Moulik, B.K. Paul, Structure, dynamics and transport properties of microemulsions, Adv. Colloid Interface Sci. 78 (1998) 99–195.
[15] S.P. Moulik, G.C. De, B.B. Bhowmik, A.K. Panda, Physicochemical studies on microemulsions. 6. Phase behavior, dynamics of percolation, and energetics of droplet clustering in water/AOT/n-heptane system influenced by additives (sodium cholate and sodium salicylate), J. Phys. Chem. B 103 (1999) 7122–7129.
[16] S.P. Moulik, L.G. Digout, W.M. Aylward, R. Palepu, Studies on the interfacial composition and thermodynamic properties of W/O microemulsions, Langmuir 16 (2000) 3101–3106.
[17] S.P. Moulik, S. Ghosh, Surface chemical and micellization behaviours of binary and ternary mixtures of amphiphiles (Triton X-100, Tween-80 and CTAB) in aqueous medium, J. Mol. Liq. 72 (1997) 145–161.
[18] M. Gradzielski, H. Hoffmann, Structural investigations of charged O/W microemulsion droplets, Adv. Colloid Interface Sci. 42 (1992) 149–173.
[19] C. Stubenrauch, B. Paeplow, G.H. Findenegg, Microemulsions supported by octyl monoglucoside and geraniol. 1. The role of the alcohol in the interfacial layer, Langmuir 13 (1997) 3652–3658.
[20] M. Fanun, Phase behavior, transport, diffusion and structural parameters of nonionic surfactants microemulsions, J. Mol. Liq. 139 (2008) 14–22.
[21] B. Lindman, M.C. Puyal, N. Kamenka, B. Brun, G. Gunnarsson, Micelle formation of ionic surfactants. Tracer self-diffusion studies and theoretical calculations for sodium p-octylbenzenesulfonate, J. Phys. Chem. 86 (1982) 1702–1711.
[22] B. Lindman, K. Shinoda, M. Jonstro?mer, A. Shinohara, Change of organized solution (microemulsion) structure with small change in surfactant composition as revealed by NMR self-diffusion studies, J. Phys. Chem. 92 (1988) 4702–4706.
[23] Y. Gao, N. Li, L. Hilfert, S. Zhang, L. Zheng, L. Yu, Temperature-induced microstructural changes in ionic liquid-based microemulsions, Langmuir 25 (2009) 1360–1365.
[24] B. Bhattacharya, A. Samanta, Excited-state proton-transfer dynamics of 7-hydroxyquinoline in room temperature ionic liquids, J. Phys. Chem. B 112 (2008) 10101–10106.
[25] K. Bhattacharyya, Solvation dynamics and proton transfer in supramolecular assemblies, Acc. Chem. Res. 36 (2003) 95–101.
[26] K. Bhattacharyya, B. Bagchi, Slow dynamics of constrained water in complex geometries, J. Phys. Chem. A 104 (2000) 10603–10613.
[27] S. Cheng, X. Fu, J. Liu, J. Zhang, Z. Zhang, Y. Wei, B. Han, Study of ethylene glycol/TX-100/ionic liquid microemulsions, Colloids Surf. A 302 (2007) 211–215.
[28] A. Samanta, Dynamic stokes shift and excitation wavelength dependent fluorescence of dipolar molecules in room temperature ionic liquids, J. Phys. Chem. B 110 (2006) 13704–13716.
[29] A. Samanta, Solvation Dynamics in Ionic Liquids: What We Have Learned from the Dynamic Fluorescence Stokes Shift Studies, J. Phys. Chem. Lett. 1 (2010) 1557–1562.
[30] N. Sarkar, K. Das, A. Datta, S. Das, K. Bhattacharyya, Solvation dynamics of coumarin 480 in reverse micelles. Slow relaxation of water molecules, J. Phys. Chem. 100 (1996) 10523–10527.
[31] H. Gao, J. Li, B. Han, W. Chen, J. Zhang, R. Zhang, D. Yan, Microemulsions with ionic liquid polar domains, Phys. Chem. Chem. Phys. 6 (2004) 2914–2916.
[32] V.G. Rao, S. Ghosh, C. Ghatak, S. Mandal, U. Brahmachari, N. Sarkar, Designing a new strategy for the formation of IL-in-oil microemulsions, J. Phys. Chem. B 116 (2012) 2850–2855.
[33] O. Rojas, J. Koetz, S. Kosmella, B. Tiersch, P. Wacker, M. Kramer, Structural studies of ionic liquid-modified microemulsions, J. Colloid Interface Sci. 333 (2009) 782–790.
[34] T.L. Greaves, C.J. Drummond, Ionic liquids as amphiphile self-assembly media, Chem. Soc. Rev. 37 (2008) 1709–1726.
[35] S.K. Mehta, K. Kaur, Ionic liquid microemulsions and their technological applications, Ind. J. Chem. 49A (2010) 662–684.
[36] M. Moniruzzaman, N. Kamiya, M. Goto, Ionic liquid based microemulsion with pharmaceutically accepted components: formulation and potential applications, J. Colloid Interface Sci. 352 (2010) 136–142.
[37] M.S. Althanyan, K.H. Assi, B.J. Clark, J. Hanaee, Microemulsion high performance liquid chromatography (MELC) method for the determination of terbutaline in pharmaceutical preparation, J. Pharm. Biomed. Anal. 55 (2011) 397–402.
[38] Y. Gao, S. Wang, L. Zheng, S. Han, X. Zhang, D. Lu, L. Yu, Y. Ji, G. Zhang, Microregion detection of ionic liquid microemulsions, J. Colloid Interface Sci. 301 (2006) 612–616.
[39] Y. a. Gao, N. Li, L. Zheng, X. Zhao, S. Zhang, B. Han, W. Hou, G. Li, A cyclic voltammetric technique for the detection of micro-regions of [bmim][PF6]/Tween 20/H_2O microemulsions and their performance characterization by UV–vis spectroscopy, Green Chem. 8 (2006) 43–49.
[40] Y. Gao, J. Zhang, H. Xu, X. Zhao, L. Zheng, X. Li, L. Yu, Structural studies of 1-butyl-3-methylimidazolium tetrafluoroborate/TX-100/p-xylene ionic liquid microemulsions, Chem. Phys. Chem. 7 (2006) 1554–1561.
[41] N. Li, Y. Gao, L. Zheng, J. Zhang, L. Yu, X. Li, Studies on the micropolarities of [bmim][BF4]/TX-100/toluene ionic liquid microemulsions and their behaviors characterized by UV−visible spectroscopy, Langmuir 23 (2006) 1091–1097.
[42] Y. Zheng, W. Eli, G. Li, FTIR study of Tween80/1-butyl-3-methylimidazolium hexafluorophosphate/toluene microemulsions, Colloid Polym. Sci. 287 (2009) 871–876.
[43] A. Adhikari, D.K. Das, D.K. Sasmal, K. Bhattacharyya, Ultrafast FRET in a room temperature ionic liquid microemulsion: a femtosecond excitation wavelength dependence study, J. Phys. Chem. A 113 (2009) 3737–3743.
[44] A. Adhikari, K. Sahu, S. Dey, S. Ghosh, U. Mandal, K. Bhattacharyya, Femtosecond solvation dynamics in a neat ionic liquid and ionic liquid microemulsion: excitation wavelength dependence, J. Phys. Chem. B 111 (2007) 12809–12816.
[45] A. Adhikari, D.K. Das, D.K. Sasmal, K. Bhattacharyya, Ultrafast FRET in a room temperature ionic liquid microemulsion: a femtosecond excitation wavelength dependence study, J. Phys. Chem. A 113 (2009) 3737–3743.
[46] S. Ghosh, S. Dey, A. Adhikari, U. Mandal, K. Bhattacharyya, Ultrafast fluorescence resonance energy transfer in the micelle and the gel phase of a triblock copolymer: excitation wavelength dependence, J. Phys. Chem. B 111 (2007) 7085–7091.
[47] D. Seth, A. Chakraborty, P. Setua, N. Sarkar, Interaction of ionic liquid with water in ternary microemulsions (triton X-100/water/1-butyl-3-methylimidazolium hexafluorophosphate) probed by solvent and rotational relaxation of Coumarin 153 and Coumarin 151, Langmuir 22 (2006) 7768–7775.
[48] D. Chakrabarty, D. Seth, A. Chakraborty, N. Sarkar, Dynamics of solvation and rotational relaxation of Coumarin 153 in ionic liquid confined nanometer-sized microemulsions, J. Phys. Chem. B 109 (2005) 5753–5758.
[49] D. Seth, A. Chakraborty, P. Setua, N. Sarkar, Dynamics of solvent and rotational relaxation of Coumarin-153 in room-temperature ionic liquid 1-butyl-3-methyl imidazolium tetrafluoroborate confined in poly(oxyethylene glycol) ethers containing micelles, J. Phys. Chem. B 111 (2007) 4781–4787.
[50] W. Kunz, T. Zemb, A. Harrar, Using ionic liquids to formulate microemulsions: current state of affairs, Curr. Opin. Colloid Interface Sci., in press.
[51] J. Perrin, in: Les Atomes, Felix Alcan Paris, 1913.
[52] Y. Guo, D. He, S. Xia, X. Xie, X. Gao, Q. Zhang, Preparation of a novel nanocomposite of polyaniline core decorated with anatase-TiO_2nanoparticles in ionic liquid/water microemulsion, J. Nanomater. 2012 (2012).
[53] G. Wang, M. Lu, H. Wu, Preparation of poly(methyl methacrylate) by ATRP using initiators for continuous activator regeneration (ICAR) in ionic liquid/microemulsions, Polymer 53 (2012) 1093–1097.
[54] L. Xue, Y. Li, F. Zou, L. Lu, Y. Zhao, X. Huang, Y. Qu, The catalytic efficiency of lipase in a novel water-in-[Bmim][PF6] microemulsion stabilized by both AOT and Triton X-100, Colloids Surf. B 92 (2012) 360–366.
[55] J.L. Anderson, D.W. Armstrong, G.T. Wei, Ionic Liquids in Analytical Chemistry, Anal. Chem. 79 (2007) 4247.
[56] A.E. Visser, R.P. Swatloski, S.T. Griffin, D.H. Hartman, R.D. Rogers, Liquid/liquid, extraction of metal ions in room temperature ionic liquids, Sep. Sci. Technol. 36 (2001) 785–804.
[57] J.-P. Belieres, D. Gervasio, C.A. Angell, Binary inorganic salt mixtures as high conductivity liquid electrolytes for >100 °C fuel cells, Chem. Commun. (2006) 4799–4801.
[58] S. Paul, A.K. Panda, Physicochemical investigations on the aqueous solution of an ionic liquid, 1-butyl-3-methylimidazolium methanesulfonate, [bmim][MS], in a concentrated and dilute regime, Colloids Surf. A 404 (2012) 1–11.
[59] S. Paul, A. Panda, Physico-chemical studies on microemulsion: effect of cosurfactant chain length on the phase behavior, formation dynamics, structural parameters and viscosity of water/(polysorbate-20 n-alkanol)/n-heptane water-in-oil microemulsion, J. Surf. Detergents 14 (2011) 473–486.

[60] M. De, S.C. Bhattacharya, A.K. Panda, S.P. Moulik, Physicochemistry of mixed systems of water/AOT (surfactant)/alkanol (cosurfactant)/cycloalkanone (oil): a detailed study of phase behavior, salt effect, and conductance properties, J. Disp. Scie. Technol 30 (2009) 277–288.
[61] S.K. Hait, S.P. Moulik, Interfacial composition and Thermodynamics of formation of water/isopropyl myristate water-in-oil microemulsions stabilized by butan-1-ol and surfactants like cetyl pyridinium chloride, cetyl trimethyl ammonium bromide, and sodium dodecyl sulfate, Langmuir 18 (2002) 6736–6744.
[62] A. Acharya, S.P. Moulik, S.K. Sanyal, B.K. Mishra, P.M. Puri, Physicochemical investigations of microemulsification of coconut oil and water using polyoxyethylene 2-cetyl ether (Brij 52) and isopropanol or ethanol, J. Colloid Interface Sci. 245 (2002) 163–170.
[63] A. Acharya, S.K. Sanyal, S.P. Moulik, Physicochemical investigations on microemulsification of eucalyptol and water in presence of polyoxyethylene (4) lauryl ether (Brij-30) and ethanol, Int. J. Pharm. 229 (2001) 213–226.
[64] S. Biswas, S.C. Bhattacharya, S.P. Moulik, Characterization of reverse micelles by spectroscopic measurements, Indian J. Chem. A 40 (2001) 1210–1213.
[65] A.K. Panda, B.B. Bhowmik, A.R. Das, S.P. Moulik, Dispersed molecular aggregates. 3. Synthesis and characterization of colloidal lead chromate in water/sodium bis(2-ethylhexyl) sulfosuccinate/n-heptane water-in-oil microemulsion medium, Langmuir 17 (2001) 1811–1816.
[66] A.K. Panda, S.P. Moulik, B.B. Bhowmik, A.R. Das, Dispersed molecular aggregates. II. Synthesis and characterization of nanoparticles of tungstic acid in H2O/(TX-100 alkanol)/n-heptane w/o microemulsion media, J. Colloid Interface Sci. 235 (2001) 218–226.
[67] S.K. Hait, S.P. Moulik, M.P. Rodgers, S.E. Burke, R. Palepu, Physicochemical studies on microemulsions. 7. dynamics of percolation and energetics of clustering in water/AOT/isooctane and water/aot/decane w/o microemulsions in presence of hydrotopes (sodium salicylate, α-naphthol, β-naphthol, resorcinol, catechol, hydroquinone, pyrogallol and urea) and bile salt (sodium cholate), J. Phys. Chem. B 105 (2001) 7145–7154.
[68] M. Chakraborty, A.K. Panda, Spectral behaviour of eosin Y in different solvents and aqueous surfactant media, Spectrochim. Acta A 81 (2011) 458–465.
[69] A. Chakrabarty, A. Mallick, B. Haldar, P. Das, N. Chattopadhyay, Binding interaction of a biological photosensitizer with serum albumins: a biophysical study, Biomacromolecules 8 (2007) 920–927.
[70] A. Mallick, B. Haldar, N. Chattopadhyay, Spectroscopic investigation on the interaction of ICT probe 3-acetyl-4-oxo-6,7-dihydro-12H indolo-[2,3-a] quinolizine with serum albumins, J. Phys. Chem. B 109 (2005) 14683–14690.
[71] B.K. Paul, S.P. Moulik, Microemulsioins: an overview, J. Disp. Sci. Technol. 18 (1997) 301–367.
[72] B.K. Paul, S.P. Moulik, Uses and applications of microemulsions, Curr. Sci. 80 (2001) 990–1001.
[73] M. De, S.C. Bhattacharya, A.K. Panda, S.P. Moulik, Interfacial behavior, structure and thermodynamics of water in oil microemulsion formation in relation to the variation of surfactant head group and cosurfactant, J. Disp. Sci. Technol. 30 (2009) 1262–1272.
[74] A. Stark, A.W. Zidell, M.M. Hoffmann, Is the ionic liquid 1-ethyl-3-methylimidazolium methanesulfonate [emim][$MeSO_3$] capable of rigidly binding water? J. Mol. Liq. 160 (2011) 166–179.
[75] W. Liu, L. Cheng, Y. Zhang, H. Wang, M. Yu, The physical properties of aqueous solution of room-temperature ionic liquids based on imidazolium: database and evaluation, J. Mol. Liq. 140 (2008) 68–72.
[76] W. Liu, T. Zhao, Y. Zhang, H. Wang, M. Yu, The physical properties of aqueous solutions of the ionic liquid [BMIM][BF4], J. Sol. Chem. 35 (2006) 1337–1346.
[77] A. Stark, P. Wasserscheid, in: Handbook of Green Chemistry - Green Solvents - Ionic Liquids, Wiley-VCH, 2010.
[78] E. Ghasemian, M. Najafi, A.A. Rafati, Z. Felegari, Effect of electrolytes on surface tension and surface adsorption of 1-hexyl-3-methylimidazolium chloride ionic liquid in aqueous solution, J. Chem. Therm. 42 (2010) 962–966.
[79] L.A.S. Ries, F.A. do Amaral, K. Matos, E.M.A. Martini, M.O. de Souza, R.F. de Souza, Evidence of change in the molecular organization of 1-n-butyl-3-methylimidazolium tetrafluoroborate ionic liquid solutions with the addition of water, Polyhedron 27 (2008) 3287–3293.
[80] T. Singh, A. Kumar, Aggregation behavior of ionic liquids in aqueous solutions: effect of alkyl chain length, cations, and anions, J. Phys. Chem. B 111 (2007) 7843–7851.
[81] N.M. Vaghela, N.V. Sastry, V.K. Aswal, Effect of additives on the surface active and morphological features of 1-octyl-3-methylimidazolium halide aggregates in aqueous media, Colloids Surf. A 373 (2011) 101–109.
[82] C. Petit, A.S. Bommarius, M.P. Pileni, T.A. Hatton, Characterization of a four-component cationic reversed micellar system: dodecyltrimethylammonium chloride/hexanol/n-heptane and 0.1 M potassium chloride solution, J. Phys. Chem. 96 (1992) 4653–4658.
[83] W. Gerbacia, H.L. Rosano, Microemulsions: formation, stabilization, J. Colloid Interface Sci. 44 (1973) 242–248.
[84] K. Maiti, D. Mitra, R.N. Mitra, A.K. Panda, P.K. Das, A.K. Rakshit, S.P. Moulik, Self-aggregation of synthesized novel bolaforms and their mixtures with sodium dodecyl sulfate (SDS) and cetyltrimethylammonium bromide (CTAB) in aqueous medium, J. Phys. Chem. B 114 (2010) 7499–7508.
[85] M. De, S. Bhattacharya, S. Moulik, A. Panda, Interfacial composition, structural and thermodynamic parameters of water/(surfactant n-butanol)/ n-heptane water-in-oil microemulsion formation in relation to the surfactant chain length J. Surf, Detergents 13 (2010) 475–484.
[86] L. Digout, K. Bren, R. Palepu, S.P. Moulik, Interfacial composition, structural parameters and thermodynamic properties of water-in-oil microemulsions, Colloid Polym. Sci. 279 (2001) 655–663.
[87] S.P. Moulik, W.M. Aylward, R. Palepu, Phase behaviours and conductivity study of water/CPC/alkan-1-ol (C4 and C5)/1-hexane water/oil microemulsions with reference to their structure and related thermodynamics, Can. J. Chem. 79 (2001) 1–12.
[88] F. Wang, Z. Zhang, D. Li, J. Yang, C. Chu, L. Xu, Dilution method study on the interfacial composition, thermodynamic properties, and structural parameters of the [bmim][BF4] Brij-35 1-butanol toluene microemulsion, J. Chem. Eng. Data 56 (2011) 3328–3335.
[89] N. Li, Q. Cao, Y. Gao, J. Zhang, L. Zheng, X. Bai, B. Dong, Z. Li, M. Zhao, L. Yu, States of water located in the continuous organic phase of 1-butyl-3-methylimidazolium tetrafluoroborate/triton X-100/triethylamine reverse microemulsions, Chem. Phys. Chem. 8 (2007) 2211–2217.
[90] I. Chakraborty, S.P. Moulik, Physicochemical studies on microemulsions. 9. Conductance percolation of AOT-derived W/O microemulsion with aliphatic and aromatic hydrocarbon oils, J. Colloid Interface Sci. 289 (2005) 530–541.
[91] C.J.F. Böttcher, The dielectric constant of crystalline powders, Recl. Trav. Chem. 64 (1945) 47–51.
[92] C.G. Granqvist, O. Hunderi, Conductivity of inhomogeneous materials: effective-medium theory with dipole–dipole interaction, Phys. Rev. B 18 (1978) 1554.
[93] S. Kirkpatrick, Classical transport in disordered media: scaling and effective-medium theories, Phys. Rev. Lett. 27 (1971) 1722.
[94] B. Lagourette, J. Peyrelasse, C. Boned, M. Clausse, Percolative conduction in microemulsion type systems [10], Nature 281 (1979) 60–62.
[95] J.C. Maxwell, in: Electrochemistry and Magnetism, Third ed., 1892.
[96] N. Li, Y. Gao, L. Zheng, J. Zhang, L. Yu, X. Li, Studies on the micropolarities of bmimBF4/TX-100/toluene ionic liquid microemulsions and their behaviors characterized by UV–visible spectroscopy, Langmuir 23 (2006) 1091–1097.